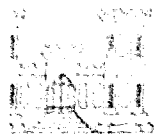


AD A029161



TECHNICAL REPORT S-76-7

THE CHANGEABLE INTERACTION BETWEEN SOILS AND PRESSURE CELLS: TESTS AND REVIEWS AT THE WATERWAYS EXPERIMENT STATION

by

M. Juul Hvorslev

Soils and Pavements Laboratory
U. S. Army Engineer Waterways Experiment Station
P. O. Box 631, Vicksburg, Miss. 39180

June 1976

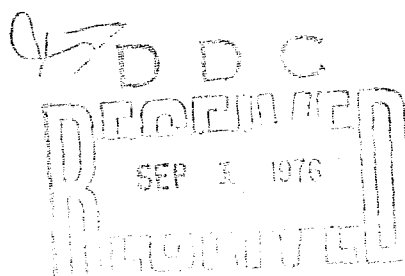
Final Report

Approved For Public Release; Distribution Unlimited

COPY AVAILABLE TO DDC DOES NOT
PERMIT FULLY LEGIBLE PRODUCTION



Reproduced From
Best Available Copy



Destroy this report when no longer needed. Do not return
it to the originator.

**Reproduced From
Best Available Copy**



NO COPY REFER TO

DEPARTMENT OF THE ARMY
WATERWAYS EXPERIMENT STATION, CORPS OF ENGINEERS
P. O. BOX 631
VICKSBURG, MISSISSIPPI 39180

23 August 1976

Errata Sheet

No. 1

THE CHANGEABLE INTERACTION BETWEEN SOILS AND PRESSURE CELLS;
TESTS AND REVIEWS AT THE WATERWAYS EXPERIMENT STATION

Technical Report No. S-76-7

June 1976

Traced Figures

- Fig. 1-A Show single, slightly curved tube from cell to surface gage.
Fig. 5-A Note that there is no lateral or radial force acting on side-walls of cell during calibration.
Fig. 17 Change ordinate from " σ_c/σ_z " to " σ_c/σ_x ."
Fig. 28B Upper right corner. Change " $D = 2P = 6$ in." to " $D = 2B = 6$ in."
Fig. 37B Left center note should read $\sigma_F = 73$.
Fig. 45 Upper sketch. Change " $h = 0.4D$ " to " $h = 0.2D$."
Fig. 53 Change ordinate to " $\sigma_3 = -u$." (Max $u = 13.26$ psi.)
Fig. 54 Title should read: "Measured Stresses at Midheight for Deadweight and with Forming Jacket On."
Fig. 66A Bottom abscissae should read: " $\epsilon_e = (\epsilon_z - \epsilon_c)$."
Fig. 74 Left center note. Change "See Figure 76" to "See Figure 75."
Fig. 76 Top left. Change "See Figure 76" to "See Figures 77 and 78."
Fig. 80 Bottom reference. Change "See Fig. 83" to "See Fig. 82."
Fig. 83 Bottom reference. Change "See Fig. 78" to "See Figs. 79-81."
Fig. 85B Add indicator line from left center note to solid registration ratio diagram.
Fig. 87 Add Note: Test data for specimen 70, cell 119, at 26-in. elev.
Fig. 88 Add Note: Test data for specimen 68, cell 119, at 26-in. elev.
Fig. 89 Add Note: Test data for specimen 72, cell 89, at 44-in. elev.
Fig. 91 Add Note: Test data for specimen 67, cell 85, at 26-in. elev.
Fig. 92 Add Note: Test specimen 79.
Fig. 93 Add Note: Test data for specimen 70, cell 83, at 26-in. elev.
Fig. 94 Add Note: Test data for specimen 70, cell 83, at 26-in. elev.
Fig. 95 Note below table should read: Data from fourth load cycle in Fig. 97.
Fig. 96A Upper left corner. Change "Fig. 97" to "Fig. 95."
and B

Text and Equations

- Abstract Page II, Line 8: Change "magnitude and direction" to "magnitude, direction, and ratio"
Page 18, Line 6 from bottom: Add before (Figure 4): "in the WES cell"

Page 22, Line 5 from top: Change "Figure 2" to "Figure 22"
 Page 31, Line 7 from bottom: change "Figure 95" to "Figures 95 and 97"
 Page 31, Line 6 from bottom: Add "Terzaghi" before Figure 126-b.
 Page 34, Line 11 from bottom: Add "the elevation" after "influence of"
 Page 37, Line 4 from top: Change "soil" to "oil"
 Page 37, Line 7 from top: Change "1/24" to "1/25"
 Page 37, Line 4 from bottom: Change "relative" to "relatively"
 Page 39, Line 3 from top: Change "radial" to "axial"
 Page 41, Line 3 from top: Change "stresses" to "stress"
 Page 45, Equation 6b: Change " $\sigma_x - \sigma_s$ " to " $\sigma_c - \sigma_s$ "
 Page 53, Equation 21b: Change " $\sigma_s - \delta_c$ " to " $\delta_s - \delta_c$ "
 Page 57, Line 8 from top: Change " σ_c/σ_z " to " σ_c/σ_x "
 Page 57, Line 9 from top: Change "and" to "with"
 Page 57, Line 12 from top: Change "Figure 16." to "Figure 17."
 Page 59, Line 3, para 43: Change to read: may be formed by improper installation and...."
 Page 65, Equation at top: Enclose the two fractions in parentheses.
 Page 75, Line 2 from bottom: Change "Figure 31." to "Figure 34."
 Page 77, Line 5 from top: Change "Figure 31B." to "Figure 34B."
 Page 77, Bottom line: Change "are in" to "is defined by"
 Page 90, Line 10 from bottom: Change "Figure 26." to "Figure 25."
 Page 169, Line 7 from bottom: Change "Figure 62." to "Figure 63."
 Page 193, Equation (99): Change " M_x " to " M_s "
 Page 229, Line 4 from top: Change "modulus" to "moduli"
 Page 231, Line 4 from bottom: Change "14.1 psi" to "14.3 psi"
 Page 234, Line 15 from bottom: Change "Figure 89" to "Figure 86"
 Page 234, Line 1 from bottom: Delete "additional"
 Page 240, Line 21 from top: Change to read: "...vertical soil pressure cell measuring horizontal stresses are...."
 Page 246, Line 7 from top: Change "Figure 97" to "Figure 95"
 Page 246, Line 14 from bottom: Change "Figure 95a" to "Figure 96a"
 Page 246, Line 13 from bottom: Change "Figure 95b" to "Figure 96b"
 Page 246, Line 5 from bottom: Change "Figure 96" to "Figure 97"
 Page 252, Line 2 from top: Change "Figure 11" to "Figure 12"
 Page 256, Line 1 from top: Change "Figure 5a" to "Figure 51a"
 Page 256, Line 10 from top: Change "Figure 5b" to "Figure 51b"
 Page 256, Line 4 from bottom: Change "tests" to "test"
 Page 257, Line 16 from top: Change "Figures 80-91" to "Figures 86-91"
 Page 260, Line 5 from bottom: Change "but were" to "which is"
 Page 261, Line 10 from bottom: Delete "and" at start of line.
 Page 262, Line 11 from bottom: Change "of compacted" to "in compacted"
 Page 266, Paragraph 7 from top: Add "for measuring of horizontal stresses"
 Page 269, Reference 5: Change "by" to "bei"
 Page 270, Reference 1: Change "Chelapati" to "Chelapati"
 Page 270, Reference 1: Change "Test Note" to "Tech. Note"
 Page 270, Last Reference: Change titles of paper and publication to "Ein Neues Hydraulisches Fernmessverfahren für Mechanische Spannungen und Drücke. Archiv für Technisches Messen"
 Page A1, Line 9 from bottom. Change "Fig. 32a" to "Figure 35a"

Unclassified

WES-TR-S-76-7

SECURITY CLASSIFICATION OF THIS PAGE (When Data Entered)

REPORT DOCUMENTATION PAGE		READ INSTRUCTIONS BEFORE COMPLETING FORM
1. REPORT NUMBER Technical Report S-76-7	2. GOVT ACCESSION NO.	3. RECIPIENT'S CATALOG NUMBER
4. TITLE (and Subtitle) THE CHANGEABLE INTERACTION BETWEEN SOILS AND PRESSURE CELLS; TESTS AND REVIEWS AT THE WATERWAYS EXPERIMENT STATION.	5. TYPE OF REPORT & PERIOD COVERED Final report.	
6. AUTHOR(s) Juul Hvorslev	7. PERFORMING ORG. REPORT NUMBER	
9. PERFORMING ORGANIZATION NAME AND ADDRESS U. S. Army Engineer Waterways Experiment Station Soils and Pavements Laboratory P. O. Box 631, Vicksburg, Miss. 39180	10. PROGRAM ELEMENT, PROJECT, TASK AREA & WORK UNIT NUMBERS	
11. CONTROLLING OFFICE NAME AND ADDRESS	12. REPORT DATE June 1976	
14. MONITORING AGENCY NAME & ADDRESS (if different from Controlling Office) 12 284p.	13. NUMBER OF PAGES 275	
	15. SECURITY CLASS. (of this report) Unclassified	
15a. DECLASSIFICATION/DOWNGRADING SCHEDULE		
16. DISTRIBUTION STATEMENT (of this Report) Approved for public release; distribution unlimited.		
17. DISTRIBUTION STATEMENT (of the abstract entered in Block 20, if different from Report)		
18. SUPPLEMENTARY NOTES		
19. KEY WORDS (Continue on reverse side if necessary and identify by block number) Pressure cells (soils) Soil-pressure cell interaction		
20. ABSTRACT (Continue on reverse side if necessary and identify by block number) The principal subjects of the report are the often neglected changes in the interaction of soil and pressure cells with consequent changes in relative errors in cell registrations. The report contains (a) a brief account of the development and use of soil pressure cells; (b) a review of proposed theories for soil-cell interaction; (c) a delayed account of tests with Waterways Experiment Station pressure cells placed in a large triaxial device; and (d) tentative conclusions plus suggestions for calibration, installation, and measuring (Continued)		

DD FORM 1 JAN 73 1473 EDITION OF 1 NOV 65 IS OBSOLETE

Unclassified

SECURITY CLASSIFICATION OF THIS PAGE (When Data Entered)

Reproduced From
Best Available Copy

038100

Unclassified

SECURITY CLASSIFICATION OF THIS PAGE(When Data Entered)

20. ABSTRACT (Continued).

procedures. Early theories may yield acceptable explanations of the action of soil pressure cells, but corresponding numerical data are not reliable because these theories were based on the Boussinesq equations for forces on the free soil surface, whereas the Mindlin equations should be used for forces acting in the interior of a soil mass. Theory and experiments show lateral stresses may increase or decrease the axial stresses, normal to the faces of a cell, that is, the calibration factor of a soil pressure cell is not a constant but varies with the configuration of the cell, with the magnitude and direction of the principal soil stresses, and with the value of the Poisson ratio in addition to the moduli of deformation of cell and soil. Registration of soil pressure cells may become quite variable and unreliable when the stress conditions in the soil approach those of failure with corresponding changes in soil deformations and properties.

ACCESSION for	
NTIS	Whole Section <input checked="" type="checkbox"/>
DOC	Full Section <input type="checkbox"/>
UNANNOUNCED	<input type="checkbox"/>
JUSTIFICATION	
BY	
DISTRIBUTION AVAILABILITY CODES	
Dist.	Avail. Code
A	

Unclassified

SECURITY CLASSIFICATION OF THIS PAGE(When Data Entered)

Reproduced From
Best Available Copy

PREFACE

At a meeting in June 1953 the Board of Consultants for the Soils Division, Waterways Experiment Station (WES), approved construction of a large triaxial compression device of the vacuum type and performance of tests with WES soil pressure cells placed in test specimens of this device. The triaxial device was built and the recommended tests were made in 1954-55. However, difficulties were encountered in evaluation of the test data and in preparation of a report on the tests, because the test results in many cases did not seem to agree with the then commonly used theories for soil-cell interaction. Preparation of the report was suspended in 1957 for lack of funds and assignments with a higher priority rating. Work on the test data and the report were resumed in 1970 on an intermittent basis.

The original tests were performed and intermittent and very brief memoranda were prepared by Mr. H. H. Ulery under direct supervision of Mr. R. G. Ahlvin, and general supervision by Mr. W. J. Turnbull, Chief of the Soils Division. During this period Major General (then Colonel), A. P. Rollins was Director and Mr. J. B. Tiffany was Technical Director of WES.

The report was prepared by Dr. M. J. Hvorslev, officially retired but reemployed on a part-time basis. During preparation of the final report, Mr. J. P. Sale was Chief of the Soils and Pavements Laboratory, BG E. D. Peixotto and COL G. H. Hilt were Directors, and Mr. F. R. Brown was Technical Director of WES.

CONTENTS

	<u>Page</u>
PREFACE	1
CONVERSION FACTORS, U. S. CUSTOMARY TO METRIC (SI)	
UNITS OF MEASUREMENT	10
PART I: DEVELOPMENT OF SOIL PRESSURE CELLS	11
Introduction	11
Initial Developments	12
The WES Soil Pressure Cell	15
Recent Types of Soil Pressure Cells	32
Installation of Pressure Cells	39
PART II: THEORIES OF SOIL-CELL INTERACTION	40
Principal Problems and Simplified Analysis	40
Review of Proposed Theories for Soil-Cell Interaction	92
PART III: TRIAXIAL TESTS WITH SOIL PRESSURE CELLS AT WES IN 1954-55	136
Background Data	136
Theoretical Stress Distribution in Cylinders with Restrained Ends	140
Testing Equipment and Procedures	144
Stress Distribution Tests of 1954	151
Cell Action Tests of 1955	177
PART IV: SUMMARY AND CONCLUSIONS	253
General Data	253
Hypotheses for Soil-Cell Interaction	254
WES Experimental Data of 1954-55	255
Principal Pressure Cell Parameters and Design Data	258
Types of Cells, Sensors, and Soils	259
Calibration of Soil Pressure Cells	261
Installation of Soil Pressure Cells	262
Operating Procedures	263
PART V: SUGGESTIONS FOR ADDITIONAL INVESTIGATIONS	265
REFERENCES	268
APPENDIX A: NOTATION	

Reproduced From
Best Available Copy

LIST OF FIGURES

	<u>Page</u>
1 Early Soil Pressure Measurements	13
2 Soil Pressure Cell with Exposed Diaphragm	14
3 Carlson Stress Meter	16
4 WES Soil Pressure Cell	17
5a Double Diaphragm Calibration Chamber	20
5b Stacked Ring Compression Chamber	21
6 Model of Deformation for WES Soil Pressure Cells	24
7 Influence of Load Eccentricity or Pressure Gradient . . .	26
8 Stress Distribution on and near a Soil Pressure Cell	30
9 Double Diaphragm Pressure Cell with Inactive Rim	33
10 Glötzl Hydraulic Soil Pressure Cell	35
11 URS-Mason Free Field Soil Stress Gage	36
12 Principles of SMRL Soil Stress Cell	38
13 Simplified Stress Relations for Cell in a Free Field	44
14 Influence of some Factors on the Indentation Ratio K_s	48
15 Registration Ratios of Soil Pressure Cells in a Free Field	51
16 Registration Ratios for Vertical Stresses, Earth Pressures at Rest	55
17 Registration Ratios for Horizontal Stresses, Earth Pressure at Rest	56
18 Installation Problems	60
19 Stress Bulbs Below Circular Load	67
20 Trapdoor Experiments after Terzaghi	70
21 Registration Ratios for Cells in Rigid Slab - Uniaxial Stress Changes	72
22 Registration Ratios for Cells in Rigid Slab - Earth Pressure at Rest	74
23 Registration Ratios for Cells in Rigid Wall - Earth Pressure at Rest	76

LIST OF FIGURES

	<u>Page</u>
24 Soil Pressure Cells at Interface of Compressible Strata	78
25 Pressure Cell Error Ratios for Normal and Extraneous Deformations	88
26 Boussinesq Versus Mindlin Equations for Interior Point Loads	91
27a Pressure Cell Error Ratios for Various Soil Types and Pressures	96
27b Influence of Thickness-Diameter Ratio of Cell on Its Registration Error	97
28a Comparison of Active and Passive Sand Pressures on Circular Trapdoor	100
28b Initial Values of Pressure Versus Displacement Ratios for Sand on Circular Trapdoor	101
29 Definitions for Mason-URS Pressure Cell Theory	104
30a Limiting Stress Change Versus Soil Cover	107
30b Change Ratio Versus Depth and Differential Deformation Ratios	108
31 Comparison of Theoretical and Experimental Trapdoor Active Pressures	109
32 Comparison of Theoretical and Experimental Trapdoor Passive Pressures	110
33 Kallstenius-Bergau Soil Pressure Cell for Rigid Walls	113
34 Soil Deformation and Pressure Conditions at Rigid Walls	115
35 Stresses in and at Rigid Ellipsoidal Inclusions	121
36 Stresses in Fluid Filled Ellipsoidal Cavity	124
37 Stresses on Cell with Inactive Rim and Exposed Diaphragms	127
38 Grids for Finite Element Analysis of the SMRL Soil Pressure Cell	128
39 Stress Distribution on the SMRL Pressure Cell for Axial Major Stress	130
40 Stress Distribution on the SMRL Pressure Gage for Lateral Major Stress	131
41 Inclusion Effect of the SMRL Soil Pressure Gage	132

LIST OF FIGURES

	<u>Page</u>
42	Correction Factors for Calibration of the SMRL Soil Pressure Gage
	134
43	Triaxial Calibration Tests by Plantema 1953
	137
44	Theoretical Axial Stress Distribution in Restrained Cylinder by Filon
	141
45	Theoretical Axial Stress Distribution in Restrained Cylinder by Balla
	143
46	WES Large Triaxial Compression Device - Vacuum Type
	145
47	Diagram of WES Equipment for Large Triaxial Tests - Vacuum Type
	146
48	Grain-Size Distribution of Sand Used in Large Triaxial Tests
	148
49	Modulus M_s for Mortar Sand and Constant Lateral Stress σ_3
	149
50	Apparent and Actual Moduli for Mortar Sand Versus Principal Stress Ratios
	150
51	Arrangement of WES Pressure Cells in Principal Tests
	153
52	Stress-Strain Diagrams for Medium Dense Sand in Uniaxial Compression
	157
53	Soil-Cell Stress Diagram at Midheight for Uniaxial Compression
	158
54	Measured Stresses at Midheight for Deadweight
	163
55	Measured Stresses at Midheight for Deadweight Plus Vacuum
	164
56	Measured Stresses at Midheight for Applied Axial Load of 13.26 psi
	165
57	Measured Stresses at Midheight for Applied Load Interval, 0-25 psi
	166
58	Measured Stresses at Midheight for Applied Load Interval, 25-30 psi
	167
59	Typical Soil-Cell Stress Diagrams for Base of Test Specimen
	170
60	Measured Stresses at Specimen Base for Applied Loads of 20-30 psi
	171

LIST OF FIGURES

	<u>Page</u>
61 Summary of Theoretical and Experimental Data on Axial Stresses	173
62 Changes in Incremental Registration Ratios with Increasing Applied Axial Load	176
63 Measured Residual Stresses After Initial Loading Cycle	178
64 Axial Stress-Strain Diagrams for Specimen 70 - Uniaxial Stage Loading	181
65 Soil-Cell Stress Diagrams for Uniaxial Stage Loading . .	189
66a Cell Overregistration Versus Axial Strain Differential at Midheight; Uniaxial Stage Loading, Specimen 70 - Cell 82, Elevation 26 in., Cycles 1, 2, and 3	190
66b Cell Overregistration Versus Strain Differentials; Axial Stress-Uniaxial Stage Loading, Specimen 70 - Cell 82, Elevation 26 in., Cycle 4	191
67 Deformation Moduli for Unaxial Stage Loading	196
68a Incremental and Total Registration Ratios for Uniaxial Loading	198
68b Alternative Diagram for Incremental Registration Ratios	199
69a Plate Loading Tests in Yuma Sand	202
69b Plate Loading Tests in Buckshot Clay	203
70 Axial Stress-Strain Diagrams for Principal Stress Ratio 3.0	212
71 Soil-Cell Stress Diagrams for Principal Stress Ratio 3.0	213
72 Axial Registration Ratios for Principal Stress Ratio 3.0	214
73 Axial Stress-Strain Diagrams for Principal Stress Ratio 2.5	215
74 Soil-Cell Stress Diagrams for Principal Stress Ratio 2.5	216
75 Axial Registration Ratios for Principal Stress Ratio 2.5	217
76 Axial Stress-Strain Diagrams for Principal Stress Ratio 2.0	218

LIST OF FIGURES

	<u>Page</u>
77 Soil-Cell Stress Diagrams for Principal Stress Ratio 2.0	219
78 Axial Registration Ratios for Principal Stress Ratio 2.0	220
79 Axial Stress-Strain Diagrams for Principal Stress Ratio 1.5	221
80 Soil-Cell Stress Diagrams for Principal Stress Ratio 1.5	222
81 Axial Registration Ratios for Principal Stress Ratio 1.5	223
82 Axial Stress-Strain Diagrams for Approximate Principal Stress Ratio 1.0	224
83 Soil-Cell Stress Diagrams for Approximate Principal Stress Ratio 1.0	225
84 Axial Registration Ratios for Approximate Principal Stress Ratio 1.0	226
85 Comparison of Registrations for Constant Principal Stress Ratios	228
86 Measured Radial Stresses for Uniaxial Stage Loading . . .	232
87 Measured Radial Stresses in Each Loading Stage	233
88 Measured Radial Stresses for Principal Stress Ratio 2.5	235
89 Measured Tangential Stresses for Uniaxial Stage Loading	236
90 Measured Tangential Stresses in Each Loading Stage . . .	237
91 Measured Tangential Stresses for Principal Stress Ratio 2.5	239
92 Diagonal Stress-Strain Diagrams for Uniaxial Stage Loading	242
93 Diagonal Soil-Cell Stress Diagram for Uniaxial Stage Loading	243
94 Diagonal Cell Registration Ratios for Uniaxial Stage Loading	245
95 Summary of Test Data for WES Pressure Cell Plus Inactive Rim	247

LIST OF FIGURES

		<u>Page</u>
96	Soil-Cell Stress Diagrams for WES Cell Plus Inactive Rim	248
97	Registration Ratios for WES Pressure Cell Plus Inactive Rim	251

LIST OF TABLES

	<u>Page</u>
1 Density Data for Sand in Triaxial Test Specimens, 1954 Test Series	154
2 Axial and Lateral Deformations of Triaxial Test Specimens, 1954 Test Series	155
3 Applied and Measured Stresses in Triaxial Test Specimens, 1954 Test Series	159
4 Summary of Applied and Measured Stresses in Triaxial Test Specimens, 1955 Test Series	183
5 Summary of Deformations and Moduli of Sand in Triaxial Test Specimens, 1955 Test Series	186
6 Average Registration Ratios of Pressure Cells in Triaxial Test Specimens, 1955 Test Series	187

Tables 1-5 are copies of tables in memoranda on the 1954-55 test series, but Table 6 was prepared for this report. Corrections of data in Tables 1-5 have not been made, but data which may be unreliable because of leaking of a cell or problems in seating the cell are indicated by special marks when used in figures for this report.

CONVERSION FACTORS, U. S. CUSTOMARY TO METRIC (SI)
UNITS OF MEASUREMENT

U. S. customary units of measurement used in this report can be converted to metric (SI) units as follows:

<u>Multiply</u>	<u>By</u>	<u>To Obtain</u>
inches	0.0254	metres
square inches	6.4516	square centimetres
cubic feet	0.02831685	cubic metres
pounds (mass)	0.4535924	kilograms
pounds (mass) per cubic foot	16.01846	kilograms per cubic metre
kips	4448.222	newtons
pounds (force) per square inch	6.894757	kilopascals
degrees (angle)	0.01745329	radians
Fahrenheit degrees	5/9	Celsius or Kelvins degrees*

* To obtain Celsius (C) temperature readings from Fahrenheit (F) readings, use the following formula: $C = (5/9)(F - 32)$. To obtain Kelvin (K) readings, use: $K = (5/9)(F - 32) + 273.15$.

THE CHANGEABLE INTERACTION BETWEEN SOILS AND PRESSURE CELLS;
TESTS AND REVIEWS AT THE WATERWAYS EXPERIMENT STATION

PART I: DEVELOPMENT OF SOIL PRESSURE CELLS

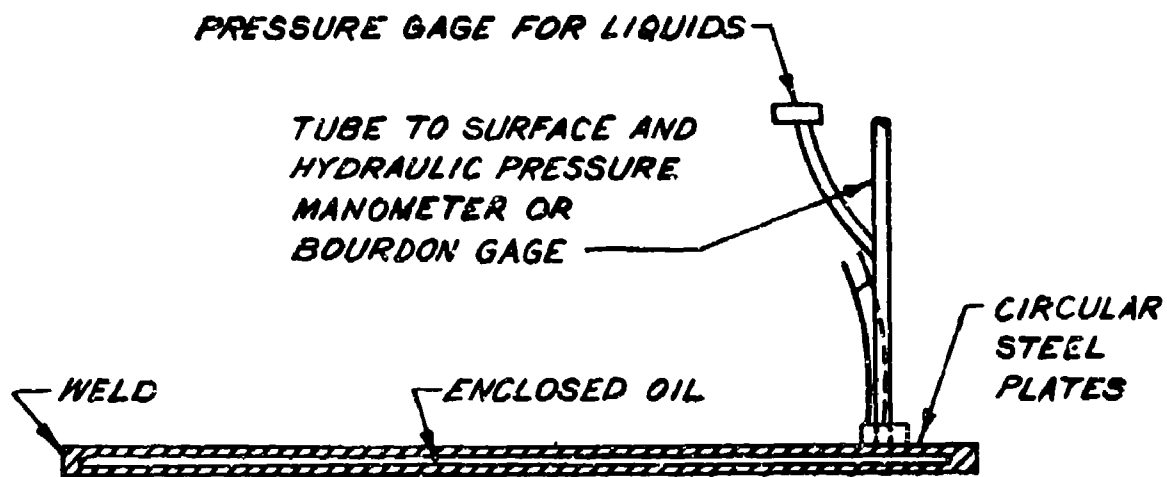
Introduction

1. This report contains a long delayed account of tests with the Waterways Experiment Station (WES) soil pressure cells and of changes in the soil-cell interaction and the corresponding errors in the registration of the pressure cells, which often appear to be overlooked in discussions of test data and measurements. Part I of the report presents a brief account of design and operation of the principal types of pressure cells, currently available, and of early tests on WES soil pressure cells, which were placed in a solid-walled shallow container filled with sand and subjected to confined compression. The results of these tests are described in a report of 1944, which for many years was a principal source of data on soil pressure cells. To obtain data on the action of pressure cells for various loading conditions, the early experiments were supplemented in 1954-55 by tests on WES soil pressure cells placed in test specimens of a large triaxial compression device. The test data did not yield fully conclusive information on the soil-cell interaction, but some of the data are, nevertheless, significant. The evaluation of the test data and preparation of a final report were interrupted in 1956, because priority was given to other investigations, but the work was resumed in 1970 as a part-time assignment. An important objective of the investigations was to determine the validity or limitations of theories for soil-cell interaction, and this objective governed in part the plan of tests and the preparation of the report. Therefore, the second part of the report is a fairly detailed review of a considerable variety of theories for soil-cell interaction, which have been proposed to date and are based on different simplifying assumptions. The third and main part of the report contains a summary of the results obtained in the 1954-55 tests and comparison of these data with the theories for

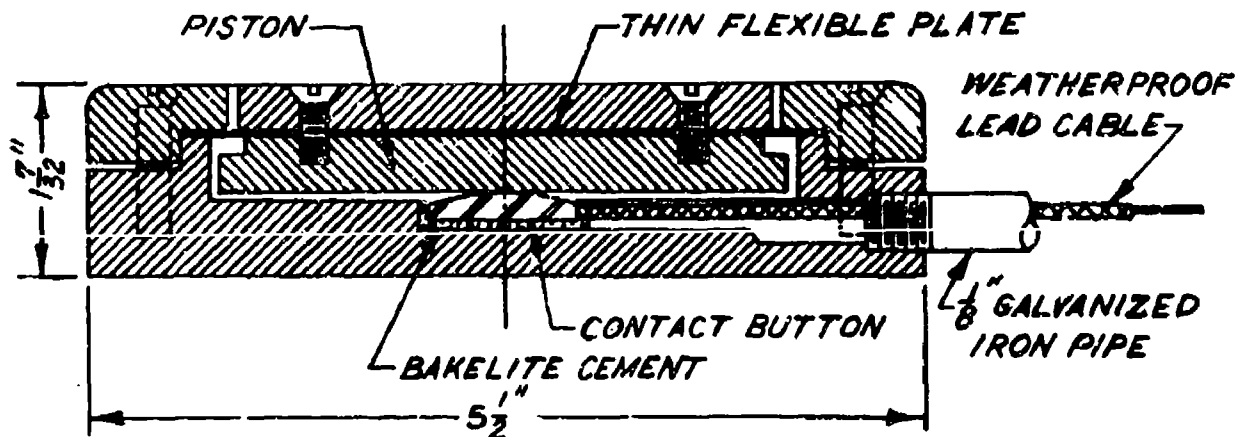
cell action. The various types of soil pressure cells described and the theories for soil-cell interaction discussed in the report do not constitute an encyclopedic review of the rapidly increasing literature on the subject. Furthermore, papers and reports published after January 1971 may be mentioned but are not reviewed in the report.

Initial Developments

2. One of the earliest soil pressure cells for field use was developed by Goldbeck (1916)* and is shown in Figure 1. The central and active part of the relatively thick face plate is connected to another plate or piston through a thin and flexible plate which acts as a hinge and allows small axial movements of the sensitive part of the face plate. The piston is normally supported by an insulated button in the base plate. The button is connected to the surface by an insulated wire inside a small tube. The latter permits changing the air pressure inside the cell. To make a measurement of the soil pressure, the air pressure is increased until the electrical connection between button and piston is broken, whereupon the air pressure is decreased until the electrical connection is reestablished. Difficulties were encountered in actual field installations. Pressure on the face plate may be increased by the counter movement required to break the electrical connection, which also is influenced by moisture conditions in the cell and by deformations of the pipe and cable. In Germany a very simple pressure cell, called a pressure pad and shown in Figure 1-B, was developed concurrently. It consists of two large circular plates, welded together but a short distance apart. The interior space was filled with oil and connected by a tube to the soil surface and a simple gage for measuring liquid pressures. Difficulties were encountered which are attributed to temperature variations and deformations of the tube between the pad and the soil surface. Another simple and frequently used pressure cell is shown in Figure 2. It has an inactive rim, and the active part of the face plate is thin enough to form a measuring diaphragm. Soil pressure is correlated with strains in the diaphragm, which are measured by



A. SCHEMATIC OF GERMAN HYDRAULIC PRESSURE PAD



FROM WES, TM 210-1, 1944

B. GOLDBECK SOIL PRESSURE CELL

FIGURE 1. EARLY SOIL PRESSURE MEASUREMENTS

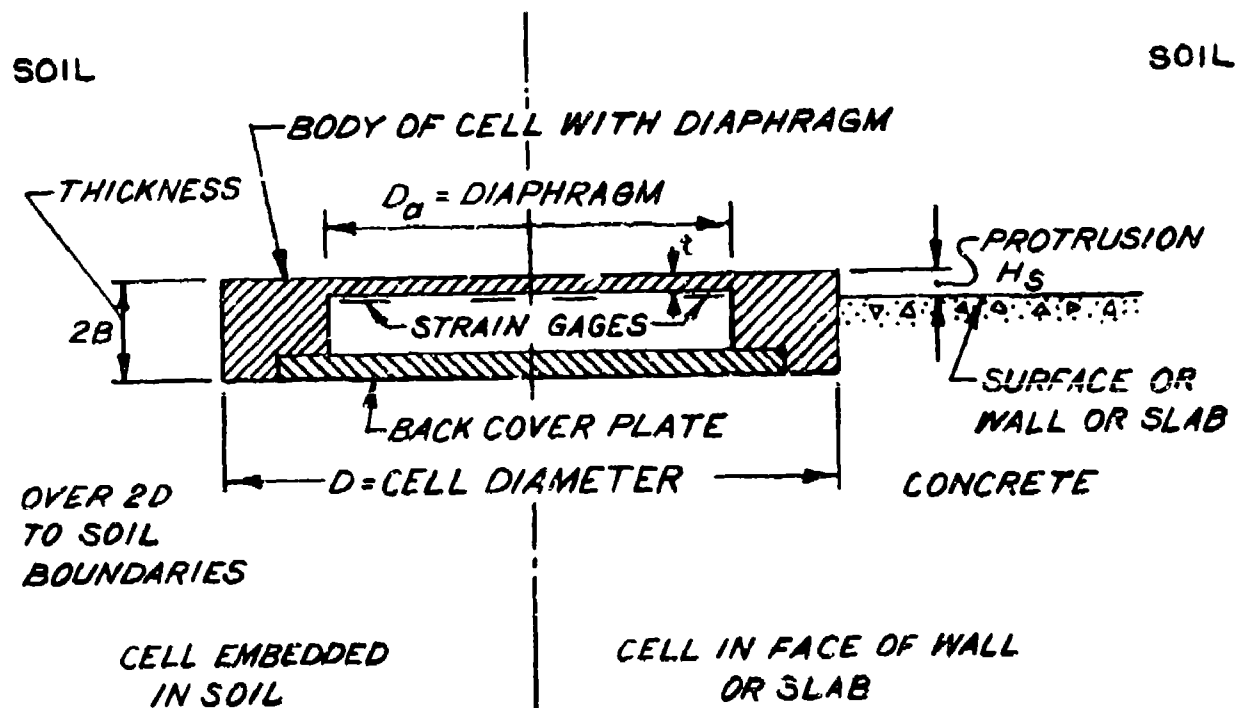


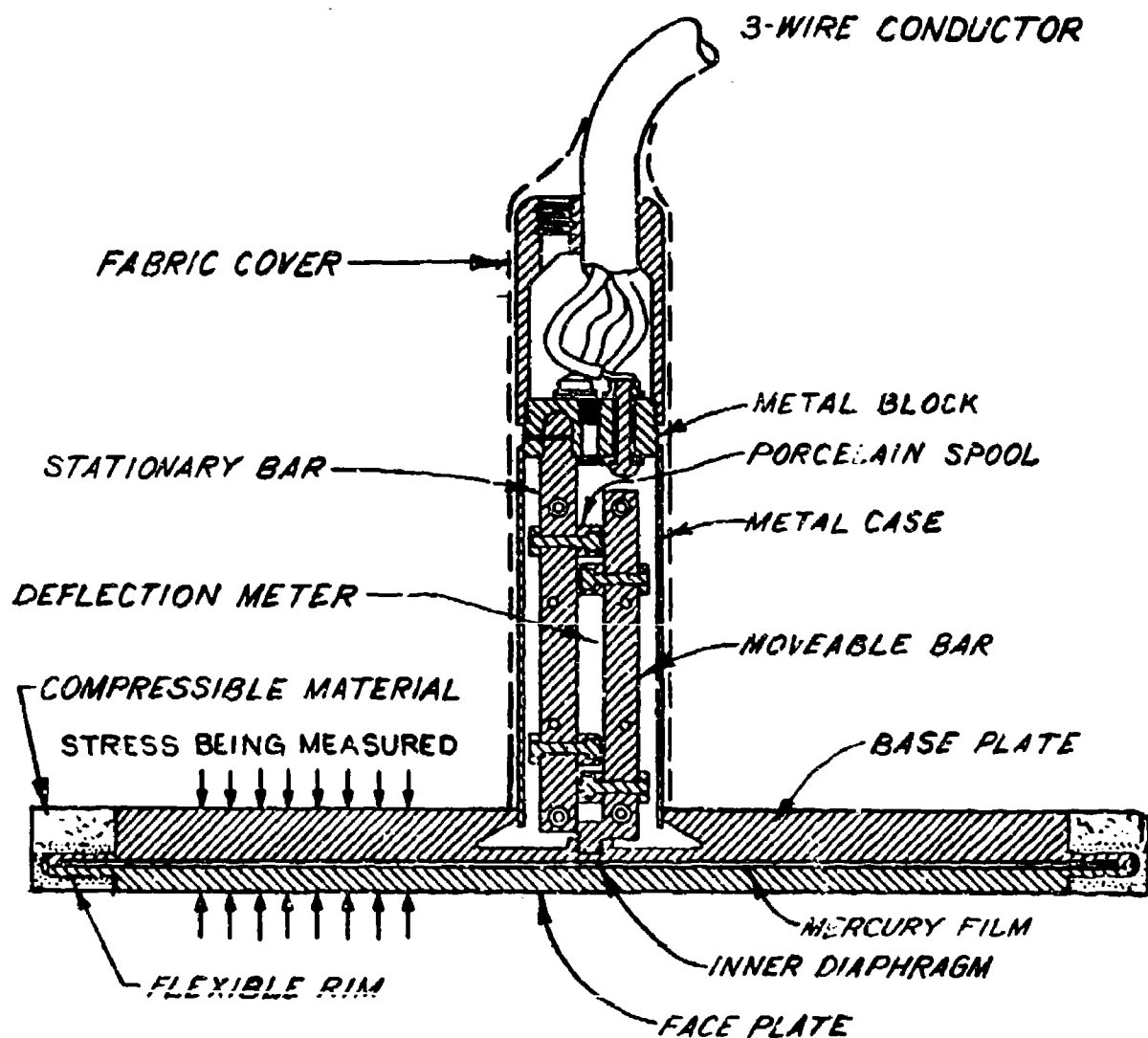
FIGURE 2. SOIL PRESSURE CELL WITH EXPOSED DIAPHRAGM

electrical resistivity foils or unbounded gages. This type of pressure cell may be used to advantage in fairly fine-grained and uniform soils; however, stones in the soil may cause eccentric load concentrations and also damage the diaphragm. These disadvantages are reduced in the Carlson stress meter, Figure 3, and in the WES soil pressure cell, Figure 4. Both of these cells use a fairly thick face plate with a flexible rim, which transfer the load to a thin layer of confined liquid and acts on an interior measuring diaphragm; but other details of the cells are quite different, and they were developed concurrently and independently of each other and are used in soils, rock, and concrete. The Carlson stress meter is described in greater detail by Carlson (1939), Carlson and Pirtz (1952), and also in TM 210-1, 1944, by the WES. A revised design of the Carlson stress meter has recently been developed, but details are not available, pending completion of trial tests.

The WES Soil Pressure Cell

General design data

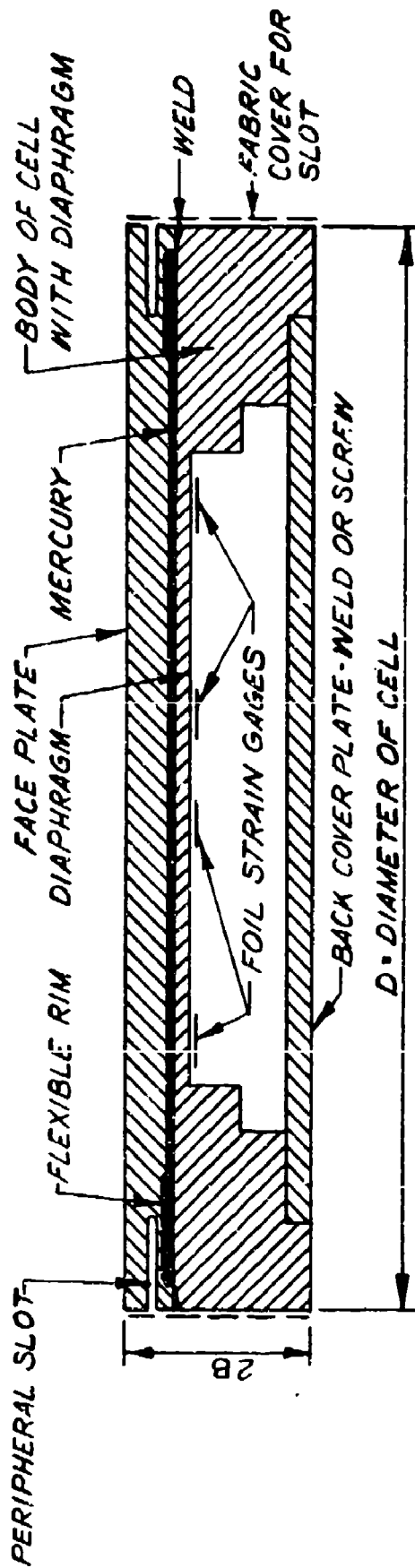
3. The principal features of the original WES soil pressure cell are shown in Figure 4-A and were developed by J. O. Osterberg during his employment at the WES. The cell consists of a face plate and a base plate, both fairly heavy and welded together at the outer edge but leaving a thin interspace in the central part which is filled with mercury. A thin slot is machined in the face plate, so that a flexible rim is formed and the load on the face plate is transmitted to the thin mercury layer, which acts on a thin diaphragm in the base plate. This arrangement decreases the influence of a concentration and eccentricity of the load on the face plate. The stresses in the diaphragm and corresponding pressure in the mercury are determined by means of strain gages, cemented to the diaphragm and connected into a Wheatstone bridge. Originally the strains in the central part of the diaphragm were determined by two radial wire strain gages, and two dummy gages provided temperature compensation. This arrangement was later changed to a pair of foil strain gages near the center and a corresponding pair near the



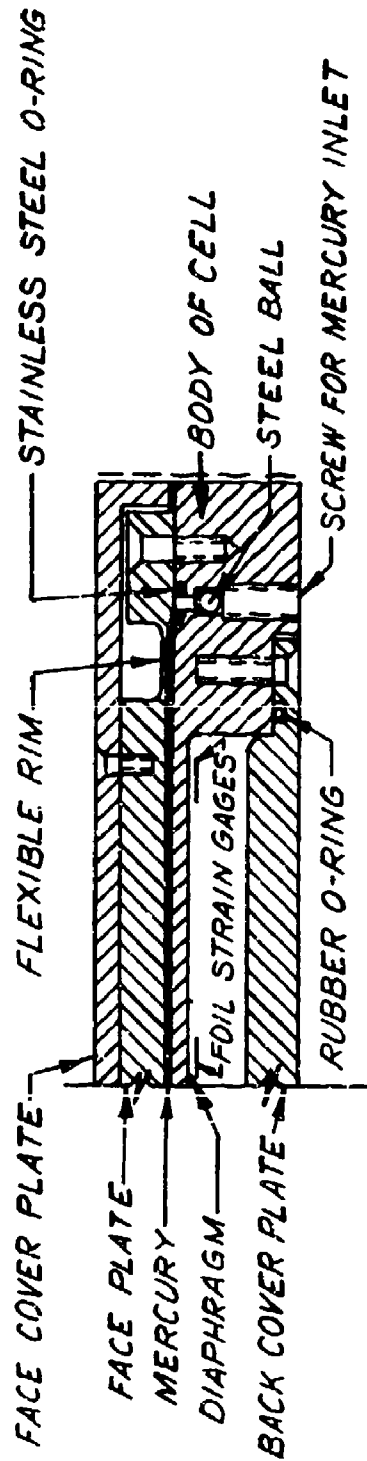
THE THICKNESS OF THE FACE PLATE IS INCREASED TO $\frac{3}{4}$ IN. WHEN METER IS USED CLOSE TO ROCK OR SOIL WITH STONES.

FROM WES TM 210-1, 1944

FIGURE 3. CARLSON STRESS METER



a. ORIGINAL DESIGN



b. 1969 EXPERIMENTAL DESIGN

FIGURE 4. WE'S SOIL PRESSURE CELL.

outer edge of the diaphragm. One pair undergoes positive strains and the other pair negative strains; this arrangement yields a higher degree of resolution in comparison with the original design. Wires from the strain gages lead to an outside cable through a radial fitting and flexible tubing with a hermetic seal. Most of the soil pressure cells were built in two sizes with diameters of 6 in.* and 12 in., both with a thickness of 1 in. Further details may be found in WES Technical Manual No. 210-1 of 1944 and also in the paper by Woodman (1955).

4. Some difficulties have been encountered in the manufacture and use of the WES soil pressure cells, Figure 4-A. It is not easy to machine the peripheral slot in the face plate with adequate accuracy to form a flexible rim of the desired thickness. The original cells were made of stainless steel, type 416, but this steel has presented difficulties in welding and has required special treatment to prevent progressive changes in its elastic properties. Tests are currently being made with cells of an experimental design shown in Figure 4-B. The face plate now consists of two parts, one forming an outer cover and the other an inner plate with a slot forming the flexible rim. Welding is eliminated in favor of screw joints and O-rings. The material has been changed to a free cutting carbon-manganese steel with stable elastic properties, and corrosion resistance is obtained by application of rust protectors.

5. The pressure cell designs in Figures 3 and 4 have in common that the pressure on the cell is determined by calibration with the strain of electrical resistance in the wire or foil sensor. In Figure 3 forces and movements are transmitted by mechanical means whereas this transmission is obtained by epoxy cements (Figure 4). Many other designs have been developed and some will be described after summarizing results of initial tests with cells of the design shown in Figure 4-A. Pressure cells of this design are called "Waterways Experiment Station Soil Pressure Cell" when discussed in this report. An entirely different type of pressure cell utilizes calibration of the pressure on the cell against

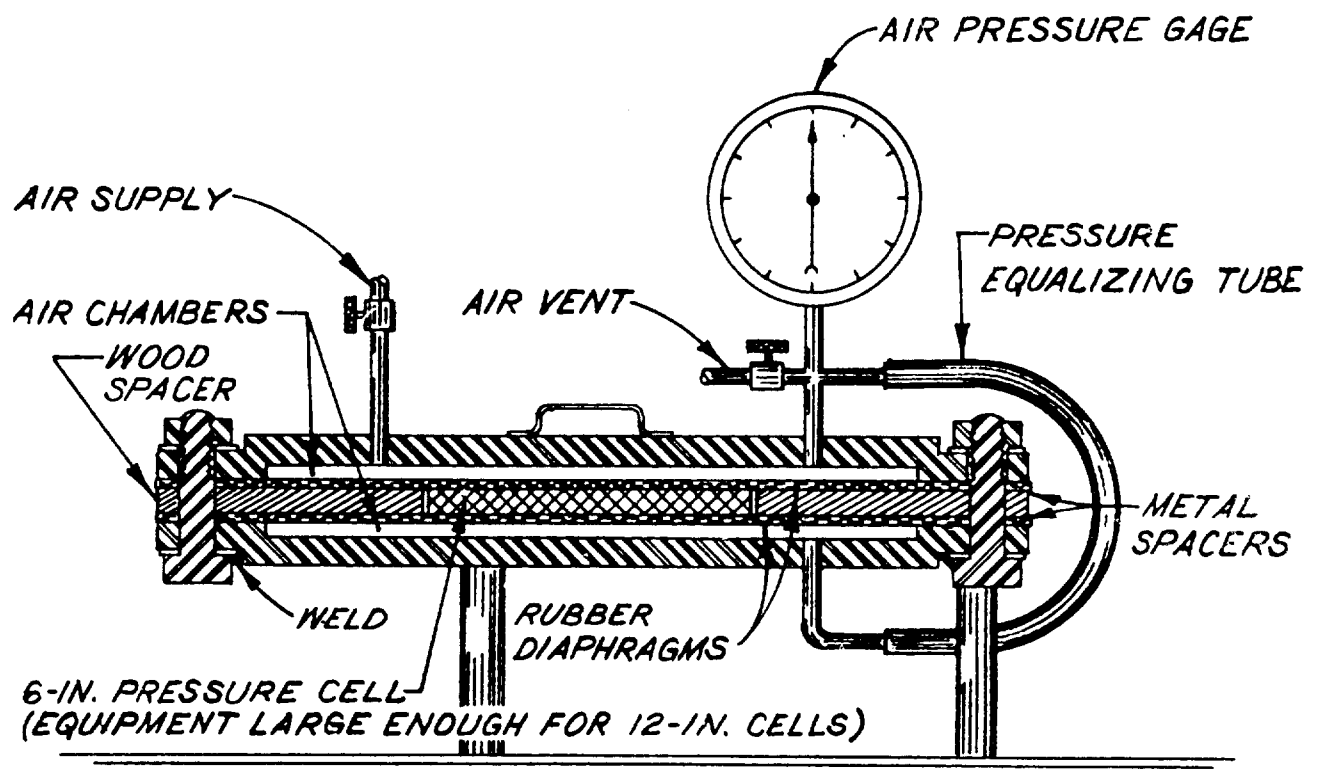
* A table of factors for converting U. S. customary units of measurement to metric (SI) units is presented on page 10.

changes in vibrations of a taut wire sensor. Pressure cells of this type are primarily used in Europe and are not considered in this report.

6. The WES soil pressure cells are calibrated in a double diaphragm chamber, Figure 5-A, where air pressure can be applied to the top and bottom surfaces of the cell, but is prevented from acting on the cylindrical surfaces and in the peripheral slot, Woodman (1955). Calibration factors obtained by this loading are slightly different from those yielded by hydrostatic air or liquid pressure on all surfaces of a cell. Both calibration factors are needed in use of the WES soil pressure cell. The cell reading corresponds to the sum of soil and pore pressure; the latter is measured separately or estimated and the corresponding reading is subtracted from the total reading to obtain the effective soil pressure. As discussed later in greater detail, the inclusion effect and the registration of a pressure cell depend not only on the field stress normal to the cell but to some extent also on lateral field stresses. Therefore, it is desirable, at least for each type of cell and soil, to check the routine calibration with a test in which the cell is embedded in soil and subjected to inclusion effects and lateral stresses. Confined compression in a chamber of stacked rings with rubber spacers, Figure 5-B, may be used for this purpose. The sidewall friction in such a chamber is decreased to a negligible amount. A compression chamber formed by separated rings was first used by the Swedish Geotechnical Institute in tests with gravel; finer grained material may enter the open space between the rings. Rubber spacers between the rings was introduced by Seaman (1966), who used rubber spacers cemented to the rings, whereas the design shown in Figure 5-B was developed at the WES.

Initial investigations of soil-cell interaction

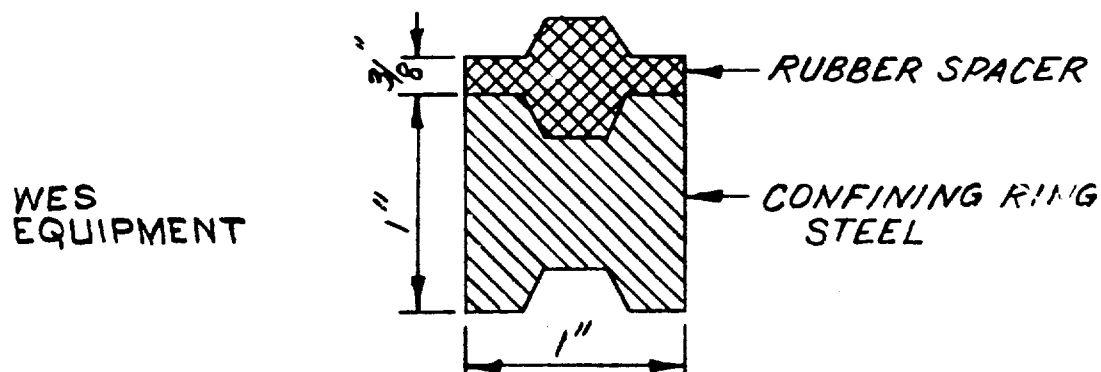
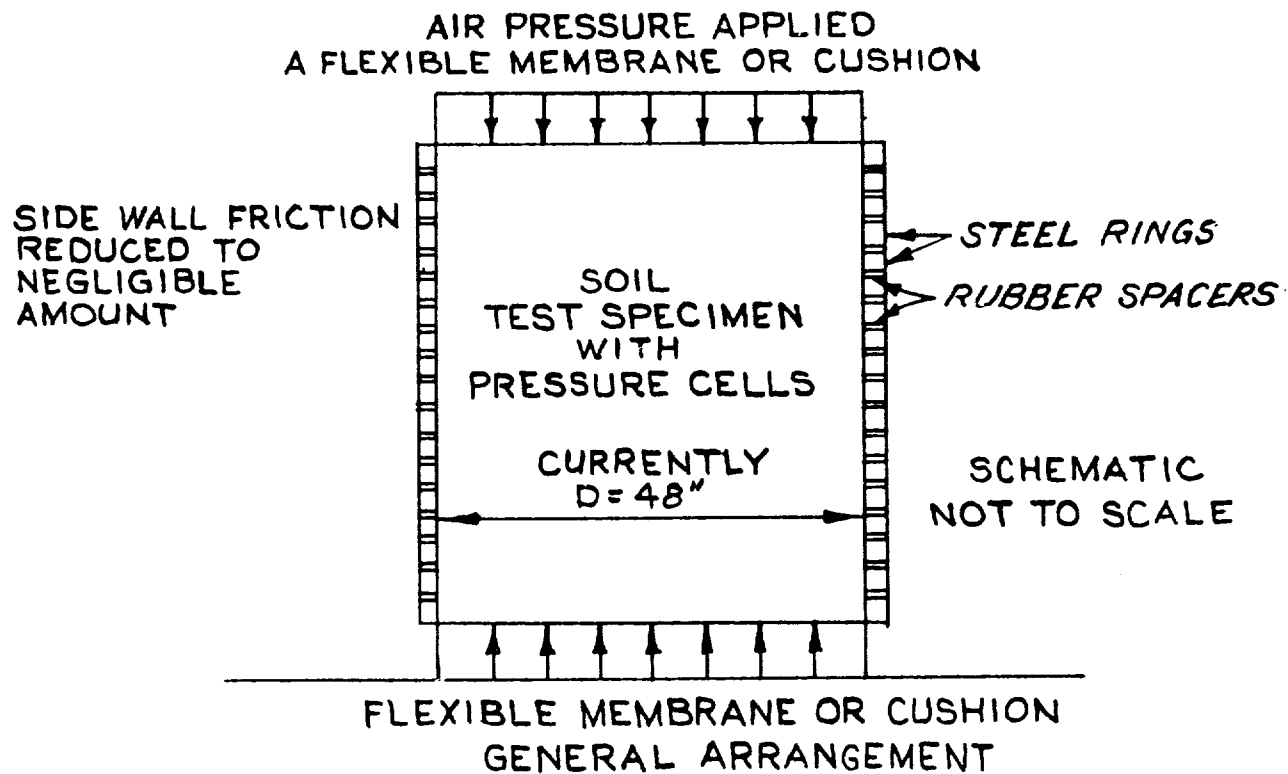
7. Observations by Benkelman and Lancaster (1940) show that the soil pressures registered by a pressure cell may vary with the thickness-diameter ratio of the cell and with the relative stiffness of cell and soil. In an attempt to obtain more quantitative data, WES soil pressure cells were tested in a pressure chamber with a diameter of 28 in. and a height of 10 in. The chamber was filled with standard Ottawa sand



FROM WES BULLETIN NO. 40, 1955

FIGURE 5A. DOUBLE DIAPHRAGM CALIBRATION CHAMBER.

Reproduced From
Best Available Copy



DETAIL OF RINGS AND SPACERS

FIGURE 5B. STACKED RING COMPRESSION CHAMBER.

and covered with a rubber membrane for transmission of air pressure above the sand. In some tests the pressure cells were placed at mid-height in the sand and in other tests the cells were embedded in a layer of plaster-of-Paris below the sand. The protrusion ratio of these cells, $H_s/2B^*$, varied from 0 to 1.0; see Figure 2. The tests are described in WES Technical Manual No. 210-1, 1944. The results obtained are summarized in the following paragraphs, where σ_s is the actual soil stress, σ_c is the stress indicated by the pressure cell; σ_c/σ_s is called the registration ratio and $(\sigma_e/\sigma_s) = (\sigma_c - \sigma_s)/\sigma_s$ is the error ratio.

- a. Changes in the stiffness of a thin pressure cell in loose sand has little influence on the registration ratio when the diameter-deflection ratio, D/δ_c , is greater than 2000, in which case registration ratios of 1.00 to 1.50 were obtained.
- b. The registration ratio of a stiff pressure cell decreases with decreasing thickness of the cell, but this change is small when the diameter-thickness ratio, $D/2B$, is greater than 5, in which case registration ratios of 1.00 to 1.20 were obtained.
- c. A pressure cell mounted flush with a stiff boundary or the bottom of the chamber underregisters, but this underregistration decreases with increasing stiffness of the cell, and changes in registration are small when the diameter-deflection ratio is greater than 1000. On the other hand, the registration ratios decrease rapidly with decreasing stiffness or diameter deflection ratios, D/δ_c , of the cell.
- d. The registration ratio of a pressure cell increases with increasing protrusion of the cell from a stiff boundary. Registration ratios of 0.90 to 1.00 were obtained with diameter-protrusion ratios $(D/H_s) = 30$ or less. (The underregistration changes to overregistration when the protrusion ratio is large or the cell just rests on the rigid boundary.)

8. Numerical values of test data summarized in paragraph 7 were probably influenced by the shallow depth of the sand layer and the use of a rigid test bin, but the general relationships are undoubtedly correct and are widely quoted. They also agree with relations obtained by

* For convenience, symbols and unusual abbreviations are listed and defined in the Notation (Appendix A).

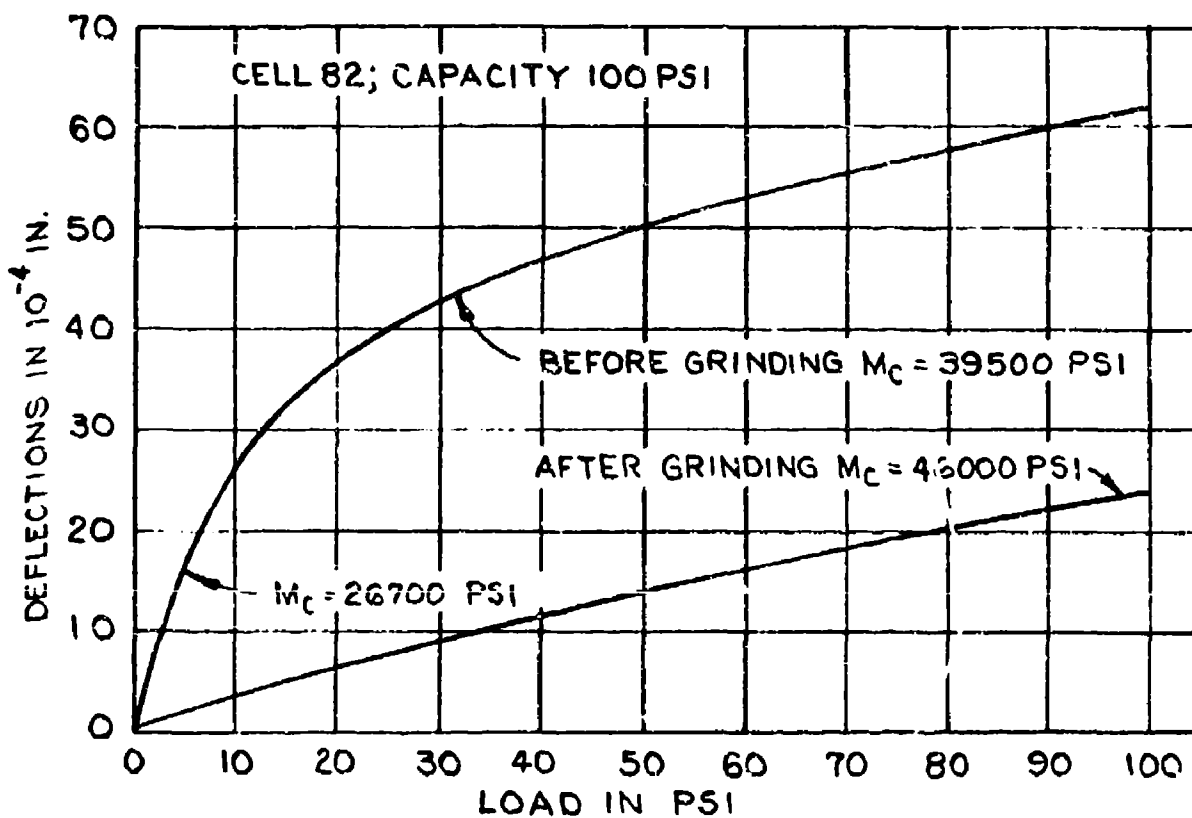
theories developed in later years, which may be summarized or restated as follows:

- a. The registration ratio of a pressure cell in a free field or in surface contact with a rigid boundary is greater than 1.0 when the cell is stiffer than the soil, but this ratio is smaller than 1.0 when the cell is more compressible than the soil.
- b. The registration ratio of a pressure cell embedded in a rigid boundary material may be greater or smaller than 1.0 depending on the relative stiffness of soil and cell and on the protrusion ratio of the cell, H_s/D .
- c. The error ratio of a pressure cell $(\sigma_c - \sigma_s)/\sigma_s$, is generally proportional to the thickness-diameter ratio of the cell, $2B/D$.
- d. These relations and the numerical data in paragraph 7 should be reconsidered and restated when the pressure cell has an inactive rim and the maximum deflection occurs in the center of the cell.

Structural action
of the WES pressure cell

9. Design, calibration, and structural action of WES pressure cells have been the subject of several investigations, which are discussed in the report "Summary of Earth Pressure Cell Development of 1954," WES Miscellaneous Paper No. 5-21. A few of these investigations are described in the following paragraphs.

10. Modulus of deformation. The registration ratio of a given pressure cell and soil is a function of the overall deformations of the pressure cell, which are not easy to determine with sufficient accuracy. Small irregularities in the surface of the cell cause the stress-strain diagrams to become curved, as shown in Figure 6. After grinding the faces of a cell, a much flatter but still curved diagram is obtained, which yields a tangent modulus of 26,700 psi at the start of the test and 46,000 psi at the rated capacity of the cell. The final tangent modulus of the cell before grinding is 39,500 psi whereas the modulus computed in design of the cell is 53,200 psi, disregarding the stiffness of the flexible rim. However, the measured and computed moduli at rated cell capacity are of the same order of magnitude. The moduli for hydrostatic loading were not determined experimentally but obtained by



CELL CAPACITY	MEASURED M_c - PSI		COMPUTED M_c - PSI	RATIO C_h / C_d
	MIN.	MAX.		
50 PSI	14,300	18,000	21,900	1.24
100 PSI	26,700	46,000	53,200	1.15

C_h = CALIBRATION FACTOR FOR HYDRAULIC LOADING

C_d = CALIBRATION FACTOR FOR DIRECT LOADING, FIG. 5

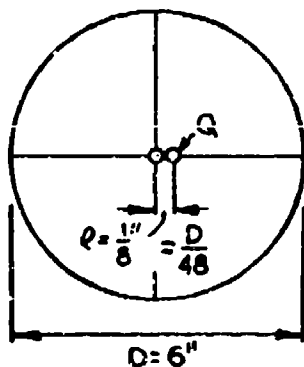
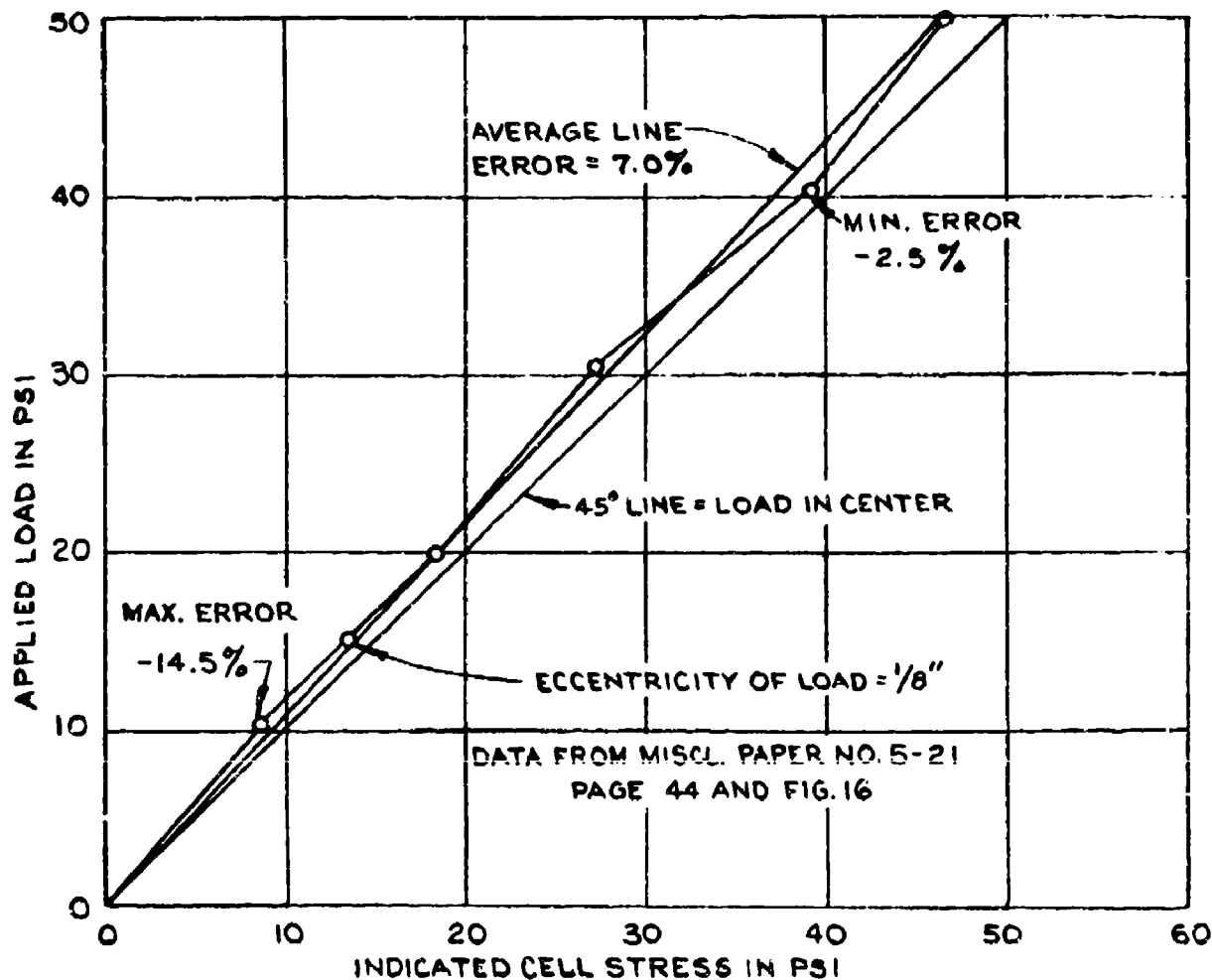
FIGURE 6. MODULI OF DEFORMATION FOR WES SOIL PRESSURE CELLS.

assuming proportionality between moduli and calibration factors.

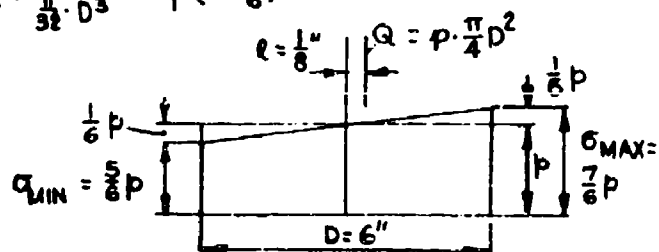
11. Carlson (1952) encountered similar difficulties in determining the deformation moduli of his stress meters. He solved the problem by developing an interferometer technique for measuring the change in thickness of the meter while it is being subjected to all-round air pressure. The interferometer can be observed through a window in the pressure chamber.

12. Influence of nonuniformity of loading. It has been mentioned already that the WES soil pressure cell is less sensitive to a nonuniformity of load elements than is a common pressure cell of the type shown in Figure 2; that is, the registration of a given annular load should vary relatively little with the radius of the annulus for the WES pressure cell, whereas for the cell in Figure 2 the registration for such loads varies from zero at the edge to a maximum in the center. The effect of an eccentricity of the total load, or a pressure gradient across the face of the cell may be quite different. This case was investigated in a single test in which the load was applied through a movable knife edge on top of the solid steel cylinder, covering the face plate of the cell. The results obtained for an eccentricity of 1/8 in. or a pressure gradient of 33 percent are shown in Figure 7, and the diagram shows a decrease in cell registration varying from a maximum of 14.5 percent at low loads to a minimum of 2.5 to 7.0 percent at high loads. Dials attached to the loading block indicated tipping of the face plate, which may be the direct cause of underregistration. The results obtained are quite erratic, and additional tests should be made before attempting to formulate the relationship between a stress gradient and change in cell registration. The influence of the radius of uniform annular loading should also be investigated for the WES pressure cell.

13. Effect of lateral forces on a pressure cell. An increase of radial pressure on the cylindrical surface of the pressure cell will cause an increase of lateral compression in the body of the cell and, by reason of the Poisson effect, also an increase in thickness of the pressure cell and a corresponding increase in cell registration. These changes in thickness and cell registration are very small because of



$$\sigma = \frac{Q}{\frac{\pi}{4} D^2} \pm \frac{Q \cdot e}{\frac{\pi}{32} D^3} = p \left(1 \pm \frac{1}{6} \right)$$



$$\text{PRESSURE GRADIENT} = \frac{\sigma_{MAX} - \sigma_{MIN}}{\sigma_{AV}} = \frac{1}{3} = 33\%$$

A LOAD ECCENTRICITY OF $\frac{1}{8}''$ FOR A 6-IN. CELL, CORRESPONDING TO A PRESSURE GRADIENT OF 33% OVER FACE OF CELL, CAUSES AN ERROR VARYING FROM 14.5% AT LOW LOADS TO A MINIMUM OF 2.5% AT HIGHER LOADS. THE TEST RESULTS ARE ERRATIC AND THE AVERAGE ERROR IS 7.0% UNDER REGISTRATION.

WES SOIL PRESSURE CELL

FIGURE 7. INFLUENCE OF LOAD ECCENTRICITY OR PRESSURE GRADIENT.

the large modulus of deformation of the steel, and they are usually negligible in comparison with the influence of other factors. However, Carlson and Pirtz (1952) suggest that an increase in radial pressures may magnify the transverse deflection of the inner diaphragm and thereby increase the registration of the stress meter. It was assumed that the radial pressures were caused by temperature variation of a meter in direct contact with concrete. Placing compressible material around the cylindrical surface of the meter, and reducing the thickness of the mercury film to one-third of its original values, caused a very material decrease in the temperature compensation factor. These comments refer primarily to the pressure cell itself, but lateral pressures may cause considerable changes in the deformations and stresses in the soil.

14. The cylindrical surface of the WES soil pressure cell is covered with adhesive tape to prevent soil from entering the peripheral slot. A test was made with a cell having its cylindrical surface covered with several layers of adhesive tape to prevent soil from entering the peripheral slot. The test was inconclusive possibly because it was made in a large vacuum type triaxial specimen where changes in effective confining pressures and pore pressures may compensate each other. It was observed that pressure cells placed on edge in a triaxial specimen for measurement of radial and tangential stresses had considerably smaller registration ratios than cells for measuring axial and diagonal stresses.

15. It has been suggested that lateral or shear forces on the face surfaces of a soil pressure cell may influence cell registration. A single improvised test with such shear forces, made at the Waterways Experiment Station, indicated that shear forces had very little influence on the cell registration. Detailed test data are not available now, and the test results were not conclusive. In summary, the influence of radial pressures and shear forces on a soil pressure cell has not yet been determined conclusively by experiments. However, as will be discussed later on, Askegaard (1963) and Bates (1969) have shown theoretically that a change in lateral earth pressure may have considerable influence on the axial earth pressure and on the corresponding registration of a soil pressure cell.

16. Temperature corrections. The influence of temperature changes on the output of the electrical circuits can be compensated automatically by proper design of the bridge formed by the four strain gages, when all parts of the cell body are made of the same steel. A uniform change in temperature should not give rise to disturbing stress changes, but the difference between volume changes of the cell body and the surrounding soil may cause a slight change in cell registration. However, this does not apply to the mercury film below the face plate, since the volume change of mercury for a given temperature change is thirteen times as great as that of steel. The results of an increase in temperature will be an excess increase in volume of the mercury, which raises the face plate and increases the deflections of the diaphragm by an amount which depends on the resistance offered by the soil. The magnitude of this difference in volume changes, and its influence on cell registration can be reduced by using a smaller amount of mercury. Carlson and Pirtz (1952) reduced the original thickness of the mercury film from 0.03 in. to 0.01 in., and the temperature correction was thereby decreased to 1 psi per degree Fahrenheit temperature change for cells embedded in concrete.

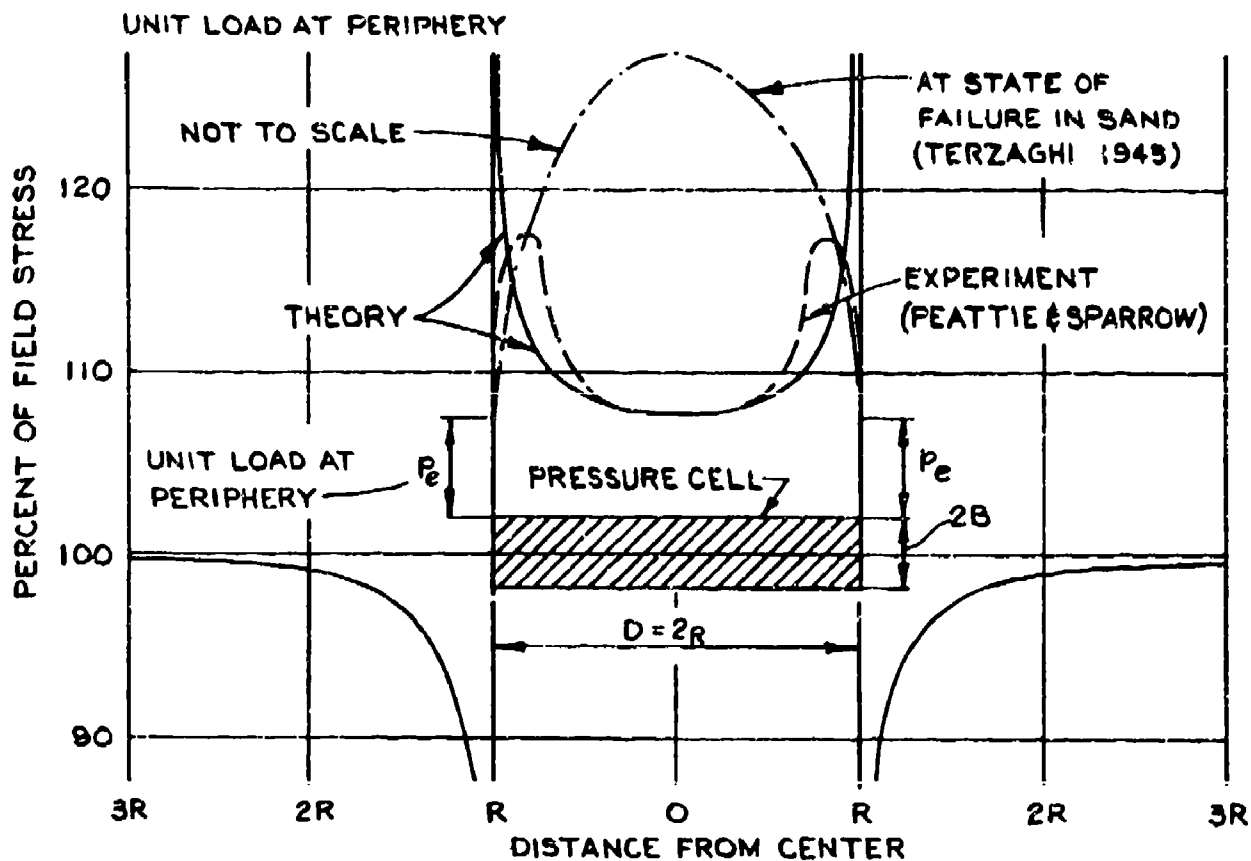
17. The thickness of the mercury layer in WES soil pressure cells is about 0.03 in. In the WES Miscellaneous Paper No. 5-21, 1952, it is stated that it was desired to reduce the temperature compensation to 0.01 percent of the full capacity of the cell for each degree Fahrenheit temperature change. Tests on 51 soil pressure cells built before 1951 indicated that the temperature compensation for forty of these cells was greater than the above mentioned 0.01 percent, but none was greater than 0.05 percent of the rated capacity per degree Fahrenheit. It is emphasized that the actual temperature compensation depends on the reaction of the soil to change in thickness of the pressure cell. It is also stated that cells buried deep in a body of soil undergo only very small temperature changes, and that the influence of temperature changes is slight compared to that of variations in installation techniques.

Contact pressures and inactive rims

18. Stress distribution at soil pressure cells. Embedment of a

pressure cell will change the stress conditions in the surrounding soil unless the cell has the same deformation properties as the soil. The general form of the stress distribution at a pressure cell which is stiffer than the soil is shown in Figure 8. Considerable overstress occurs in a narrow zone near the edge of the cell, and a corresponding understress exists in the soil outside the perimeter of the cell. Stress conditions in the overstressed zones above and below the cell usually cause partial failure of the soil with consequent plastic deformations and a reduction of the peak overstress, so that the stress distribution is changed to that indicated by the dashed line in Figure 8. The numerical values depend on the ratio of the moduli of deformation of the cell and the soil and on the diameter-thickness ratio of the cell. For a pressure cell which is more compressible than the surrounding soil, understress occurs above and below the cell and overstress just outside the perimeter of the cell. Theoretical investigations of the stress conditions around a pressure cell placed in an ideal elastic material have been made by Monfore (1950) and were verified in experiments by Peattie and Sparrow (1954), Figure 8. The stress distribution at a pressure cell, which is stiffer than the soil, is similar to that existing below and around a stiff foundation slab, which has been treated by many investigators and is summarized by Terzaghi (1943), Taylor (1948), Terzaghi and Peck (1967).

19. The stress distributions mentioned in the foregoing paragraph apply primarily to an ideal elastic material or to purely cohesive soils. However, it appears from experiments by Peattie and Sparrow (1954) and from observations of the action of pressure cells that these stress distributions also apply to other soils, including confined cohesionless soils, provided the stress conditions do not approach those of general failure. The latter which may cause a change from elastic to plastic conditions usually changes the stress distribution; according to Terzaghi (1943, Figure 126-b), the stresses below a loaded plate at the surface of a cohesionless soil at failure reach a maximum in the center and approach zero at the edges. For a plate or pressure cell below the surface the stress at the periphery will probably not be zero but correspond



AFTER TERZAGHI (1943), MONFORE (1950), PEATTIE AND SPARROW (1954)
 FIGURE B. STRESS DISTRIBUTION ON AND NEAR A SOIL PRESSURE CELL.

to the confining pressure and to the cohesion in soils with both friction and cohesion components of strength, as shown by the dash-dot diagram in Figure 8, whereas the maximum stress still occurs at the center. Such a change in stress distribution when passing from the elastic to the plastic state of the soil probably occurs gradually and would affect the registration ratio of pressure cells for which the sensitivity varies with the distance from the center of the diaphragm as in Figure 2.

20. Pressure cells with an inactive rim. The stress concentrations near the edge of stiff soil pressure cells caused Peattie and Sparrow (1954) to suggest that such pressure cells should be built with an inactive rim, Figure 2, and that the diameter of the central and active part should only be about half the outside diameter of the entire cell. Many tests have verified that the overregistration of such a cell under the usual stress conditions is much smaller than for a pressure cell with a full active face. However, the sensitivity of pressure cell diaphragm of the type shown in Figure 2 increases from zero at the edge of the diaphragm to a maximum in the middle, and this type should only be used in soils without stones and far enough away from boundary irregularities. Furthermore, the overregistration of such a pressure cell would be increased when stress condition in a friction type soil approaches that of failure, causing the stress distribution above and below the cell to change to the form shown by the dash-dot line in Figure 8. The WES conducted tests with the standard 6-in. WES soil pressure cell, Figure 4-A, provided with a 3-in. wide inactive rim. The registration ratio of these cells was close to 100 percent for low principal stress ratios but it rose to 153-172 percent when the stress conditions in the soil approached the failure conditions, see Part III, Figure 95. These results of the WES tests are an experimental verification of the diagrams suggested by Terzaghi in 1943, Figure 126-b. A similar rise in registration ratios when approaching failure conditions of the soil was exhibited by WES soil pressure cells without an inactive rim. In general, the principle of an inactive rim simplifies the construction of a soil pressure cell and improves the reliability of the registration when the cell is used in soils without stones and under

fairly uniform stress conditions, but the possibility of a change in stress distribution and its effect on the cell registration when approaching failure conditions should be borne in mind and deserves further investigation.

Recent Types of Soil Pressure Cells

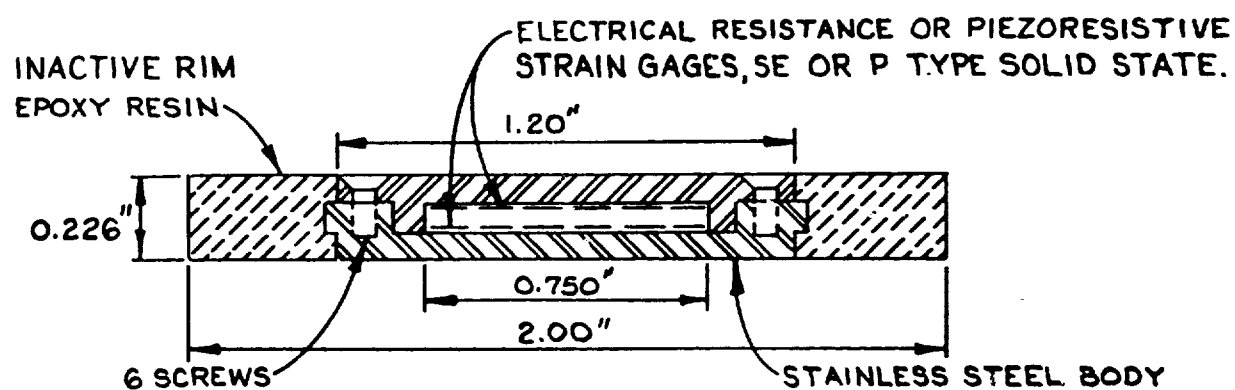
21. A great variety of soil pressure cells has been developed over the years. In many cases the difference between such cells is in minor mechanical details or in methods for measuring strains or deflections of diaphragms, such as bonded electrical resistance foils, non-bonded resistance wires, or a vibrating wire. Some recently developed or proposed types of soil pressure cells are described briefly in the following paragraphs, but it is again emphasized that this report primarily deals with the WES soil pressure cell, shown in Figure 4-A, and with its soil-cell interaction.

WES double diaphragm cell with inactive rim

22. The soil pressure cells shown in Figure 4 are primarily used in larger soil structures, and smaller cells may be needed for small models and in laboratory tests. Such cells often consist of small commercially available pressure cells which are provided with a collar or inactive rim in order to obtain a more favorable diameter-thickness ratio for the entire pressure cell. A recent WES development of small soil pressure cells is shown in Figure 9 and is described in detail in a report by J. K. Ingram (1968). The active diameter of this cell is 0.75 in., and it has a diaphragm on each side so that the cell is nearly symmetrical with respect to the midheight plane. This lightweight collar combined with the interior void causes the unit weight of the cell to be close to that of soil, and the cell is suitable for both static and dynamic experiments, provided the soil does not contain stones and the loads on the diaphragms are fairly uniformly distributed.

Glötzl hydraulic soil pressure cell

23. Early German measurements of pressures below foundation were



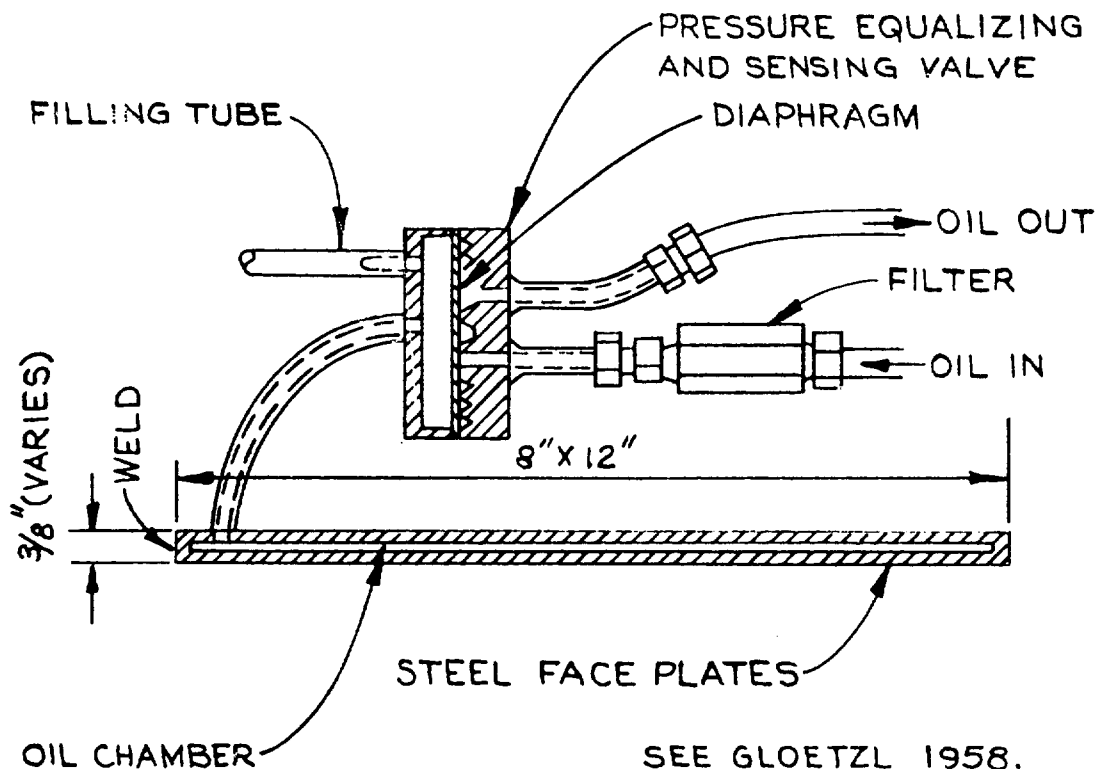
DATA FROM WES T.R. NO. 1-814, INGRAM, 1968

FIGURE 9. DOUBLE DIAPHRAGM PRESSURE CELL WITH INACTIVE RIM.

made with hydraulic pressure pads, called "druckkissen," consisting of two flexible steel plates welded together along the edges, so that they form a thin reservoir which is filled with oil and connected by a tube to a pressure gage outside the foundation. However, the pressures measured were not always reliable since they were sensitive to temperature variations and pressures on the connecting tube, and the flow of oil to or from the outside pressure gage caused too large movements of the plates. These disadvantages have been practically eliminated through introduction of a diaphragm valve by Glötzl (1958), Franz (1958), and others. The pressure pad is connected to the valve unit by a short pipe, Figure 10, forming a closed system for the oil, which acts on one side of the diaphragm in the valve, whereas the other side is supported by a dentated plate with inflow and outflow pipes. Oil is pumped slowly into the valve unit, and its pressure is measured by an outside gage. When the pressure of the inflowing oil becomes a little larger than that in the oil of the pressure pad, the diaphragm deflects a little and allows the inflowing oil to pass to the outflow pipe, and the pressure in the inflowing oil ceases to rise. The required movement of the diaphragm is much smaller than that required for the Goldbeck cell, Figure 1, and the short pipe decreases the influence of temperature changes of the oil and pressure on the pipe. The hydraulic diaphragm valve is available as a separate unit, and the advertised sensitivity or accuracy is 0.15 psi. The counterbalancing oil may be replaced by a neutral gas, which eliminates the influence of the outside pressure gage. The standard Glötzl pressure pad, Figure 10, is 8 by 10 in. with a total thickness of 3/8 in. and an effective thickness-diameter ratio of about 1/27; circular pressure cells using the same principles of design and operation have also been built. The small thickness-diameter ratios reduce the inclusion effect and the cell error, but the thin cells are easily damaged in coarse and stony soil, and they may then be replaced by thicker plates with a flexible rim, similar to the Carlson or WES stress cells.

URS - Mason soil stress cell

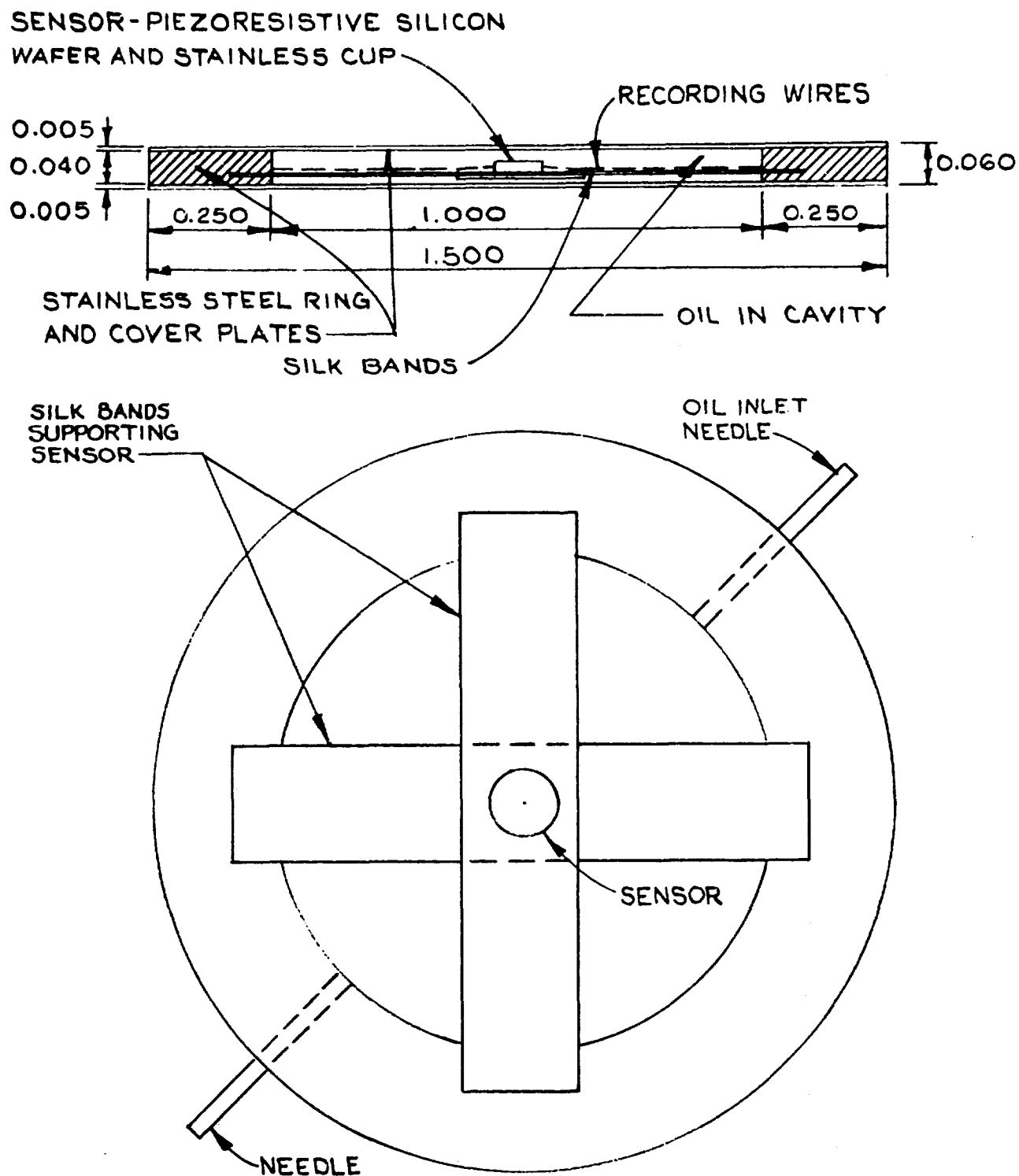
24. A small and thin soil stress cell of sophisticated design is shown in Figure 11. It was developed by the United Research Services



SEE GLOETZL 1958.

SIMILAR PRESSURE EQUALIZING VALVES HAVE BEEN BUILT BY SEVERAL INVESTIGATORS.

FIGURE 10. GLOETZL HYDRAULIC SOIL PRESSURE CELL



UNITED RESEARCH SERVICES, REPORT URS-758-6, 1971

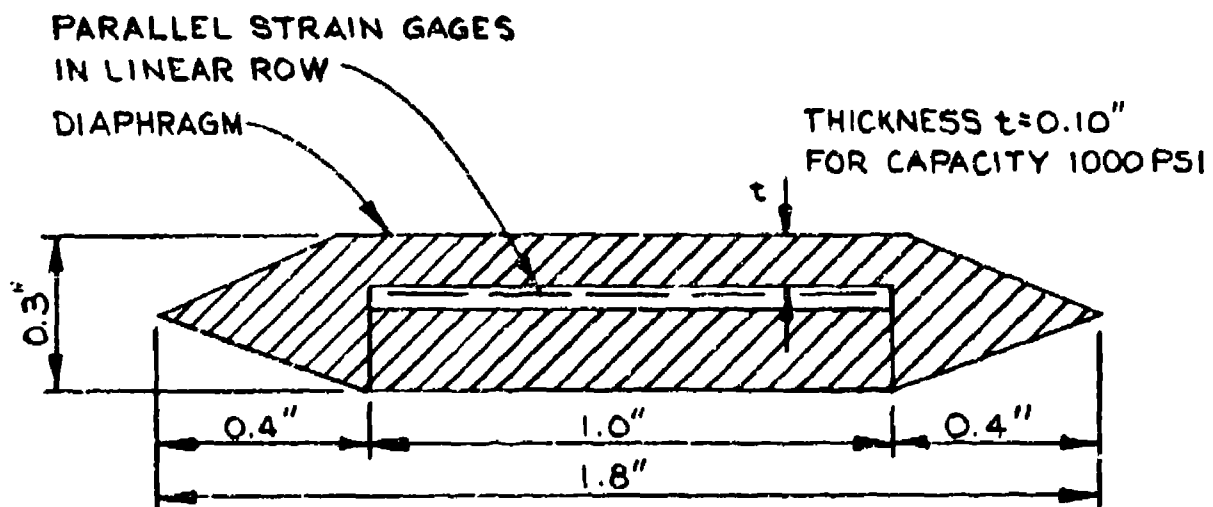
FIGURE 11. URS-MASON FREE FIELD SOIL STRESS GAGE.

under direction of Dr. H. G. Mason. All metal parts of the cell are of stainless steel. It consists of an inactive rim plus two cover plates fastened to the rim by epoxy. The central space is filled with Diala oil, and the pressure in this soil, considered equal to the soil pressure, is measured by a solid state sensor supported by two silk bands. The diameter is 1.50 in., the total thickness only 0.06 in., and the thickness-diameter ratio is $1/24$, or about the same as for the Glötzl soil stress cell. The cell can be used for both static and dynamic measurements. The use of a solid state sensor increases obtainable resolution, but such sensors represent recent developments, and definite data on their stability over long periods are not yet available. This very thin stress cell is easily damaged, and a less delicate cell may be obtained by increasing the diameter without increasing the thickness diameter ratio. The stress cells shown in Figures 10 and 11 represent opposite current limits of simplicity and sophistication in design.

The SMRL pressure
cell with bevelled rim

25. Figure 12 shows the principles of a rock and soil stress cell developed at the Spokane Mining Research Laboratory by R. C. Bates (1969), who analyzed the stress conditions in the cell and in the surrounding material of a free field by the finite element method, Part II. Bates found that lateral soil pressures may significantly increase the axial soil stresses and registration of the cell, and that the influence of the lateral soil pressures may be decreased by bevelling the outside edge of the proposed pressures cell, Figure 12. The central and active part of the cell forms an exposed and relative heavy diaphragm, but the sensitivity of the cell is increased by use of solid state strain gages.* The cell shown in Figure 12 has a rating of 1000 psi and is intended for mining investigations, but the same type of cell is also built with the

* Soil pressure gages with a vibrating wire strain gage are not described in this report; such strain gages are still commonly used in Europe but rarely in the United States. It is believed at the WES that available expoxies provide a satisfactorily strong and durable bond between a measuring diaphragm and a foil type resistivity strain gage.



CELL BODY OF STAINLESS STEEL

FROM BATES, 1969

FIGURE 12. PRINCIPLES OF SMRL SOIL STRESS CELL.

rated capacity of 100 psi for use in soils. More general and rigorous mathematical investigations by Askegaard (1963) show that lateral pressures may cause either an increase or a decrease in the radial soil stresses depending upon the values of the thickness-diameter ratio of the cell and the Poisson ratio of the soil, Figure 32.

Installation of Pressure Cells

26. Although improper installation of pressure cells may cause large errors in the cell registration, only a few experimental investigations of the problem have been made. Hadala (1967) recommends that cells be placed on a planed surface of sand deposits, whereas cells in clay should be placed in a shallow cylindrical excavation. A thin layer of fine sand is often used to improve the uniformity of contact between cell and soil; a thicker layer of sand is used when the soil contains stones or rock, but the sand body may also cause pocket action, which should be taken into consideration. As shown in this report, subjecting the cell to a seating pressure during or after installation improves contact between cell and soil, stabilizes soil properties, and cell registration and errors, but it may also cause a secondary type of pocket action. Additional systematic experimental investigations are needed, as mentioned in a more detailed review of the problem in Part II of this report.

PART II: THEORIES OF SOIL-CELL INTERACTION

27. This part of the report is divided into two sections, (a) a fairly detailed presentation of the principal problems encountered and a simplified analysis of the individual problems, and (b) a review of both simplified and more rigorous theories for soil-cell interaction. The results yielded by the more rigorous methods can often be obtained by the simplified analysis after changing the numerical values of one or more coefficients, but recent investigations indicate that some of the assumptions forming the basis for a simplified analysis may be untenable for several stress and boundary conditions. Nevertheless, the simplified analysis is presented first in this report because it illustrates the influence of special conditions, and it facilitates visualization of the influence of independent variables, whereas currently available solutions of more rigorous theories primarily cover basic stress and boundary conditions. Questionable assumptions in the simplified analysis will be emphasized and explained, when possible.

Principal Problems and Simplified Analysis

Development and assumptions

28. General objectives and procedures. The general purpose of investigations of soil-cell interaction is to obtain data for estimating over- or under-registration of a pressure cell and for evaluation of stress determinations in earth structures by means of soil pressure cells. The most commonly used method for investigating soil-cell interaction may be called the indentation analogy, which consists in estimating the difference between soil and cell deformations or the indentation and then computing the corresponding over- or under-registrations of the cell which produces the same indentation. Carlson (1939) and other investigators proposed the fundamentals of such a procedure, which will be discussed further in paragraphs 68-94. Simplified theories based on the indentation analogy have been proposed, independently of each other, by Hast (1945), Coutinho (1949) and Taylor (1945,47). The

Taylor theory in a slightly modified form is presented in the following paragraphs, and it has been extended to cover both uniaxial and triaxial stresses changes. The stresses considered are those between the soil grains or effective stresses; changes in pore water pressures are treated separately. Initially it is assumed that the cell is placed in a free stress field, and cells placed on or in rigid boundaries of a soil body are discussed in later paragraphs.

29. Usual assumptions. The following assumptions are made in most but not all proposed theories for soil-cell interaction:

- a. The pressure cell acts as a thin disk or cylindrical inclusion with uniform axial compressibility but rigid in radial directions.
- b. The influence of the radial rigidity of the cell on the surrounding soil has only a negligible influence on axial soil stresses.
- c. The influence of shear stresses on the faces of the cell and of all stresses on the cylindrical surface of the cell are negligible.
- d. A change in lateral soil stresses causes axial soil deformations corresponding to the Poisson ratio, but it does not directly influence axial soil stresses on the cell.
- e. The simplified analysis or indentation analogy considers only soil deformations in a layer with a thickness equal to that of the cell, and the force corresponding to the indentation is computed by means of the Boussinesq-Prandtl equations for the sinkage of a rigid platte at the free soil surface.

Assumption "a" is acceptable for pressure cells with fully active face plates, such as the Carlson and WES cells, but it is not correct for cells with an inactive rim and an exposed measuring diaphragm. It is best to use the finite element method of analysis for the latter type of pressure cell. Assumption "b" appears to be acceptable except in analysis of cells placed under confining conditions. Limited tests indicate that assumption "c" is acceptable, but additional investigations are desirable. Early investigations indicated that assumption "d" could be made acceptable by introduction of a minor correction factor, but more recent investigations by Askegaard and Bates show that lateral stresses may cause appreciable changes in the axial soil stresses on a cell.

Assumption "e" provides appreciable simplifications in equations for the soil-cell interaction, but these equations may in some cases yield too small values of the error in cell registrations, because the assumptions cause neglect of significant secondary soil stresses and deformations, and also because relations between stresses and deformations in the interior of a soil mass are represented by the Mindlin equations, whereas the Boussinesq equations apply to the effect of loads on the free surface of the soil. The errors caused by the above mentioned assumptions depend to a large extent on values of the Poisson ratio for the soil and on the thickness-diameter ratio of the pressure cell.

30. Definitions. The simplified analysis is actually developed for relatively small stress changes, which are designated by σ rather than by $\Delta\sigma$ because the latter is used for incremental stress changes or parts of a total stress change. The influence of a change in pore water pressure, u , is discussed in a separate paragraph, and the effective soil stress changes are then designated by $\sigma' = \sigma - u$. It will be shown that the influence of u can be taken into account by a change in the effective modulus of cell deformation, M_c . Therefore, in all other cases it is assumed that there is no change in pore water pressure or $\sigma = \sigma'$, and the prime mark indicating effective stresses is omitted in the equations for the sake of convenience in writing and reading.

Pressure cells in a free field

31. Uniaxial stress changes. The first or basic theories for soil-cell interaction were developed for the simple condition that the only stress change is in an axial direction perpendicular to the faces of the cell. Such simple stress changes can be obtained with cells embedded in a large triaxial test specimen, but the corresponding theories could theoretically also be applied to tests and field conditions in which the ratio between axial and radial stresses is constant for the stress interval under consideration provided the soil deformation modulus is determined for similar stress changes, usually by a confined compression test. The basic simplified theory for action of soil pressure cells presented in the following paragraphs is essentially that proposed by D. W. Taylor in 1945.

32. Figure 13 shows a pressure cell embedded at the depth H below the soil surface or the top of a triaxial test specimen at which depth there is no significant influence of these boundaries. With no change in the pore pressure, u , the total and effective changes in the vertical soil stress are equal and designated by σ_s , and the corresponding stress change indicated by the cell is σ_c . The overstress or understress of the cell is then

$$\sigma_e = \sigma_c - \sigma_s \quad (1)$$

and the deformation of a cell with thickness $2B$ is

$$2\delta_c = 2B \frac{\sigma_c}{M_c} \quad (2)$$

where M_c is the deformation modulus of the cell in axial direction. When the deformation modulus of the soil in the same direction is M_s , the deformation of a soil layer with thickness $2B$ and radially beyond the disturbance caused by the cell is

$$2\delta_s = 2B \frac{\sigma_s}{M_s} \quad (3)$$

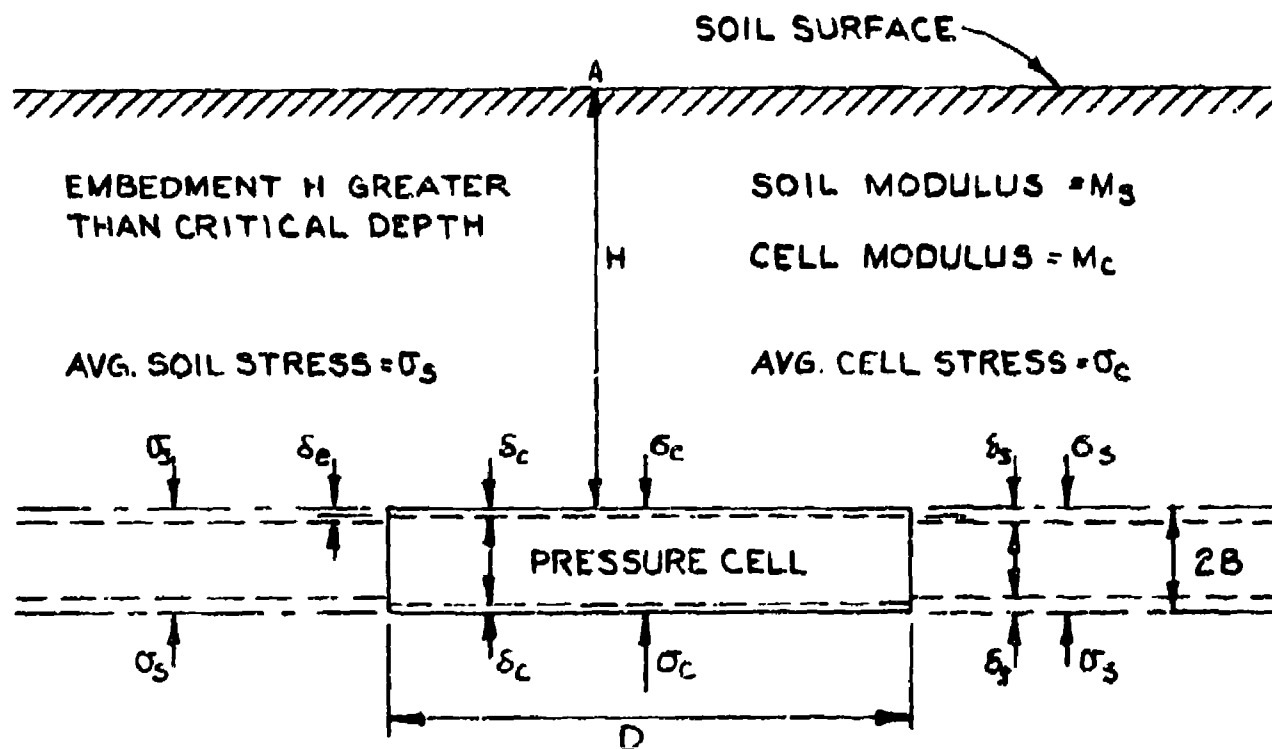
The difference between these deformations

$$2\delta_e = 2\delta_s - 2\delta_c$$

is the indentation or retraction of the cell surfaces with respect to the original planes of contact between cell and soil. Assuming symmetry of deformations of cell and soil, each side of the cell indents or retracts from the soil for the distance δ_e , or

$$\delta_e = \delta_s - \delta_c \quad (4)$$

Introducing the expressions for δ_s and δ_c in Equations 2 and 3 yield



CELL OVER OR UNDERSTRESS $\sigma_e = \sigma_c - \sigma_s$

CELL DEFORMATION $2\delta_c = 2B \cdot \sigma_c / M_c$

SOIL DEFORMATION FOR $2B$ $2\delta_s = 2B \cdot \sigma_s / M_s$

CELL INDENTATION (EACH SIDE) $\delta_e = \delta_s - \delta_c$

WITH INDENTATION COEFF. " N_s " AND $\delta_e = D \cdot \sigma_e / N_s$

$$\frac{\sigma_c}{\sigma_s} = \frac{\frac{D}{B} + \frac{N_s}{M_s}}{\frac{D}{B} + \frac{N_s}{M_c}} = \frac{\frac{D}{B} + K_s}{\frac{D}{B} + K_s \frac{M_s}{M_c}} ; \text{ WHERE } K_s = \frac{N_s}{M_s}$$

$$\frac{\sigma_e}{\sigma_s} = \frac{\sigma_c}{\sigma_s} - 1 = \text{ERROR RATIO}$$

NOTE: FORMULAS DO NOT INCLUDE THE INFLUENCE OF LATERAL SOIL STRESSES

FIGURE 13. SIMPLIFIED STRESS RELATIONS FOR CELL IN A FREE FIELD.

$$\delta_e = D \left(\frac{\sigma_B}{M_B} - \frac{\sigma_C}{M_C} \right) \quad (5)$$

Taylor (1945) and others now assume that δ_e is similar to the indentation of a circular plate or punch into an elastic solid under the load $\sigma_e = \sigma_C - \sigma_B$ and that this also will apply to a saturated clay and to confined sand provided the stress change, σ_B , does not approach the confining stress in the cohesionless soil or causes stress changes approaching those of failure. The indentation δ_e may then be expressed by

$$\delta_e = D \frac{\sigma_e}{N_B} \quad (6)$$

where D is the diameter of the plate or cell and N_B is an indentation coefficient which is a function of the deformation characteristics of the soil. Values of N_B are discussed in subsequent paragraphs. Combining Equations 1, 5, and 6 yields

$$\frac{\sigma_C - \sigma_B}{N_B} D = B \left(\frac{\sigma_B}{M_B} - \frac{\sigma_C}{M_C} \right)$$

and

$$\sigma_C \left(\frac{D}{N_B} + \frac{B}{M_C} \right) = \sigma_B \left(\frac{D}{N_B} + \frac{B}{M_B} \right)$$

The registration ratio is then

$$\frac{\sigma_C}{\sigma_B} = \frac{\frac{D}{N_B} + \frac{B}{M_B}}{\frac{D}{N_B} + \frac{B}{M_C}} = \frac{\frac{D}{B} + \frac{K_B}{M_B}}{\frac{D}{B} + \frac{K_B}{M_C}} \quad (7)$$

where $K_B = N_B/M_B$ may be called the soil indentation ratio. Equation 7 is basically that proposed by Taylor (1945), and equations derived

independently by Hast (1945) and Coutinho (1949) can be reduced to the same form. As indicated by Equation 7, the registration ratio increases with increasing stiffness of the cell, M_c , and approaches a limiting maximum value obtained for $M_s/M_c = 0$, or

$$\frac{\sigma_c}{\sigma_s} (\text{lim}) = \frac{\frac{D}{B} + K_s}{\frac{D}{B}} = 1 + K_s \frac{B}{D} \quad (8)$$

that is, the limiting value of the registration ratio increases linearly with increasing thickness-diameter ratio.

33. Values of the indentation parameters. Theoretical values of N_s and K_s may be expressed by the theories of Boussinesq, assuming that the soil acts as an elastic solid. For an infinitely rigid circular plate or punch at the soil surface, the theoretical value of the indentation δ_e for the unit load σ_e is also given by Timoshenko-Goodier (1951; p. 372)

$$\delta_e = \sigma_e \frac{\pi}{4} D^2 \frac{(1 - \nu^2)}{DM_s} = \sigma_e \frac{\pi}{4} D \frac{1 - \nu^2}{M_s} \quad (9)$$

where ν is the Poisson ratio of the soil. The coefficient N_s in Equation 6 may then be expressed by

$$N_s = \frac{4}{\pi} \frac{M_s}{1 - \nu^2} \quad (10)$$

and the indentation ratio

$$K_s = \frac{N_s}{M_s} = \frac{4}{\pi} \frac{1}{1 - \nu^2} \quad (11)$$

With $\nu = 1/3$, Equation 11 yields

$$K_s = \frac{49}{\pi 8} = 1.43$$

Reproduced From
Best Available Copy

which may apply to a pressure cell with heavy face plates. For pressure cells with face plates which are thin enough to act as measuring diaphragms, it will be of interest to compare the average deflection of flexible face plates with the same diameter and total load but various types of stress distribution. The following general relations apply

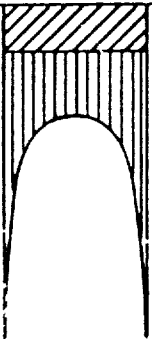
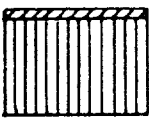
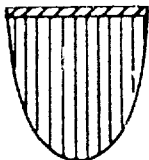
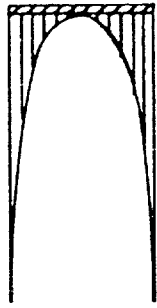
$$\delta_{e,av} = \sigma_e D \frac{1 - \nu^2}{M_s} C = \frac{\sigma_e}{N_s} D \quad (12)$$

$$N_s = \frac{\sigma_e D}{\delta_{e,av}} = \frac{M_s}{(1 - \nu^2)C} \quad (13)$$

$$K_s = \frac{N_s}{M_s} = \frac{1}{(1 - \nu^2)C} \quad (14)$$

The values of the coefficients C and K_s for rigid flexible plates at the free surface of a soil body with various load distributions are summarized in Figure 14. The data are based on equations by Boussinesq and the details were obtained from Hast (1945) and Timoshenko-Goodier (1951). As shown in this figure and first noted by Hast (1945), the distribution of the reaction stress for a given total load has relatively little influence on the average deflection of the plate. However, the values of these parameters decrease to unity as the depth of burial decreases and the pressure cell approaches the free soil surface, Figure 29.

34. The Poisson ratio, ν , for soils varies greatly with the soil type, the relative density, state of consolidation, and the stress conditions during shear tests and triaxial tests. Dense cohesionless soils and strongly overconsolidation cohesive soils undergo a volume increase instead of a decrease during shear and triaxial tests, corresponding to values of ν greater than 0.5. As mentioned, most of the early investigators determined the modulus of deformations of soils, M_s , for confined conditions, and it would seem appropriate to consider the corresponding values of the Poisson ratio in the simplified analysis.

PLATE	RIGID		FLEXIBLE	
LOAD DISTRIBUTION	ANY	UNIFORM	PARABOLIC MAX. CENTER	PARABOLIC ZERO CENTER
CASE NO.	1	2	3	4
SOIL LOAD OR REACTION DISTRIBUTION				
COEFF. e IN. EQ. 12-14	0.785	0.849	0.903	0.793
$k_s = \frac{N_s}{M_s} = \frac{1}{(1-\nu^2) \cdot C}$ EQ. 14 AND $\nu = 1/3$	1.43	1.33	1.24	1.42
NOTE: PLATE AT FREE SOIL SURFACE				

EQ. 12: $\delta_a = \sigma_e \cdot D \cdot \frac{1-\nu^2}{M_s} \cdot C$ OR $\delta_a = D \frac{\sigma_e}{N_s}$; $k_s = \frac{N_s}{M_s}$

BASED ON DATA BY TIMOSHENKO, 1932 AND NILS HAST, 1943.

A. EFFECT OF LOAD DISTRIBUTION

							OUTSIDE USUAL THEORY			
ν	0	0.1	0.2	0.3	0.4	0.5	0.6	0.7	0.8	0.9
ν^2	0	0.01	0.04	0.09	0.16	0.25	0.36	0.49	0.64	0.81
$1-\nu^2$	1.00	0.99	0.96	0.91	0.84	0.75	0.64	0.51	0.36	0.19
k_s	1.27	1.29	1.33	1.40	1.52	1.70	2.00	2.51	3.55	6.73

RIGID PUNCH = $C = \frac{\pi}{4} = 0.786$ $k_s = \frac{1}{(1-\nu^2) \cdot C} = \frac{1.27}{1-\nu^2}$

B. EFFECT OF POISSON'S RATIO

THESE VALUES OF k_s AND EQUATIONS IN FIGURE 13 APPLY ONLY TO A RIGID PLATE AT THE FREE SURFACE OF A SEMI-INFINITE SOIL DEPOSIT.

FIGURE 14. INFLUENCE OF SOME FACTORS ON THE INDENTATION RATIO k_s .

For confined compression, $\sigma_x = \sigma_y = \sigma_3$ is the confining pressure and $\sigma_z = \sigma_1$ is the axial pressure. The relation between the coefficient of earth pressure at rest, K_0 , and the Poisson ratio is

$$K_0 = \frac{\sigma_3}{\sigma_1} = \frac{\nu}{1 - \nu} \quad (15-A)$$

But the value of K_0 for granular materials can also be obtained by the Jaky equation

$$K_0 = 1 - \sin \phi \quad (15-B)$$

The two equations yield the following relation between the angle of internal friction, ϕ , and the Poisson ratio

$$1 - \sin \phi = \frac{\nu}{1 - \nu}$$

and numerical values shown in the tabular form

ϕ	20°	25°	30°	35°	40°	45°	50°
$\sin \phi$	0.342	0.423	0.500	0.574	0.643	0.707	0.766
K_0	0.658	0.577	0.500	0.426	0.357	0.293	0.240
ν	0.400	0.365	0.333	0.295	0.262	0.226	0.194

Many of the computations and figures were completed 15 years ago, and the value $\nu = 1/3$ was used for convenience but only for illustrative purposes.

35. Taylor (1945) suggests that the probable value of N_s is close to that of M_s , corresponding to $K_s = 1.0$. Such values of N_s and K_s are also used by Peattie and Sparrow (1954). However, these investigators treat tests in a solid-walled cylindrical test bin as a case of uniaxial compression but they also suggest that the modulus of deformation of the soil, M_s , be determined for the same stress conditions or by means of a confined compression test, i.e. a consolidation test. In such a test the lateral stresses are

$$\sigma_x = \sigma_y = \sigma_z \frac{\nu}{1 - \nu} \quad (15-C)$$

where $\sigma_z = \sigma_s$ is the axial soil stress acting on the faces of the pressure cell. The axial soil deformation is then

$$\delta_s = \delta_z = \frac{\sigma_z - \nu(\sigma_x + \sigma_y)}{M_s}$$

or by use of Equation 15-C

$$\sigma_s = \delta_z = \frac{\sigma_z}{M_s} \left(1 - \frac{2\nu^2}{1 - \nu} \right) \quad (16)$$

and for $\nu = 1/3$

$$\delta_s = \frac{\sigma_z}{M_s} \frac{2}{3} = \frac{\sigma_z}{1.5M_s} \quad (17)$$

or an equivalent value of M_s equal to 1.5 times that which would be obtained in an unconfined or uniaxial compression test. This corresponds to a value of K_s close to 1.5 which agrees with that shown in Figure 14 for cases 1 and 4. Much greater values of N_s and K_s were obtained in some experiments as described in the following paragraph and in Part III of this report. It is again emphasized that the theoretical equations and values of the indentation parameters, mentioned in the foregoing paragraphs, represent only rough approximations of the actual stresses and deformations.

36. Theoretical values of σ_c/σ_s versus M_c/M_s , Equation 7, are shown in Figure 15 for various values of K_s . The lower value, $K_s = 1.33$, corresponds to a uniform stress distribution on the cell as shown in Case 2 of Figure 14. The higher value $K_s = 3$, was obtained from the average indications of WFS pressure cells embedded in triaxial test specimens of fairly dense sand subjected to uniaxial cyclic loading.

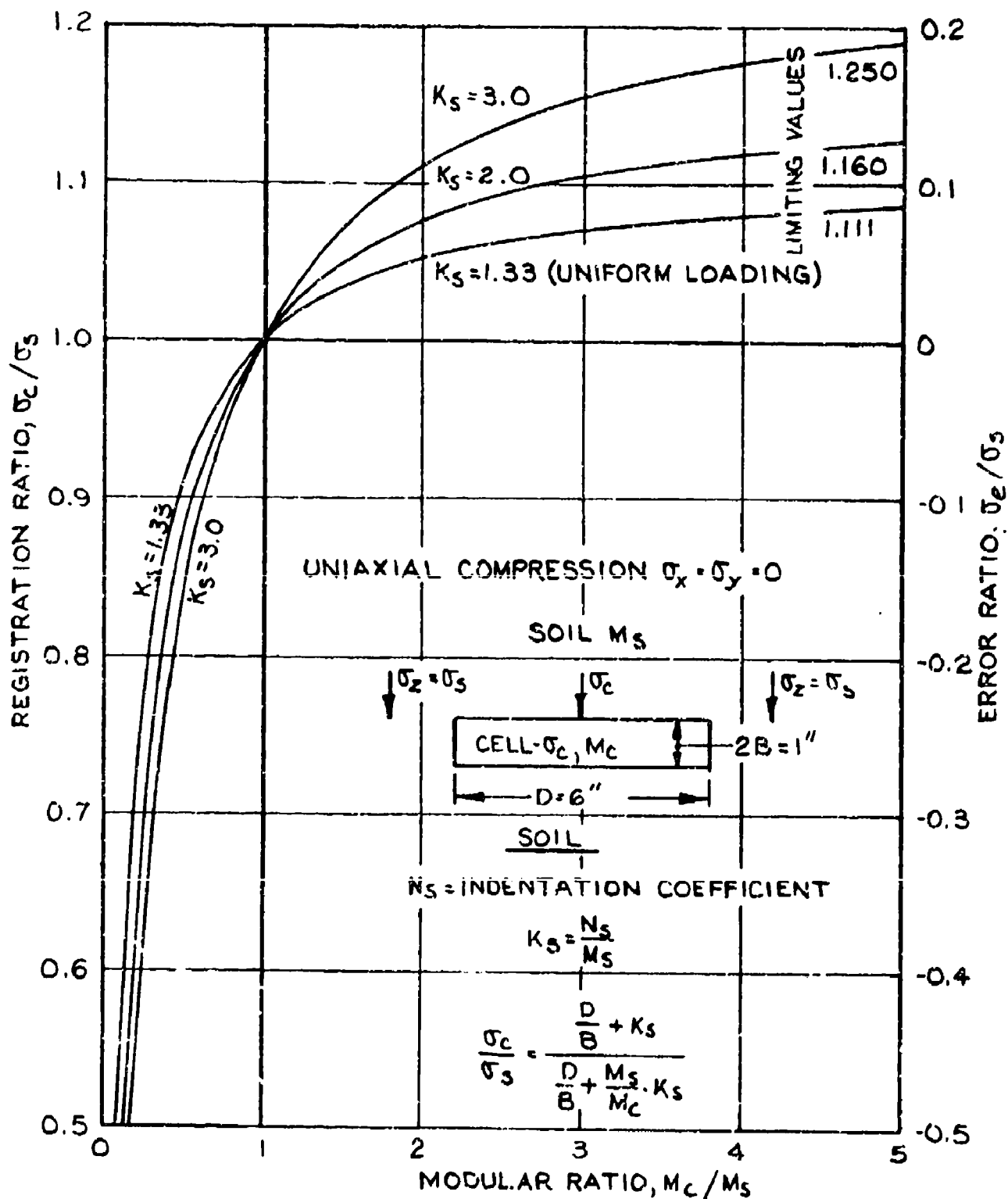


FIGURE 15. REGISTRATION RATIOS OF SOIL PRESSURE CELLS IN A FREE FIELD.

Still higher values of K_s were found when the stress conditions in the sand approach those of failure. The registration ratio σ_c/σ_s approaches the limiting values, given by Equation 8, with increasing modular ratios, M_c/M_s , whereas σ_c/σ_s decreases to zero with decreasing modular ratios, or increasing M_s/M_c . The shape of the diagrams in Figure 15 agrees in form with experimental data corresponding to confined compression, but K_s is larger for dense sand. Unconfined compression or uniaxial loading combined with a curved stress strain diagram produces great variations in M_s and K_s as the unit load increases.

37. Error ratio. Referring to Equation 1, the relative error or error ratio, σ_e/σ_s in the pressure cell indication is determined by

$$\frac{\sigma_e}{\sigma_s} = \frac{\sigma_c}{\sigma_s} - 1 \quad (18)$$

A graphical diagram of σ_e/σ_s versus M_c/M_s can be obtained from Figure 15 simply by changing the ordinate scale as shown on the right-hand side of this figure. An analytical expression for the error ratio can be derived from Equations 7 and 18 which yield

$$\frac{\sigma_e}{\sigma_s} = K_s \frac{B}{D} \frac{1 - \frac{M_s}{M_c}}{1 + K_s \frac{B}{D} \frac{M_s}{M_c}} \quad (19)$$

The limiting positive values of σ_e/σ_s is obtained for $(M_s/M_c) = 0$

$$\frac{\sigma_c}{\sigma_s} (\text{lim}) = K_s \frac{B}{D} \quad (20)$$

which shows that the limiting values are proportional to B/D . This proportionality applies also to finite values provided M_s/M_c and B/D are small, as shown by Peattie and Sparrow (1954).

38. Triaxial stress changes. As shown in the foregoing

paragraphs, some problems involving triaxial stress changes may be solved by the equations for uniaxial stress changes perpendicular to the pressure cell, provided the soil modulus of deformation is determined for the same direction and triaxial stress changes. However, equations which consider arbitrary stress changes in the three principal directions, the influence of the Poisson effect, and the usual modulus of deformation should provide solutions of much wider applications. Assuming as before that there is no change in the pore water pressure and that the total and effective stress changes are σ_x , σ_y , and σ_z , Equations 1, 2, and 4 still apply, and deformation of the cell is represented by

$$2\delta_c = 2B \frac{\sigma_c}{M_c} \quad (2 \text{ bis})$$

but the deformation of a soil layer with thickness $2B$ is now

$$2\delta_s = 2E \frac{\sigma_z - \nu(\sigma_x + \sigma_y)}{M_s} \quad (21)$$

With $\sigma_e = \sigma_c - \sigma_s$, the indentation of the cell into the soil is defined as before by

$$\delta_e = \sigma_s - \delta_c = \frac{\sigma_e}{N_s} D$$

which combined with Equation 21 yields

$$\frac{\sigma_e}{N_s} = \frac{B}{D} \left(\frac{\sigma_z}{M_s} - \nu \frac{\sigma_x + \sigma_y}{M_s} - \frac{\sigma_c}{M_c} \right) \quad (22)$$

and with $\sigma_e = \sigma_c - \sigma_s$, $K_s = N_s/M_s$, and $\sigma_s = \sigma_z$

$$\frac{\sigma_c}{\sigma_s} = \frac{\sigma_c}{\sigma_z} = \frac{\frac{D}{B} + K_s \left(1 - \nu \frac{\sigma_x + \sigma_y}{\sigma_z} \right)}{\frac{D}{B} + K_s \frac{M_s}{M_c}} \quad (23)$$

The limiting value of σ_c/σ_s for large values of M_c or M_s/M_c approaching zero are similar to those given by Equation 8 or

$$\frac{\sigma_c}{\sigma_s} (\text{lim}) = 1 + K_s \frac{B}{D} \left(1 - \nu \frac{\sigma_x + \sigma_y}{\sigma_z} \right) \quad (24)$$

Equation 23 applies to measurement of vertical stresses, σ_z , in the usual coordinate system. For measurement of a lateral stress, for example σ_x , interchange σ_z and σ_x , and with $\sigma_s = \sigma_x$ Equation 23 becomes

$$\frac{\sigma_c}{\sigma_s} = \frac{\sigma_c}{\sigma_x} = \frac{\frac{D}{B} + K_s \left(1 - \nu \frac{\sigma_y + \sigma_z}{\sigma_x} \right)}{\frac{D}{B} + K_s \frac{M_s}{M_c}} \quad (25)$$

When σ_z is greater than σ_x and σ_y , Equation 25 will usually yield values of σ_c/σ_x which are smaller than 1.0; see Figure 16. Furthermore, the friction between the soil and the end surfaces of the cell may be greater than between soil and cylindrical surface for a horizontal cell, corresponding to Equation 23 and Figure 17.

39. Examples of applications. In case of earth pressure at rest or confined virgin consolidation, the theoretical relation between the Poisson ratio and the principal stress ratio is

$$\frac{\sigma_3}{\sigma_1} = \frac{\sigma_x}{\sigma_z} = \frac{\nu}{1 - \nu} \quad (26)$$

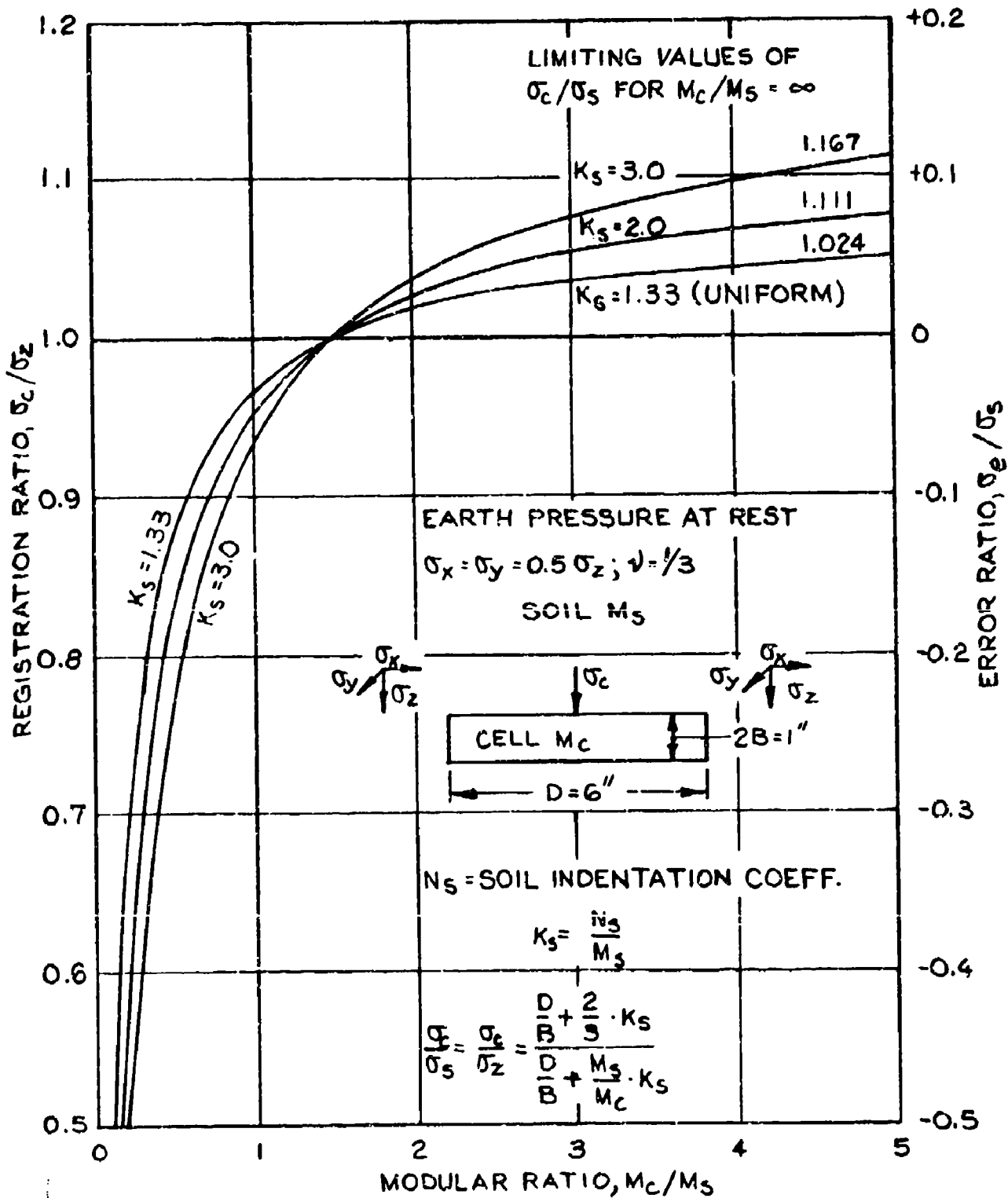


FIGURE 16. REGISTRATION RATIOS FOR VERTICAL STRESSES, EARTH PRESSURES AT REST.

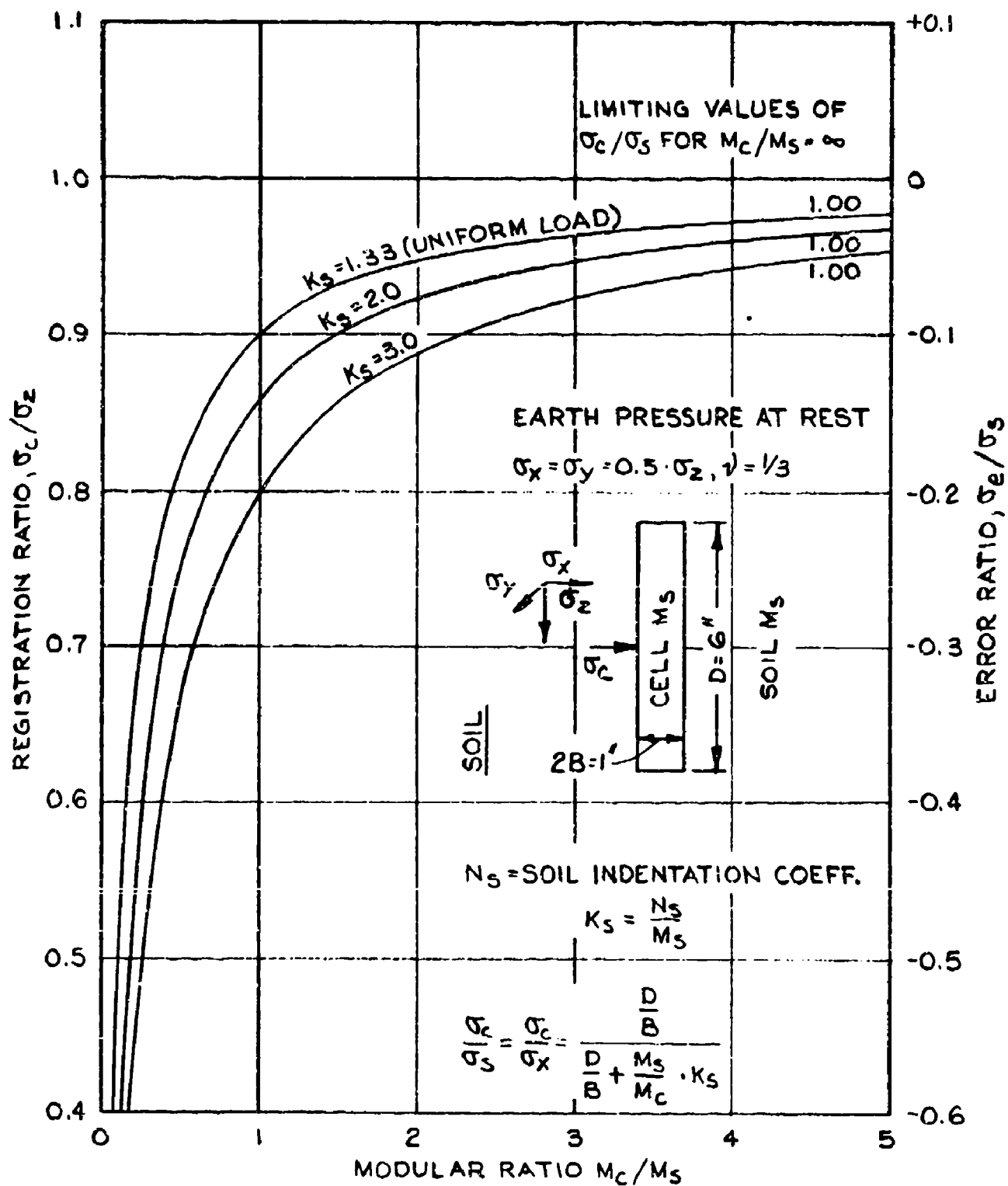


FIGURE 17: REGISTRATION RATIOS FOR HORIZONTAL STRESSES, EARTH PRESSURE AT REST

or for $\nu = 1/3$, $\sigma_x = \sigma_y = 0.5\sigma_z$. Equations 23 and 25 then become

$$\frac{\sigma_c}{\sigma_z} = \frac{\frac{D}{B} + \frac{2}{3} K_s}{\frac{D}{B} + K_s \frac{M_s}{M_c}} \quad (27)$$

and for Equation 25

$$\frac{\sigma_c}{\sigma_x} = \frac{\sigma_c}{\sigma_y} = \frac{\frac{D}{B}}{\frac{D}{B} + K_s \frac{M_s}{M_c}} \quad (28)$$

A graphical representation of Equation 27 is shown in Figure 17 for various values of K_s . It is noted that $\sigma_c/\sigma_z = 1.0$ for $M_c/M_s = 1.0$ and for any value of K_s and $M_c/M_s = 1.5$. This is in agreement with a previous statement that the apparent modulus of axial deformation for confined compression is 1.5 times that for unconfined compression when $\nu = 1/3$. Diagrams for σ_c/σ_x in Equation 28 are shown in Figure 16. In this case the cell stresses, σ_c , are smaller than σ_x and σ_y but they approach each other for large values of the modular ratio M_c/M_s .

40. For the rare case of uniform pressure change, $\sigma_x = \sigma_y = \sigma_z$, Equations 23 and 25 become

$$\frac{\sigma_c}{\sigma_x} = \frac{\sigma_c}{\sigma_y} = \frac{\sigma_c}{\sigma_z} = \frac{\sigma_c}{\sigma_s} = \frac{\frac{D}{B} + K_s(1 - 2\nu)}{\frac{D}{B} + K_s \frac{M_s}{M_c}} \quad (29)$$

and with $\nu = 1/3$

$$\frac{\sigma_c}{\sigma_s} = \frac{\frac{D}{B} + \frac{2}{3} K_s}{\frac{D}{B} + K_s \frac{M_s}{M_c}} \quad (30)$$

41. Comparisons. The foregoing examples of the action of

pressure cells in case of triaxial stress changes in the soil show that the simplified theory yields registration ratios, σ_c/σ_s , for vertical or normal stresses which decrease with increasing values of the Poisson ratio and the lateral stress changes. In contrast thereto, the more rigorous investigations by Askegaard (1963) indicate that the influence of the Poisson ratio is smallest for $\nu = 0.3$ and increases for lower and higher values of ν , Figure 32A. The simplified theory usually yields underregistration of cells placed to measure minor horizontal stresses, Figure 17. Triaxial tests at the WES show only small under- or over-registrations in the measurement of radial and tangential stresses. Additional data or investigations are needed, and the influence of lateral stresses on the registration of stresses normal to the cell should not be confined to the Poisson effect of lateral deformations, as assumed in the simplified theory.

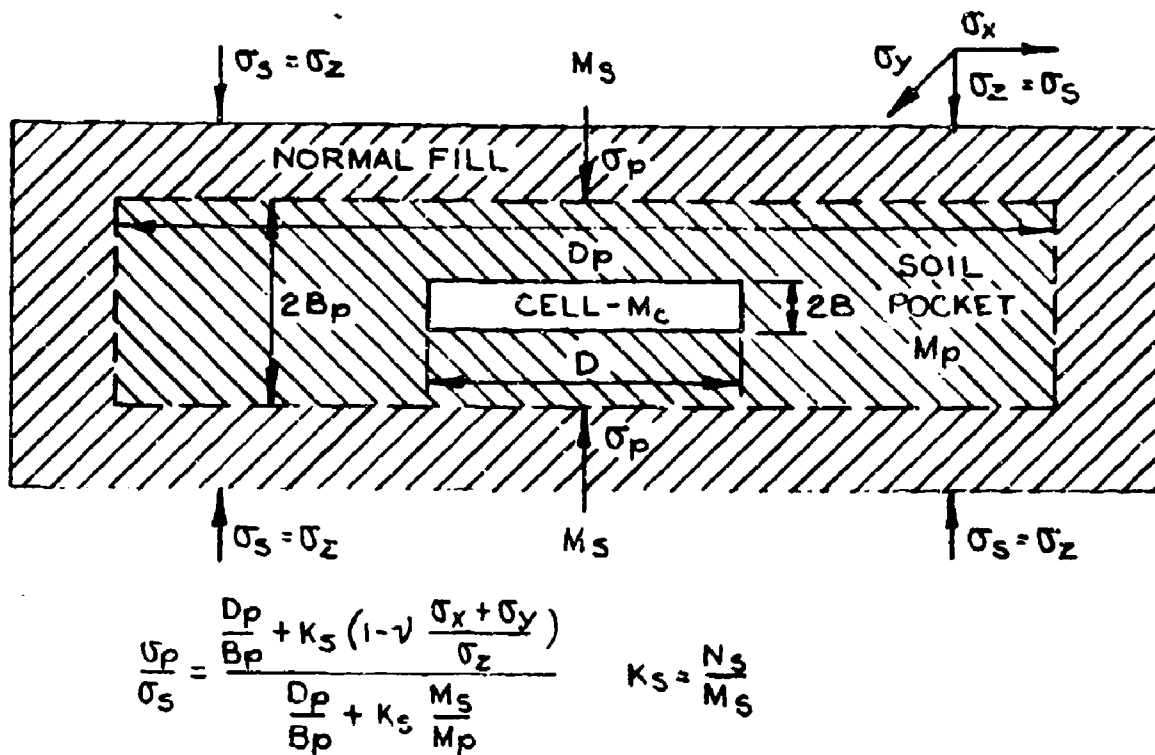
Installation problems

42. Seating load. Great errors in pressure cell indications may be caused by improper installation of a cell. Recent and very interesting research on the installation of small pressure cells of the type shown in Figure 9 has been performed and reported by Hadal (1967). Additional research and a manual on installation of soil pressure cells in general are needed. It is practically impossible to install a pressure cell in virgin soil without disturbing the soil and the stress conditions, first by excavating a hole, secondly by placing the cell and backfilling the hole without attaining the original soil properties and stress conditions. The difficulties are reduced but not eliminated when the pressure cell is installed during construction in a fill or at the contact between backfill and another structure or virgin soil. Coarse or stony soils cause additional problems which will be mentioned later, but even in sand and finer graded soil it may be difficult to obtain good contact between cell and soil and to avoid differences in physical properties of the soil close to the cell and those of the main body of soil. Overcompaction causes an increase in cell registration, called pocket action or cover action by Taylor (1945), whereas undercompaction or too compressible soil has the opposite effect. Observations during

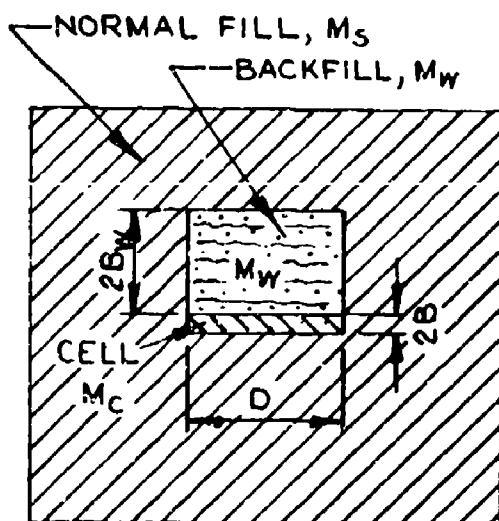
the 1954-55 test series indicate that irregularities in soil deformations and cell indications in the first loading cycle are decreased in subsequent loading cycles. It appears that a certain seating pressure on cell and soil cover is needed to obtain satisfactory contact and stress conditions between cell and soil. Residual strain and stresses are created by such a seating load and should be taken into consideration by a new zero setting of the cell. It is possible that the residual strain and stresses may be increased too much by repetitive loading in tests on soil in a solid walled container, because of the influence of sidewall friction. Experimental data on the optimum magnitude of such a seating load are not yet available. At this time it can only be suggested that a moderate seating load be applied during installation of the cell, and that a larger seating load, about equal to the anticipated maximum load, be applied when the cell is covered by enough soil to protect it from damage by passage of construction equipment. Proper placement and pre-loading of cells placed on edge for measuring lateral or inclined stresses is particularly difficult. Additional systematic investigations of these problems are needed. Comments in the following paragraphs may be of assistance in the planning of such tests.

43. Soil pocket formation. A body of soil around a pressure cell, of limited extent and with properties different from those of the main soil mass, may be considered as an inclusion, and the average stresses in such a soil pocket may be computed by methods similar to those for pressure cells in a uniform soil mass. As a first approximation, it may be assumed that the soil pocket forms a cylindrical disk with the diameter D_p and the thickness $2B_p$ as shown in Figure 18A. With the average modulus of deformation M_p , the average load on the soil pocket may be computed by inserting D_p , B_p , and M_p in Equation 23 instead of D , B , and M_c , which yields

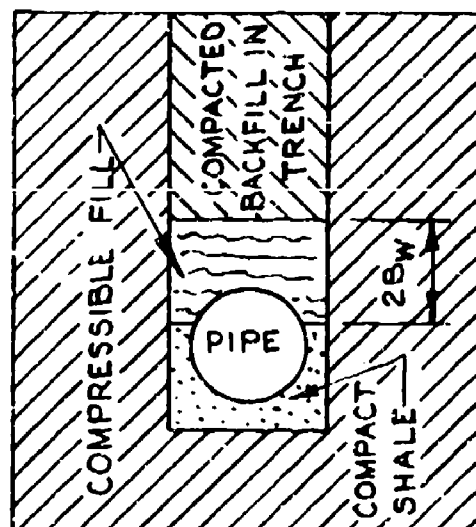
$$\frac{\sigma_p}{\sigma_s} = \frac{\frac{D_p}{B_p} + K_s \left(1 - \nu \frac{\sigma_x + \sigma_y}{\sigma_z} \right)}{\frac{D_p}{B_p} + K_s \frac{M_s}{M_p}} \quad (31)$$



A. SOIL POCKET AROUND PRESSURE CELL



B. COMPRESSIBLE COVER OF PRESSURE CELL



C. COMPRESSIBLE COVER FOR BURIED PIPE

FIGURE 18. INSTALLATION PROBLEMS

The ratio σ_p/σ_s increases with increasing stiffness of the soil in the pocket or with decreasing values of M_s/M_p , but there is a limiting value of σ_p/σ_s corresponding to $M_s/M_p = 0$, or

$$\frac{\sigma_p}{\sigma_s} (\text{lim}) = 1 + \frac{B_p}{D_p} K_s \left(1 - \nu \frac{\sigma_x + \sigma_y}{\sigma_z} \right) \quad (32)$$

which is equivalent to Equation 24. It should be noted that M_s , N_s , and $K_s = N_s/M_s$ refer to the main soil mass which has not been changed by the pocket formation. As shown in Figure 14, N_s and K_s are fairly independent of the pressure distribution. If the pocket actually has the shape of a cylindrical disk, there should be a stress concentration at the edges and the stress in the center would then be smaller than the average stress, σ_p , which would decrease the influence of a soil pocket on the load acting on the pressure cell. The soil pocket may be lenticular in shape which would decrease stress variations. However, the load on the cell would be increased when the modulus of the cell is greater than that of the soil in the pocket, or $M_c > M_p > M_s$, provided the distance from the cell to the surface of the soil pocket is great enough to eliminate boundary effects, see Figure 29. The load on the pressure cell can now be determined by substituting σ_p for σ_s in the equations for interaction of cell and soil. As indicated by Equations 31 and 32, the overstress in a pocket of dense soil can be decreased to tolerable amounts by decreasing the thickness-diameter ratio of the soil pocket. On the other hand, a large overstress may occur and misleading data may be obtained when the thickness-diameter ratio of the soil pocket is large. A pocket of loose soil, $M_p < M_s$, causes understress and its relative influence on the cell registration is not as easily controlled as is that caused by overstress in a pocket of dense soil.

44. Compressible soil cover. A soil pressure cell may be placed in a carefully excavated hole in the undisturbed soil or in compacted fill, Figure 18B, but the backfill or soil covering the cell is often more compressible than the surrounding soil. Taylor (1945) terms this

condition a soil cover in contrast to a soil pocket. The action of such a soil cover is similar to that of a compressible backfill of limited thickness often used to reduce the effective load on a buried pipe, Figure 18C. The compressible cover may cause the overlying denser soil to arch over the buried cell or pipe. When complete arching does not occur, the effect of a compressible cover with thickness $2B_w$ and modulus M_w may be estimated by use of Equations 23 or 31, but the full thickness, $2B_w$, should be used instead of half the thickness, B_w , because the soil cover is bounded by the more rigid cell, similar to a pressure cell in contact with a rigid slab or wall. The equation for the approximate reduced pressure, σ_w , to be used instead of the average soil pressure σ_s , may then be written

$$\frac{\sigma_w}{\sigma_s} = \frac{\frac{D}{2B_w} + K_s \left(1 - \nu \frac{\sigma_x + \sigma_y}{\sigma_z} \right)}{\frac{D}{2B_w} + K_s \frac{M_s}{M_w}} \quad (33)$$

In case the thickness of the compressible cover is small, it may be expedient to investigate the combined effect of cover and pressure cell by use of Equation 23 for the combined thickness $2(B + B_w)$ and using an equivalent modulus, M_e , determined by

$$\frac{1}{M_e} (B + B_w) = \frac{1}{M_c} B + \frac{1}{M_w} B_w \quad (34)$$

This equation can also be used when M_w is greater than M_s and a relation similar to Equation 33 can also be derived for this condition. All the equations are subject to the limitations of the simplified cell-soil theory and can only yield roughly approximate results. However, the disturbing effect of a compressible soil cover of a cell in a hole may be much greater and more difficult to estimate than that of a soil pocket. Installation of pressure cells in soil pockets of adequate size is preferable to installation in close fitting holes.

45. Coarse and stony soils. Barring special precautions, installation of a pressure cell in stony soil may cause stress concentrations and some changes in the registration of Carlson, WES, Glötzl, and similar cells but much greater changes in registration and possible damage may occur in the case of cells with exposed measuring diaphragm. The size of pressure cells to be used in direct contact with stony soils is generally increased, but opinions concerning the required minimum size vary greatly, and a systematic experimental investigation of this problem has not yet been made. It has been suggested that the diameter of a pressure cell should be about 5 to 6 times the diameter of the largest soil particles and that the diameter should not be less than 6 to 12 in. for cells used in sand, whereas smaller cells may be used in finer grained soils. It would seem that consideration also should be given to the type of cell used; i.e. cells with a fully active face and an interior load equalizing liquid versus cells with an inactive rim and an exposed diaphragm. Referring to cells in sand without stones, it may be claimed that a cell size which has yielded satisfactory results in model and laboratory tests also should be adequate for field use in the same type of soil. Small pressure cells may possibly be used in stony soils provided they are placed in adequately proportioned pockets of finer grained soils, and that the relation of the moduli of the soils in the pocket and the main deposit be determined. In some cases it may even be sufficient to remove stones from the vicinity of the pressure cell or to pass the field soil through a sieve and use the material passing the sieve in a soil pocket for the pressure cell, but the change in the modulus of deformation of the scalped soil should also be investigated.

Influence of changes in
pressure of the pore fluids

46. Function of pore fluid. In deriving the foregoing equations it was tacitly assumed that the soil is dry or that there is no change in the pressure of water and/or air in the soil pores, that is, the measured stresses indicate a change in effective soil stresses which is equal to the change in total stresses. A change in the pore fluid alone,

without any change in the effective soil stresses, may be illustrated by a change of back pressure in triaxial soil tests. Such a change will not affect deformations of the soil but it will influence the deflections and indications of the pressure cell which represent changes in total stresses. Usually, changes in pore water pressures and effective stresses are interrelated, but the form of this relationship is often a controversial matter and is outside the scope of this report. Changes in pore water or air pressure can be measured quite easily and accurately by means of a piezometer or fluid pressure gage. The changes in effective stresses are determined by subtracting the fluid pressure changes, measured by a piezometer, from the change in total stresses measured by a soil pressure cell.

47. Basic relations. Assume that the effective change in soil stresses σ_x , σ_y , σ_z are concurrent with a change u in the pore pressure. The problem is now to determine the effect of the additional deformations of the soil pressure cell caused by the change in pore pressure. Considering stresses and deformation in the z direction, or $\sigma'_s = \sigma_z$, the deformation of the soil is that given by Equation 21

$$2\delta_s = 2B \frac{\sigma_z - v(\sigma_x + \sigma_y)}{M_s} \quad (21)$$

and the deformation of the pressure cell is

$$2\delta_c = 2B \frac{\sigma_c + u}{M_c} \quad (35)$$

In the case of the WEC soil pressure cell, the deflection of the cell caused by hydrostatic liquid or air pressure is only 80 percent to 90 percent of that for direct static loading because liquid or air entering the circumferential slot counteracts part of the loading on the face plate, or the modulus of deformation is M_h considering only hydrostatic loading of the face plate and Equation 35 would then be changed to

$$2\delta_c = 2B \frac{\sigma_c}{M_c} + \frac{u}{M_h}$$

however, the same result is obtained by using Equation 35 in combination with the effective cell diameter for liquid or air loading or the actual outside diameter and a reduced value of u obtained by multiplying the actual u with the ratio of the calibration factors for hydrostatic and direct static loading. The latter method appears to be the simpler one, and Equation 35 is used in the following derivations. As before, the indentation of the pressure cell into the soil is $\delta_e = \delta_s - \delta_c$, or using Equations 21 and 35

$$\delta_e = B \frac{\sigma_s}{M_s} \left(1 - \nu \frac{\sigma_x + \sigma_y}{\sigma_z} \right) - B \frac{\sigma_c + u}{M_c} \quad (36)$$

but δ_e is also determined by Equations 1 and 6, or

$$\delta_e = \frac{\sigma_e}{N_s} D \quad (6 \text{ bis})$$

and

$$\sigma_e = (\sigma_c + u) - (\sigma_s + u) = \sigma_c - \sigma_s$$

which is independent of the pore water pressure, and Equation 6 can then be written

$$\delta_e = \frac{\sigma_c - \sigma_s}{N_s} D \quad (37)$$

which with Equation 36 yields

$$D \frac{\sigma_c - \sigma_s}{N_s} = B \frac{\sigma_s}{M_s} \left(1 - \nu \frac{\sigma_x + \sigma_y}{\sigma_z} \right) - B \frac{\sigma_c + u}{M_c}$$

and with $K_s = N_s/M_s$

$$\frac{\sigma_c}{\sigma_s} = \frac{\frac{D}{B} + K_s \left(1 - \nu \frac{\sigma_x + \sigma_y}{\sigma_z} \right) - K_s \frac{M_s}{M_c} \frac{u}{\sigma_s}}{\frac{D}{B} + K_s \frac{M_s}{M_c}} \quad (38)$$

This equation is identical to Equation 25 except for the last term in the numerator; that is, a change in pore pressure changes the value of σ_c/σ_s by

$$\Delta \frac{\sigma_c}{\sigma_s} = - \frac{K_s \frac{M_s}{M_c} \frac{u}{\sigma_s}}{\frac{D}{B} + K_s \frac{M_s}{M_c}} \quad (39)$$

Positive values of the pore pressure change, u , cause a decrease in overregistration and an increase in underregistration whereas a negative change in pore pressure has the opposite effect. Potential errors are smaller for a negative than for a positive change in pore pressure.

48. Equivalent cell modulus. The influence of a change in pore water pressure on the registration ratio for effective stresses can also be taken into consideration and, perhaps, better visualized by introducing an equivalent cell modulus, M'_c , which yields the same deformation as Equation 35 for the unit load σ_c ; that is,

$$2B \frac{\sigma_c + u}{M_c} = 2B \frac{\sigma_c}{M'_c}$$

or

$$M'_c = M_c \frac{\sigma_c}{\sigma_c + u} \quad (40)$$

The WES soil pressure cell has the cell modulus M_c for direct loading on the face plate and the modulus M_h for hydrostatic loading, and the equations are then changed to

$$2B \left(\frac{\sigma_c}{M_c} + \frac{u}{M_h} \right) = 2B \frac{\sigma_c}{M'_c}$$

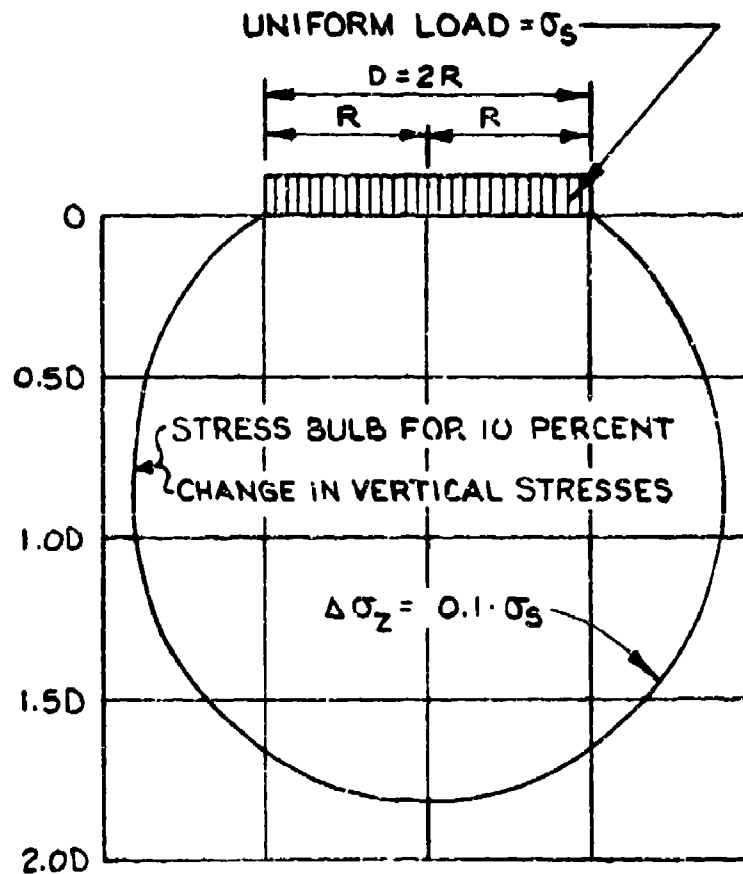
and

$$M'_c = M_c \frac{\sigma'_c}{\sigma_c + u \left(\frac{M_c}{M_h} \right)} \quad (41)$$

Estimates of M_c/M_h are usually based on the ratio of the calibration factors F_s/F_u . Values of σ_c and u are or can be measured in the field and $\sigma'_c = \sigma_c - u$, but these values must be estimated in design of pressure cells and discussion of the reliability of intended measurements. When M'_c is introduced in Equation 35 and subsequent equations, these equations become identical to those obtained for the action of soil pressure cells for stress changes without a change in pore pressure; that is, these equations and corresponding diagrams can be used without further consideration of changes in pore pressures when M_s/M_c is replaced with M_s/M'_c . This applies also to the action of pressure cells placed at the boundaries or interfaces of soil masses. For a positive change or increase in pore pressure, u , M'_c is smaller than M_c , which again emphasizes the importance of making cell modulus as large as possible and reducing the cell deformations to the minimum compatible with the required resolution of the pressure cell.

Pressure cell action influenced by boundaries

49. Cells close to the free soil surface. The simplified theory for soil-pressure cell interaction cannot be used when the cell is close to the free soil surface. Taylor (1945) states that the proposed simplified theory is based on the assumption that the embedment of a cell is large enough to permit development of a normal pressure bulb above the cell and cites the following examples. A pressure bulb indicating stresses equal to ten percent of the unit load has a height equal to 1.75 times the diameter of the cell, Figure 19, whereas a pressure bulb corresponding to two percent of the applied surface pressure



AFTER

D.W. TAYLOR, 1945

L. JURGENSON 1934, 1940

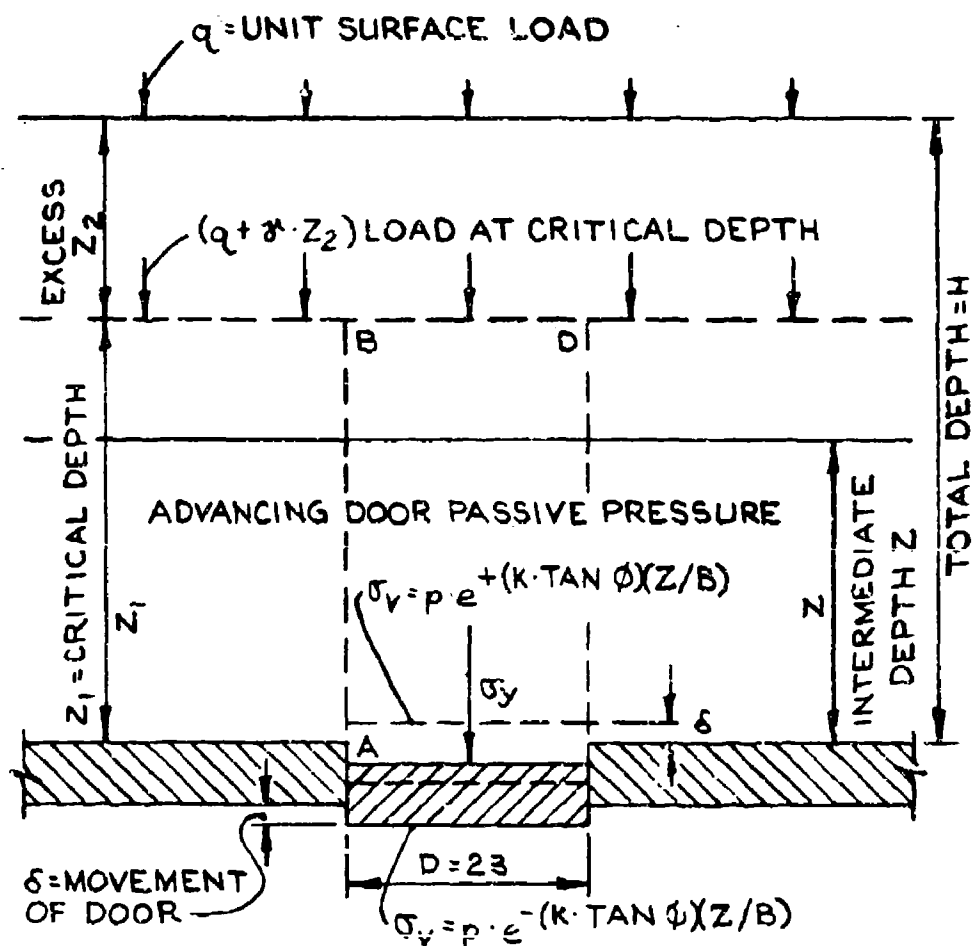
FIGURE 19. STRESS BULBS BELOW
CIRCULAR LOAD.

has a height of about four cell diameters. Estimates of the variation of pressure cell registration as a function of the depth below the free soil surface are discussed in the section on trap door analogies.

50. Terzaghi (1943, pp. 66-76) presents a theory for the approximate pressure of sand on a long or strip-type trap door, Figure 20. He states that effective arching in sand ceases to exist at a distance above the door equal to two to three times the width of a long door, depending on the properties of the soil and the movements of the door. McNulty (1965) performed extensive and carefully executed experiments with circular trap doors. He concluded that a cover with a thickness slightly less than the diameter of the door may be sufficient for development of active arching, and that a cover with a thickness of one to two times the diameter of the door is adequate in most practical cases for development of passive arching.

51. Mason and Associates of the United Research Services (1963, 1965, 1971) investigated arching around trap doors and inclusions by experiments, theory, and reviews. These investigations are discussed in the section on trap door analogies, and the results agree fairly well with the observations of Terzaghi and McNulty as shown in Figures 30A and 30B. The ratio of cell stress to surface load or field stress is 1.0 at the surface, and it increases or decreases exponentially with increasing depth ratio, z/R , until the ultimate overregistration or underregistration of the cell is attained. The depth at which the influence of the free soil boundary becomes unimportant varies with the cell diameter, the cell and soil properties, the stress level, and the differential deformations of soil and pressure cell.

52. Pressure cells at rigid boundaries. This section deals with pressure cells flush inserted, straddling, or just in contact with a foundation slab or a backfilled retaining wall which can be considered rigid in comparison with the soil. The simplified theory cannot yet be extended to cells which are close to but not in contact with such a boundary. To simplify derivation and comparison of basic equations, it is assumed that only the effective stresses but not the pore pressures are undergoing a change. A change in the pore water pressure can



YIELDING DOOR ACTIVE PRESSURE
AFTER TERZAGHI (1943)

THE EQUATIONS SHOWN APPLY TO A STRIP TYPE DOOR.

FIGURE 20. TRAP DOOR EXPERIMENTS AFTER TERZAGHI.

be taken into consideration by using a modified modulus of the pressure cell, equivalent to the pore pressure change as explained in paragraphs 56 and 57.

53. To be considered is a pressure cell with diameter D and thickness $2B$, set in a horizontal surface of a rigid material with a protusion H_s into the soil, Figure 21. For the stress changes σ_x , σ_y , σ_z of the soil, the vertical deformation δ_z of a soil layer with thickness H_s is

$$\delta_z = \delta_s = \left[\sigma_z - \nu(\sigma_x + \sigma_y) \right] \frac{H_s}{M_s} \text{ and } \sigma_s = \sigma_z \quad (42)$$

and the deformation of the pressure cell, for its total thickness, is

$$\delta_s = \frac{\sigma_c}{M_c} 2B \quad (43)$$

The indentation or penetration of the cell into the soil caused by the stress change is

$$\delta_e = \delta_s - \delta_c = \left[\sigma_z - \nu(\sigma_x + \sigma_y) \right] \frac{H_s}{M_s} - \frac{\sigma_c}{M_c} 2B \quad (44)$$

As before, it is assumed that δ_e also can be expressed by

$$\delta_e = \frac{\sigma_e}{N_s} D \text{ where } \sigma_e = \sigma_c - \sigma_s \quad (45)$$

Equations 44 and 45 yield

$$\frac{\sigma_c - \sigma_s}{N_s} D = \left[\sigma_s - \nu(\sigma_x + \sigma_y) \right] \frac{H_s}{M_s} - \frac{\sigma_c}{M_c} 2B$$

After reduction and with $K_s = N_s/M_s$, the equation can be written as

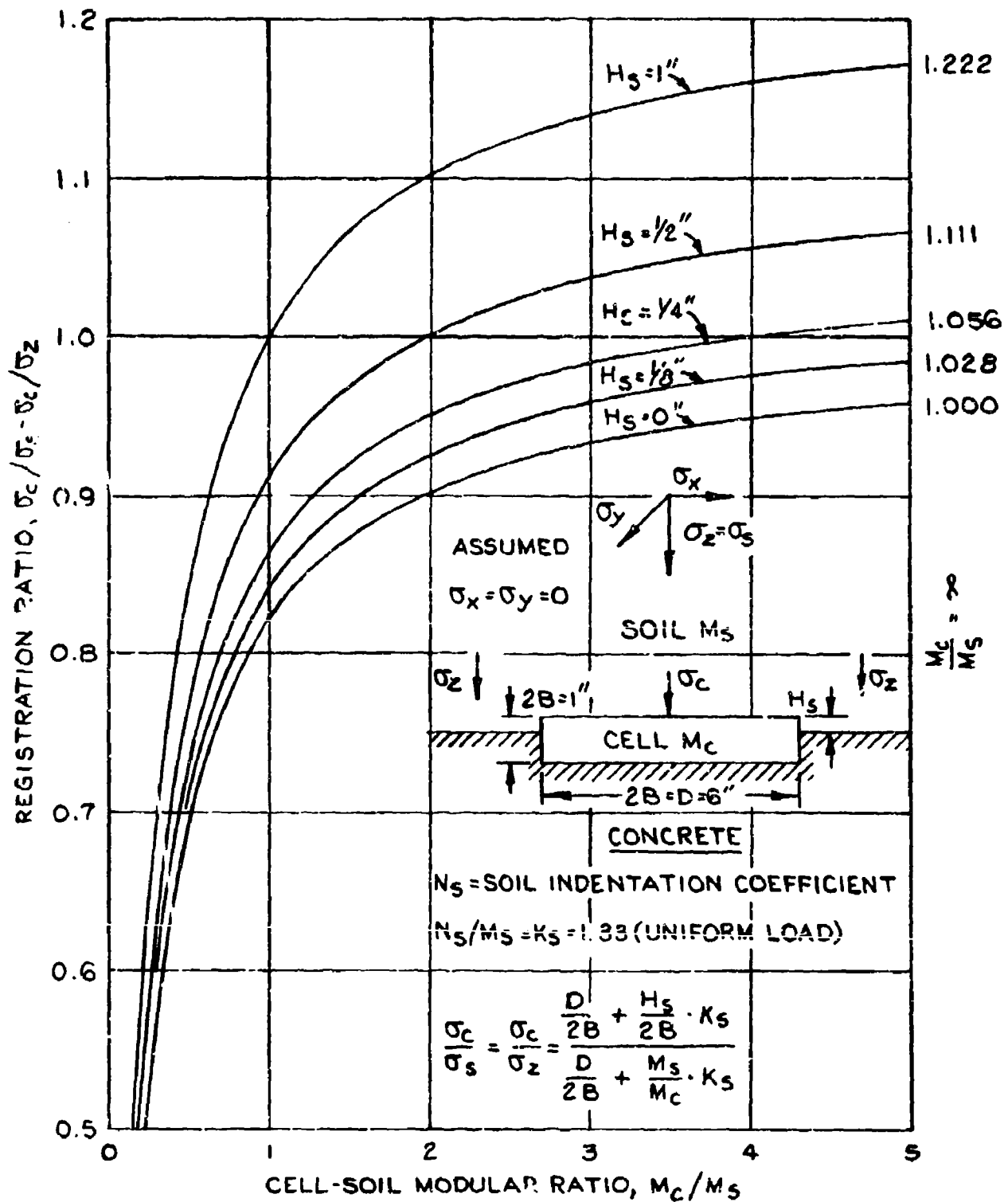


FIGURE 21. REGISTRATION RATIOS FOR CELLS IN RIGID SLAB-
UNIAXIAL STRESS CHANGES.

$$\frac{\sigma_c}{\sigma_s} = \frac{\frac{D}{2B} + \left(1 - \nu \frac{\sigma_x + \sigma_y}{\sigma_z}\right) \frac{H_s}{2B} K_s}{\frac{D}{2B} + \frac{M_s}{M_c} K_s} \quad (46)$$

Equation 46 applies to pressure cells embedded in a horizontal slab for measuring vertical stresses. For pressure cells in a vertical wall and measurement of horizontal stresses, for example σ_x , Equation 46 changes to

$$\frac{\sigma_c}{\sigma_s} = \frac{\sigma_c}{\sigma_x} = \frac{\frac{D}{2B} + \left(1 - \nu \frac{\sigma_y + \sigma_z}{\sigma_x}\right) \frac{H_s}{2B} K_s}{\frac{D}{2B} + \frac{M_s}{M_c} K_s} \quad (47)$$

54. Some examples of applications of Equations 46 and 47 are discussed in this paragraph. Consider first a pressure cell embedded in a horizontal slab, Figure 21, and subjected to a uniaxial stress change or $\sigma_x = \sigma_y = 0$; Equation 46 is then reduced to

$$\frac{\sigma_c}{\sigma_s} = \frac{\sigma_c}{\sigma_z} = \frac{\frac{D}{2B} + \frac{H_s}{2B} K_s}{\frac{D}{2B} + \frac{M_s}{M_c} K_s} \quad (48)$$

For earth pressure at rest and $\nu = 1/3$, or $\sigma_x = \sigma_y = \sigma_z/2 = \sigma_s/2$, Equation 46 becomes

$$\frac{\sigma_c}{\sigma_s} = \frac{\sigma_c}{\sigma_z} = \frac{\frac{D}{2B} + \frac{2}{3} \frac{H_s}{2B} K_s}{\frac{D}{2B} + \frac{M_s}{M_c} K_s} \quad (49)$$

Graphical illustrations of Equations 48 and 49 are shown in Figures 21 and 22 for $D = 6$ in., $2B = 1$ in., and $K_s = 1.33$. Comparison with the corresponding equations and Figures 15 and 16 for pressure cells in

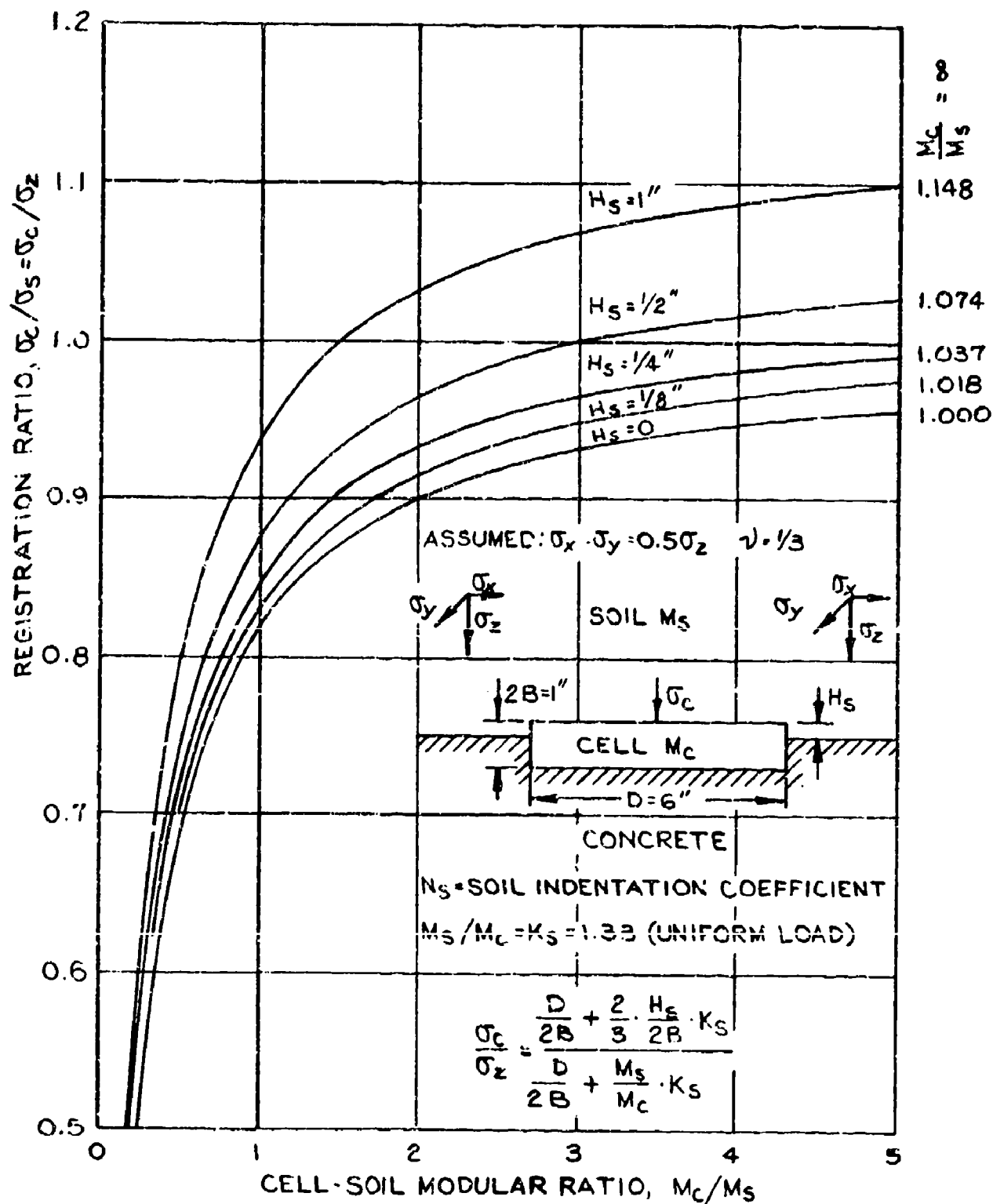


FIGURE 22. REGISTRATION RATIOS FOR CELLS IN RIGID SLAB-EARTH PRESSURE AT REST.

a free field shows that a pressure cell in contact with but not embedded in a rigid horizontal slab, $H_s = 2B$, acts as a cell in a free field with the double thickness, $2B =$ half thickness, and that the limiting potential error ratio is twice as great as for a cell in a free field. On the other hand, a pressure cell flush embedded, $H_s = 0$, in a rigid structure always underregisters, and only for the ultimate condition ($M_s/M_c = 0$), is the registration ratio $(\sigma_c/\sigma_s) = 1.0$. For intermediate conditions it is possible to determine a value of the protrusion, H_s , which yields 100 percent registration or $(\sigma_c/\sigma_s) = 1.0$ for given values of the deformation moduli M_c and M_s , but these conclusions do not apply to pressure cells in contact with or embedded in a rigid vertical wall. For such cells and stress change conditions for earth pressure at rest or $\nu = 1/3$ and $\sigma_x = \sigma_y = \sigma_z/2$, Equation 47 applies but is reduced to

$$\frac{\sigma_c}{\sigma_s} = \frac{\sigma_c}{\sigma_x} = \frac{\frac{D}{2B}}{\frac{D}{2B} + \frac{M_s}{M_c} K_s} \quad (50)$$

The conditions represented by Equation 50 are illustrated by Figure 23. It is seen that the registration ratio is independent of the protrusion H_s and is less than unity; that is, a pressure cell embedded in or in contact with a rigid vertical wall, and with earth pressure at rest, underregisters and is not influenced by protrusion of the cell; therefore, such pressure cells are generally flush mounted in order to avoid damage to a protruding edge during the backfill and compaction operations.

55. The numerical examples in Figures 21, 22, 23 are primarily intended for illustration and comparison and the diagrams are computed for the same values of N_s and K_s used in previous examples, whereas the values of N_s and K_s increase at rigid boundaries as shown in the special investigations by Walen (1942), Gravesen (1959-B) and Askegaard (1959, 1961) are summarized in Figure 31. These investigations also indicate that the use of relations based on simplifications or



approximations should be confined to very small deformations of a pressure cell embedded flush with the surface of a rigid slab or wall, since the area of contact between the soil and the pressure cell decreases with increasing deformation and becomes zero for a relatively small deformation, Figure 31B.

56. Pressure cells at interface of materials with different compressibility. The foregoing paragraphs deal with the action of pressure cells in a uniform free field or at the boundary of compressible and incompressible materials. The more general condition of a pressure cell at the interface of two different but compressible strata is discussed in the following paragraphs, primarily for the purpose of enumerating the many factors to be considered and to demonstrate some general relationships. Figure 24 shows a pressure cell straddling the interface to the two strata. The modulus for deformation of the softer materials is designated by M_s and the more rigid stratum by M_r ; furthermore, the cell is oriented to measure the vertical or major principal stress, $\sigma_s = \sigma_z$. The embedments of the cell in the two strata are H_s and H_r , and

$$H_s + H_r = 2B \quad (51)$$

As before, the deformation of the cell caused by the stress change σ_c , corresponding to σ_s in the soil, is

$$2\delta_c = \frac{\sigma_c}{M_c} 2B \quad (2 \text{ bis})$$

whereas the corresponding deformation of soil strata with a total thickness $2B$ and the stress change $\sigma_s = \sigma_z$ is

$$2\delta_s = \sigma_z \left(1 - \nu \frac{\sigma_x + \sigma_y}{\sigma_z} \right) \left(\frac{H_s}{M_s} + \frac{H_r}{M_r} \right) \quad (52)$$

The average change in penetration into new soil by the two faces of the cell are in Equation 4

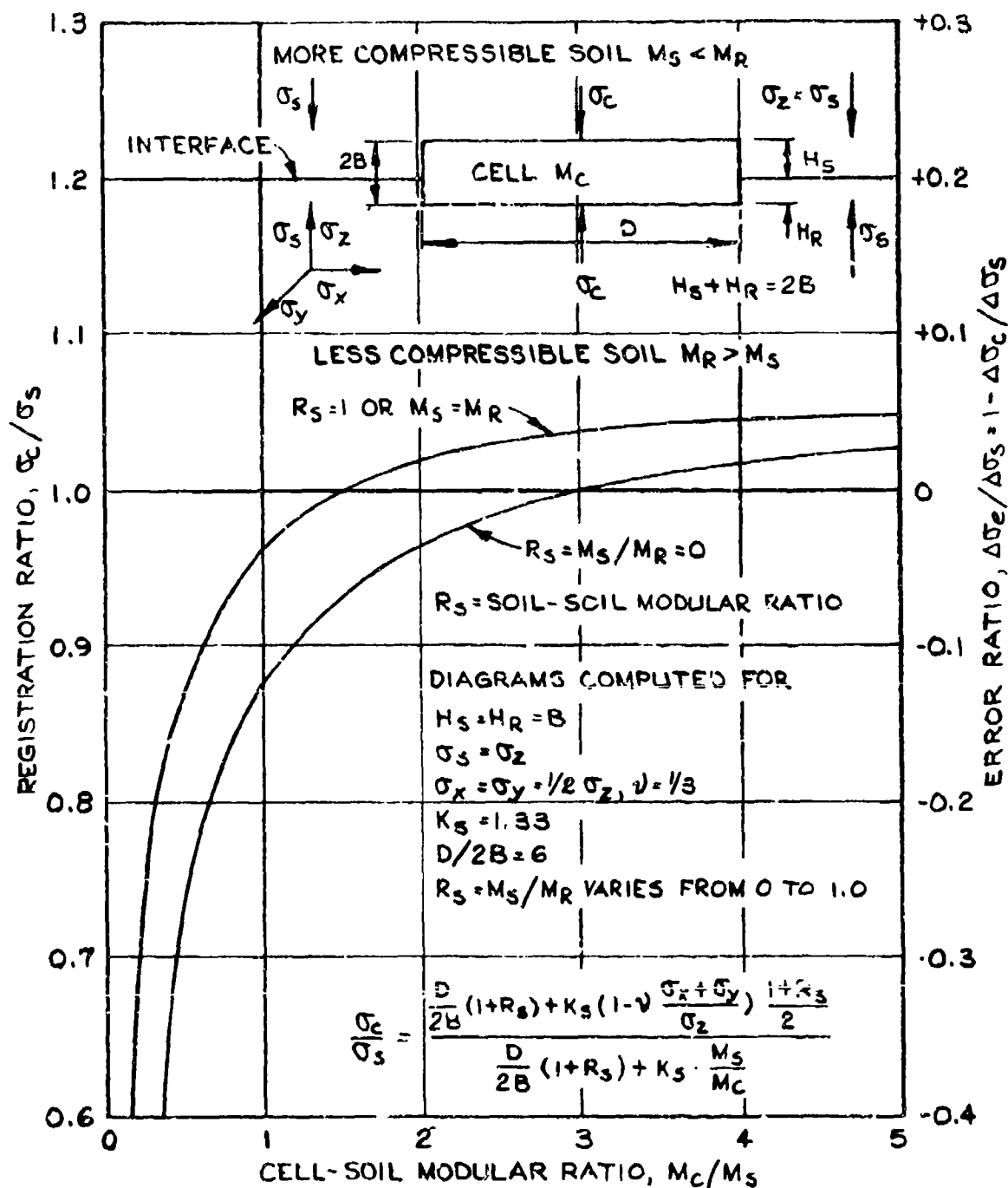


FIGURE 24. SOIL PRESSURE CELLS AT INTERFACE OF COMPRESSIBLE STRATA

$$\delta_e = \delta_s - \delta_c \quad (4 \text{ bis})$$

The overstress or understress, σ_e , is defined by Equation 1, or

$$\sigma_e = \sigma_c - \sigma_s \quad (1 \text{ bis})$$

and is the same for both faces of the cell when the friction and adhesion on the sidewall of the cell is negligible. Referring to Equation 6, the total change in penetration, δ_e , can also be expressed by

$$2\delta_e = \frac{\sigma_e}{N_s} D + \frac{\sigma_e}{N_r} D = \sigma_e D \left(\frac{1}{N_s} + \frac{1}{N_r} \right) \quad (53)$$

Where the indentation coefficients N_s and N_r are functions of the properties of the materials and the ratios

$$\frac{N_s}{M_s} = \frac{N_r}{M_r} = K_s \quad (54)$$

are assumed to be constant, as before. Multiplying the terms in this equation by (M_s/N_r) yields

$$\frac{N_s}{N_r} = \frac{M_s}{M_r} = R_s = K_s \frac{M_s}{N_r} \quad (55)$$

and the modular ratio of two given soils is constant. Equations 1, 2, 4, 52, and 53 yield

$$(\sigma_c - \sigma_s) D \left(\frac{1}{N_s} + \frac{1}{N_r} \right) = \sigma_s \left(1 - \nu \frac{\sigma_x + \sigma_y}{\sigma_z} \right) \left(\frac{H_s}{M_s} + \frac{H_r}{M_r} \right) - \frac{\sigma_e}{M_c} 2B$$

Introducing the modular ratio R_s , Equation 55, and rearranging yield

$$\sigma_c \left[\frac{D}{N_s} (1 + R_s) + \frac{2B}{M_c} \right] = \frac{\sigma_s}{N_s} D (1 + R_s) + \frac{\sigma_s \left(1 - \nu \frac{\sigma_x + \sigma_y}{\sigma_z} \right)}{M_s} (H_s + R_s H_r)$$

or

$$\frac{\sigma_c}{\sigma_s} = \frac{\frac{1}{N_s} D(1 + R_s) + \left(1 - \nu \frac{\sigma_x + \sigma_y}{\sigma_z} \right) (H_s + R_s H_r)}{\frac{1}{N_s} D(1 + R_s) + \frac{2B}{M_c}}$$

Multiplying by N_s and introducing K_s from Equation 54 produces the equation

$$\frac{\sigma_c}{\sigma_s} = \frac{D(1 + R_s) + K_s \left(1 - \nu \frac{\sigma_x + \sigma_y}{\sigma_z} \right) (H_s + R_s H_r)}{D(1 + R_s) + K_s \frac{2B}{M_c}} \quad (56A)$$

or the alternative form with individually dimensionless component elements

$$\frac{\sigma_c}{\sigma_s} = \frac{\frac{D}{2B} (1 + R_s) + K_s \left(1 - \nu \frac{\sigma_x + \sigma_y}{\sigma_z} \right) \frac{H_s + R_s H_r}{2B}}{\frac{D}{2B} (1 + R_s) + K_s \frac{M_s}{M_c}} \quad (56B)$$

These equations constitute a general expression for the registration ratio, σ_c/σ_s , obtained by the extended Taylor theory.

57. Simpler forms of Equations 56 for definite values of H_s , H_r , and the modular soils ratio, R_s , are discussed in this paragraph. For $M_s = M_r$ or $R_s = 1$ and with $H_s + H_r = 2B$ Equation 56B becomes

$$\frac{\sigma_c}{\sigma_s} = \frac{\frac{D}{B} + K_s \left(1 - \nu \frac{\sigma_x + \sigma_y}{\sigma_z} \right)}{\frac{D}{B} + K_s \frac{M_s}{M_c}}$$

which is identical to Equation 23 as it should be since the conditions specified correspond to those for a pressure cell in uniform soil. For M_r infinite or $M_s/M_r = R_s = 0$, Equation 56A becomes

$$\frac{\sigma_c}{\sigma_s} = \frac{\frac{D}{2B} + K_s \left(1 - \nu \frac{\sigma_x + \sigma_y}{\sigma_z} \right) \frac{H_s}{2B}}{\frac{D}{2B} + K_s \frac{M_s}{M_c}}$$

which is identical with Equation 46 for a pressure cell at an incompressible boundary and protruding the distance H_s into the soil. The influence of the modular ratio, $R_s = M_s/M_r$, on the registration ratio, σ_c/σ_s , varies with the relative values of H_s and H_r and is best examined for symmetrical conditions or $H_s = H_r = B$, in which case Equation 56B reduces to

$$\frac{\sigma_c}{\sigma_s} = \frac{\frac{D}{2B} (1 + R_s) + K_s \left(1 - \nu \frac{\sigma_x + \sigma_y}{\sigma_z} \right) \frac{1 + R_s}{2}}{\frac{D}{2B} (1 + R_s) + K_s \frac{M_s}{M_c}} \quad (57)$$

This equation shows that maximum values of σ_c/σ_s are obtained for $R_s = 1.0$ and minimum values for $R_s = 0$, which also are the limiting values of R_s considering the definition of M_s and M_r . A numerical example indicating possible variations of σ_c/σ_s and σ_e/σ_s for the maximum and minimum values of R_s is shown in Figure 24. It is assumed that $(D/2B) = 6.0$, $K_s = 1.33$, $\nu = 1/3$, and $\sigma_x = \sigma_y = \sigma_z/2$. The numerical form of Equation 57 is then

$$\frac{\sigma_c}{\sigma_s} = \frac{6.44(1 + R_s)}{6.0(1 + R_s) + 1.33 \frac{M_s}{M_c}} \quad (58)$$

Values of σ_c/σ_s as a function of M_c/M_s are shown in Figure 24 for

$R_s \approx 0$ and $R_s = 1.0$. It is seen that the soil-soil modular ratio, R_s , has relatively little influence on σ_c/σ_s when the cell-soil modular ratio is greater than 1.0.

58. A remaining problem concerns the placement of a pressure cell at the interface of two different soils; that is, the values of H_s and H_r which yield the optimum value of σ_c/σ_s . These optimum values depend on many factors, but the following discussion is confined to the influence of the relative value of M_c with respect to M_s and M_r , and it does not consider possible singular solutions for special stress conditions or values of σ_x , σ_y , and σ_z . As defined, M_r is the modulus of the less compressible soil layer and is greater than M_s , the modulus of the more compressible soil layer. Also by definitions

$$H_s + H_r = 2B$$

and introducing

$$\frac{H_s}{H_r} = n$$

yields

$$H_s = 2B \frac{n}{1+n} \quad (59)$$

$$H_r = 2B \frac{1}{1+n} \quad (60)$$

The last term in Equation 56b can then be written

$$\frac{H_s + R_s H_r}{2B} = \frac{n + R_s}{n + 1} \quad (61)$$

where $R_s = M_s/M_r$ is a constant for given soils and n is the variable for which the optimum value is sought.

59. When M_c is smaller than M_s the pressure cell will always

underregister, and the optimum value of "n" is that which produces the maximum value of σ_c/σ_s in Equation 56. The only variable on the right side of this equation is the term shown in Equation 61, and the maximum value of this term is obtained for n equal to infinite or $1/n = 0$, which yields

$$H_r = 0 \text{ and } H_s = 2B$$

that is, the pressure cell should be placed entirely in the more compressible layer but in contact with the interface between the two layers.

60. For M_c greater than M_s but smaller than M_r , the registration ratio σ_c/σ_s may vary from smaller than 1.0 to greater than 1.0 with changes in H_s and H_r . The optimum values of H_s and H_r or of the ratio n are those which produce $\sigma_c/\sigma_s = 1.0$. Equation 56B may then be reduced to

$$K_s \frac{M_s}{M_c} = K_s \left(1 - v \frac{\sigma_x + \sigma_y}{\sigma_z} \right) \frac{H_s + R \frac{H_r}{s_r}}{2B}$$

and by use of Equation 61

$$\frac{M_s}{M_c} = \left(1 - v \frac{\sigma_x + \sigma_y}{\sigma_z} \right) \frac{n + R \frac{H_r}{s_r}}{n + 1} \quad (62)$$

from which "n" and the corresponding optimum values of H_s and H_r can be determined; see also Figures 21-24.

61. In case M_c is greater than M_r , the pressure cell will always overregister and the optimum value of "n" is that producing the minimum value of σ_c/σ_s in Equation 56B, or Equation 61, since $R \frac{H_r}{s_r}$ is smaller than one. The minimum value of the term $(n + R \frac{H_r}{s_r})/(n + 1)$ occurs for $n = 0$ or $H_s = 0$ and $H_r = 2B$; that is, the pressure cell should be placed in the less compressible layer but in contact with the interface between the two soil layers.

62. Important limitations. The special case of a pressure cell

located at the interface of two compressible but different soil strata has not yet been treated in available publications. The foregoing discussion and mathematical analysis of the problem is based on the same assumptions as the simplified analyses of the soil-cell interaction in a free field; that is, the method is a simplified indentation analogy, in which the soil deformations are determined by simplified equations and the indentation forces are obtained by the Boussinesq equations for a load at a free soil surface. The direct influence of lateral stresses on the axial stresses is not considered. It is probable that the resulting explicit formulas yield an indication of the form of relationships under investigation, but the numerical results may not be reliable, and the errors in cell registration are generally larger than those obtained by the simplified equations and diagrams. Improved results may be obtained by multiplying the independent coefficients in the equations, especially K_s , with a correction factor. Such a correction factor is not yet available or even constant, but the maximum values are indicated by the limiting diagrams for σ_c/σ_s or σ_e/σ_s in Figure 24, and the difference in ordinates of the two limiting diagrams is not large. These limiting diagrams may also be obtained by other and more reliable methods of analysis, as described in the following summary of currently available theories for soil-cell interaction. Finally, it is to be noted that the simplified analysis can only be applied to a pressure cell straddling or in contact with an interface or boundary but not to cells a short distance from such discontinuity.

Influence of extra-neous soil deformations

63. Definitions. The simplified theory for the interaction of soil and pressure cells, discussed in the foregoing paragraphs, is confined to conditions of corresponding changes in stresses, strains, or deformations of the soil, which may be expressed by

$$\epsilon_s = \frac{\sigma_s}{M_s} \quad \text{and} \quad 2\delta_s = 2B\epsilon_s = 2B \frac{\sigma_s}{M_s} \quad (63)$$

where σ_s and ϵ_s are corresponding changes of stress and strain in the soil, and δ_s is the deformation of a soil layer with thickness $2B$ equal to that of the pressure cell. It should be noted that the modulus M_s here has the same numerical value as that used in determining the indentation coefficient and ratio, N_s and K_s , as discussed in paragraph 32. These deformations may be called stress-dependent or normal deformations. However, strains and deformations may take place without a change in stresses and may be designated by

$$\epsilon_{se} \text{ and } 2\delta_{se} = 2B\epsilon_{se} \text{ but}$$

$$\text{without a corresponding change in soil stress or } \sigma_s = 0 \quad (64)$$

Such strains and deformations are nonstress dependent or extraneous deformations, which may be caused by creep, loading followed by unloading or vice versa, shrinkage or swelling, and by temperature changes, Carlson (1939) and Monfore (1950). Unrestricted shrinkage or swelling occur without a change in outside forces and total stresses. The influence of temperature changes discussed in this report refers only to the effect of a difference in volume changes of cell and soil for a given temperature change. The influence of temperature changes on the internal parts of a pressure cell are usually made nearly self compensating so that they do not cause any change in the calibration of a cell or the indication of the cell for a given, effective load change.

64. Errors caused by extraneous deformations. The following analysis is confined to pure extraneous deformations at zero stress changes, corresponding to Equation 64. The methods and assumptions of this simplified analysis are similar to those previously used for normal or stress-dependent deformations and are subject to the same limitations. Referring to Equation 64, the extraneous deformation for a soil layer with thickness $2B$ and at a strain ϵ_{se} is

$$2\delta_{se} = 2B\epsilon_{se}$$

This soil deformation causes a change in deformation, $2\delta_{ce}$, and a corresponding change in stress registration, σ_{ce} , of the pressure cell. Since $\sigma_s = 0$, the change σ_{ce} is also the error in cell registration, or $\sigma_e = \sigma_{ce}$. The total change in deformation of the cell, $2\delta_{ce}$, is then

$$2\delta_{ce} = 2B \frac{\sigma_e}{M_c} \quad (65)$$

The indentation of the soil by each side of the cell is

$$\delta_e = \delta_{se} - \delta_{ce} = B \left(\epsilon_{se} - \frac{\sigma_e}{M_c} \right) \quad (66)$$

According to Equation 6, δ_e can also be determined by

$$\delta_e = D \frac{\sigma_e}{N_s} \quad (6 \text{ bis})$$

which combined with Equation 66 yields

$$B \left(\epsilon_{se} - \frac{\sigma_e}{M_c} \right) = D \frac{\sigma_e}{N_s}$$

or by resolving for σ_e

$$\sigma_e = \frac{B \epsilon_{se}}{\frac{D}{N_s} + \frac{B}{M_c}} = \frac{B}{D} \frac{\epsilon_{se} N_s}{1 + \frac{B}{D} K_s \frac{M_s}{M_c}} \quad (67)$$

where K_s is defined by Equation 7 or

$$K_s = \frac{N_s}{\gamma_s}$$

The error in cell indication can then be determined by Equation 67 when the extraneous strain ϵ_{se} is known, but comparisons with similar equations for normal or stress-dependent deformations is facilitated by introducing an equivalent stress, σ_{se} , which corresponds to the strain ϵ_{se} and the current value of the modulus of deformation of the soil, M_s , or

$$\sigma_{se} = \epsilon_{se} M_s \quad (68)$$

Dividing Equation 67 with Equation 69 yields the error ratio for extraneous deformations

$$\frac{\sigma_e}{\sigma_{se}} = \frac{B}{D} \frac{\frac{N_s}{M_s}}{1 + \frac{B}{D} K_s \frac{M_s}{M_c}}$$

$$\frac{\sigma_e}{\sigma_{se}} = \frac{B}{D} K_s \frac{1}{1 + \frac{B}{D} K_s \frac{M_s}{M_c}} \quad (69)$$

Values of σ_e/σ_{se} as a function of M_s/M_c or M_c/M_s are shown by the upper diagram in Figure 25 for a WES soil pressure cell with $D = 6.0$ in., $2B = 1.0$ in., and $K_s = 1.33$. The error ratio varies from zero at $M_c/M_s = 0$ to a maximum of 0.111 at $M_s/M_c = 0$. There is very little variation in σ_e/σ_{se} when M_c is larger than M_s . As before, σ_e is positive when it represents an increase in cell registration and compression, whereas ϵ_{se} and δ_{se} are positive when they indicate a decrease in thickness of soil layers and an increase in soil compression above and below the cell. Strains and stresses of opposite sign occur in soil outside but close to the periphery of the cell.

65. Comparison of errors by normal and extraneous deformations.
Equation 69 and the upper diagram in Figure 25 represent errors in cell

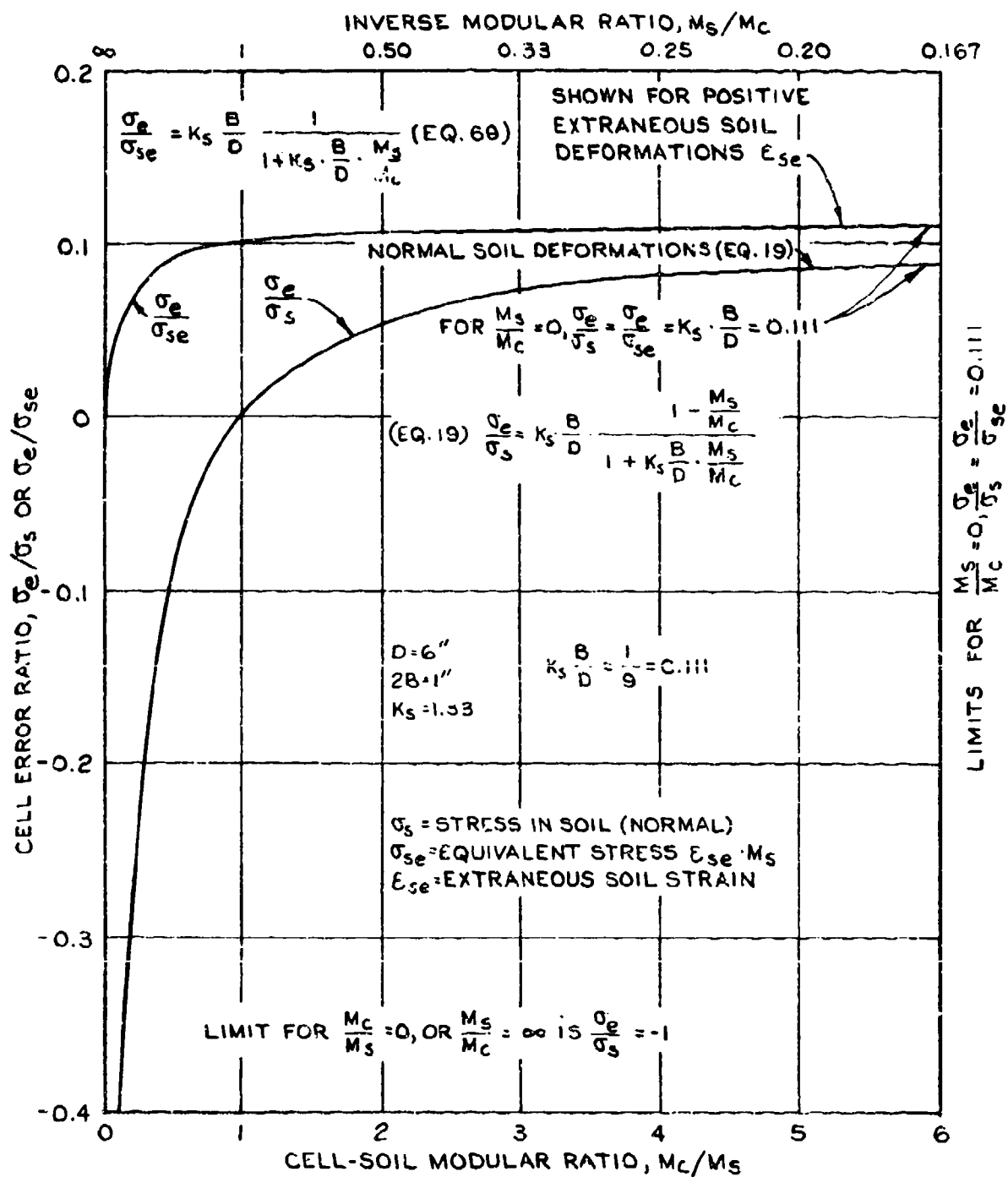


FIGURE 25. PRESSURE CELL ERROR RATIOS FOR NORMAL AND EXTRANEEOUS DEFORMATIONS.

indications caused by extraneous deformations. Corresponding values of the error ratio for normal or stress-dependent deformations may be determined by Equation 19 or

$$\frac{\sigma_e}{\sigma_s} = \frac{B}{D} K_s \frac{1 - \frac{M_s}{M_c}}{1 + \frac{B}{D} K_s \frac{M_s}{M_c}} \quad (19 \text{ bis})$$

and the relationship is shown by the lower diagram in Figure 25. The maximum value of σ_e/σ_s occurs at $M_s/M_c = 0$ and is 0.111 or the same as for σ_e/σ_{se} . However, for $M_s = M_c$ the error ratio $\sigma_e/\sigma_s = 0$ whereas $\sigma_e/\sigma_{se} = 0.10$, and for values of M_c smaller M_s there is not only a great numerical difference between the error ratios for stress-dependent and extraneous deformations but these ratios and the needed corrections are of opposite sign. These results are important in case normal and extraneous deformations occur at the same time; for further discussion of this problem see paragraph 67.

66. Influence of temperature changes. A change in temperature of a pressure cell and the medium in which it is embedded may affect the indicated pressure in several ways, which may be summarized as follows:

- a. A temperature change will affect the electrical conductivity of wire or foil strain gages in a pressure cell, but the connections of these gages are usually so designed that positive and negative errors practically compensate each other.
- b. The steel or other metals in a pressure cell has a much greater thermal expansion or contraction than the matrix in which the cell is embedded. Consequently a temperature change will cause a movement of the cell with respect to the surrounding medium, and the sum of the movements of both faces of the cell may be expressed by

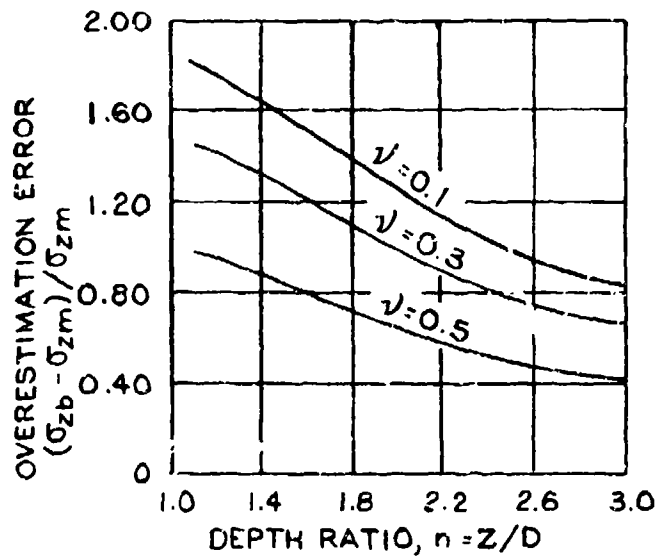
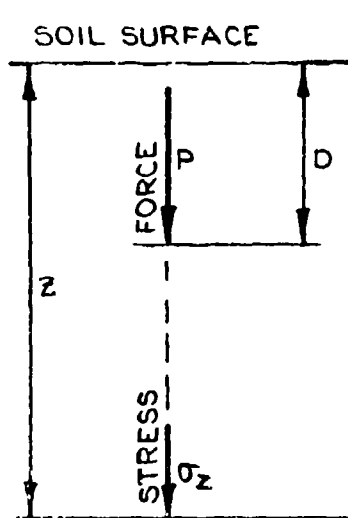
$$2\delta_{se} = 2B(\alpha_c - \alpha_s)T^0 \quad (70)$$

where α_c is the coefficient of linear thermal expansion of the cell, α_s is the corresponding coefficient for

the surrounding material, and T° is the temperature change. The relative movement of each face of the cell, δ_{se} , may then be considered and treated as an extraneous deformation.

- c. The third type of error caused by temperature changes apply only to pressure cells in which the pressure on the face plate is transmitted through a liquid film to an interior measuring diaphragm, such as in the Carlson and WES pressure cells. The volume change of the liquid, oil or mercury, is greater than that of the cell material for the same temperature change. Furthermore, the liquid film is more or less laterally confined and a volume change primarily occurs as a change in thickness of the liquid film, which in turn causes changes in the pressure of the liquid and in indications by the measuring diaphragm. This influence of temperature changes cannot be eliminated completely but it can be reduced materially by making the film as thin as is consistent with the manufacturing process, usually between 0.01 in. and 0.03 in., and necessary corrections can be determined during calibration and expressed by a general equation, Carlson and Pirtz (1952).

67. Mixed normal and extraneous deformations. Soil and concrete subjected to creep or plastic flow and to cycles of loading and unloading exhibit both normal and extraneous deformations. The latter are of special importance when it is desired to determine the total stress changes rather than those caused by the last load increment. The pressure cell will indicate a stress corresponding to the stress change since placement of the cell, but the indicated stress is subject to errors, and the needed corrections are quite different for normal and extraneous deformations, except when the cell-soil modular ratio, M_c/M_s , is large as shown in Figure 26. Use of a single correction equation or no corrections at all may lead to misleading results when the modular ratio is small, especially when it is less than unity. In such cases it is advisable to supplement a series of pressure cells with a few strain meters, Carlson and Pirtz (1952), which may furnish data making it possible to separate the two types of deformations and corresponding corrections. Further investigations of this problem are needed. In general, strain meters are useful even when the cell-soil modular ratio is large, because these meters furnish information on residual strains, creep, and rate of creep, which is needed for estimation of the



BOUSSINESQ:

$$\sigma_{zb} = \frac{k_b}{(n-1)^2} \cdot \frac{P}{D^2}$$

MINDLIN:

$$\sigma_{zm} = k_m \cdot \frac{P}{D^2}$$

ERROR RATIO:

$$\frac{\sigma_{zb} - \sigma_{zm}}{\sigma_{zm}} = \left(\frac{k_b}{k_m (h-1)^2} - 1 \right)$$

DATA BY GEDDES 1966

FIGURE 26. BOUSSINESQ VERSUS MINDLIN EQUATIONS FOR INTERIOR POINT LOADS.

ultimate deformation of earth and foundation structures.

Review of Proposed Theories for Soil-Cell Interaction

68. The general objectives of this section are to enumerate the most important methods for estimating the interaction of soil and pressure cells, to present a brief summary of the general principles and results which are of particular importance for discussions in this report. Although a soil pressure cell may be considered as an inclusion in soil or rock, the following comments do not include the more elaborate theories for stresses on buried structures, except some parts which may be used to advantage in the analysis of the action of pressure cells. Most theories consider the soil surrounding a pressure cell to be an elastic material with constant properties, whereas the deformation characteristics of soils usually change with the stress.

Simplified methods in a free stress field

69. Indentation analogies. One of the earliest and most commonly used pressure cell theories obtain closed equations for the cell action by analogy with the indentation of a rigid cylinder or punch into the surface of a semi-infinite, elastic body, and the simplified theory discussed in this report belongs to this group of theories. The general principles of the theory have been explained in the foregoing part of the report, but they will be summarized here to emphasize their advantages and limitations. The method bypasses determination of the actual stress distribution and is primarily concerned with average stresses and strains. Equations are written for deformation of the pressure cell under its registered load and for a soil layer under the nominal field stress load and having a thickness equal to that of the cell. The difference between these deformations is the indentation or retraction of the two faces of the cell with respect to the soil. The force corresponding to this positive or negative indentation is then to be estimated by means of the Boussinesq equation for the indentation of the surface of an elastic body by a smooth and rigid cylinder, and this

equation together with the deformation equations make it possible to solve the problem. This method has been used by Taylor (1945), Nils Hast (1945), Coutinho (1949), Peattie and Sparrow (1954), and others. The analysis is simplified and deals primarily with stresses and strains normal to the pressure cell although the Poisson effects of known lateral strains are considered in this report, directly or indirectly. The numerical results may be in need of appreciable correction factors, but the method is very flexible and yields a logical explanation of the cell action plus relative relationships for conditions not yet covered by rigorous analysis, which are very helpful in the planning of further analytical or experimental research.

70. Limitations - Boussinesq versus Mindlin equations. The principal causes of numerical errors in results obtained by the indentation analogy are

- a. Simplifications in computing stresses and deformations of soil close to the rim of the pressure cell.
- b. The influence of lateral stresses in the soil are only indirectly taken into consideration by the Poisson effect of lateral stresses on axial strain.
- c. A major source of error occurs when translating soil-cell differential deformations into stress or force by analogy with a rigid disk at the soil surface. The indentations later are determined by the Boussinesq equations, but these equations are not valid in the interior of a soil mass, where the Mindlin equations should be used. The relations between stress and indentation of a rigid disk in the interior of a soil mass have not yet been determined, but comparisons of Boussinesq and Mindlin equations to an interior point load by Geddes (1966) are shown in Figure 26 and give an indication of the magnitude of errors which may be caused by use of the Boussinesq instead of the Mindlin equations. The diagrams in Figure 26 apply only to points directly below a point load. The error decreases with radial distance, and a reversal must ultimately occur, so that an integration of stresses on a horizontal plane will yield the total force P.
- d. Nonlinear stress-strain relations, hysteresis, and residual stresses and strains may affect total registrations of a pressure cell but the influence of these factors are small for incremental registration ratios. The remarks about the Boussinesq versus Mindlin equations apply

not only to the indentation analogy but whenever the Boussinesq equations for stresses and deformations caused by forces on the soil surface are applied to forces in the interior of a soil mass.

71. Use of finite annular elements. The following comments apply only to pressure cells in a free field, whereas cells at or in a rigid boundary will be discussed later. It is assumed that a plane through the midheight of the cell remains plane in both cell and soil during and after a load change, and the normal stress on a series of annular elements is altered until this requirement is fulfilled. Only normal stresses on the annuli are considered, and they are computed by means of the Boussinesq equations. This leads to a series of simultaneous equations which can be solved by various methods, and the resulting loads of the elements indicate the stress distribution on the cell and errors in its registration. The solution of the simultaneous equations can be facilitated by use of a computer, and is similar in principle to that used in the finite element method of analysis. In the two examples discussed in the following paragraphs the pressure cells are assumed to be inclusions with uniform, elastic properties, but the method can be extended to a pressure cell with an inactive rim and an active diaphragm or cell when the finite element method of analysis is used.

72. In an unpublished thesis, Carlson (1939) used the method of finite annular elements for analysis of the response of a pressure cell. Results of subsequent refinements of the original analysis are presented in a paper by Carlson and Pirtz (1952), but this paper does not contain all the details of the computations. However, the paper is extended to cover the influence of extraneous soil deformations and temperature changes. Carlson and Pirtz (1952) also suggest that lateral or radial stresses in some cases also may have considerable influence on the cell registration of axial stresses. The simultaneous equations are solved by trial and error, similar to the method used in the trial load analysis of arch dams. The results are in good agreement with both the original analysis and later solutions by others using the same or more systematic methods. Monfore (1950) has performed a detailed and very efficient analysis of the influence of a pressure cell, considered as a

uniform inclusion, on the pressures in the surrounding soil. The method of annular rings was used, and the task was facilitated by preparing tables of terms or ratios in the simultaneous equations which are independent of the properties of the materials, and solving the equations by systematic divisions. An easier solution could be obtained by use of matrixes and electronic computers, but they were not available when the paper was prepared. The influence of the diameter-thickness ratio of the cell, and of the cell-soil modular ratios, M_c/M_s , were determined and are shown graphically. Extraneous deformations of the soil and temperature changes in cell and soil were also considered. All the results are in general agreement with those yielded by previously mentioned methods. Numerical results were obtained for a uniform inclusion with a diameter of 2.5 inches and embedded in concrete. The value of Poisson's ratio was assumed to be $\nu = 0.2$ for concrete, and minor variations are not important since this ratio appears only in the term $(1 - \nu^2)$. A special analysis was made for a pressure cell with the dimensions of the Carlson pressure cell, and the result of the analysis by Carlson was verified.

73. Influence of an inactive rim. Monfore (1950) noted that the error in pressure cell registration would be reduced from 9.0 percent to 5.0 percent when only the stresses on the central part of the entire cell are considered. This theoretical result was later verified by Peattie and Sparrow (1954), who investigated the influence of an inactive rim of cells in various types of soils. The experiments were made with soil and cells in a solid-walled container. The soil was subjected to surface loading, and corrections were made for the influence of side-wall friction. A special cell was built which makes it possible to change the active area, Figure 27A. The authors suggest that the active area of a pressure cell should be between 0.25 and 0.45 times the total area of the cell. Peattie and Sparrow also suggest that the modular ratio, M_c/M_s , should not be less than ten, in which case the simple equation $\sigma_c/\sigma_s = C_a(B/D)$ may be used. The results of tests with cells with an inactive rim and with a full active face are compared in Figure 27A. The maximum error in registrations of cells with a full active

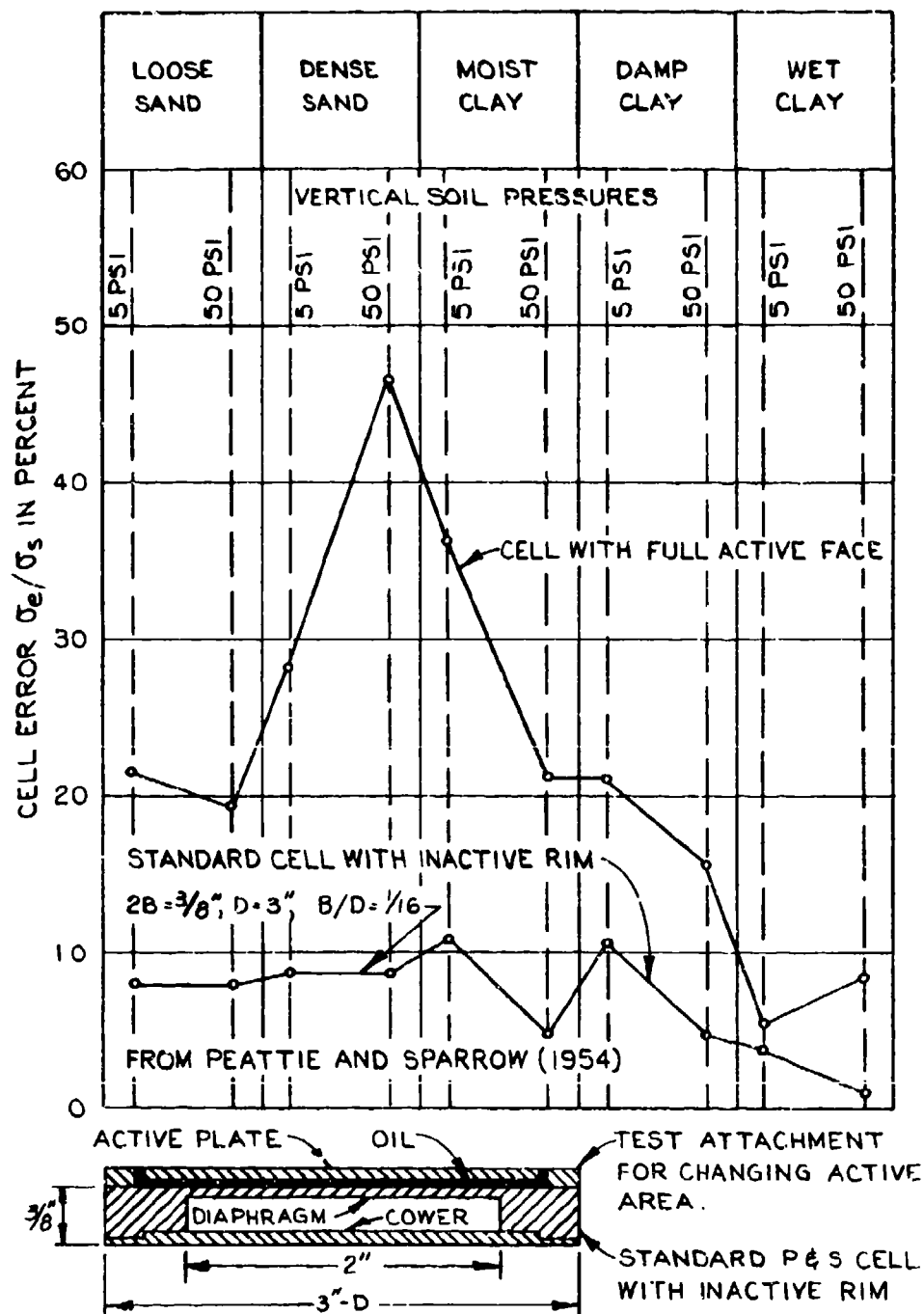
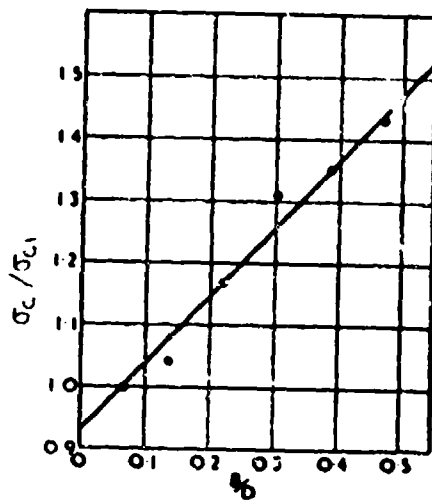
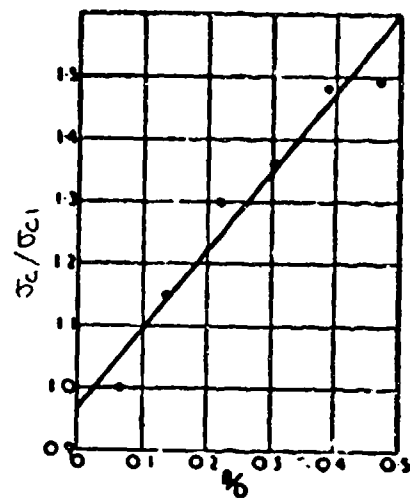


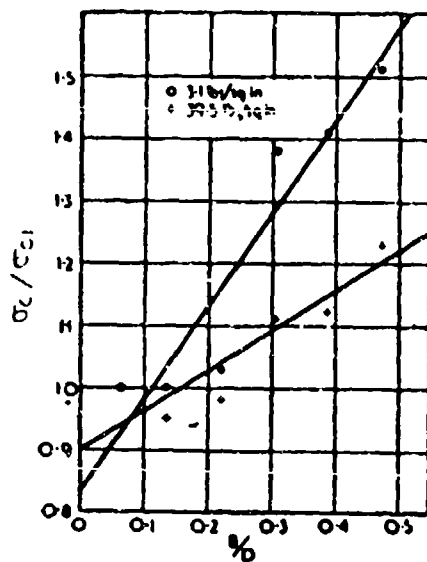
FIGURE 27 A. PRESSURE CELL ERROR RATIOS FOR VARIOUS SOIL TYPES AND PRESSURES.



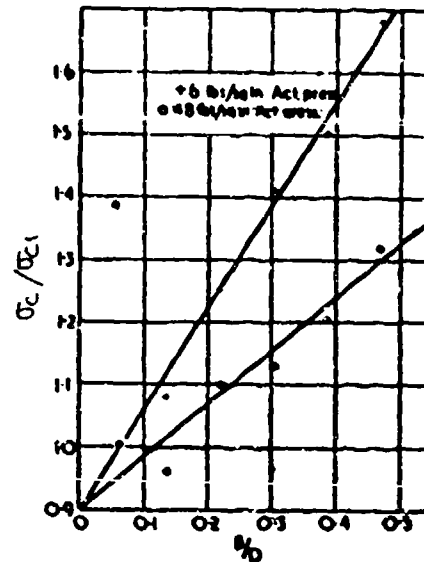
B-1. LOOSE MOIST SAND



B-2. DENSE MOIST SAND



B-3. BRICK EARTH AT 13.5 PERCENT MOISTURE CONTENT



B-4. BRICK EARTH AT 16 PERCENT MOISTURE CONTENT

FROM PEATTIE AND SPARROW (1954)

σ_{c1} = VALUE OF σ_c FOR MINIMUM (B/D) USED IN THE EXPERIMENTS

FIGURE 27B. INFLUENCE OF THICKNESS-DIAMETER RATIO OF CELL ON ITS REGISTRATION ERROR

face was found to be 47 percent for cells in dense sand. The average error in registrations of cells with an inactive rim was consistently smaller than the error for cells with a full active face, irrespective of the type of soil in which the cells were embedded. However, tests at the Waterways experiment Station with cells in sand indicated that the registrations of cells with an inactive rim approach those of cells with a full active face when the stress conditions in the surrounding soil approach those of failure; see Part III of this report, Figures 95-97. Experimental data shown in Figure 27B show that the stress ratio σ_c/σ_{ci} is a linear function of the thickness-diameter ratio, B/D .

Trapdoor analogies

74. The Terzaghi analysis. In the trapdoor analogy the force corresponding to a differential deformation of soil and pressure cell is estimated by comparison with the forces on a yielding or advancing trapdoor at the bottom of a soil-filled bin. Many papers on the trapdoor problem have been published over the years; the analysis presented by Terzaghi (1936, 1943) is illustrated in Figure 20. Active or passive arching occurs in the soil over the trapdoor, but the arching does not affect the soil beyond a critical distance or cover z_1 , and the weight of soil above this depth merely increases the effective surface load, Figure 20. Terzaghi has analyzed the forces acting on a long rectangular or strip-type trapdoor, to or below the critical depth z_1 , and he simplified the problem by replacing some curved and inclined failure surfaces with plane and vertical surfaces. This analysis yielded the following equation for the force, σ_v , acting on a yielding trapdoor and corresponding to active soil pressure over the door:

$$\sigma_v = \frac{B[\gamma - (c/B)]}{K \tan \phi} \left[1 - e^{-K \tan \phi (z/B)} \right] + q e^{-K \tan \phi (z/B)} \quad (71A)$$

where z is the depth of soil above the door and K is the coefficient of earth pressure. The value of z used in this equation should not be greater than z_1 . In sand or sandy soils it is generally adequate to consider only the effect of the surface load, which yields

$$\sigma_v = qe^{-K \tan \phi (z/B)} \quad (71B)$$

The corresponding equation for an advancing door and passive earth pressure is

$$\sigma_v = qe^{+K \tan \phi (z/B)} \quad (71C)$$

The equations furnish limiting values of σ_v for a depth or cover z , smaller than z_1 . The movements, δ , of the door do not enter into these equations, and it is tacitly assumed that the movements are large enough to mobilize the peak soil strength. Terzaghi (1943) states that smaller movements of the door produces smaller pressures on the door, but a possible relation between δ and σ_v is not suggested. Terzaghi (1943) found that the critical depth, z_1 , is between $2D$ and $3D$ for a yielding door and active earth pressure. Terzaghi states that the relative merit of proposed trapdoor theories, including the theory presented by him, is still unknown - in 1943.

75. Experiments by McNulty. Extensive and carefully executed experiments with circular trapdoors were performed by McNulty (1965) at the WES. In addition, reviews are presented of initial investigations of the trapdoor problem by Terzaghi (1936-1943) and of recent publications on the more general problem of soil-structure interaction by Spangler (1948). The McNulty experiments were made with two diameters of the trapdoor, 3 and 6 in., placed at the bottom of a test bin with a diameter of 46.75 in. Two types of medium grained sand were used, placed at average unit weights of 100 and 106 pcf, corresponding to relative densities of 72 and 76 percent, which were obtained by means of a mechanical spreader and final vibration. The depth of the sand varied for individual tests but did not exceed twice the diameter of the trapdoor used in the test. Results of tests for various depths of sand in the bin are shown in Figure 28A, where q is the surface pressure and σ_v is the unit pressure on the trap door. Diagrams for active and passive pressures are quite different but have a common tangent for zero movement of the door. Data for very small movements of the door are

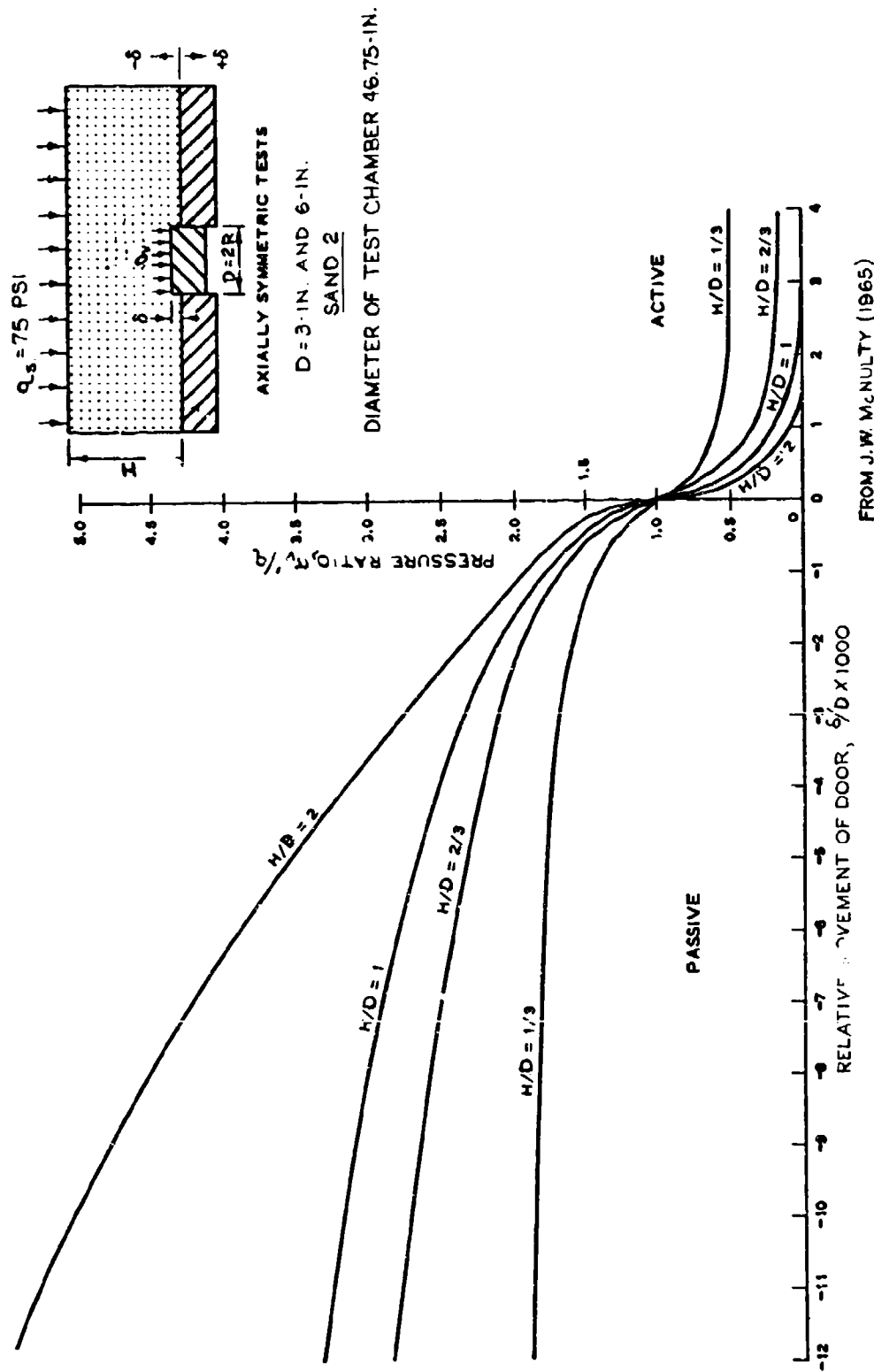


FIGURE 28A. COMPARISON OF ACTIVE AND PASSIVE SAND PRESSURES ON CIRCULAR TRAP DOOR.

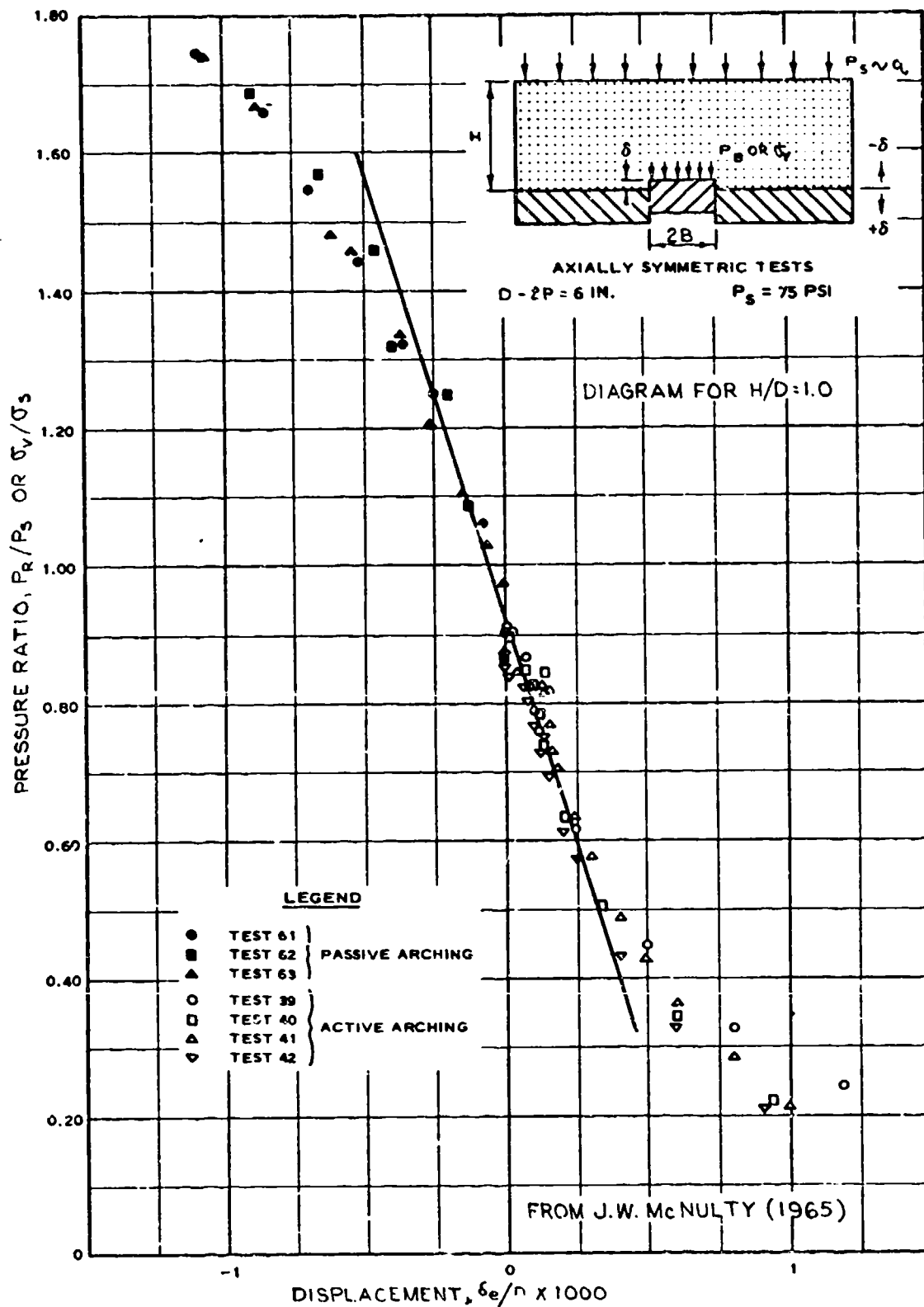


FIGURE 28B. INITIAL VALUES OF PRESSURE VERSUS DISPLACEMENT RATIOS FOR SAND ON CIRCULAR TRAP DOOR.

shown in enlarged scale in Figure 28B, which shows that nearly linear relations exist to a movement of about 0.0002 times the diameter of the trapdoor. As pointed out by McNulty, such a small movement may change the pressure on the trapdoor by about 50 percent. Experiments with circular trapdoors form excellent models for the action of pressure cells placed flush with the surface of a rigid boundary for the soil. However, the reliability of trapdoor experiments as models for the action of pressure cells in a free stress field is still open to question, because lateral movements of soil near a trapdoor are hindered by friction between the soil and the rigid boundary. Notations used by Terzaghi, McNulty, Mason, and other authors are quite different in some instances which may cause misunderstandings. Therefore, the notation in figures and equations by these authors have been changed when they are used or quoted in this report.

76. In the theoretical evaluation of the test data, McNulty considers first elastic conditions for the nearly linear part of the load-deflection diagrams, Figure 28B. Here the Boussinesq equations should apply. One form of these equations is reported by Timoshenko-Goodier (1951) and is shown in Equation 9 of this report, that is

$$\delta_v = \sigma_v \frac{\pi}{4} D \frac{1 - \nu^2}{M_s} \quad (9 \text{ bis})$$

This equation may be used to estimate the slopes of the initial parts of diagrams for both active and passive pressures or, conversely, to compute the moduli of soil deformation when δ_v and σ_v are known. The ultimate values of σ_v are in the plastic region and may be determined by the Terzaghi Equations 71a, b, c when they are transformed from a strip-type to a circular trapdoor. This transformation yields, considering only uniform surface loads,

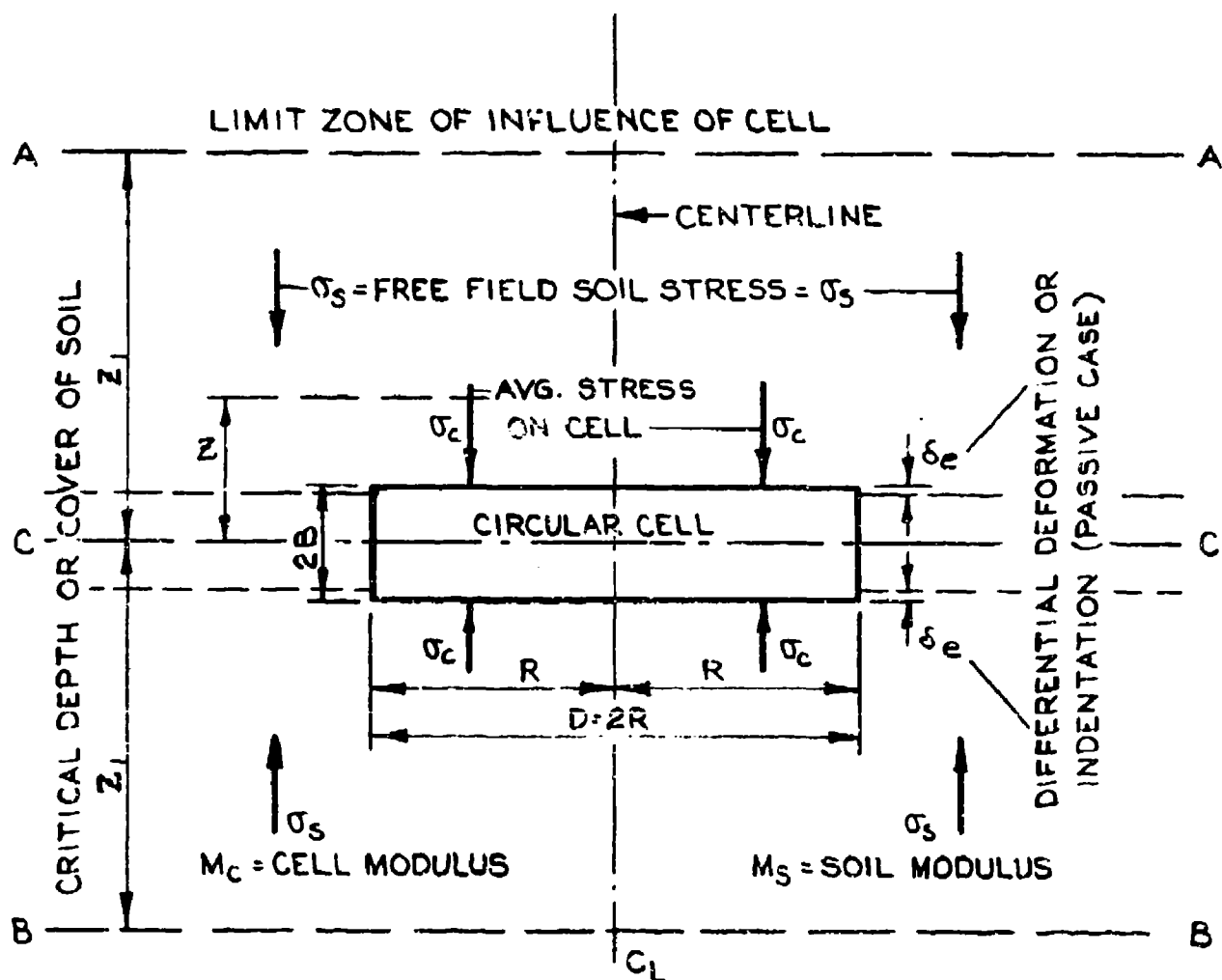
$$\sigma_v = 1e^{\sqrt{2}K \tan \phi} (H/R) \quad (72)$$

which agrees fairly well with test data for active pressures, excluding small values of (H/R) . For passive pressures McNulty adopts the rigid body approach, in which a soil cylinder above the trapdoor is assumed to be rigid and subjected only to sidewall friction on the cylindrical surface, $2\pi RH \cdot q \cdot K \cdot \tan \phi$, which yields the equation

$$\sigma_v = q[1 - 2K \tan \phi (H/R)] \quad (73)$$

this agrees fairly well with passive pressures for (H/R) greater than 2. These equations apply to initial and ultimate values of σ_v and δ_v . McNulty suggests a semi-empirical method for determination of σ_v corresponding to intermediate values of δ_v or (δ_v/D) , using experimentally determined diagrams for (δ_v, σ_v) in combination with a secant analysis. Approximate analytical solutions have been suggested by Mason (1965), which are discussed in the following paragraphs. More rigorous mathematical solutions have been developed by Askegaard (1959) and Gravesen (1959); see paragraphs 84 and 85.

77. Investigations by Mason and Associates. Trapdoor experiments and the theory by Terzaghi (1936, 1943) constitute an excellent model of the actions of a soil pressure cell placed flush with the surface of a rigid boundary. A rigid boundary restricts lateral movements of the soil, but the Terzaghi trapdoor theory does not consider the influence of lateral soil stresses and strains. This applies also to the theory proposed by Mason and Associates (1965) of the United Research Services for determination of the approximate axial stresses on a pressure cell in a free stress field. The problem is illustrated in Figure 29, where z_1 corresponds to the critical depth of soil cover over a trapdoor. Deformations and stresses of soil at distances greater than z_1 above or below the cell are not affected by the presence of the cell. With a uniform stress σ_s in the free soil or a uniform load σ_s at the critical distances, the theory considers only the average stress $\sigma_c = \sigma_s + \sigma_e$ within a soil cylinder above and below the cell, which may be expressed by an equation similar to that for a trapdoor, Equation 72, or



OVER-OR UNDERSTRESS $\sigma_e = \sigma_c - \sigma_s$, OR $\sigma_c = \sigma_s + \sigma_e$

SOIL DEFORMATION FOR THICKNESS $2B = 2\delta_s = 2B \sigma_s / M_s$

CELL DEFORMATION $= 2\delta_c = 2B \sigma_e / M_c$

DIFFERENTIAL DEFORMATION OR INDENTATION, $\delta_e = \delta_s - \delta_c$

FIGURE 29. DEFINITIONS FOR MASON-URS PRESSURE CELL THEORY.

$$\frac{\sigma_z}{\sigma_c} = e^{\pm 2K \tan \phi (z/R)} \quad (74)$$

At the critical distance, z_1 , the stress is σ_s , but it is σ_c at the cell, which yields the following relation between z_1 and (σ_c/σ_s) ,

$$z_1 = \frac{R}{2K \tan \phi} \ln \left(\frac{\sigma_c}{\sigma_s} \right) \quad (75)$$

Integration of soil deformations from the critical distances to the centerline of the cell yields the following equations for differential settlements, corresponding to the indentation used in the simplified theory; for passive pressure,

$$\frac{\delta_e}{R} = \frac{\sigma_s}{M_s \cdot 2K \tan \phi} \left(\frac{\sigma_c}{\sigma_s} - 1 - \ln \frac{\sigma_c}{\sigma_s} \right) \quad (76a)$$

and for active pressure,

$$\frac{\delta_e}{R} = \frac{\sigma_s}{M_s \cdot 2K \tan \phi} \left(\ln \frac{\sigma_c}{\sigma_s} - 1 + \frac{\sigma_c}{\sigma_s} \right) \quad (76b)$$

The integrations also yield the following relations between the stress ratio (σ_c/σ_s) , and the modular ratio (M_s/M_c) , for passive pressure

$$\frac{M_s}{M_c} = \frac{1 - \left(\frac{\sigma_c}{\sigma_s} \right) + \ln \left(\frac{\sigma_c}{\sigma_s} \right) + \left(\frac{B}{R} \right) 2K \tan \phi}{\left(\frac{B}{R} \right) \left(\frac{\sigma_c}{\sigma_s} \right) 2K \tan \phi} \quad (77a)$$

and for active pressures

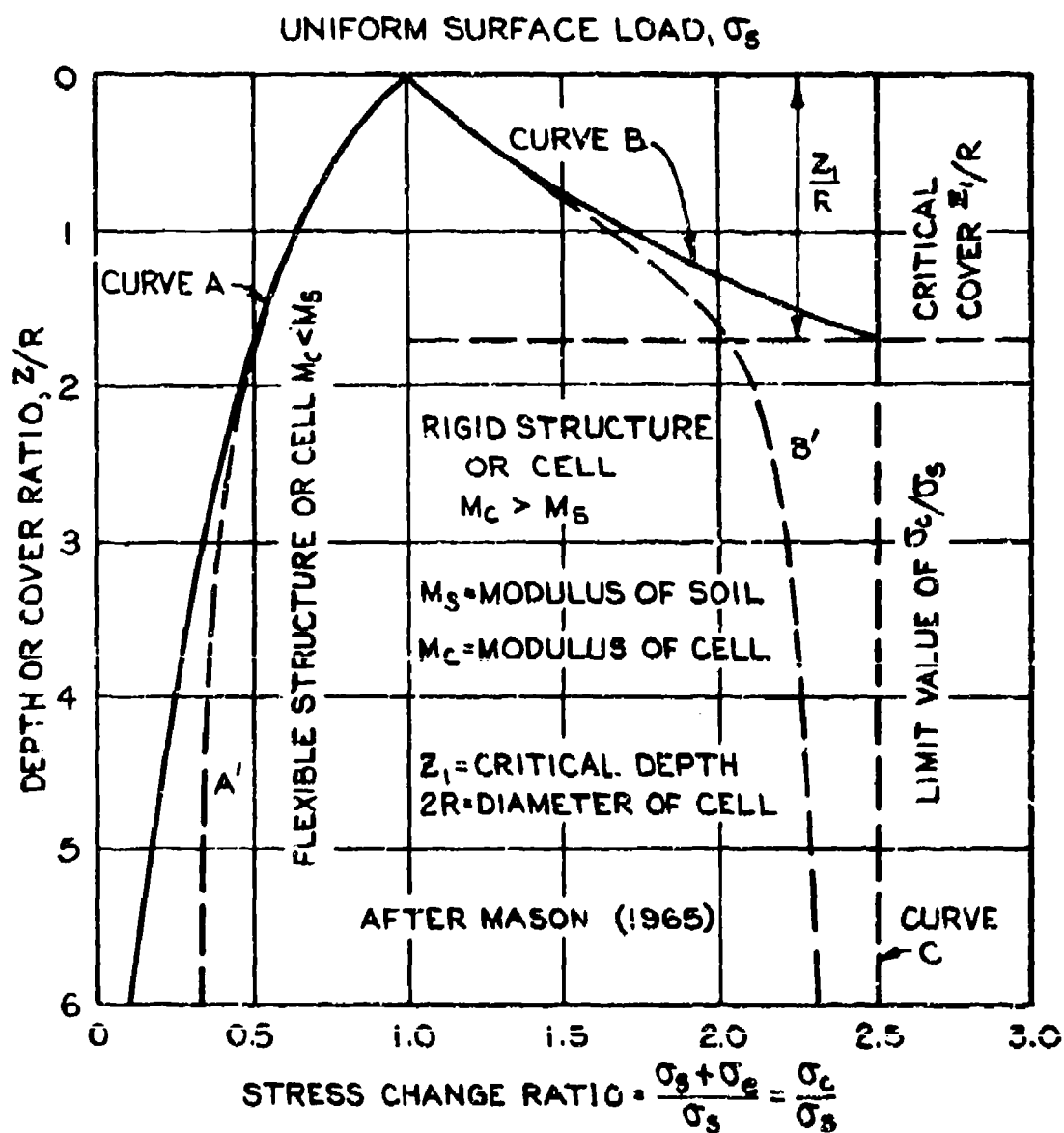
$$\frac{M_s}{M_c} = \frac{\ln \left(\frac{\sigma_s}{\sigma_c} \right) - 1 + \left(\frac{\sigma_c}{\sigma_s} \right) + \left(\frac{B}{R} \right) \cdot 2K \tan \phi}{\left(\frac{B}{R} \right) \left(\frac{\sigma_c}{\sigma_s} \right) 2K \tan \phi} \quad (77b)$$

Similar equations were also derived for nonlinear stress-strain relations represented by the equation

$$\epsilon_s = \left(\frac{\sigma_s}{M_s} \right)^{2/3} \quad \text{or} \quad \sigma_s = M_s \epsilon^{3/2} \quad (78)$$

In some cases the nonlinear stress-strain relationship yields better agreement between theory and experimental data.

78. In initial experiments by United Research Services small test bodies were placed in much larger triaxial test specimens. The results of these tests plus theoretical considerations yield the general diagrams shown in Figure 30A. Active stresses decrease and passive stresses increase with increasing depth below the free soil surface until a critical depth is reached, whereupon the stresses remain constant with additional increases in depth. In Figure 30A the full drawn diagrams represent original theoretical relations and the dashed diagrams experimental data. The experiments indicated a more gradual transition to constant values of (σ_c/σ_s) . Additional experimental data indicated that the critical depths and the ultimate values of the stress ratio, (σ_c/σ_s) also increase with increasing deformation ratios (δ_c/R) , Figure 30B. More detailed comparisons of the theory with the experimental trapdoor experiments by McNulty (1965) are shown in Figures 31 and 32. In general, good agreement exists for small deformation ratios (δ_e/l') and in some cases also for larger deformations in combination with the larger depth of cover. Figure 32A shows that apparent agreement to a large extent depends on the soil parameters inserted in the theoretical equations. It may be noted that the theory by Mason and Associates also can yield diagrams of the same form as those shown in Figure 28. A later report by United Research Services, prepared by



NOTE: DASHED CURVES, A' AND B', REPLACE CURVES A AND B FOR LIMITED AND SMALL DIFFERENTIAL MOVEMENTS δ OR CORRESPONDING MOVEMENTS OF A TRAP DOOR.

FIGURE 30A. LIMITING STRESS CHANGE VERSUS SOIL COVER.

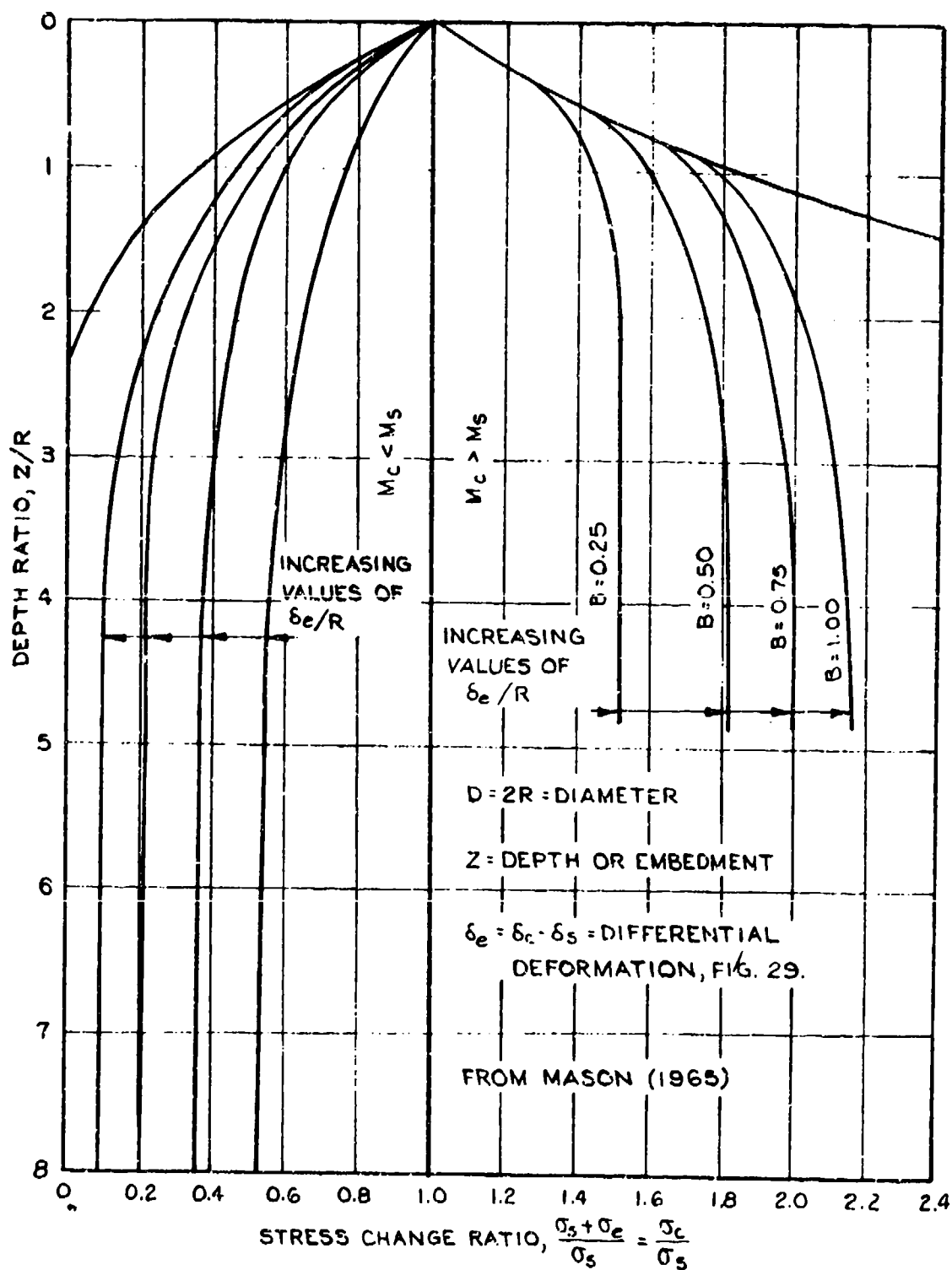
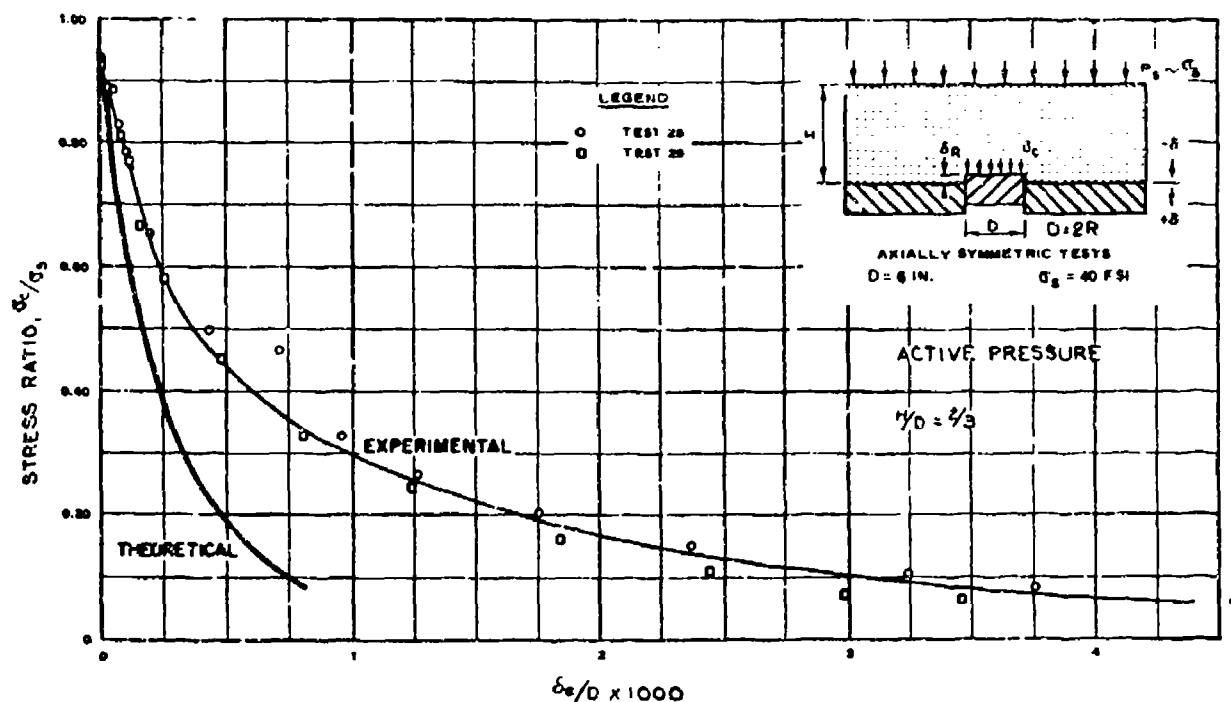
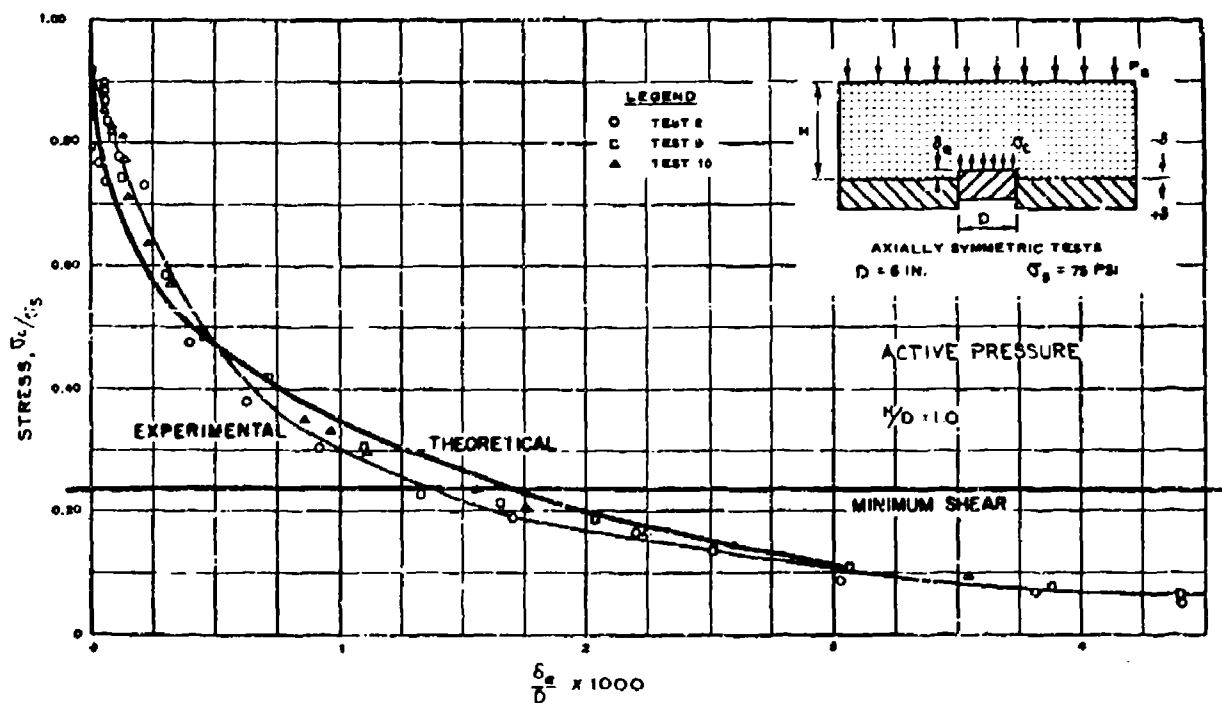


FIGURE 30B. CHANGE RATIO VERSUS DEPTH AND DIFFERENTIAL DEFORMATION RATIOS.

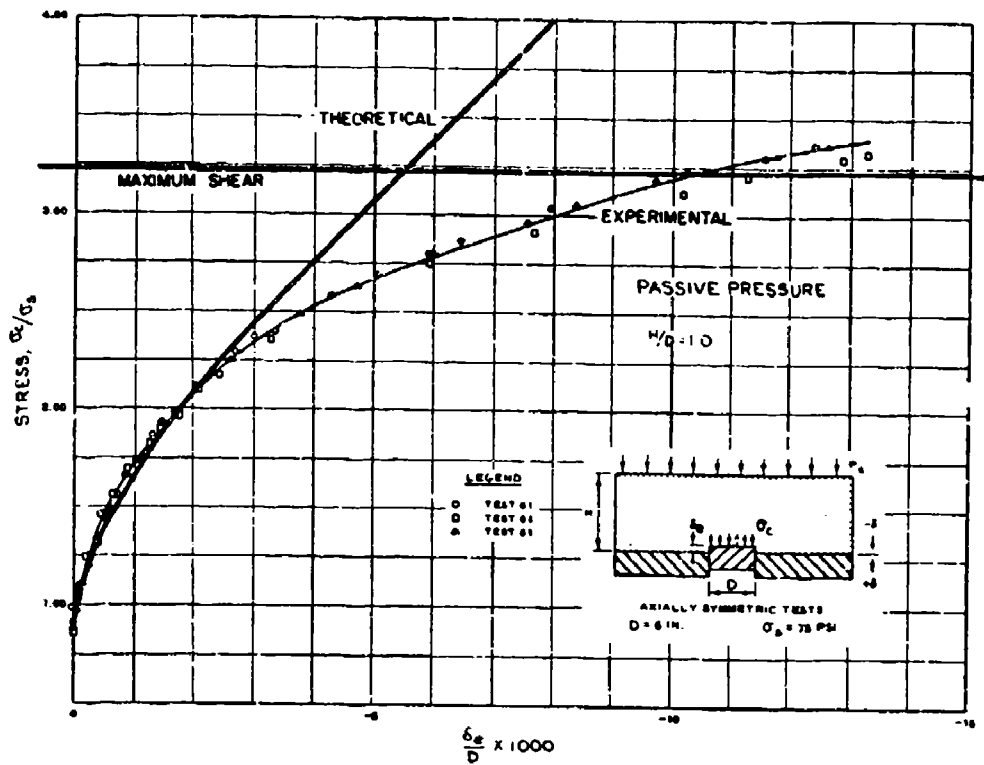


A. COMPARISON OF EXPERIMENTAL DATA BY McNULTY AND THEORY BY MASON AND ASSOCIATES - ACTIVE PRESSURES.

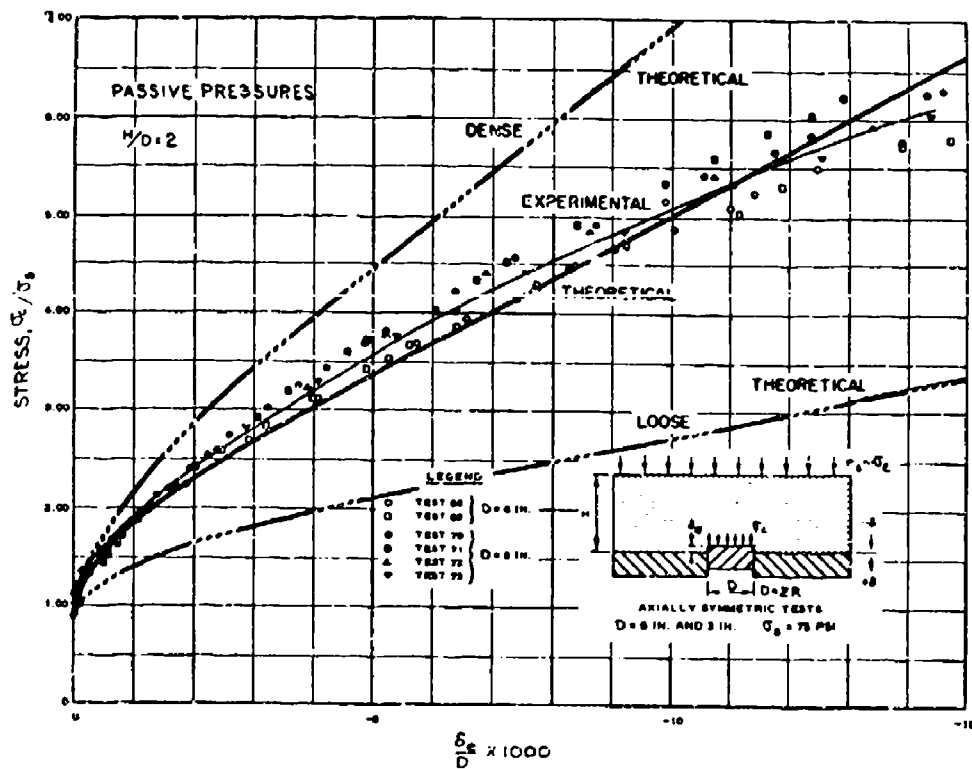


B. COMPARISON OF EXPERIMENTAL DATA BY McNULTY AND THEORY BY MASON AND ASSOCIATES - ACTIVE PRESSURES.

Figure 31. Comparison of Theoretical and Experimental Trapdoor Active Pressures



A. COMPARISON OF EXPERIMENTAL DATA BY McNULTY AND THEORY BY MASON AND ASSOCIATES-PASSIVE PRESSURES.



B. COMPARISON OF EXPERIMENTAL DATA BY McNULTY AND THEORY BY MASON AND ASSOCIATES-PASSIVE PRESSURES.

Figure 32. Comparison of Theoretical and Experimental Trapdoor Passive Pressures

Walter-Kriebel-Kaplan (1971) but not Mason, describes the design and evaluation of the URS free field stress gauge, shown in Figure 11 of this report. A similar pressure cell was developed and used by Askegaard (1963), Figure 35b. The 1971 URS report presents the following simplification of Equation 77a

$$\frac{\sigma_e}{\sigma_s} = \frac{\sigma_c - \sigma_s}{\sigma_s} = \sqrt{\frac{B}{R} \left(1 - \frac{M_3}{M_c} \right)} \quad (79)$$

which may be used for small differential deformations, $\delta_e = \delta_s - \delta_c$, but it yields diagrams of greater curvature and departure from linear relations than Equation 77a. The simplified Equation 79 indicates that the error or overstress is a function of the square root of (B/R) , whereas the original simplified theory shows that (σ_e/σ_s) is a linear function of (B/R) , and this result was also found in many experiments by Peattie and Sparrow (1954) with both sands and clays, Figure 27b. Furthermore, a rigorous mathematical analysis of the stresses at and in a rigid ellipsoidal inclusion in an elastic matrix yields a nearly linear relation between stresses in the matrix and in the inclusion, Figure 35c, Askegaard (1963). The 1971 URS report presents results of tests with the Mason-URS stress gage in reconstituted and consolidated clays, and the agreement between the test results and the theory is generally satisfactory. However, the test data and Equations 77-79 do not agree well with published experiments by Peattie and Sparrow (1954), WES (this report), and others, especially when considering that the experiments were performed with stress gages having a much greater thickness-diameter ratio than the Mason-URS gage. The 1971 URS report will not be reviewed in greater detail, because it was published after the official cutoff date for publications to be considered in this report, and because of the above mentioned areas of disagreement, which will require considerable clarification of the test data to permit a reliable comparison. However, the URS-Mason theory is an improvement of several other proposed and approximate solutions of the problem. It should be noted that the registration ratio, σ_c/σ_s , is not determined

by indentations and the Boussinesq equations but by progressive solution of the equations by Mason and associates, summarized in this section.

Special problems at rigid boundaries

79. Objectives and definitions. The action of pressure cells built into a rigid wall or slab has been analyzed by several investigators, using the indentation analogy, the trapdoor analogy, finite annular elements, or more rigorous mathematical methods. The principal papers or methods are summarized in the following paragraphs. Comparisons are in some cases facilitated by expressing the Boussinesq indentation equation for a flat and rigid punch

$$\delta_e = \sigma_e \frac{\pi}{4} D \frac{1 - \nu^2}{M_s} \quad (9 \text{ bis})$$

in terms of the total differential load on the cell

$$P_e = \frac{\pi}{4} D^2 \delta_e$$

which yields

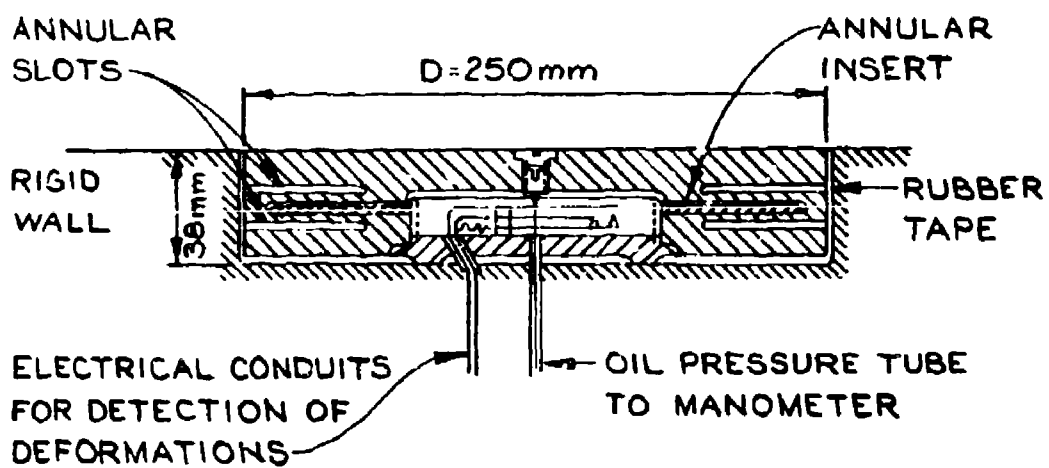
$$\delta_e = \frac{P_e}{D} \frac{1 - \nu^2}{M_s} \quad (80a)$$

and inversely

$$P_e = \frac{\delta_e D M_s}{1 - \nu^2} \quad (80b)$$

where δ_e is uniform for the entire area of a rigid punch. These equations apply to the free surface of a semi-infinite elastic body. Correction factors must be added when the equations are used for the indentation of an elastic boundary within a compressible matrix.

80. Swedish pressure cell. Kallstenius and Bergau (1956) report on the development of a soil pressure cell for use in rigid walls, Figure 33. The face of the cell is fully active and rather heavy so that



FROM KALLSTENIUS AND BERGAU (1956)

FIGURE 33. KALLSTENIUS-BERGAU SOIL PRESSURE CELL FOR RIGID WALLS.

it will not be damaged by coarse backfill. The interior of the cell is filled with oil, and its pressure is measured by an outside manometer, which is a part of a closed hydraulic system. The amount of oil in the system, and the influence of temperature changes, is reduced by annular plate inserts. The faces of the cell move in proportion to the pressure changes and the flow of oil to the manometer. The measured pressures and deflections were compared to those corresponding to the Boussinesq indentation equations (7 and 80), which indicated that it was necessary to use a correction factor of 1.7 or a soil modulus of 1.7 times M_s , and even then some underregistration was encountered. Deviations were attributed to the influence of several factors, primarily the boundary conditions and the small size of the test bin. It should be noted that calibration factor for soil will not be the same as for water or air, since the latter may enter the peripheral slots in the cell.

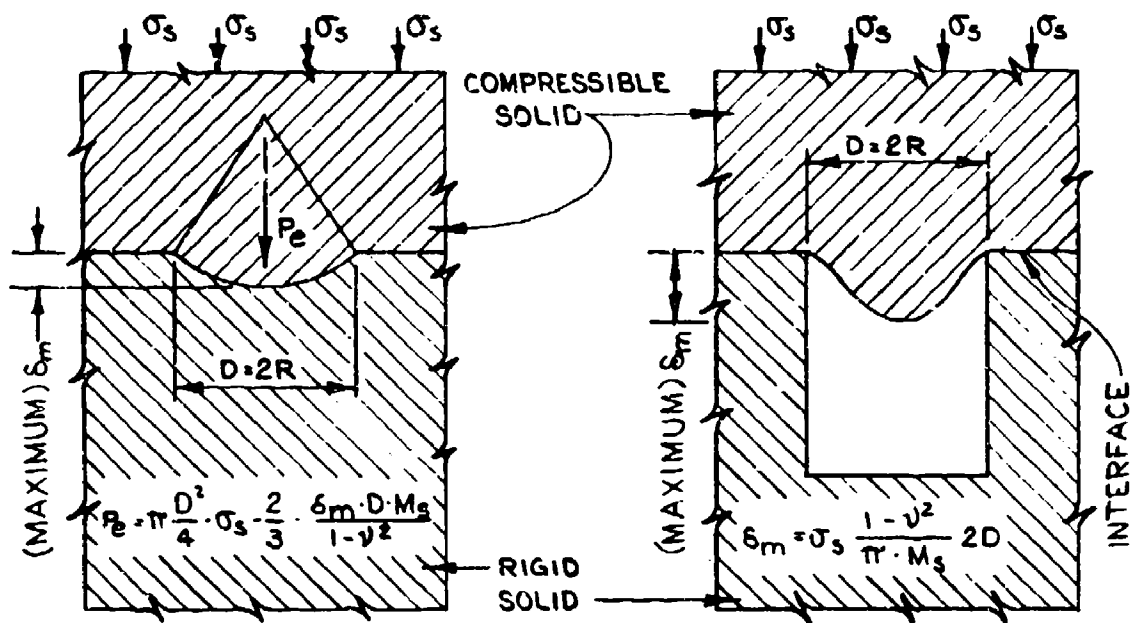
81. Spherical surface cavity. Walén (1942) has developed theoretical expressions for stresses in a compressible elastic material which is forced into a spherical surface depression or cavity in a more rigid material. The original paper by Walén was not available to the writer, and the following comments are based on quotations and references in other papers. According to Askegaard (1959), Walén found that the pressure on the walls of a shallow spherical surface cavity are those shown in Figure 34a, or

$$P_e = \frac{\pi}{4} D^2 \sigma_s - \frac{2}{3} \delta_m D \frac{M_s}{1 - \nu^2} \quad (81)$$

Kallstenius and Bergau (1956) state that Walén also found that contact between the bottom of the cavity and the compressible elastic material is discontinued when

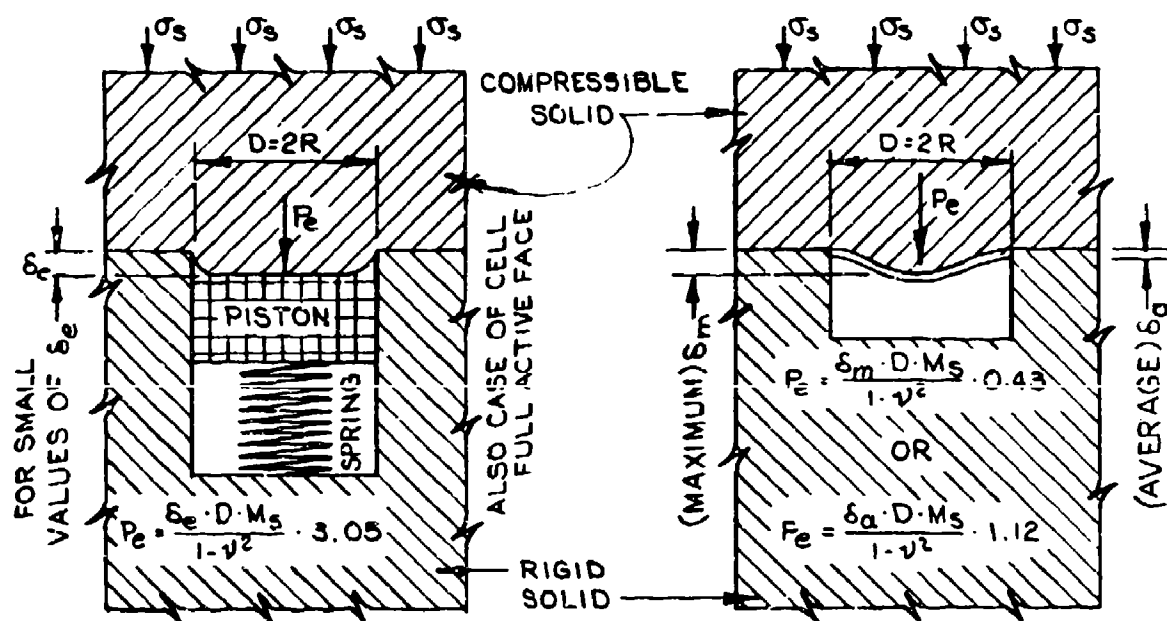
$$\delta_m > \frac{1}{2} \sigma_s D \frac{1 - \nu^2}{M_s} \quad (82)$$

Cessation of contact at the bottom does not necessarily indicate that



A. SPHERICAL RECESS, WALEN 1942, ASKEGAARD 1959.

B. OPEN HOLE-SMOOTH INTERFACE, GRAVESEN 1959-B.



C. HOLE AND PISTON, GRAVESEN-ASKEGAARD, 1959.

D. HOLE AND DIAPHRAGM, ASKEGAARD, 1961.

NOTE: COEFFICIENT IN ALL EQUATIONS ARE AVERAGE FOR SMALL DEFLECTIONS.

FIGURE 34. SOIL DEFORMATION AND PRESSURE CONDITIONS AT RIGID WALLS.

P_e in Equation 81 is zero. In these equations δ_m is the maximum depth of the cavity. The equations could also be rewritten in terms of the average depth for comparison with the Boussinesq indentation equation, but it is also stated by Askegaard (1959), that the Boussinesq equations are not valid at a rigid boundary.

82. Hole in rigid wall. Gravesen (1959-B) has developed equations for stresses and deformations in an elastic material bounded by a rigid wall with a circular hole. Actually, the problem was converted into the inverse problem of stresses and deformations in the elastic material loaded in succession with a single force, a circular line load, and finally a uniform load on a circular area with a diameter equal to that of the hole. With a smooth rigid wall or an interface which does not exert any restrictions on lateral movements, Gravesen found that the maximum deflection of the elastic material into the hole, Figure 34b, may be expressed by

$$\delta_m = \frac{\sigma_s D}{\pi M_s} 2(1 - \nu^2) \quad (83)$$

On the other hand, when the rigid wall is rough, and lateral movement of the elastic material is completely restricted, the maximum deformation in the center of the hole is reduced to

$$\delta_m = \frac{\sigma_s D}{\pi M_s} \frac{(1 + \nu)(3 - 4\nu)}{2(1 - \nu)} \quad (84)$$

The difference between deflections for the two conditions depends on the Poisson ratio. The difference attains a maximum of 25 percent for $\nu = 0$ and it decreases with increasing values of ν to zero for $\nu = 0.5$. It is emphasized that these deformations apply to an elastic material, and it is tacitly assumed that σ_s and D are smaller than those which would cause plastic deformations. The above mentioned data were later used in determination of the forces on a piston in the hole or on a pressure cell with a fully active face plate.

83. Hole with piston in rigid wall. When a hole in a rigid wall is provided with a piston and a spring, as shown in Figure 34c, the conditions correspond to those of a pressure cell with a fully active face plate. A theoretical solution of this problem has been developed by Gravesen (1959), who uses his theory concerning a hole in a rigid wall, discussed in the foregoing paragraph, in combination with loads, stresses, and deflections of annular segments. The results are presented in the form of tables and a few closed equations. Askegaard (1959, 1961) discusses applications of these theories and verified them experimentally, using an artificial material, "araldite," which obeys Hooke's law even at relatively large strains. As the piston is pushed into the hole, the area of contact between the piston and the outside elastic material decreases, and the relation between the total pressure on the piston, P_e , and the deflection, δ_e , is curved and not linear as in cases represented by the Boussinesq and Walén indentation equations. However, the decrease of the area of contact is nearly negligible and the relation between P_e and δ_e is practically linear for very small deformations such as those occurring in a pressure cell. For such small deformations P_e may be determined approximately by, quoting Askegaard (1959), and assuming that there is no friction between the compressible material and the rigid wall,

$$P_e = \delta_e \frac{DM_s}{1 - \nu^2} 3.05 \quad (85)$$

or with

$$P_e = \sigma_e \frac{\pi}{4} D^2$$

$$\delta_e = \sigma_e \frac{D}{M_s} \frac{\pi}{4} \frac{1 - \nu^2}{3.05} \quad (86)$$

According to Equations 6 and 10, the corresponding values N_s and K_s are

$$N_s = \frac{\sigma_e^D}{\delta_e} = 3.05 \frac{4}{\pi} \frac{M_s}{1 - \nu^2} \quad (87)$$

and

$$K_s = \frac{N_s}{M_s} = 3.05 \frac{4}{\pi} \frac{1}{1 - \nu^2} \quad (88)$$

That is, the values of P_e , N_s , K_s , and the cell error or under-registration are 3.05 times as large as those obtained by the simplified theory for a cell in a free field. The theory and numerical values of the coefficients were verified in small-scale tests on elastic materials by Askegaard. The calibration factors for changes in air and water pressures may or may not be the same as those for changes in soil pressures, depending on the design of the pressure cell.

84. Hole with diaphragm in rigid wall. Askegaard (1961) has also investigated stresses and deformations at a hole covered by a fixed but flexible diaphragm, Figure 34d. The problem is solved by means of finite annular elements and the requirement that the deflections of the diaphragm should be equal to the deformations of the soil for the same annular loading conditions. The approximate solution of the problem may be expressed by the following equation, for the average incremental force is Askegaard (1961), page 12,

$$P_e = \delta_m \frac{DM_s}{1 - \nu^2} 0.43 \quad (89a)$$

where δ_m is the maximum deflection in the center of the diaphragm. Substituting δ_m with the average deflection, δ_a , yields the equation

$$P_e = \delta_a \frac{DM_s}{1 - \nu^2} 1.12 \quad (89b)$$

which is about one-third of the force on a piston, Figure 34c.

Equation 89 yields values of P_e which are slightly larger than those obtained by the Boussinesq equations for a pressure cell in a free field and a fully active face plate. The arrangement in Figure 34d may serve as a pressure cell at a rigid boundary when the cavity below the diaphragm is filled with a liquid which acts on an smaller measuring diaphragm in the bottom of the cavity.

85. A pressure cell in a free field with an inactive rim and exposed diaphragms presents a problem similar to that for a hole with a flexible diaphragm, but the stress increase caused by the inclusion effect of the entire cell must also be considered. Tory and Sparrow (1967) have solved these problems, using the methods by Askegaard and matrix inversion. It was found that the cell error can be expressed as a function of the

$$\text{Flexibility Ratio} = \frac{M_s \cdot d^3}{E_c \cdot D^3} \quad (90)$$

where E_c is Youngs modulus for the cell material, d is the diameter of the diaphragm, D diameter of the cell, and the other parameters are defined in Figure 37. Simplified final equations similar to Equation 89 are not presented, but the simultaneous equations are arranged for computer solution. A diagrammatic solution for a specific case is shown in Figure 37; it is seen that the cell error decreases with the overall thickness-diameter ratio of the cell and with increasing flexibility ratio. It is assumed that Poisson's ratio is 0.5 for the soil and 0.33 for the cell material. Several minor assumptions and simplifications have been made in obtaining these solutions, the results in Figure 34b are only approximately correct.

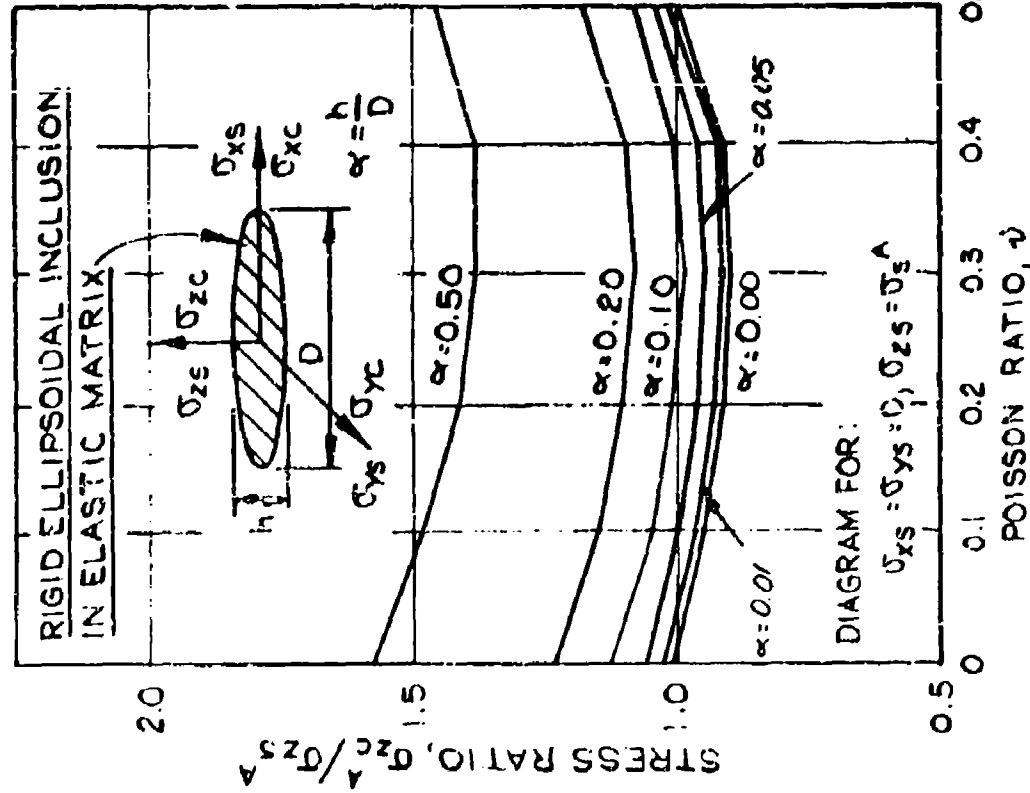
Ellipsoidal inclusion in a free stress field

86. Initial investigations. The theories discussed in the foregoing paragraphs deal primarily with stresses and deformations normal to the face of a pressure cell; the effect of lateral forces and the Poisson ratio is only partially considered. A rigorous solution with

full consideration of all stresses and strains is very difficult to obtain by conventional mathematical methods. However, Eshelby (1957) found that simplifying conditions exist for an axisymmetrical ellipsoidal inclusion in a uniform matrix, and that the strains in such a body are uniform and can be expressed by elliptical integrals. On basis of the Eshelby equations, Askegaard (1963) obtained equations for stresses in a rigid elliptical inclusion and also for the pressure in a liquid-filled ellipsoidal cavity, as summarized in the following paragraphs and figures. In general, it is assumed that the inclusion is infinitely rigid, and that the materials in the surrounding matrix, or soil, are isotropic and fully elastic. It is also assumed that both normal and tangential forces can be transferred between the inclusion and the matrix without slippage. Stresses in the matrix are designated by σ_{xs} , σ_{ys} , σ_{zs} and those in the inclusion by σ_{xc} , σ_{yc} , σ_{zc} , whereas stresses caused by a uniaxial stress change will be indicated by the superscript "A" and those caused by a triaxial or hydrostatic stress change are designated by the superscript "T."

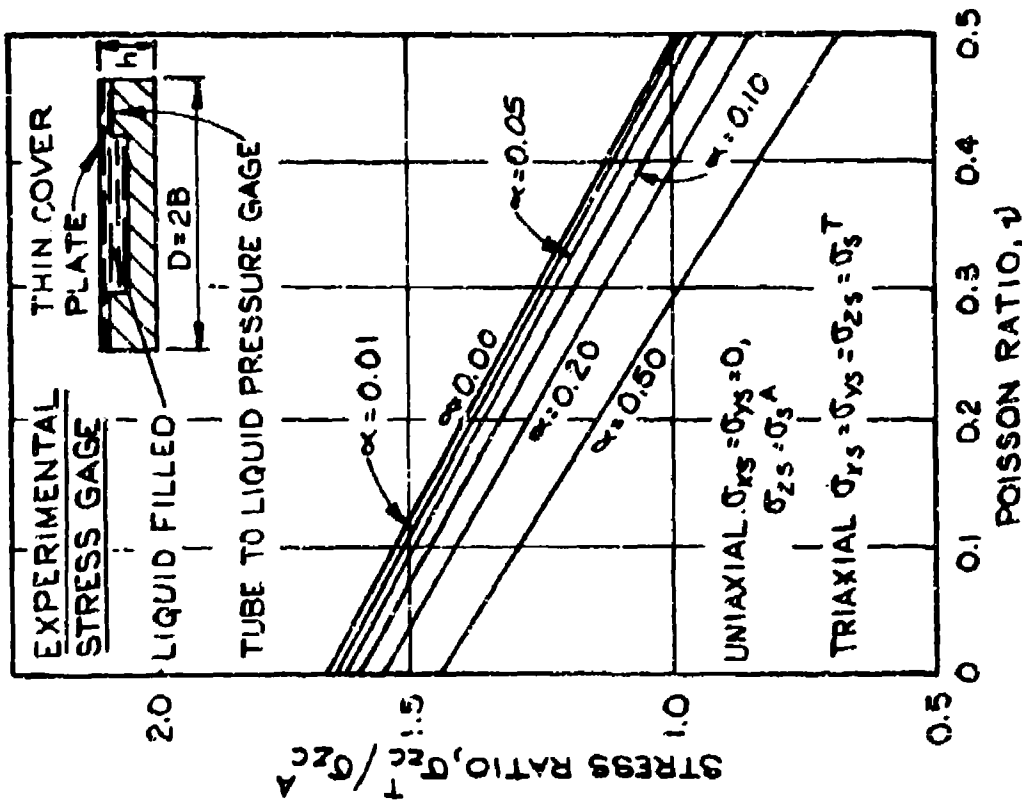
87. Rigid ellipsoidal inclusion. The solutions obtained by Askegaard (1963) for stresses in a rigid ellipsoidal inclusion are presented in the form of short equations in tensor notation and also as much longer series of equations in conventional mathematical notation. A graphical summary of the results are shown in Figure 35 which are supplemented by tables in the text. The stresses caused by a uniaxial stress change in the matrix are shown in Figure 35a, where the stress ratio ($\sigma_{zc}^A / \sigma_{zs}^A$) is plotted as a function of the Poisson ratio, ν . In contrast to data obtained by the simplified theory, the influence of ν is small but not negligible; it is a maximum for medium values of the ratio and attain minima for $\nu = 0$ and $\nu = 0.5$.

88. The stresses caused by a triaxial or hydrostatic stress change in relation to those caused by a uniaxial stress change are shown in Figure 35b as a function of the Poisson ratio, ν , and the thickness-diameter ratio, h/D . The ratio ($\sigma_{zc}^T / \sigma_{zc}^A$) also indicates the influence of lateral stresses. Figure 35b shows that axial stresses in the inclusion may be increased by an increase of the lateral stresses in



MATRIX OR SOIL: $\sigma_{xs}, \sigma_{ys}, \sigma_{zs}$, OR σ_s
 INCLUSION: $\sigma_{xc}, \sigma_{yc}, \sigma_{zc}$, OR σ_c

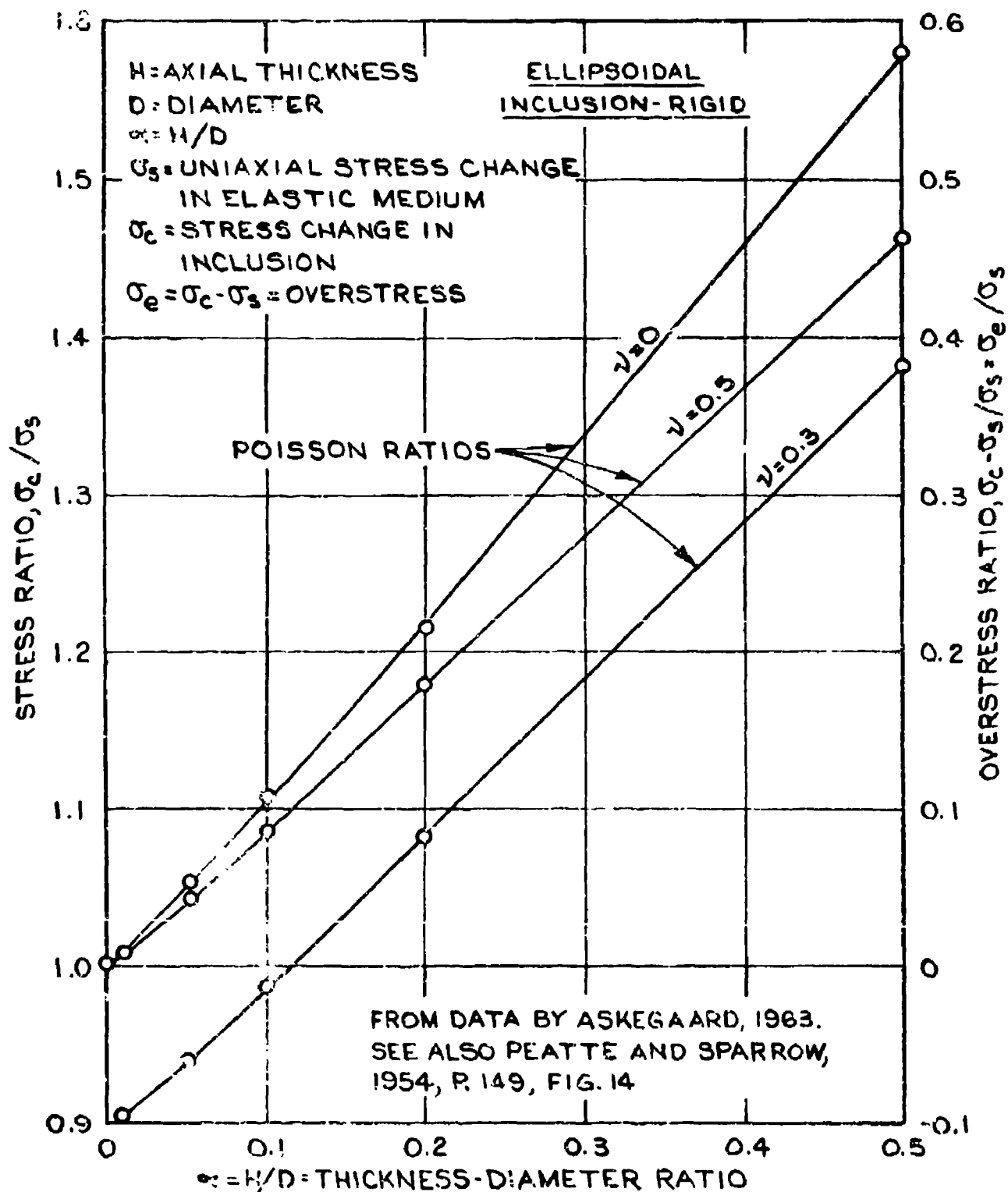
A. UNIAXIAL STRESS CHANGE IN MATRIX.



FROM ASKEGAARD, 1963

B. TRIAXIAL STRESS CHANGE IN MATRIX.

FIGURE 35. STRESSES IN AND AT RIGID ELLIPSOIDAL INCLUSIONS.



C. INCLUSION STRESS VERSUS CELL THICKNESS-DIAMETER RATIO

FIGURE 35. (CONTINUED)

matrix when the thickness-diameter ratio of the inclusion is small, but such an increase in axial stresses in the inclusion may change to a decrease for larger values of h/D combined with large values of ν . Therefore, generalization of the results of a numerical analysis of a specific problem, or given values of h/D and ν may be misleading, as will be shown in later paragraphs.

89. The simplified analysis of soil-cell interaction, Equations 19 and 20, as well as initial experiments by Peattie and Sparrow (1954), Figure 27b, show that errors in pressure cell indications are nearly linearly proportional to the height-diameter ratio of the cell, h/D . These relations can also be deduced from the figures and tables in the paper by Askegaard (1963), which are shown in Figure 35c for minimum, medium, and maximum values of ν . This figure verifies the results of the simplified analysis and of experiments by Peattie and Sparrow, but it disagrees with theoretical data by Mason and Associates, Equation 79, which indicate that the error in cell registrations is proportional to the square root of h/D .

90. Liquid-filled ellipsoidal cavity. Askegaard (1963) also investigated the changes of pressures in a liquid filling an ellipsoidal cavity in a uniform elastic matrix. Both uniaxial and triaxial stress changes in the matrix are considered. The pressure in the liquid, p , was found to be a function of the stress change in the matrix, the relative compressibilities of matrix and liquid, the height-diameter ratio of the cavity, and the Poisson ratio for the matrix. The pressure in the liquid approaches the axial stress change in the matrix with decreasing height-diameter ratio of the cavity. Some of the principal relations are summarized in Figure 36, which also shows that the pressures in the liquid are much less sensitive to changes in lateral stresses in the matrix than are the stresses in a rigid inclusion, Figure 35b. This insensitivity to changes in lateral stresses would be of great advantage in stress measurements, but it is difficult to produce suitable cavities in undisturbed soil. However, several types of cells for measuring soil stresses are based on measuring pressure changes in a liquid filling a very shallow cavity in the cell.

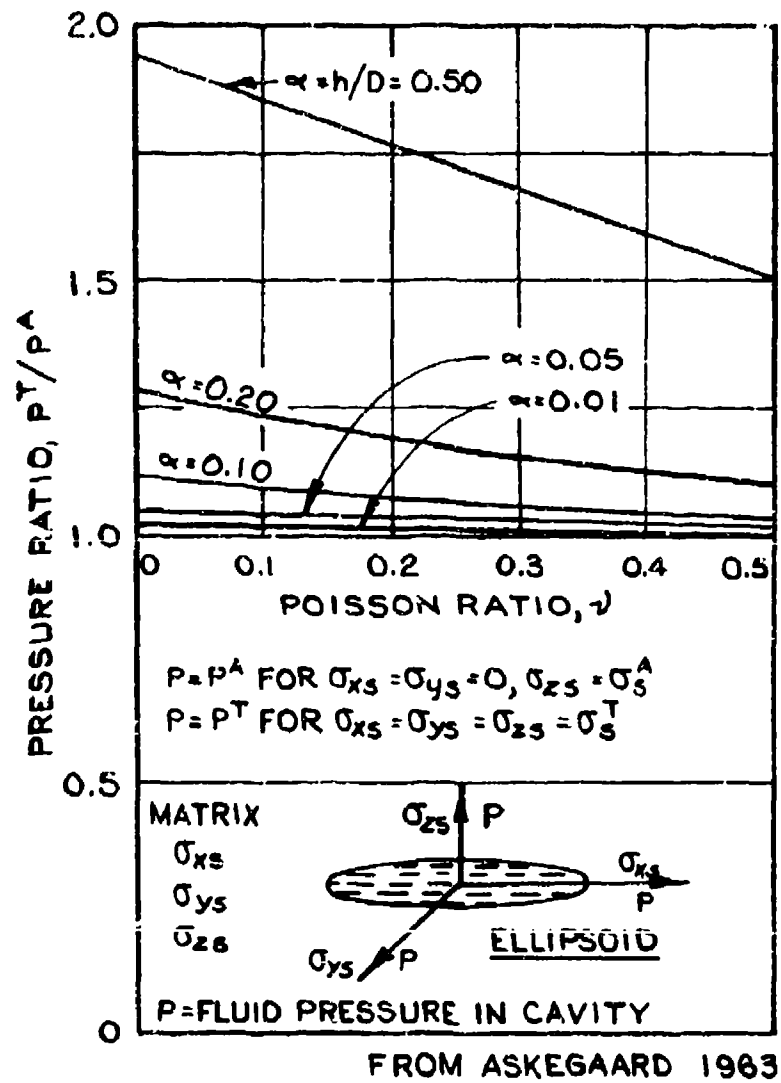


FIGURE 36. STRESSES IN FLUID FILLED ELLIPSOIDAL CAVITY.

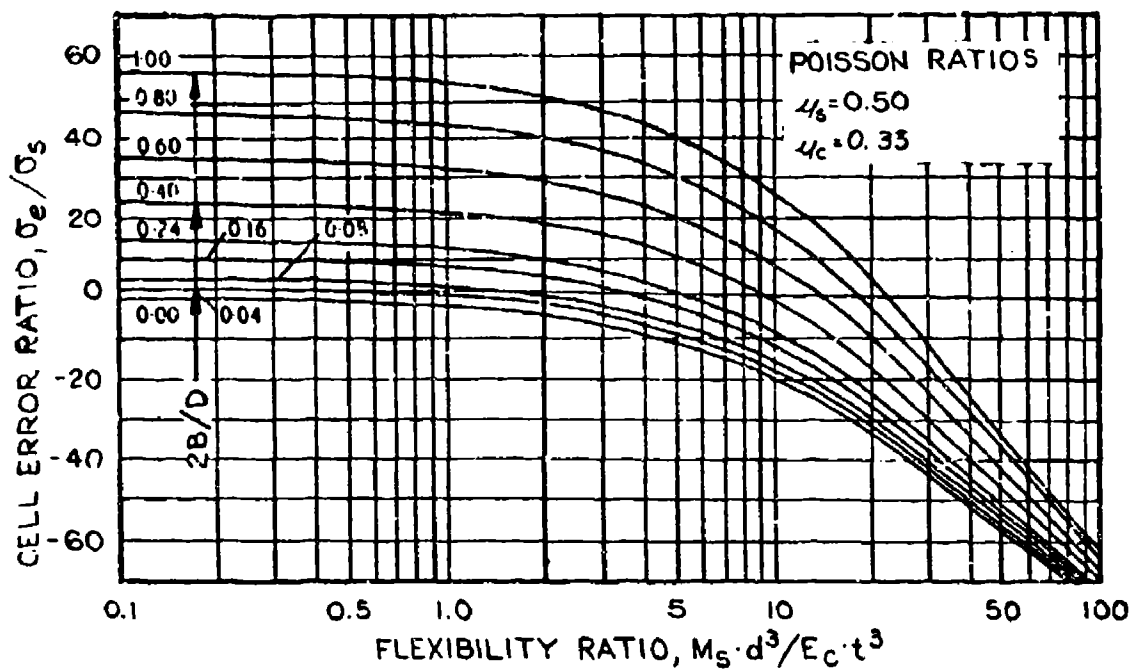
91. Experimental data. Stress relations discussed in the foregoing paragraphs and shown in Figures 35 and 36, represent theoretical data. Askegaard attempted to obtain verification of the theories by small-scale laboratory experiments. He used a 20- by 20- by 20-cm cube of an elastic plastic, araldite, as the matrix and the type of pressure cell outlined in Figure 35b for the stress measurements. The results verified the general form and trend of the theoretical relations, but there were minor numerical differences in individual tests. These deviations are probably caused by representing a semi-infinite matrix by a small cube, and by using a thin cylindrical disk instead of an ellipsoidal inclusion. It should be noted that the theories by Askegaard are based on free field stress conditions.

Finite element method of analysis

92. Introductory comments on method. Investigations of soil-cell interaction discussed in the foregoing paragraphs were in some cases based on extensive simplifications of the problem, and in other cases solutions were obtained by use of annular elements. The latter are in fact a type of finite element analysis, but solution of corresponding simultaneous equations were obtained by progressive approximations or iteration but without modern electronic computers. The finite element method combined with a computer provides a very versatile tool for investigating soil-cell interaction for most shapes and properties of the pressure cell or inclusion, stress conditions and soil properties, and it can be applied for both linear and nonlinear stress-strain conditions and also to pressure cells with an inactive rim. However, in most cases the method yields only a numerical solution for specific values of the independent variables and not a general solution of the problem. Introduction of the finite method of analysis by Bates (1969) is most commendable, although initial investigations yielded the expected result that changes in radial stresses also caused material changes in axial stresses and in stress indications by the pressure cell. This result agrees with the findings by Askegaard (1959), since a height-diameter ratio of 1/6 and a Poisson ratio $\nu = 0.3$, used by Bates, indicates an increase of axial stresses for an increase of radial stresses,

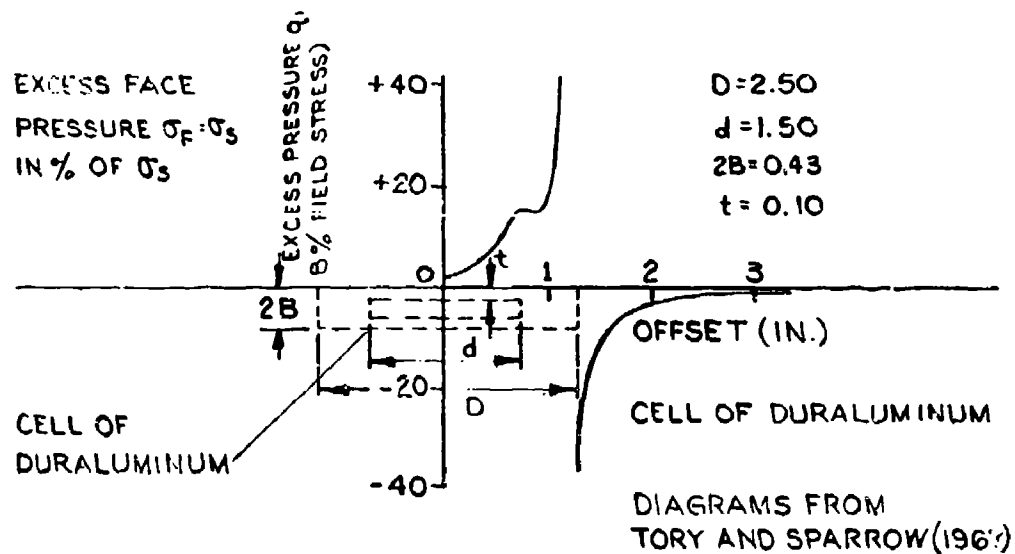
Figure 35b. However, this figure also shows that an increase in radial stresses may cause a decrease of axial stresses when the height-diameter ratio, h/D , and the Poisson ratio, ν , are large. Bates found that the influence of the radial stresses on the axial stresses could be decreased materially by tapering the outer rim of the cell, or giving it a lenticular form. The result is shown in Figure 12 and is called the SMRL pressure cell since it was designed in the Spokane Mining Research Laboratory (SMRL). It was also found that the sensitivity to radial stresses in one direction can be decreased by arranging the strain gages of the diaphragm linearly in a perpendicular direction. So far, the SMRL pressure cells have been built with two maximum capacities, 1000 psi for use in tunnels and 100 psi for shallow soil applications. In the following review it is assumed that the cells are used under free field stress condition.

93. Analysis of the SMRL soil pressure cell. The principles of the finite element method of analysis are assumed to be known and are not described in the paper by Bates or in this report. The initial and principal analysis by Bates utilizes a conventional triangular grid, Figure 38a. It appears, but not stated directly, that the analysis is two-dimensional in character and applies to a section through the center of the cell. A limited analysis was also made with an axisymmetrical, quadrilateral grid, Figure 38a, but computer programs for such elements were not fully developed at that time. The data obtained by the conventional analysis were used to construct equal stress contours as shown in Figures 39 and 40 for axial and radial stress changes in the matrix. The stresses acting on the surface of the diaphragm can be determined from these contours. The ratio between the average stress on the surface of the diaphragm, σ_c , and the field stress, σ_s , represents the overstress or inclusion effect, and it is shown in Figure 41 as a function of the modulus of the matrix. For this cell and the moduli assumed for soil and steel, the inclusion effect is 9.5 percent for axial loads, and it increases to 54 percent for radial loads. These results indicate that the overregistration of a soil stress cell depends not only on the dimension of the cell and on the deformations of soil and cell but also



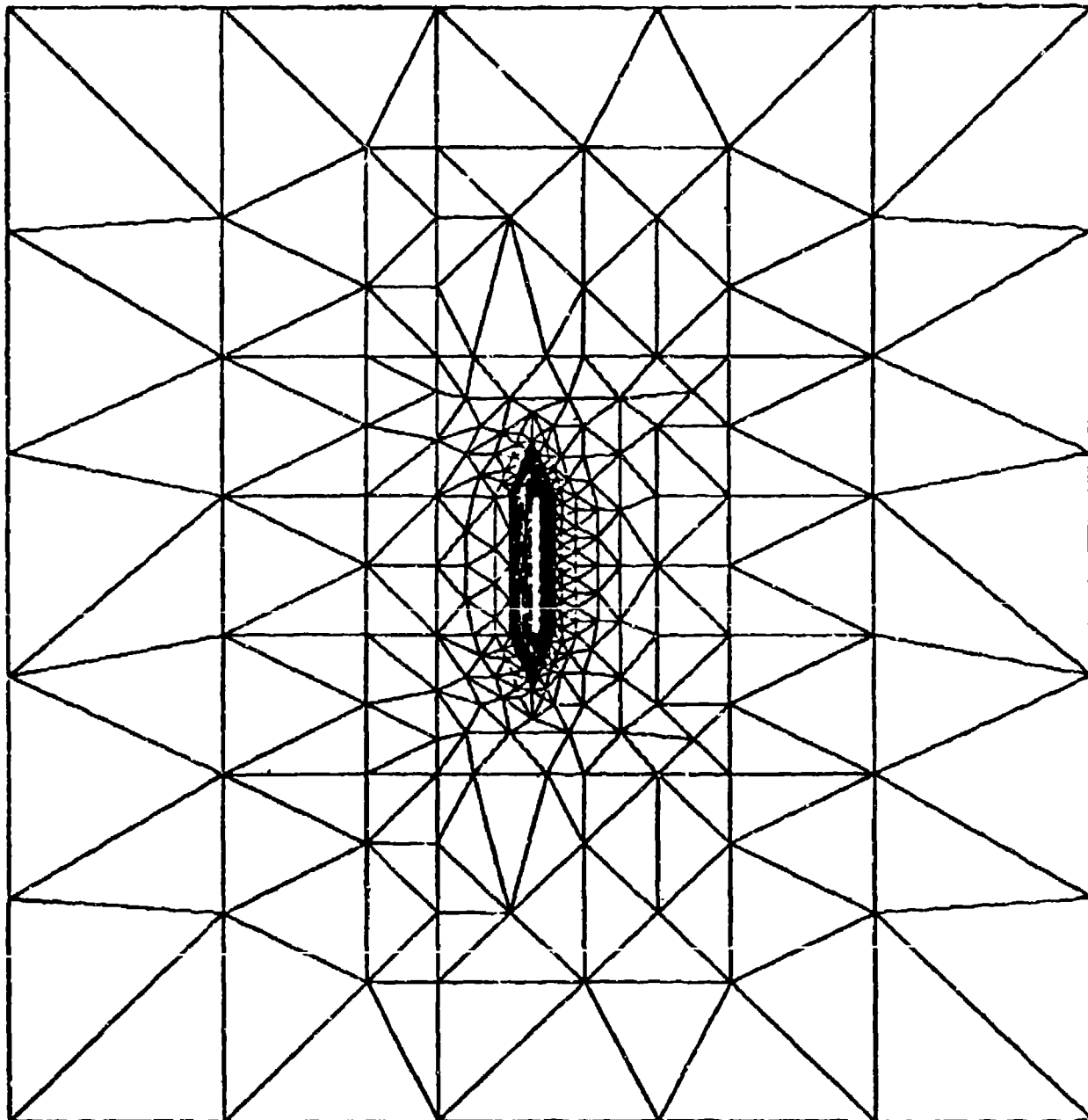
M_s = MODULUS OF DEFORMATION FOR SOIL
 E_c = YOUNG'S MODULUS FOR CELL MATERIAL

A. CELL ERROR RATIO VERSUS FLEXIBILITY RATIO.



B. VARIATION OF NORMAL STRESS ON CELL FACE

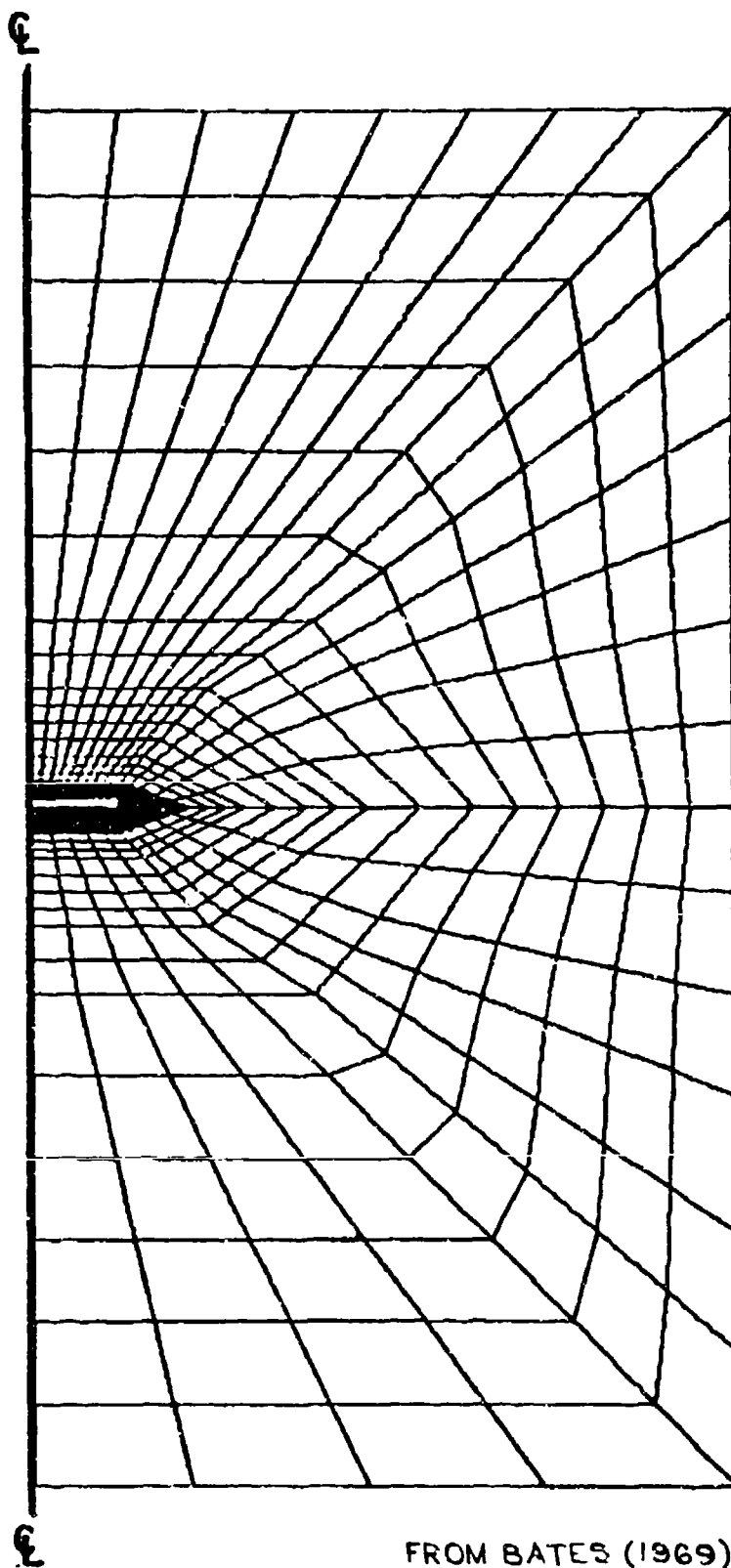
FIGURE 37. STRESSES ON CELL WITH INACTIVE RIM AND EXPOSED DIAPHRAGMS.



From Bates (1969)

A. TRIANGULAR FINAL ELEMENT GRID

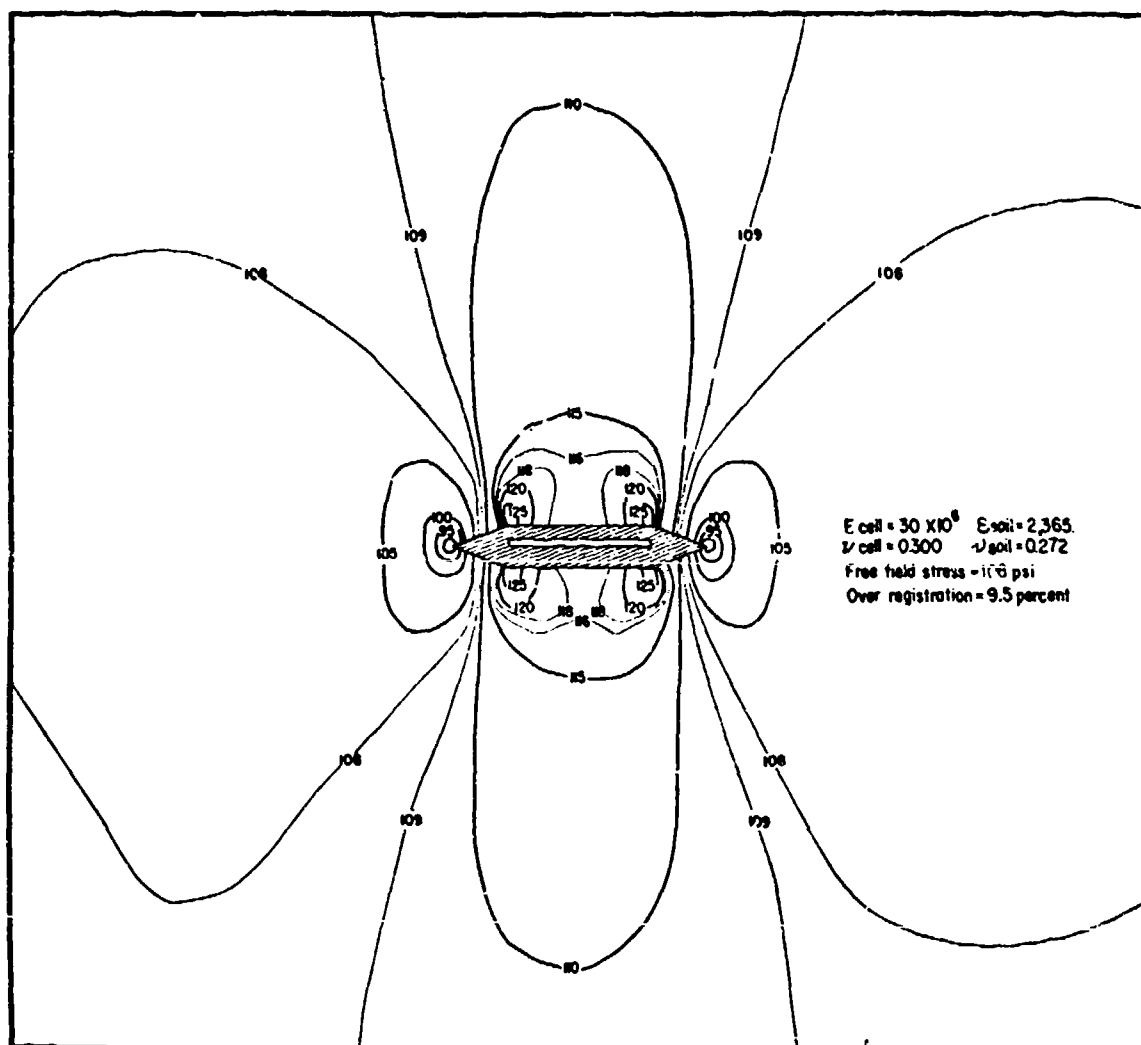
FIGURE 3G GRIDS FOR FINITE ELEMENT ANALYSIS OF THE SMRL SOIL PRESSURE CELL.



FROM BATES (1969)

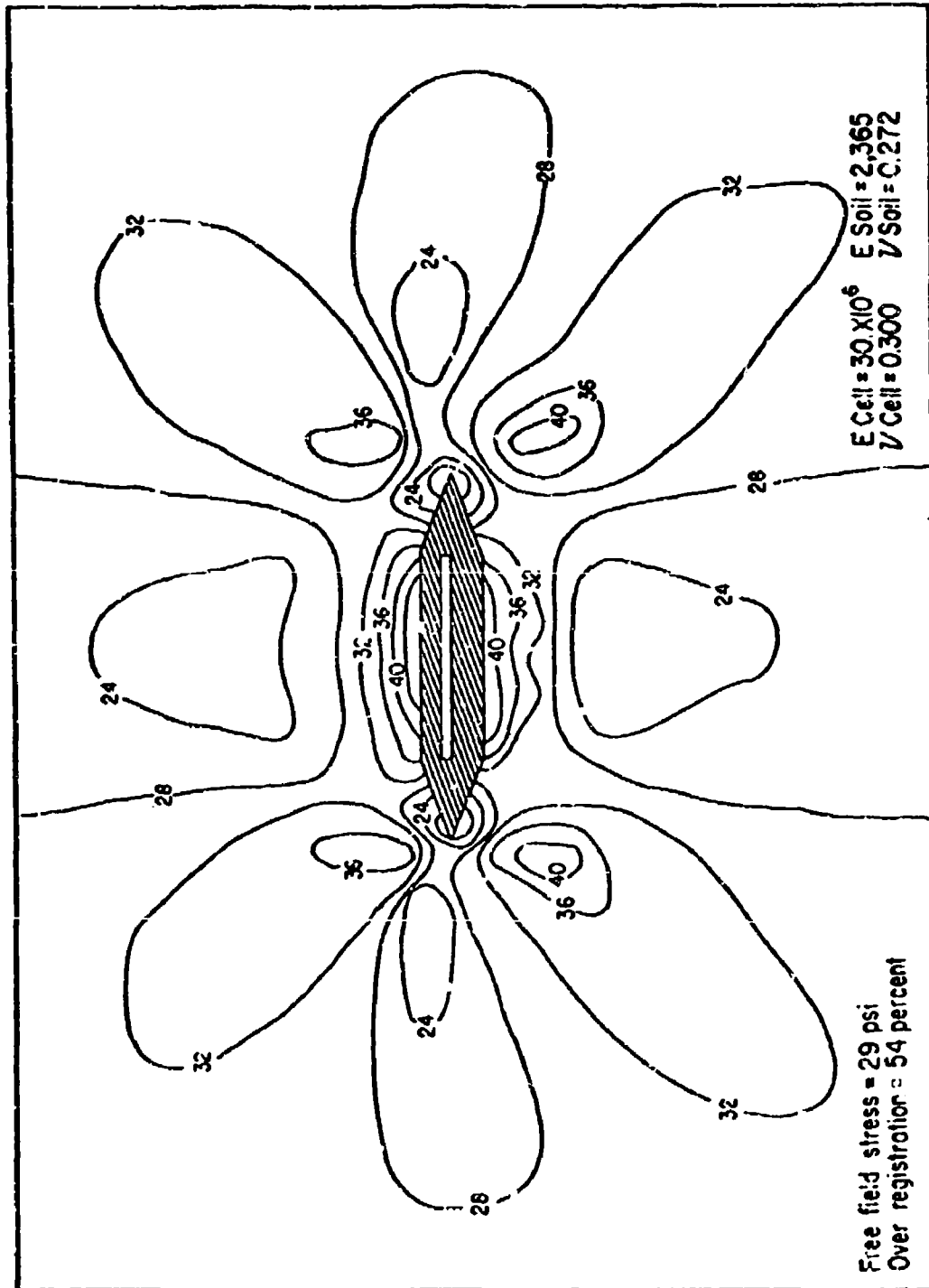
B. AXISYMMETRIC QUADRILATERAL GRID

FIGURE 3B (CONTINUED)



FROM BATES (1969)

FIGURE 39. STRESS DISTRIBUTION ON THE SMRL PRESSURE CELL
FOR AXIAL MAJOR STRESS.



FROM BATES (1969)

FIGURE 40. STRESS DISTRIBUTION ON THE SMRL PRESSURE GAGE FOR LATERAL MAJOR STRESS.

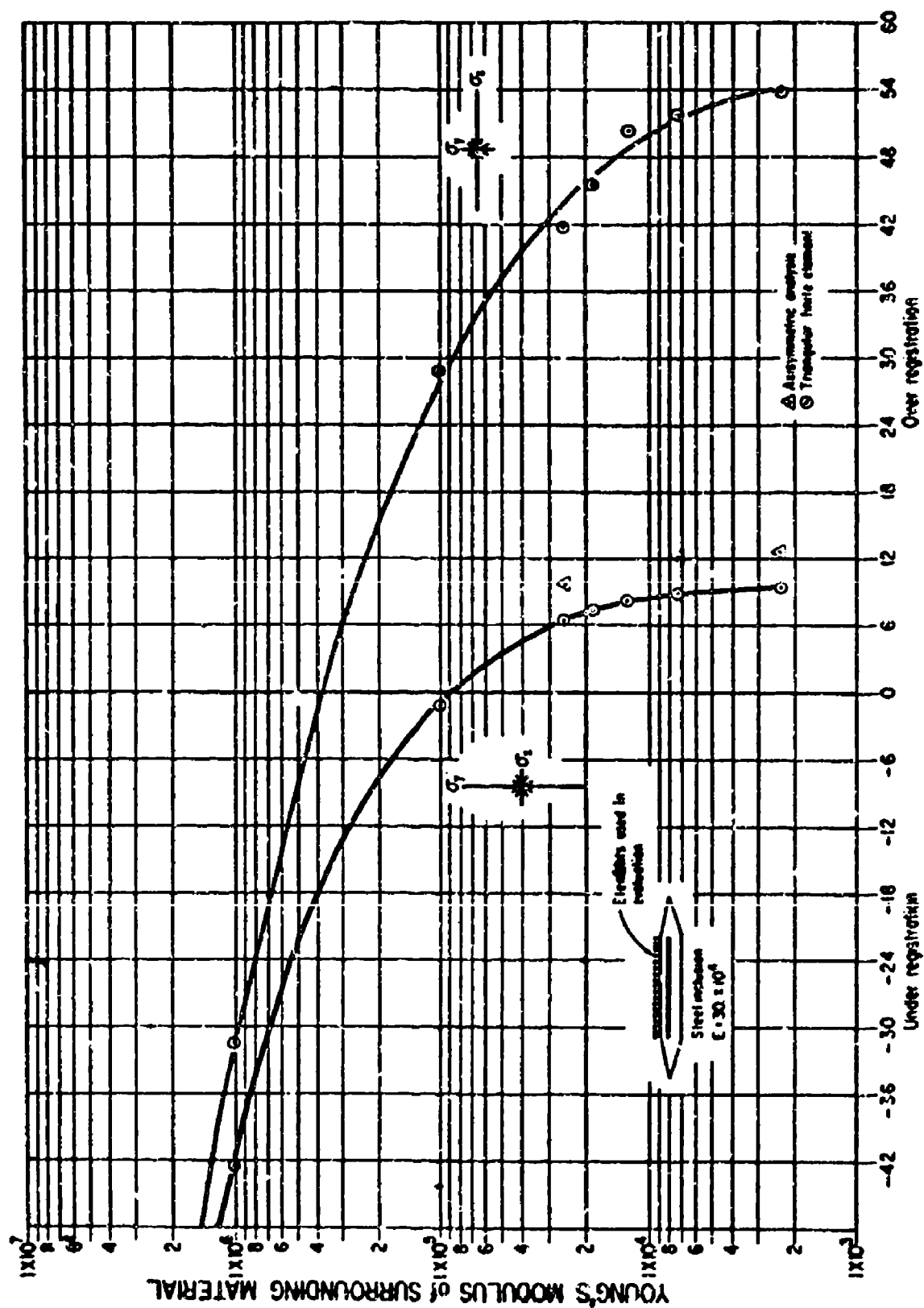
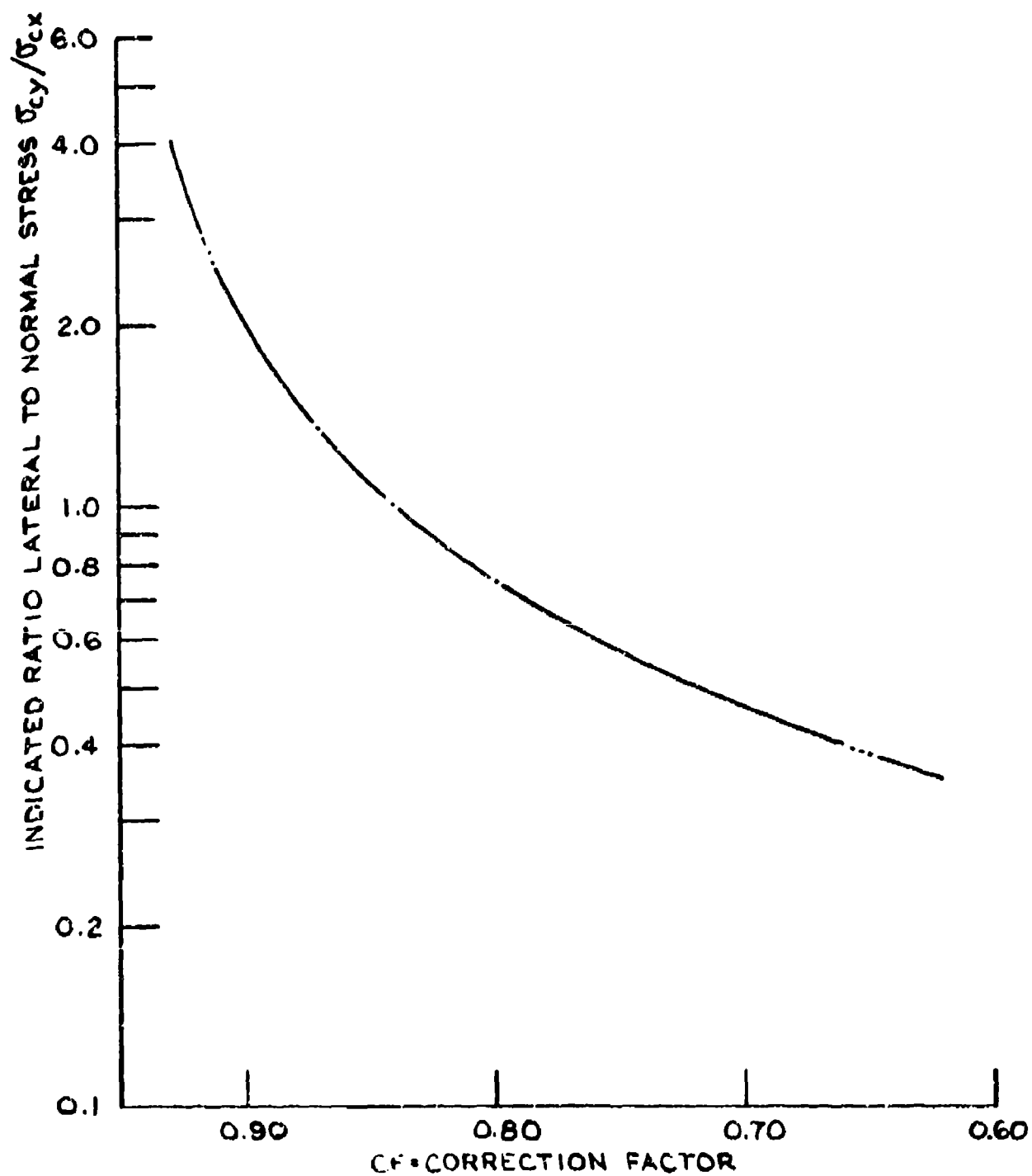


FIGURE 41. INCLUSION EFFECT OF THE SMRL SOIL PRESSURE GAGE.

on the ratio of axial to radial stress changes in the soil or matrix. It would be desirable to find a shape of the cell which would yield the same registration ratio or have the same calibration factor for horizontal and vertical positions for the cell.

94. Calibration and correction factors. The SMRL cells were calibrated for uniform axial loads in equipment similar to that used by the WES, Figure 5. The results of such a calibration must be modified by a correction factor which is a function of the various independent variables including the ratio of axial to lateral stresses. The cells were also tested in a relatively small test bin with sand. The bin had a rectangular cross section, 20 by 22 in., and was 30 in. high. Ingenious auxiliary equipment and procedures were developed for taking the influence of the sidewall friction into consideration, and the results obtained agree fairly well with the theory. Finally, Bates developed a diagram for the correction factor to be applied to the experimental calibration factor, Figure 42. This diagram applies only to the calibrated cell, to a soil with a Poisson ratio of 0.3, and to free field placement of the cell. The correction factor is presented as a function of the ratio of measured lateral and normal stresses on the cell, which represents a combination of several variables, and its reliability may possibly be subject to some limitations.

95. Advantages and limitations of a finite element analysis. One of the principal advantages of the finite element method of analysis is that it generally can be applied successfully when other currently available methods of analysis are too simplified to yield a sufficiently accurate, closed mathematical expression for the reliability or error in measurement of soil stresses. The finite element method can be used irrespective of stress conditions and stress history, for most designs of a cell or inclusion, for most properties of cell and soil, and for either no slippage or no friction or adhesion between cell and soil. It can be used to estimate the soil-cell interaction for a pressure cell with an inactive rim and an exposed measuring diaphragm, a problem which is very difficult to solve by means of other currently available methods. The principal limitation of the finite element method is that it yields



FROM BATES (1969)

FIGURE 42. CORRECTION FACTORS FOR CALIBRATION OF THE SMRL SOIL PRESSURE GAGE.

only a numerical solution for a specific set of values of the independent variables. Generalizations cannot safely be made from a single solution unless the influence of changes of the other variables is considered. The basic equations for deformations of individual elements are generally developed on the assumption that the materials are elastic and/or plastic; both linear and nonlinear stress-strain curves can be considered, but satisfactory methods for treating stress-strain diagrams which exhibit a peak strength followed by a decrease in strength under continuing deformation have not yet been developed. Furthermore, some soils are expansive, such as dense sands and strongly overconsolidated clays, and undergo a volume decrease by an increase in stress, which may yield an apparent value of the Poisson ratio greater than 0.5. Other soils, underconsolidated or only slightly overconsolidated may be subject to a volume decrease by an increase in pure shear stresses. These special manifestations of some soils require a revision of the constituent equations for their behavior when subjected to stress changes, and this applies not only to the finite element methods but to all other methods for analyzing stresses and strains in soils.

PART III: TRIAXIAL TESTS WITH SOIL PRESSURE
CELLS AT WES IN 1954-55

Background Data

Purposes of the WES tests

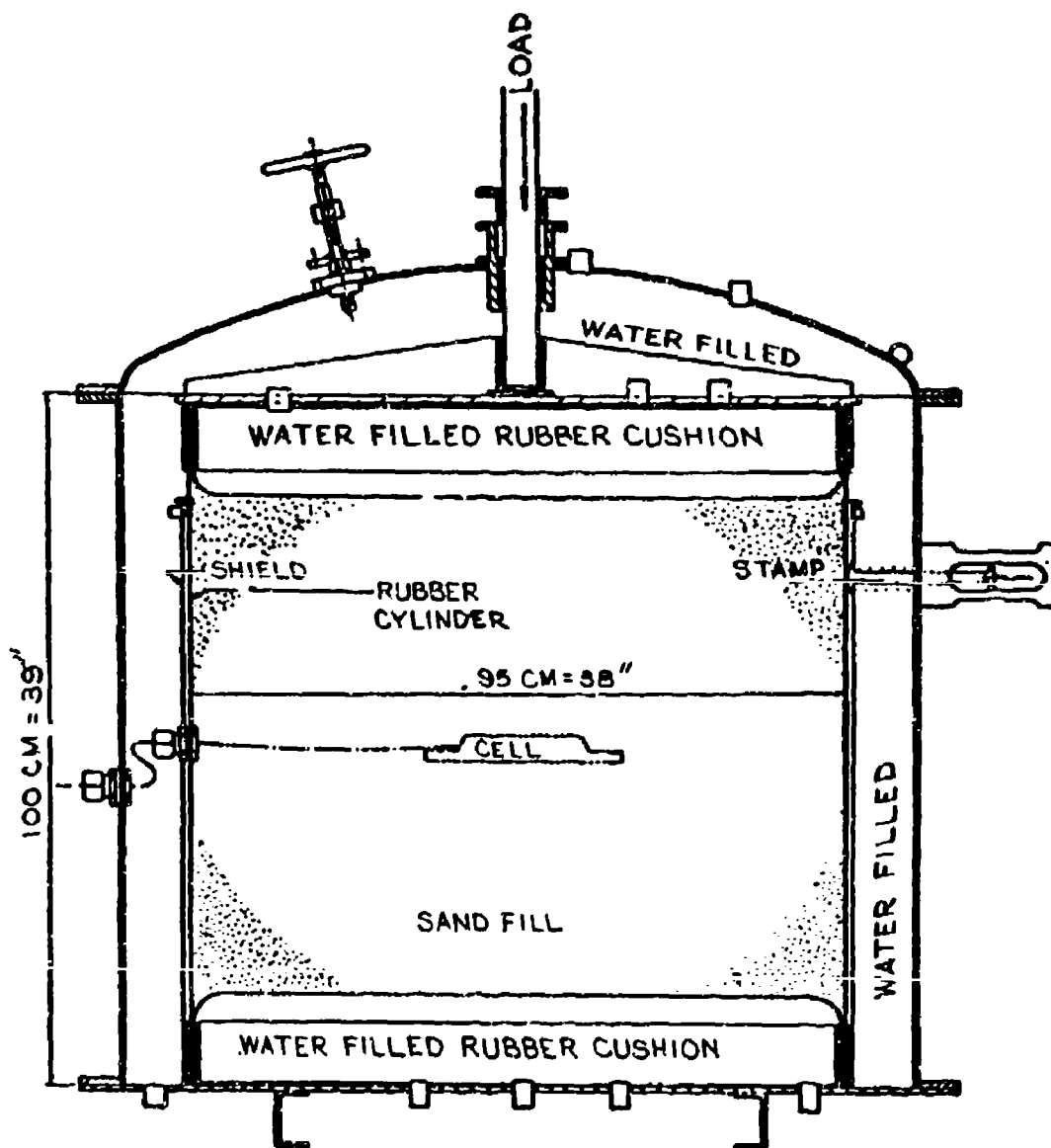
96. Initial tests with the WES soil pressure cells, described in the report of 1944, were performed with the pressure cells buried in sand in a fairly rigid and shallow container. The sand was subjected to known axial surface pressures, but the lateral or confining pressures could not be varied independently of the axial pressure and could not be determined accurately. Furthermore, sidewall friction caused the axial pressure in the sand to decrease with increasing depth. It was desired to perform tests on pressure cells in a triaxial device in which axial and lateral stresses could be varied independently of each other and where sidewall friction is eliminated. However, it was also known that the stress distribution in a triaxial test specimen might be nonuniform because of the influence of rough and rigid end plates. Therefore, the principal objectives of the triaxial tests with soil pressure cells were:

- a. To determine experimentally the existence and magnitude of nonuniformities of stress distribution within a large triaxial test specimen having the commonly used height-diameter ratio of 2:1.
- b. To verify or correct the standard calibration of the pressure cells and investigate the influence of lateral soil stresses or the orientation of a pressure cell with respect to the principal soil stresses.

A brief description of the equipment used in the above mentioned tests and a summary of the principal results obtained are presented in this report.

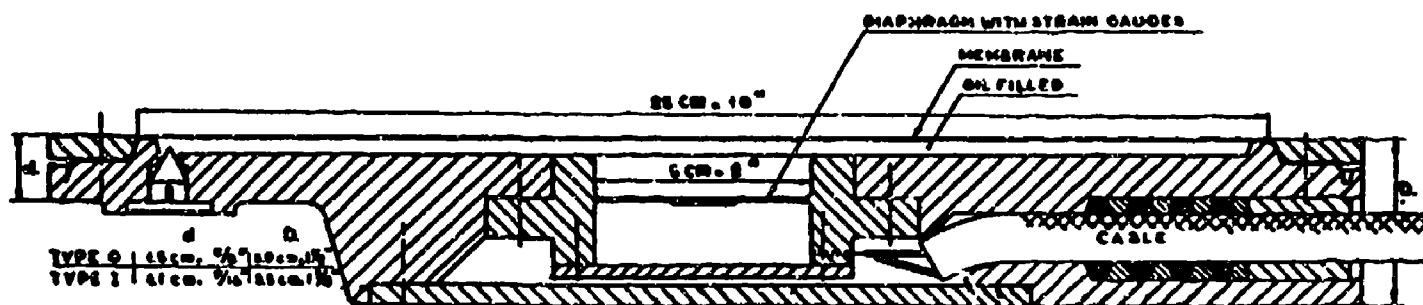
Early triaxial calibration tests

97. Plantema (1953) developed a short triaxial apparatus for calibration of large soil pressure cells, Figure 43. The pressure cell is placed in the center of the triaxial test specimen of sand, which has a diameter of 95 cm and a height of 62 cm, whereas the pressure cell had

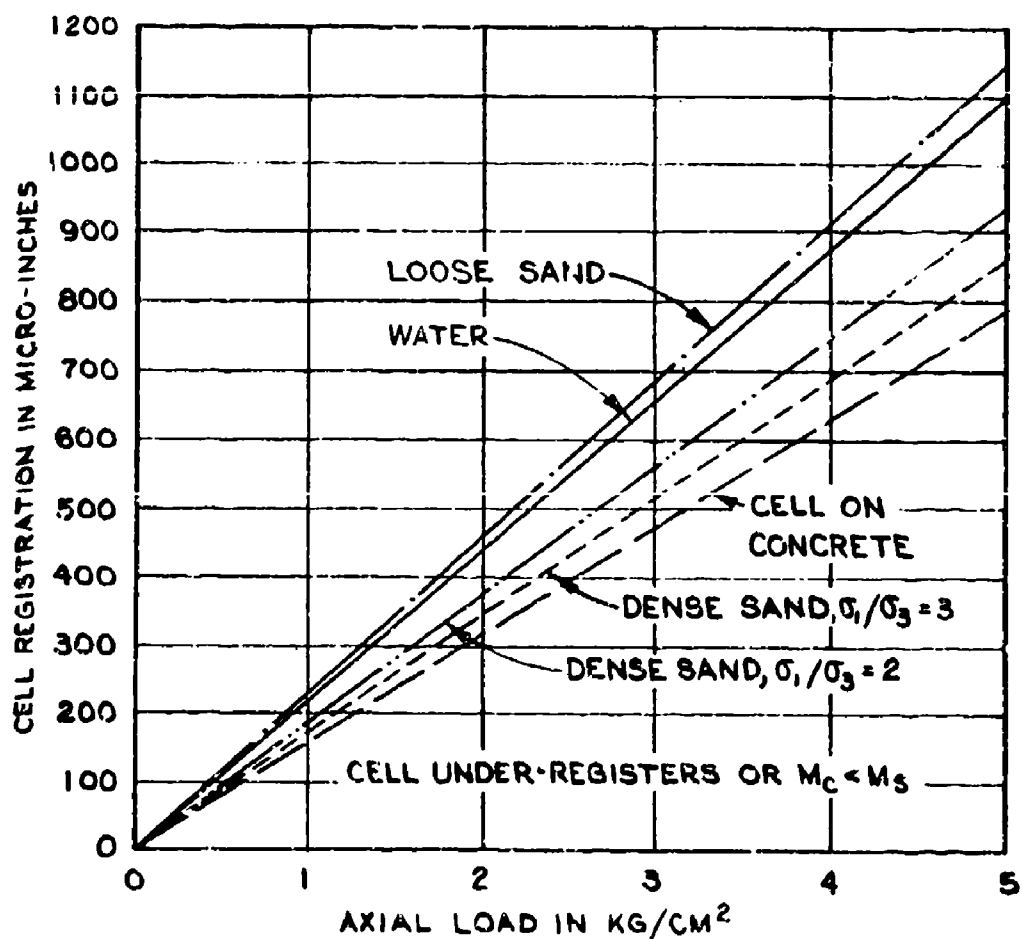


A. TRIAXIAL CALIBRATION EQUIPMENT

FIGURE 43. TRIAXIAL CALIBRATION TESTS BY
PLANTEMA, 1953.



B. SOIL PRESSURE CELL BY PLANTEMA



C. EXAMPLES OF CALIBRATION DIAGRAMS

FIGURE 43 (CONTINUED)

a diameter of 25 cm. Both the top and bottom end plates in the triaxial apparatus are provided with rubber-water cushions, which contribute to a more uniform distribution of the axial load. However, the restraining steel rims will cause some stress concentration along the cylindrical edge of the test specimen, and the influence of this stress concentration may extend to the midheight plane because of the small height-diameter ratio, but data on the actual stress distribution in the short test specimen are not available. The pressure cells were also designed by Plantema (1953) and had a face of a flexible membrane, fastened to a narrow rim and underlain by a thin layer of oil; the pressure in the oil was measured by means of a secondary diaphragm in the cell body. This cell should be satisfactory in fairly fine-grained soils and uniform stress conditions but it is probably also very sensitive to stress concentrations in gravelly and stony soils. The pressure cells were oriented to measure axial stresses, and it was found that the registration ratio increased with increasing ratios of radial to axial stress changes in the sand, which agrees in principle with the theoretical investigations by Askegaard (1963), Bates (1969).

Memoranda on the WES triaxial tests.

98. The WES triaxial tests on WES pressure cells were performed with a vacuum type triaxial apparatus and a test specimen with the commonly used length-diameter ratio of 2.0. A brief description of this apparatus and the raw test data obtained are presented in memoranda for the WES Stress Distribution Conferences of 1954 and 1955. Condensed descriptions of the equipment and summaries of the results obtained in the 1954 tests are given in the papers by Ahlvin (1956) and by Shockley and Ahlvin (1960). For convenience, a brief description of the equipment and testing procedures is also given in this report which contains a discussion of the test data obtained in both 1954 and 1955. As an introduction to this discussion, theoretical solution for the stress distribution in short and long cylinders with restrained ends and subjected to both uniaxial and triaxial stress changes is presented in the following two paragraphs.

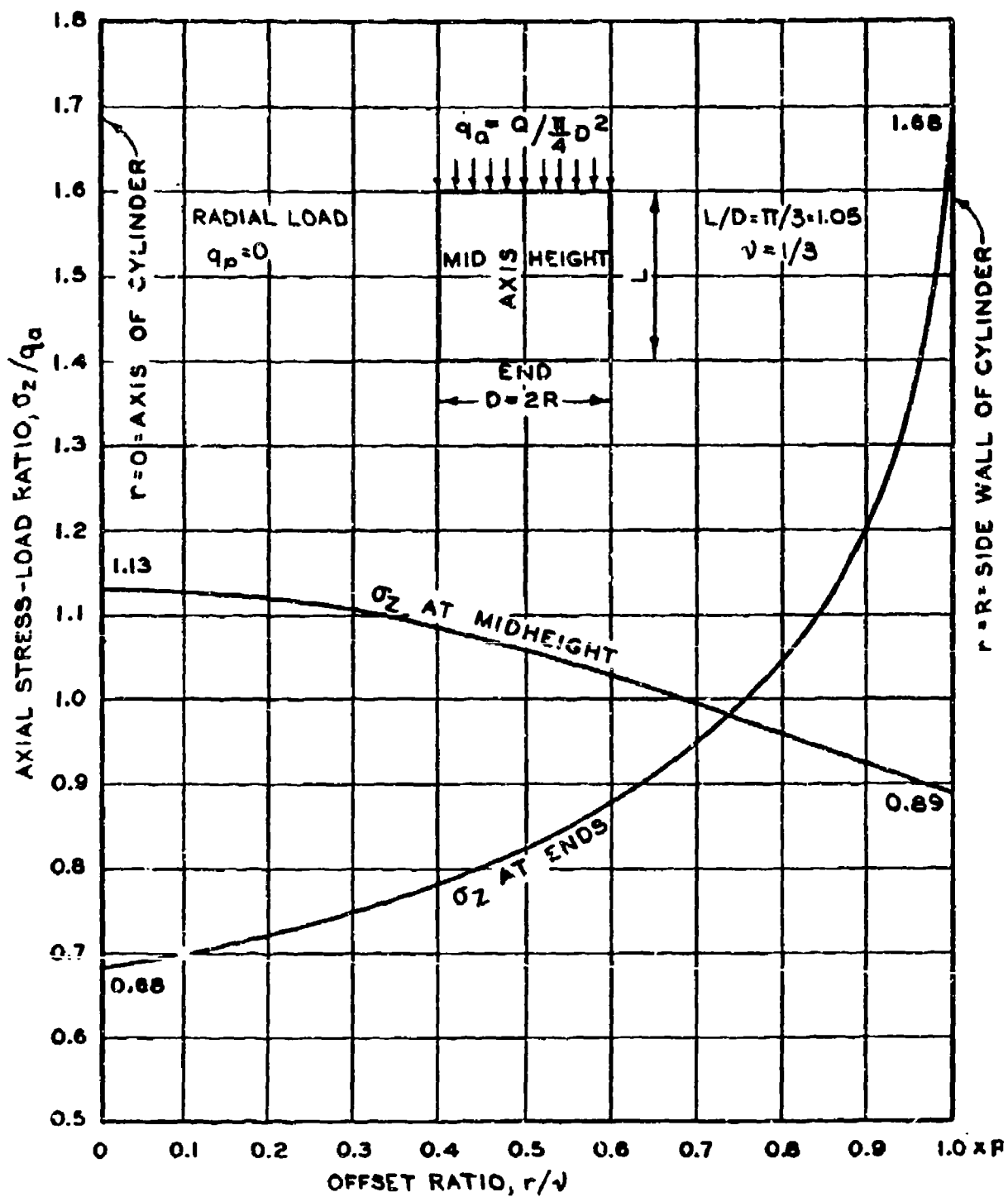
Theoretical Stress Distribution in Cylinders with Restrained Ends

Uniaxial compression of short cylinders

99. Until about 50 years ago, compression tests on metals, wood, rock, and concrete were usually performed on cubes and cylinders with a length-diameter ratio of about 1.0, and it was realized that the restraint caused by applying the compressive axial force through rough end plates created nonuniform stress conditions in the test specimens. Filon (1902) developed very completed solutions for the stress conditions in a test specimen with the length-diameter ratio of $\pi/3 = 1.05$ and subjected to uniaxial compression, q_a . He used rigorous mathematical methods for elastic materials and assumed that the end restraint is produced by fictitious narrow bands or radial surface forces at the ends, which were determined by the condition that the radial displacement at the circumferential surface should be zero at the ends. The results obtained for vertical or axial stresses, σ_z , on the end and midheight planes are shown in Figure 44. The axial stress at the center of the ends is only $0.68 \times q_a$ and it increases to $1.68 \times q_a$ at the cylindrical surface. The opposite variation occurs at the midheight plane where the vertical stress at the center is $1.13q_a$ and the stress at the surface is $0.89q_a$. Similar results for the axial stress were obtained by Pickett (1944) using the Fourier Series and by D'Appolonia and Newmark (1951) by means of the lattice analogy method. Pickett and D'Appolonia and Newmark assume a length-diameter ratio of 1.0 and that there is no displacement of any point on the end surfaces. These three investigations yielded good agreement on axial stresses but there are significant differences in the values obtained for radial, tangential, and shear stresses.

Triaxial compression of long cylinders

100. Triaxial tests on soils are commonly performed on a cylindrical test specimen with a length-diameter ratio of 2.0 and subjected to varying axial and radial loads. It was contemplated to use a similar test specimen and loading conditions in the tests with WES pressure



σ_z = THEORETICAL AXIAL STRESS
 q_a = AXIAL UNIT LOAD

FROM FILON (1902)

FIGURE 44. THEORETICAL AXIAL STRESS DISTRIBUTION IN RESTRAINED CYLINDER BY FILON.

cells. Balla (1961) succeeded in determining the stresses and strains in such a cylinder, using the theory of elasticity and a stress function. He assumes that the soil is elastic, that radial shear stresses vary linearly with the distance from the center, that the ends of the cylinder remain plane, and are acted upon by radial forces corresponding to the friction. In the numerical examples and tables it is further assumed that the friction is large enough to prevent any radial displacement and that the Poisson ratio is equal to $1/3$. The results obtained for two special loading conditions are shown in Figure 45. At the ends the vertical stresses for uniaxial compression are smallest in the center and the stress distribution resembles that obtained by Filon for a short cylinder. At midheight the vertical stresses are also largest in the center, but the numerical values of σ_z/q_a at the center of midheight are much smaller than for a short cylinder. These stress variations are reversed for uniform triaxial loading or $q_r = q_a$. At the ends the stresses attain a maximum at the center but reach a minimum there at midheight. Stress variations at the distance of $0.4 H$ from midheight are also shown and are nearly equal to those at midheight; this is of interest since the pressure cells in the 1955 tests were placed at a distance of 9 in. or $0.26 H$ above and below the midheight plane and 9 in. offset from the centerline of the tests specimen, Figure 51 (page 153). The theory of elasticity indicates that there should not be any radial displacements for the load ratio

$$\frac{\sigma_x}{\sigma_z} = \frac{\sigma_y}{\sigma_z} = \frac{\nu}{1 - \nu} = \frac{1}{2} \quad \text{for } \nu = \frac{1}{3} \quad (91)$$

These stress variations with a change in load ratios must be borne in mind when interpreting pressure cell indications for various ratios of the radial to axial unit loads. A solution for elastic conditions but without special assumptions for the shear stresses has recently been obtained by Brady (1971). The difference between the solutions by Balla and Brady occurs primarily at the end surfaces, and there is but little difference between the two solutions near midheight of the test specimen.

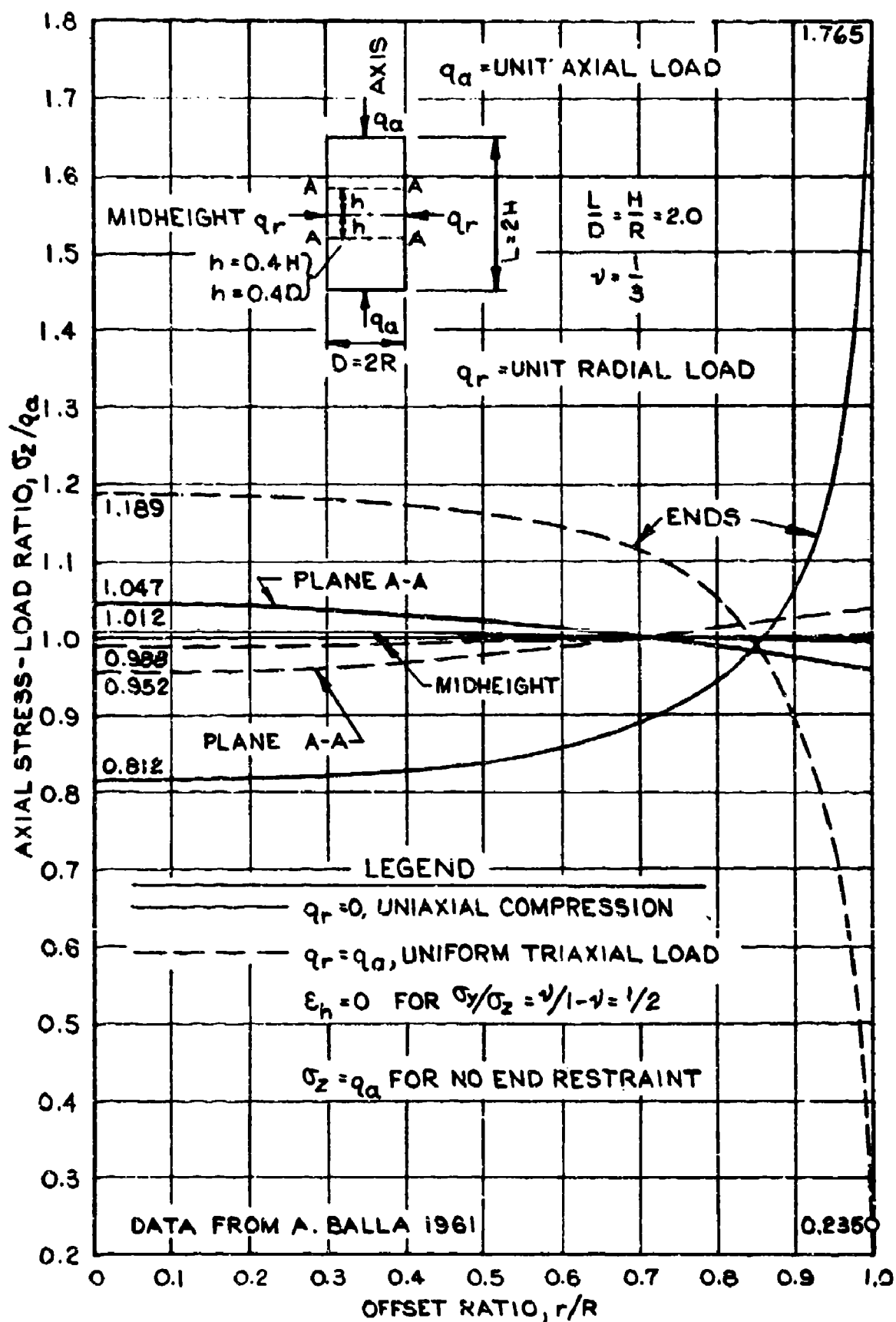


FIGURE 45. THEORETICAL AXIAL STRESS DISTRIBUTION IN RESTRAINED CYLINDER BY BALLA.

A solution for materials with nonlinear stress-strain relations has been proposed by Girijavallabhan and Mehta (1969). Discussions in this report are based on the analysis by Balla (1961).

Testing Equipment and Procedures

General requirements

101. It was desired to test groups of 6-in. WES soil pressure cells and in separate tests individual 12-in. cells consisting of a 6-in. cell plus a 3-in. wide inactive rim. It was estimated that a test specimen about 3 ft in diameter and 6 ft long would be needed. A pressure vessel large enough to accommodate such a test specimen was not available, and the tests were performed in the open using vacuum in the test specimen to produce the radial or confining stresses, although the limitations of this method were realized. Tests were to be performed with both 50- and 100-psi WES pressure cells.

The WES large triaxial device

102. The device is shown in the photograph, Figure 46, and a schematic form of the testing arrangement is presented in Figure 47. The test specimen has a height of 70 in. and a diameter of 35.68 in. corresponding to a cross-sectional area of 1000 sq in. The specimen is confined by vulcanized rubber membrane and two rigid end plates. The upper plate is a hollow disk of internally braced welded steel plates. The lower plate consists of porous concrete within a shallow steel container with an outlet for cables to the pressure cells and a pipe to the vacuum pump. It rests on a reinforced concrete base plate. Axial loads are applied by a hydraulic jack through a load cell to a reaction truss, which had been used for other loading tests. Supports are provided for dials measuring axial and radial deformations, and strain meters were placed in some test specimens. The vacuum is produced by a hand operated pump and is measured at both top and bottom of the test specimen.

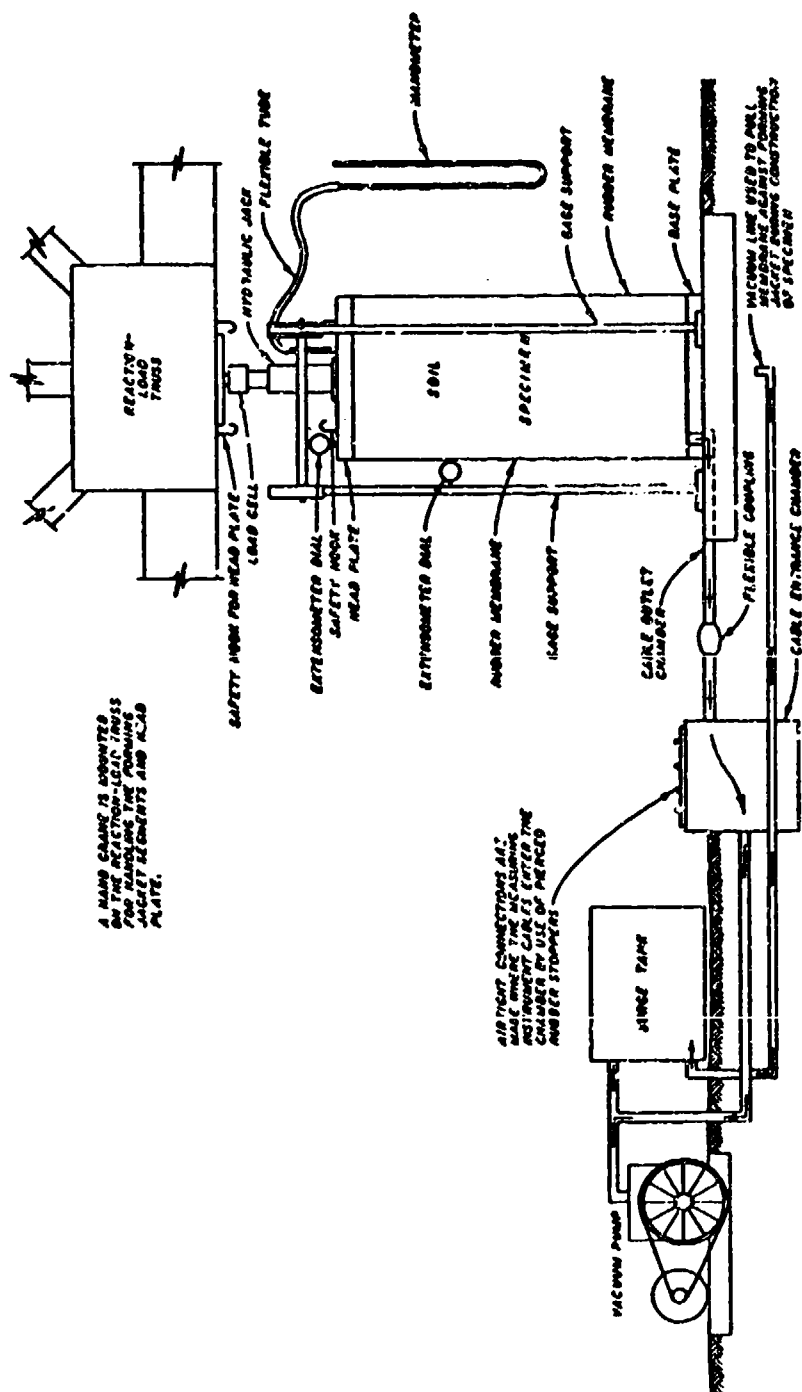
Soil used in tests

103. All tests were performed with a processed and air dry mortar



From Ahlvin (1956)

Figure 46. WES Large Triaxial Compression Device - Vacuum Type



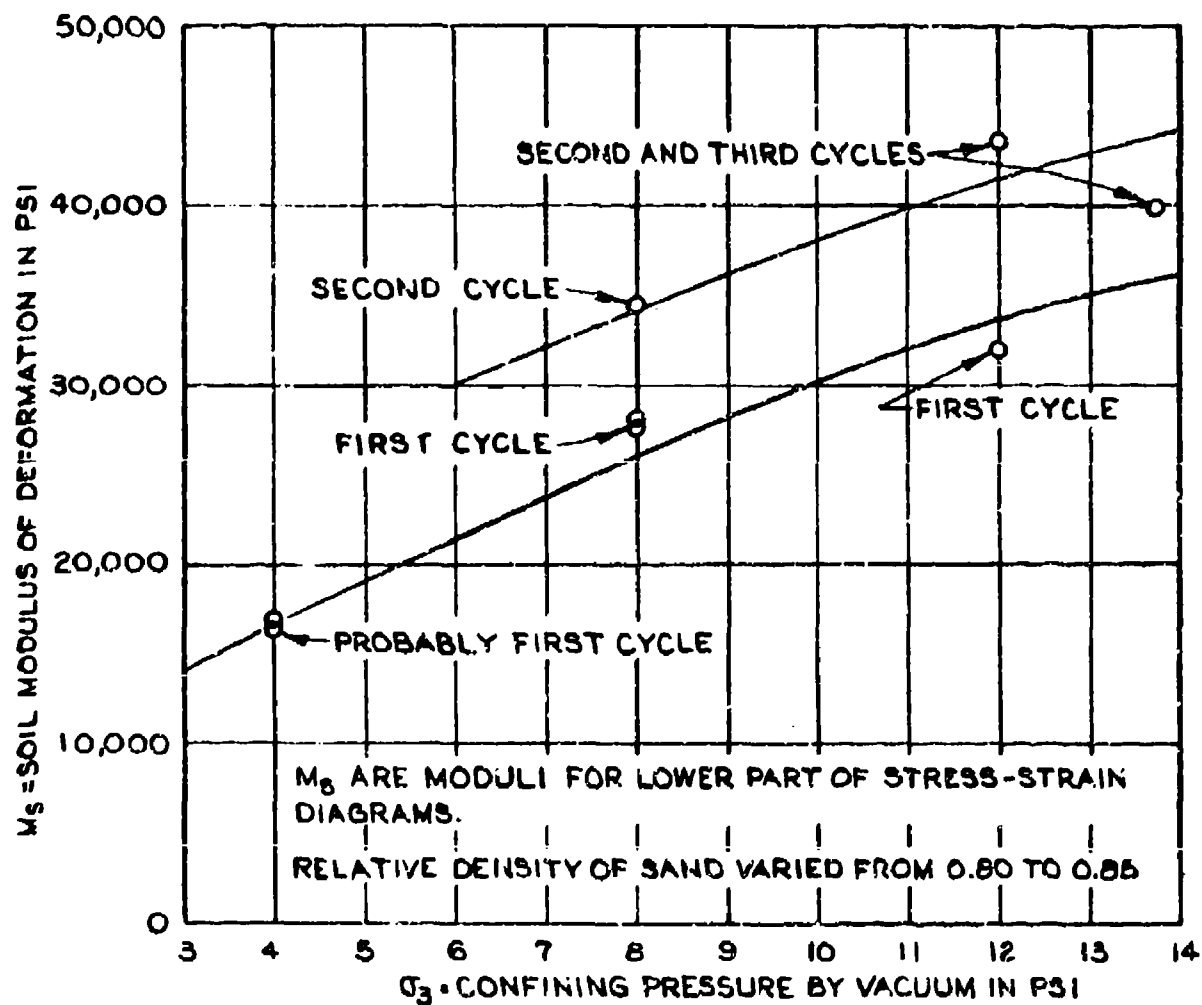
FROM SHOCKLEY AND AHLVIN (1960)

FIGURE 47. DIAGRAM OF WES EQUIPMENT FOR LARGE TRIAXIAL TESTS-VACUUM TYPE

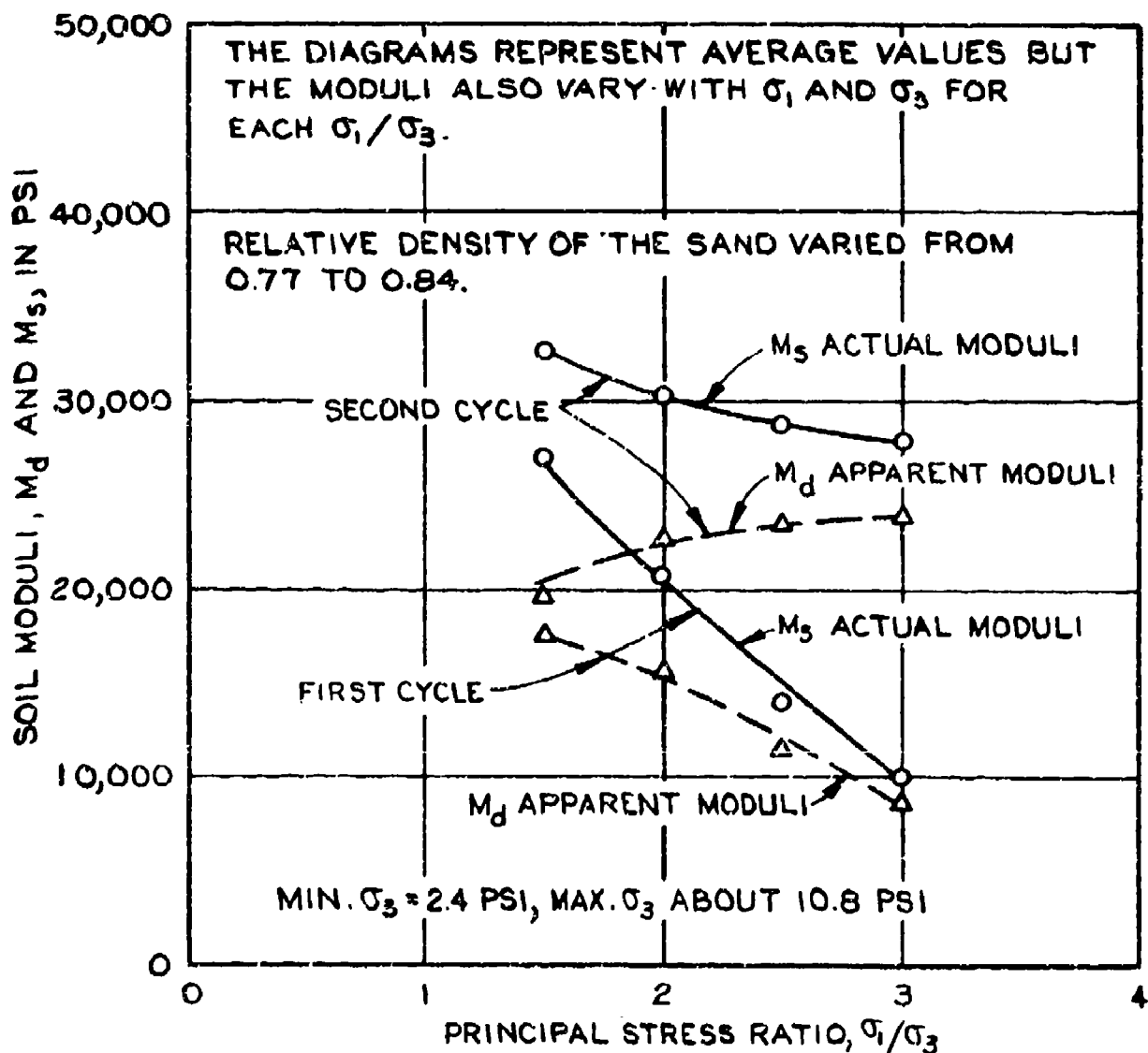
sand, used in other tests at the WES. The grain-size distribution curve for this rather fine-grained and uniform sand is shown in Figure 48. Initial tests were made with sand in both loose and dense consistencies, but most tests in 1955 were performed with a medium dense sand, with initial unit weights of 108 to 109 pcf corresponding to a relative density of 80 to 85 percent. The modulus of deformation varies with the confining pressure or vacuum and with the loading conditions. The relations for uniaxial compression or constant vacuum in each individual test are shown in Figure 49. The maximum vacuum applied was usually 27 in. of mercury or 13.26 psi. There is a conspicuous increase in the values of the moduli between the first and second cycles of loading and only a minor increase with additional cycles. Corresponding moduli for increasing stresses but constant stress ratio, σ_1/σ_3 , are shown in Figure 50. The dashed lines represent observed or apparent moduli which apply only to stress conditions with the same stress ratio as that for which the modulus was determined. To obtain the actual moduli of deformation, corrections must be made for the influence of the Poisson effect, as shown in Figure 50 for a Poisson ratio $\nu = 1/3$. The moduli shown in Figures 49 and 50 are average moduli for the first part of each loading cycle. The moduli decrease with increasing load for uniaxial compression and high values of σ_1/σ_e and change gradually to the opposite trend for uniform triaxial compression, $\sigma_1 = \sigma_e$. The peak axial stress was determined for several large test specimens and loading procedures, which yielded an average angle of internal friction of the mortar sand of $\phi = 39.5$ deg. Standard laboratory test on test specimens with a diameter of 2.8 in. yielded approximately $\phi = 38.5$ deg.

Preparation of test specimen

104. A steel forming jacket of three bolted segments supports the rubber membrane during preparation of the test specimen. The sand was poured in and compacted in batches of 200 to 400 lb, corresponding to lifts of 2-1/2 in. to 5 in., or relative densities of 80 to 85 percent. Compactive efforts were increased as the height of the specimen increased in order to obtain the same densities in the lower and upper



DATA FROM 1955 TEST SERIES, TABLE 4 AND 5, THIS REPORT
 FIGURE 49. MODULUS, M_s , FOR MORTAR SAND AND CONSTANT
 LATERAL STRESS, σ_3 .



NOTE: DATA FROM 1955 TEST SERIES, TABLES 4 AND 5 OF THIS REPORT.

$$\text{DEVIATOR MODULUS/APPEARANT MODULUS } M_d = \frac{\sigma_1 - \sigma_3}{\epsilon_1}; \frac{\sigma_1}{\sigma_3} = n,$$

$$\nu = \frac{1}{3} \text{ (ASSUMED)}$$

$$\text{ACTUAL MODULUS, } M_s \text{ AND } \epsilon_1 = \frac{\sigma_1}{M_s} - \frac{2\nu\sigma_3}{M_s}$$

$$M_s = M_d \left(1 - \frac{2\nu}{n}\right) \left(\frac{n}{n-1}\right) = M_d \left(1 - \frac{2}{3}\right) \left(\frac{n}{n-1}\right)$$

FIGURE 50. APPARENT AND ACTUAL MODULI FOR MORTAR SAND VERSUS PRINCIPAL STRESS RATIOS.

parts of the test specimen. Special templets were used to hold the pressure cells in the desired position until sand had been carefully hand-tamped around them. The height of the specimen was determined after placement of the top plate. The registration of the pressure cells were determined before and after their placement in the test specimen. A vacuum was applied after placement of the top plate and before removal of the forming jacket. Changes in height of the test specimen and in the registration of the cells during these operations were observed. Large changes in initial deformations and pressures usually correspond to large differences between the first and second cycles of loading and may indicate not only changes in the modulus but also unsatisfactory placement of the pressure cell and doubtful reliability of the cell indications, at least for the first two or three cycles of loading. The sand used in preparation of a test specimen was weighed and the corresponding average initial density of the specimen determined. Densities after completion of a test were determined by sampling and weighing at various levels during dismantling of the test specimen. Different testing procedures were used in the various test series and are described in paragraphs dealing with the particular test series.

Stress Distribution Tests of 1954

General features

105. Dual objectives. The objectives of the 1954 test series were two-fold, i.e. (a) to determine the stress distribution in a restrained cylinder with axial loading, and (b) to investigate the over- or underregistration of the pressure cells. The two objectives are interdependent, and a solution cannot be obtained without recourse to assumptions or simplified theoretical relationships. The principal objective of the 1954 test series may be said to be determination of the stress distribution by temporary neglect of the over- or underregistration of the cells. The tests also yielded some information on the action of pressure cells, but this problem was investigated in greater detail in the 1955 test series. The tests were performed with

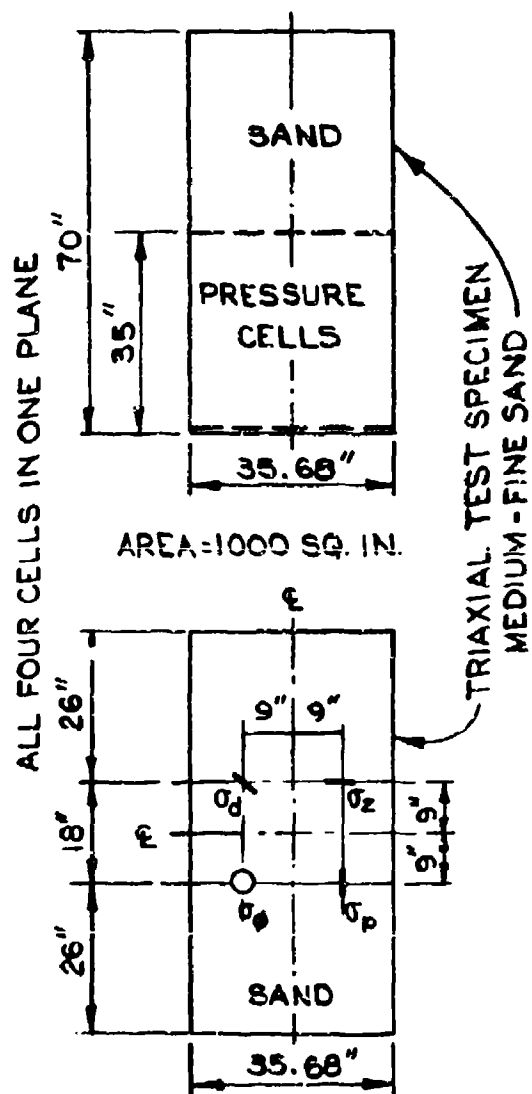
WES pressure cells of 50 and 100 psi rated capacities. The corresponding average moduli of deformation of the cells are shown in Figure 6, and the modulus of the 50 psi cells is slightly below and that of the 100 psi cells slightly above the modulus of the sand in the triangular test specimen. Therefore, the test yields only two points of the unknown curve representing the relation between compressibilities and registration ratios.

106. Placement of the cells. All cells in the 1954 test series were arranged in horizontal positions for measurement of axial stresses in the triaxial test specimen. The cells were placed at midheight and base of the test specimen as shown in Figure 51a. The cells at the base were set directly on top of the base plate, and the cells at midheight were inserted in a shallow hole carefully excavated in a test specimen. The space around the cells was carefully backfilled with sand and hand-compacted in an attempt to obtain uniform density. A slight seating pressure was applied in some of the early tests and a temporarily increased all-round pressure or vacuum in all later tests. Such a seating pressure increases the uniformity and reliability of cell indications, especially in the first loading cycle.

107. Testing procedures. All tests of the 1954 test series were performed with a constant vacuum and corresponding confining pressure of 13.26 psi. The axial or applied loads were increased or decreased in increments of 5 psi, and five or six complete loading cycles were used in most tests. Both cell indications, axial and lateral deformations, were observed for each load increase or decrease. The initial determinations of the average density of the specimen, determined during its preparation, were generally supplemented by sampling and density determinations at several levels during dismantling of the test specimen upon completion of a test.

Principal test data

108. Densities and deformations. Basic density data for the test specimens of the 1954 test series are summarized in Table 1; whereas observed axial and lateral deformations and corresponding values of the Poisson ratios and changes in volume and density are shown in Table 2.



A. 1954 TEST SERIES

50 PSI AND 100 PSI CELLS AT MIDHEIGHT, AND BOTTOM WITH VARIOUS RADIAL OFFSETS. AXIAL STRESSES MEASURED-MOST TESTS WITH 6-IN. CELLS; SOME TESTS WITH 12-IN. CELLS HAVING A 3-IN. INACTIVE RIM.

B. 1955 TEST SERIES

100 PSI AND A FEW 50 PSI CELLS PLACED AT 9-IN. RADIAL OFFSETS FOR MEASUREMENT OF AXIAL, DIAGONAL, RADIAL AND TANGENTIAL STRESSES, ALL FOUR CELLS USUALLY IN ONE PLANE 9-IN. ABOVE OR 9-IN. BELOW MIDHEIGHT.

FIGURE 51. ARRANGEMENT OF WES PRESSURE CELLS IN PRINCIPAL TESTS.

Table 1

Density Data for Sand in Triaxial Test Specimens
1954 Test Series

Specimen No.	Wt of Sand lb	Density				Dif-ference lb/cu ft	Compaction Procedure (18 lb, 8- x 8-in. tamper falling approximately 18 in.)	
		Initial		Sampled				
		lb/cu ft	Relative Percent	Min lb/cu ft	Max Average lb/cu ft			
7	4300	106.2	70	105.0	109.6	107.1	+0.9	400-lb lifts, 35 blows per lift
8	4375	108.0	80	106.0	109.0	107.7	-0.3	400-lb lifts, 40 blows on 1st and 2nd lifts and increased 2 blows per 2 lifts thereafter
9	4020	99.2	28	103.0	105.5	104.2	+5.0	Placed loose using elephant nose type device having horizontal baffle at lower end to dissipate energy
10	4410	109.0	85	105.0	110.7	108.0	-1.0	400-lb lifts and vibrated 2 minutes on each lift
11	4450	110.0	90	106.5	110.3	108.7	-1.3	400-lb lifts and vibrated 2 minutes on each lift
12	3975	98.3	22	103.0	105.0	103.9	+5.6	Placed loose using elephant nose type device having horizontal baffle at lower end to dissipate energy
13	4380	108.3	81	105.0	108.8	107.2	-1.1	400-lb lifts, 40 blows on 1st and 2nd lifts and increased 2 blows per 2 lifts thereafter
14	4460	110.5	92	106.0	110.0	108.4	-2.1	400-lb lifts and vibrated 2 minutes on each lift
15	4065	100.6	37	102.4	104.5	103.3	+2.7	Placed loose using elephant nose type device having horizontal baffle at lower end to dissipate energy
16	4473	110.0	95	105.7	109.6	107.7	-3.3	400-lb lifts and vibrated 2 minutes on each lift
18	4268	105.5	66	103.0	107.2	105.4	-0.1	400-lb lifts, 15 blows on 1st and 2nd lifts and increased 5 blows per 2 lifts thereafter
19	4297	106.2	70	103.6	108.0	105.7	-0.5	400-lb lifts, 15 blows on 1st and 2nd lifts and increased 5 blows per 2 lifts thereafter
20	4275	103.2	52	102.4	106.2	104.7	+1.5	Poured from a bucket with a 3-ft drop, further compacted by man walking, inside cylinder
21	4198	103.8	56	103.0	106.6	104.7	+0.9	Poured from a bucket with a 3-ft drop, further compacted by man walking, inside cylinder
22	3990	98.5	24	101.5	105.0	102.8	+4.2	Poured from a bucket with a 6-in. drop, no further compaction
23	3980	98.4	23	101.5	104.0	102.5	+4.1	Poured from a bucket with a 6-in. drop, no further compaction
24	4340	107.3	76	105.3	108.8	106.6	-0.7	400-lb lifts, 40 blows on 1st and 2nd lifts and increased 2 blows per 2 lifts thereafter
25	4454	110.1	90	105.4	109.0	108.0	-2.1	200-lb lifts, 35 blows on 1st lift and increased 2 blows on each lift thereafter
26	4441	109.1	85	105.5	109.0	107.1	-2.0	200-lb lifts, 15 blows on 1st lift and increased 1 blow per lift thereafter
27	4397	108.7	83	103.5	108.5	106.4	-2.3	200-lb lifts, 12 blows on 1st lift and increased 1 blow per lift thereafter
28	4387	108.5	82	104.6	108.0	106.5	-2.0	200-lb lifts, 12 blows on 1st lift and increased 1 blow per lift thereafter
29	4301	108.6	83	105.7	107.8	106.7	-1.9	200-lb lifts, 15 blows on 1st lift and increased 1 blow per lift thereafter
30	4387	108.5	82	105.2	107.5	106.8	-1.7	200-lb lifts, 15 blows on 1st lift and increased 1 blow per lift thereafter
31	4383	108.4	81	Sampling discontinued				200-lb lifts, 15 blows on 1st lift and increased 1 blow per lift thereafter
32	4366	108.0	80					200-lb lifts, 15 blows on 1st lift and increased 1 blow per lift thereafter
33	4337	107.3	76					200-lb lifts, 15 blows on 1st lift and increased 1 blow per lift thereafter
34	4375	108.1	80					200-lb lifts, 15 blows on 1st lift and increased 1 blow per lift thereafter
35	4361	107.8	78					200-lb lifts, 15 blows on 1st lift and increased 1 blow per lift thereafter
36	4367	108.0	80					200-lb lifts, 15 blows on 1st lift and increased 1 blow per lift thereafter

Table 2
Axial and Lateral Deformations of Triaxial Test Specimens
1954 Test Series

Specimen No.	Load kips	Average* Increase in Radius in.	Area of** Lateral Change	Volume of Lateral Change	Average Vertical Deflection in.	Volume of Vertical Change cu ft	Adjusted Density lb/cu ft	Initial Density lb/cu ft	Poisson Ratio ν Average
7	30	0.127	5.93	0.385	0.720	0.417	106.2	106.1	0.71
8	30	0.079	3.69	0.239	0.407	0.236	107.9	107.9	0.74
9	20	0.063	2.95	0.191	0.728	0.421	99.8	99.2	0.33
10	30	0.094	4.39	0.285	0.614	0.355	109.2	109.0	0.61
11	30	0.104	4.85	0.315	0.574	0.332	110.1	110.05	0.70
12	20	0.056	2.61	0.169	0.676	0.391	98.8	98.3	0.33
13	30	0.0877	4.09	0.265	0.480	0.278	108.6	108.55	0.72
14	30	0.0697	3.25	0.211	0.458	0.265	110.6	110.5	0.64
15	20	0.048	2.24	0.145	0.589	0.341	101.4	100.9	0.31
16	30	0.0677	3.16	0.205	0.450	0.260	111.2	111.0	0.59
18	25	0.054	2.52	0.163	0.265	0.211	105.6	105.5	0.80
19	25	0.043	2.03	0.132	0.326	0.189	106.4	106.2	0.39
20	25	0.142	6.63	0.430	0.831	0.481	103.3	103.2	0.67
21	25	0.180	8.40	0.545	0.926	0.536	103.8	103.8	0.77
22	20	0.094	4.39	0.285	1.095	0.634	99.5	98.6	0.33
23	20	0.075	3.50	0.227	0.946	0.547	99.2	98.4	0.31
24	30	0.067	3.13	0.203	0.402	0.233	107.4	107.3	0.65
25	35	0.087	4.06	0.263	0.408	0.236	110.0	110.1	0.85
26	30	0.066	3.08	0.200	0.374	0.216	109.1	109.1	0.69
27	30	0.069	3.22	0.209	0.397	0.230	108.8	108.7	0.69
28	30	0.079	3.68	0.239	0.408	0.236	108.5	108.5	0.77
29	30	0.066	3.08	0.200	0.361	0.209	108.6	108.6	0.61
30	30	0.062	2.89	0.187	0.357	0.207	108.6	108.5	0.77
31	30	0.077	3.57	0.232	0.400	0.231	108.4	108.4	0.76
32	30	0.078	3.64	0.236	0.440	0.255	108.0	108.0	0.71
33	30	0.074	3.45	0.224	0.415	0.240	107.4	107.3	0.71
34	30	0.040	1.87	0.121	0.328	0.190	108.3	108.1	0.48
35	30	0.061	2.85	0.185	0.380	0.220	107.9	107.8	0.63
36	30	0.054	2.52	0.163	0.366	0.212	108.1	108.0	0.59

* Average of three gage readings at midheight of specimen.

** Cross-sectional area of bulge assumed to be adequately represented by a parabolic area.

Assuming no displacement at head and base: $A = 2/3 \Delta r h$

Where: Δr is average midheight radius increase

h is height of specimen

$$E_x = \nu \times E_a, \quad \nu = E_x/E_a = \Delta R/R \times H/\Delta H = \Delta R/\Delta H \times H/R = \Delta R/\Delta H \times 70.0/17.84 = \Delta R/\Delta H \times 3.91$$

Typical stress-strain relations for uniaxial compression of the sand are presented in Figure 52; this and similar diagrams were used for estimating the deformation moduli of the sand under various stress conditions. The maximum deviator stress or applied unit axial load was usually 30 psi, but in some tests the maximum load was 20, 25, or 35 psi.

109. Stress conditions at midheight of test specimen. As shown in Figure 45, the theoretical stress distribution at midheight of a cylindrical test specimen with a length-diameter ratio of 2.0 and subjected to uniaxial compression are nearly uniform, and the stresses near the axis are only slightly larger than those at the cylindrical surface. A typical soil-cell stress plot is shown in Figure 53. The definitions given in this figure apply also to the general summary of observed stresses in Table 3. The stress conditions at various stages of preparation and loading of the test specimen are illustrated in Figures 54-58 and discussed in the following paragraphs. Residual stresses at the cells are not considered here but are discussed in a separate section on the influence of secondary factors.

110. Measured stresses caused by deadweight of the sand, while the test specimen still is supported by the forming jacket, are shown in Figure 54a and b. There is considerable scatter of observed stresses but no appreciable difference between indications of 50- and 100-psi pressure cells. The scatter reflects stress changes caused by installation of the pressure cells and gives a clue to the reliability of the various indications during the first loading cycle. The scatter of observed deadweight stresses is greatest near the cylindrical surface and is undoubtedly influenced by variations in the sidewall friction between the test specimen and the forming jacket.

111. The total effect of deadweight and application of a 13.26-psi vacuum plus removal of the forming jacket is indicated by the stress observations shown in Figure 55a and b. In this case the 100-psi cells indicate slightly larger stresses than the more compressible 50-psi cells, which agrees with the general theory of pressure cells or inclusions. According to the theory by Balla, Figure 45, a uniform load increase in all directions should produce a stress distribution at

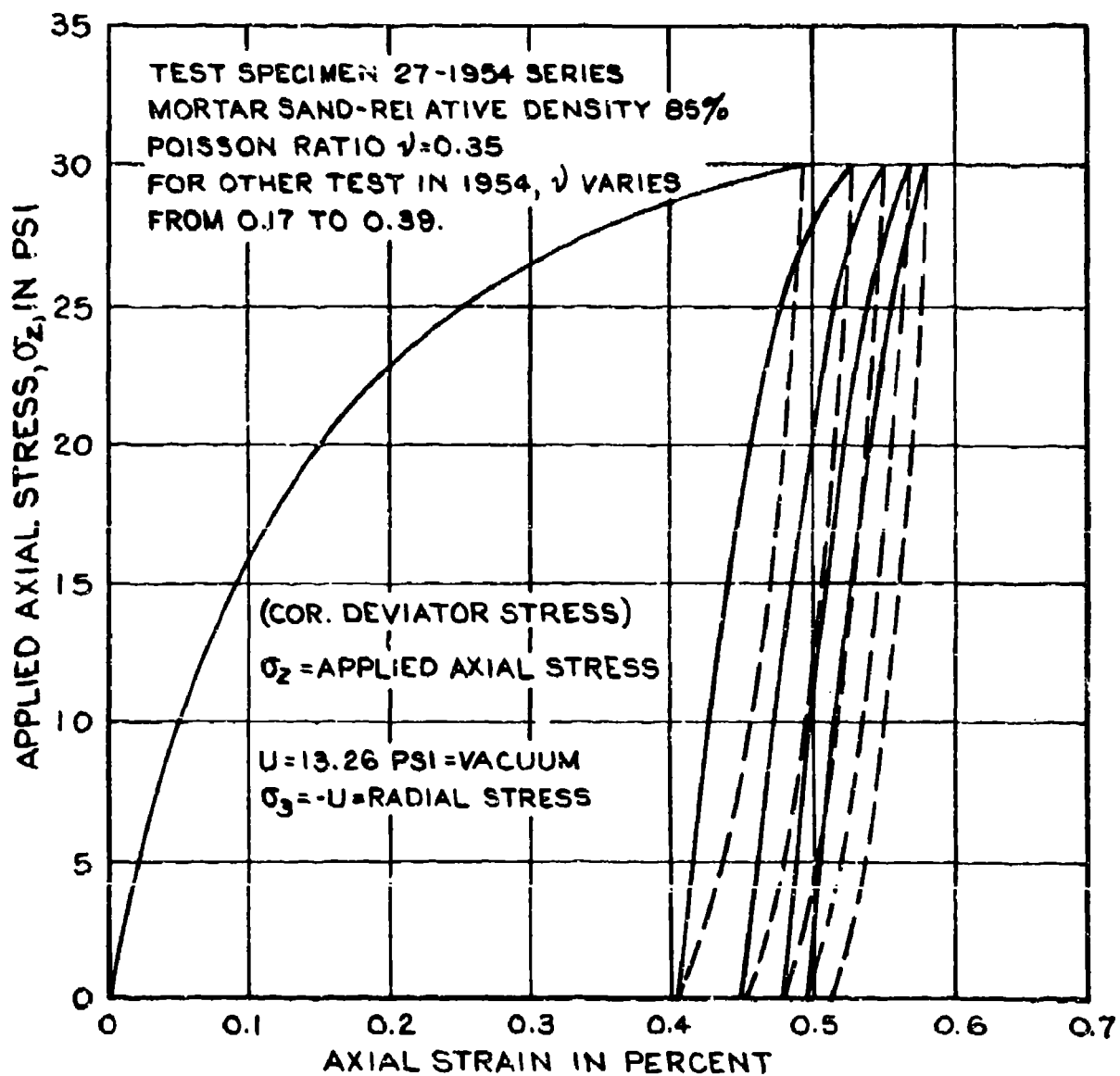


FIGURE 52. STRESS-STRAIN DIAGRAMS FOR MEDIUM DENSE SAND IN UNIAXIAL COMPRESSION.

TEST SPECIMEN 27, RELATIVE DENSITY 85 PERCENT, CELL 94,
CAPACITY 30 PSI, OFFSET 2-IN., ELEVATION 35 IN.

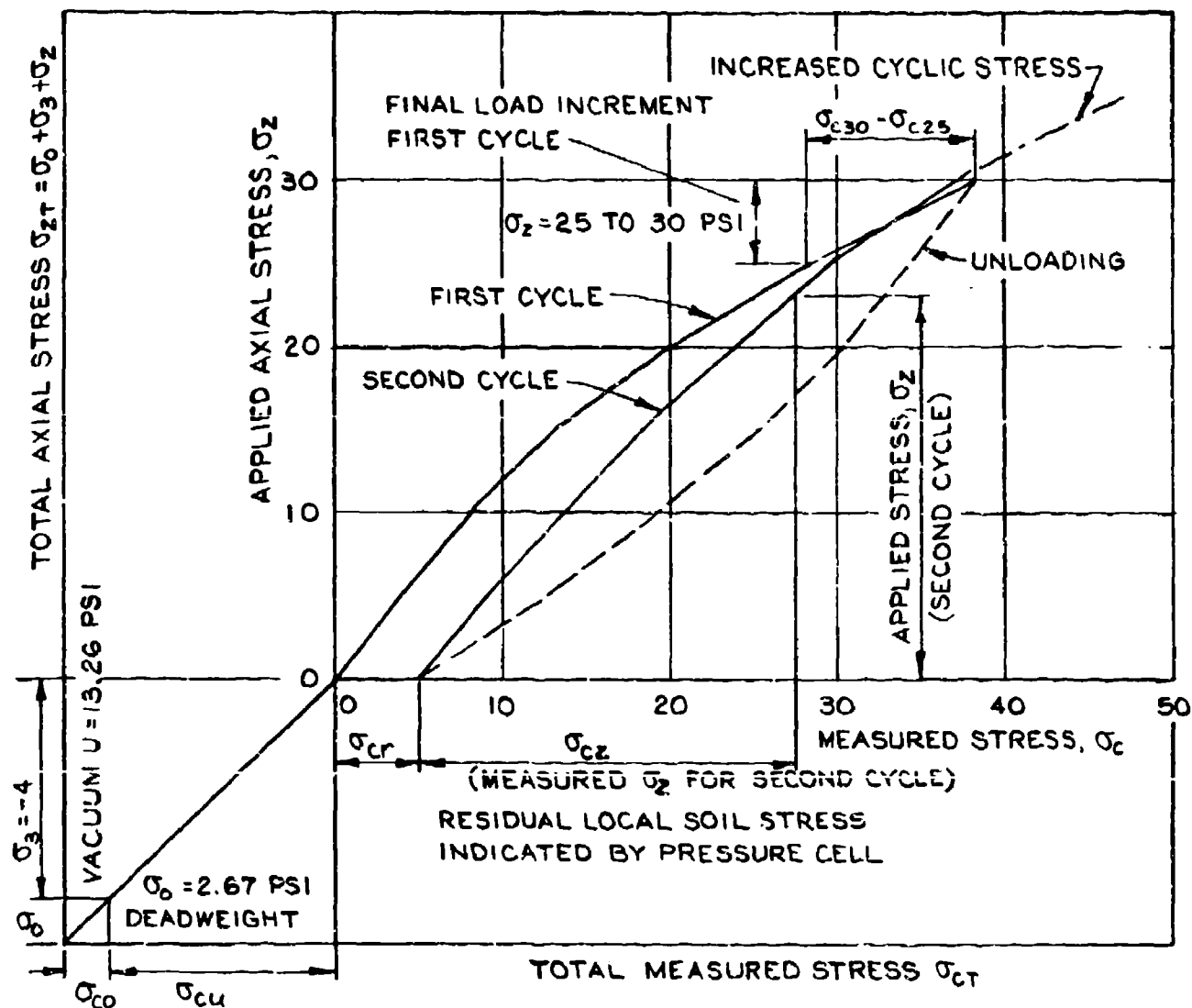


FIGURE 53. SOIL-CELL STRESS DIAGRAM AT MIDHEIGHT FOR UNIAXIAL COMPRESSION.

Tab. 3
Applied and Measured Stresses in Triaxial Test Specimens
1924 Test Series

Vertical Stresses																	
Pressure Cell						Vacuum Applied (5.26 psi)				Load Applied			Total				
Specimen No.	Initial Density lb/cu ft	Applied Load kips	Oriented Horizontally		Eleva- tion, in.	Loca- tion	Specimen Complete		Forming Jacket Off		Width of Hysteresis	Eccen- tricity, psi	Measured	Applied	Percent of Applied		
			Capac- ity, psi	Area, in.			Measure- ment	No Vacuum	Measured	Applied						psi	psi
7	106.1	30	84	50	35	12 S	1.37	2.60	14.01	15.86	12.64	6.5	27.5	4.0	+1.2	42.01	104.7
			90	50	35	0	1.81	2.60	13.35	15.86	11.25	5.5	29.0	5.0	+2.0	47.66	103.9
			94	50	35	14-1/2 N	1.72	2.60	11.27	15.86	9.55	3.7	21.6	1.7	+0.5	36.57	79.7
8	107.0	30	84	50	35	14-1/2 F	2.15	2.64	88.70	15.90	11.92	4.6	24.1	2.7	+0.7	42.80	93.2
			96	50	35	0	2.49	2.64	84.80	15.90	11.01	6.3	29.2	1.7	+1.5	45.00	106.9
			94	50	35	11 S	2.92	2.64	87.70	15.90	11.01	6.0	26.2	3.3	+1.1	46.13	100.5
9*	99.0	20	84	50	35	12 S	1.03	2.46	5.99	15.72	4.56	2.3	10.0	0.5	+0.3	17.89	50.7
			96	50	35	0	2.46	2.46	4.11	15.72	3.36	1.5	7.8	0.3	+0.3	13.43	37.6
			84	50	35	14-1/2 N	1.00	2.46	9.19	15.72	8.19	5.6	8.6	1.3	+0.4	21.39	59.9
10	100.0	30	103**	50	0	0	--	4.86	15.12	--	--	9.0	26.1	3.5	-0.5	--	--
			91	50	35	14-1/2 N	4.75	4.86	19.00	16.12	14.35	6.5	28.3	4.0	+1.2	53.30	111.8
			96	50	35	12 S	2.06	2.66	14.96	15.92	12.90	8.5	26.8	3.8	+1.2	55.56	110.1
			94	50	35	0	1.81	2.66	17.03	15.92	13.42	6.7	32.3	6.3	-2.2	58.03	126.4
			80	100	0	14-1/2 N	2.00	2.66	15.95	15.92	13.96	11.9	28.2	4.7	+1.3	55.56	121.0
11	110.1	30	84	100	0	12 S	0.92	4.83	13.48	16.09	12.57	5.0	27.8	1.7	-0.3	46.28	96.2
			83	100	0	0	3.17	4.83	23.74	16.09	20.57	5.7	26.5	0.9	-1.5	50.94	103.9
			82	100	0	14-1/2 N	1.11	4.83	19.08	16.09	17.97	5.5	31.4	2.1	0.0	55.98	110.4
			84	50	35	12 S	3.27	2.68	17.46	15.94	14.19	5.0	30.8	5.3	+1.3	53.26	115.9
			89	50	35	0	2.28	2.68	16.20	15.94	13.92	5.7	26.8	3.6	+0.8	48.70	106.0
			96	50	35	14-1/2 N	0.34	2.68	14.19	15.94	13.85	9.4	31.4	5.0	+1.3	54.99	119.7
12	98.3	20	84	100	0	12 S	2.12	3.92	14.98	17.18	11.97	2.5	16.8	0.3	-0.3	33.79	89.8
			83	100	0	0	2.35	3.92	16.42	17.18	14.07	1.5	15.7	0.5	-0.4	33.62	90.4
			82	50	35	14-1/2 N	1.39	3.92	21.62	17.18	20.03	1.0	21.3	1.1	+0.2	43.92	118.1
			94	50	35	12 S	1.02	2.44	8.69	15.70	7.66	3.6	33.9	1.4	+1.5	26.19	73.4
			89	50	35	0	0.91	2.44	5.73	15.70	4.82	1.8	9.4	0.5	+0.2	16.93	47.4
			96	100	0	14-1/2 N	0.69	2.44	4.04	15.70	3.35	1.1	7.5	0.5	+0.1	12.34	36.2
13	108.6	30	82	100	0	12 S	5.88	4.76	20.03	18.02	14.15	3.7	28.0	1.5	-0.2	51.73	107.7
			84	50	35	0	3.48	4.76	19.85	18.02	16.37	-1.7	25.0	0.0	-1.9	43.15	95.9
			83	50	35	14-1/2 N	1.38	4.76	18.08	18.02	16.70	5.5	31.9	2.8	+0.4	55.48	115.5
			94	50	35	12 S	2.58	2.64	15.95	15.90	12.47	5.0	27.8	3.7	+0.9	47.85	104.2
			89	50	35	0	2.00	2.64	15.29	15.90	13.29	5.5	29.2	5.1	+2.1	49.90	108.7
			94	100	0	14-1/2 N	2.67	2.64	15.57	15.90	12.90	3.0	24.5	3.0	+0.7	43.07	93.8
14	110.5	30	89	50	0	12 S	5.28	4.84	19.38	18.10	17.10	5.2	19.6	2.0	-0.2	44.18	91.9
			96*	50	35	0	2.84	4.84	15.00	18.10	15.16	3.5	18.4	1.3	-0.5	37.70	78.4
			84	100	35	14-1/2 N	0.89	4.04	18.40	18.10	18.31	12.0	26.3	3.9	+0.7	56.70	117.9
			84	100	35	12 S	1.36	2.68	8.18	15.94	5.82	4.0	26.9	2.5	+0.9	39.43	85.9
			82	50	35	0	1.91	2.68	13.83	15.94	11.92	-1.0	23.7	1.3	+0.7	36.53	73.5
			83	100	0	14-1/2 N	1.79	2.58	15.42	15.94	10.63	4.0	25.5	2.0	+0.7	41.92	91.2
15	100.0	20	84	100	0	5 S	2.98	4.45	12.42	17.71	9.84	0.5	14.0	0.5	0.0	26.92	71.4
			83	100	0	9 N	3.31	4.45	18.49	17.71	15.18	2.3	15.4	1.3	+0.2	36.19	96.0
			82	100	0	13-1/2 W	3.16	4.45	20.90	17.71	19.72	0.4	17.9	0.3	+0.2	40.84	108.3

(Continued)

* Vertical stresses at mid-elevation for specimens 9 and 12 are questionable since voids were found to exist beneath the cells.
 ** Cell 103 contained a partial leak which made the confining stress indeterminate. Therefore, only the residual and induced stresses are shown.
 + Cell 96 developed a total leak in specimen 14. Therefore, subsequent readings for cell 96 are not adjusted for hydrostatic pressure.

Table 3 (Continued)

Vertical Stresses																		
Specimen No.	Initial Density lb/cu ft	Applied Load kips	Pressure Cell			Specimen Complete			Vacuum Applied (15.26 psi)			Load Applied			Total			
			No.	Capacity, lbs	Extra-Location, in.	Offset, in.	No Vacuum		Measured For Forming Jacket Off		Residual	Induced	Width of Hysteresis	Hysteresis Coefficient	Measured	Percent of Applied		
							psi	psi	psi	psi							psi	psi
16	111.0	30	84	100	C		5 S	--	4.85	17.7	13.11	--	21.5	0.0	-1.3	32.00	48.11	66.5
			83				9 N	--	4.95	21.5	13.11	--	20.9	0.4	-1.0	42.43	48.11	88.2
			82				13-1/2 W	--	4.85	18.11	16.11	--	25.4	2.2	+2.0	42.43	48.11	100.0
18	104.5	25	83	100	C		12 S	5.52	4.65	26.70	17.97	15.18	24.1	1.6	0.0	48.80	42.91	113.7
			82				9 W	4.77	4.55	21.5	17.91	16.85	24.3	1.4	+0.3	42.77	42.91	99.7
			84				14-1/2 N	2.12	4.65	12.11	17.91	10.00	24.3	2.0	+0.7	40.42	42.91	94.2
			89	50	35		12 S	1.82	2.58	12.4	15.84	10.61	18.5	3.0	+1.0	37.27	40.84	91.3
			94				0	1.89	2.58	12.7	15.84	10.64	24.4	2.2	+1.0	33.73	40.84	82.6
			96				14-1/2 N	3.10	2.55	14.4	15.84	11.35	23.8	4.2	+1.7	43.25	40.84	105.9
19	106.2	25	84	100	C		5 S	4.95	4.68	17.24	17.94	12.42	21.5	1.2	-0.7	40.24	42.94	93.7
			82				9 W	5.83	4.68	22.5	17.94	16.70	20.7	0.0	-0.7	42.28	42.94	98.5
			83				13-1/2 N	4.97	4.68	19.5	17.94	14.63	24.7	2.0	+0.3	46.50	42.94	108.3
			96	50	35		12 S	2.75	2.60	14.11	15.86	11.35	22.1	3.0	+0.8	40.70	40.96	99.6
			99				0	2.37	2.60	20.93	15.86	18.56	25.3	4.3	+1.5	51.93	40.86	127.1
			94				14-1/2 N	3.28	2.60	15.35	15.86	12.11	20.7	2.2	+0.8	38.99	40.86	95.4
20	103.2	25	84	100	C		5 S	2.72	4.56	17.27	17.82	14.55	18.5	0.0	-1.2	34.27	42.82	80.0
			82				9 W	3.02	4.56	20.35	17.82	17.33	20.3	0.5	-0.3	42.60	42.82	94.8
			83				13-1/2 N	4.00	4.56	16.97	17.82	12.97	25.2	2.0	+1.0	46.17	42.82	112.5
			99	50	35		12 S	1.64	2.54	14.11	15.80	12.47	25.8	3.5	+0.9	46.11	40.80	113.7
			94				0	1.38	2.54	12.47	15.80	10.49	22.7	3.5	+1.5	41.17	40.80	100.9
			96				14-1/2 N	1.69	2.54	12.47	15.80	11.18	31.8	2.8	+1.0	40.27	40.80	96.7
21	103.8	25	84	100	C		5 S	3.03	4.58	18.75	17.84	15.76	20.1	0.0	-1.0	37.09	42.84	86.5
			82				9 W	3.50	4.58	20.83	17.84	17.33	21.8	2.0	+0.4	42.58	42.84	99.4
			83				13-1/2 N	3.04	4.58	14.96	17.84	11.86	23.5	1.5	+0.2	35.90	42.84	83.8
			89	50	35		12 S	1.09	2.55	7.01	15.81	5.92	21.3	3.1	+1.3	37.51	40.81	91.9
			96				0	1.03	2.55	5.16	15.81	4.13	18.5	3.0	+1.2	30.16	40.81	73.9
			94				14-1/2 N	0.60	2.55	6.36	15.81	5.73	19.3	3.0	+1.1	33.36	40.81	81.7
22	98.6	20	84	100	C		5 S	2.73	4.38	14.70	17.64	11.97	17.5	0.8	-0.2	34.63	37.64	90.3
			82				9 W	2.70	4.38	15.22	17.64	13.22	22.2	0.5	-0.2	34.12	37.64	90.6
			83				13-1/2 N	--	4.38	--	17.64	--	19.0	0.8	-0.1	--	37.64	--
			89	50	35		12 S	1.73	2.44	17.29	15.70	15.56	18.8	2.2	+0.4	41.09	35.70	117.4
			96				0	1.63	2.44	15.65	15.70	14.02	18.5	2.6	+0.1	37.45	35.70	104.9
			94				14-1/2 N	1.72	2.44	14.96	15.70	13.24	17.8	2.1	+0.5	37.26	35.70	104.4
23	98.4	20	84	100	C		5 S	2.98	4.37	12.27	17.63	9.39	15.3	0.2	-0.3	30.27	37.63	80.4
			82				9 W	3.18	4.37	21.5	17.63	17.97	16.6	0.5	-0.7	41.25	37.63	109.6
			83				13-1/2 N	3.04	4.37	19.04	17.63	16.00	19.0	1.0	-0.2	39.64	37.63	103.7
			89	50	35		12 S	1.18	2.44	12.83	15.70	11.65	17.8	2.4	+0.8	36.13	35.70	101.2
			96				0	1.46	2.44	12.21	15.70	10.75	16.3	2.3	+1.2	32.01	35.70	89.7
			94				14-1/2 N	1.72	2.44	14.36	15.70	12.63	17.2	2.2	+0.7	35.96	35.70	99.6
24	107.3	30	83	100	C		2-1/2 S	5.38	4.72	21.39	17.96	16.01	21.9	0.5	-0.8	43.22	47.98	90.1
			82				10-1/2 W	5.88	4.72	21.15	17.96	15.27	25.8	2.0	+0.7	47.00	47.98	98.0
			84				7 N	4.39	4.72	16.06	17.98	11.67	24.7	0.8	-0.7	37.76	47.98	78.7
			89	50	35		12 S	1.46	2.62	14.25	15.88	12.83	21.4	2.9	+1.2	45.89	45.88	100.0
			96				0	1.12	2.62	8.77	15.88	7.65	22.9	3.6	+1.7	36.47	45.88	79.5
			94				14-1/2 N	2.32	2.62	14.28	15.88	11.96	21.7	2.4	+0.6	45.88	45.88	79.6
25	110.1	35	83	100	C		2-1/2 N	6.21	4.83	23.32	18.09	17.11	24.3	0.7	-1.0	46.32	53.09	87.2
			84				7 N	6.36	4.83	19.09	18.09	12.73	27.2	1.5	-0.8	46.37	53.09	87.3
			89				10-1/2 W	6.46	4.83	21.78	18.09	15.42	25.5	2.3	+0.5	55.26	53.09	104.1
			96				12 S	3.87	2.68	13.14	15.94	9.27	26.4	2.9	+0.5	46.54	50.94	91.4

(continued)

(Sheet 2 of 4)

(Continued)

(Sheet 2 of 4)

Table 3 (Continued)

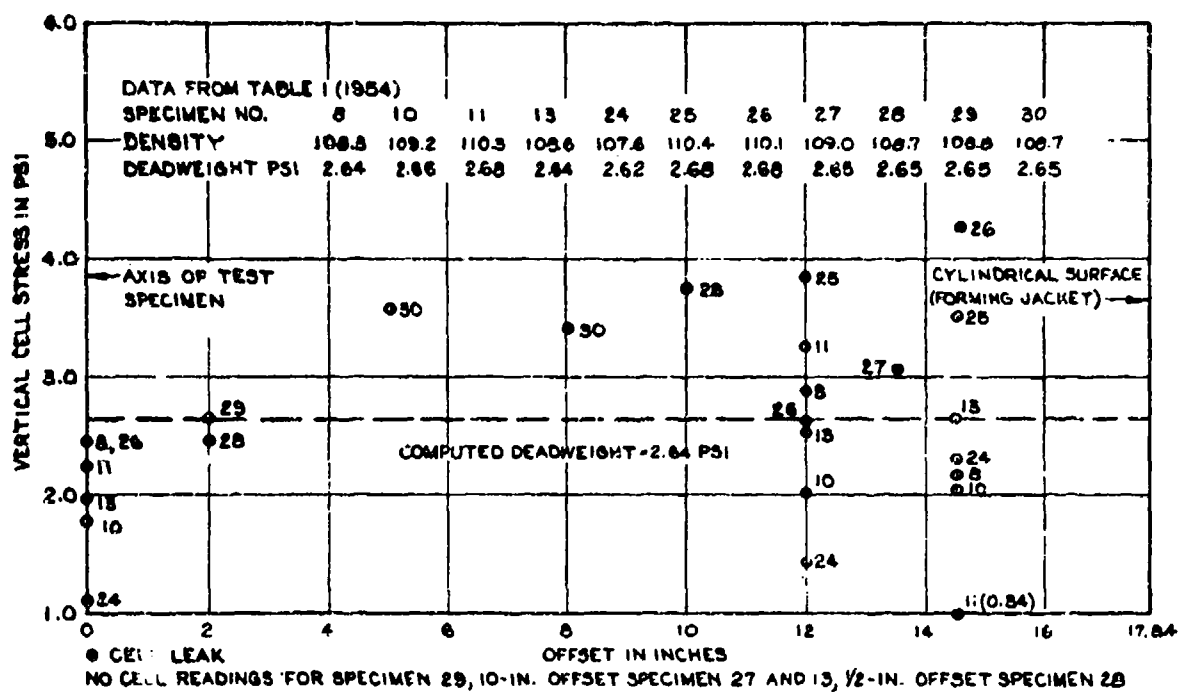
Specimen No.	Initial Density lb/cu ft	Applied Local kips	Pressure Cell			Specimen Complete			Vacuum Applied (13.26 psi)			Vertical Stresses					Total	
			No.	Capacity, psi	Elevation, ft	Location	Offset, in.	No Vacuum	Measured	Applied	psi	Residual	Induced	Load Applied	Width of Hysteresis, psi	Hysteresis Eccentricity, psi	Measured	Percent of Applied
25	120.1	35	85					6.19	2.66	21.74	15.94	15.55	8.5	36.0	7.0	+3.2	56.24	130.0
26	120.1	30	84					3.53	2.66	15.39	15.94	11.86	6.3	32.0	5.2	+0.9	53.69	105.3
27	120.1	30	82					4.93	4.82	23.21	18.06	14.28	-1.3	22.1	5.2	-0.6	44.01	91.5
28	120.1	30	83					6.21	4.82	16.33	18.06	12.12	-1.0	24.3	1.0	+0.1	41.61	85.5
29	120.1	30	84					6.83	4.82	19.32	18.06	12.14	3.0	25.8	2.0	+0.4	50.12	104.2
30	120.1	30	85					2.64	2.67	15.65	15.93	13.01	6.5	26.8	4.0	+1.5	47.96	104.4
31	120.1	30	86					2.49	2.67	15.39	15.93	12.90	3.5	26.5	5.1	+2.0	45.39	98.8
32	120.1	30	87					4.3	2.67	14.02	15.93	9.72	3.5	23.5	2.4	+0.8	41.52	90.4
33	120.1	30	88					5.30	4.78	18.65	18.04	13.33	-0.7	23.4	0.3	-1.0	41.96	87.3
34	120.1	30	89					6.52	4.78	23.37	18.04	16.85	-1.0	26.5	1.6	0.0	48.97	101.9
35	120.1	30	90					6.50	4.78	22.36	18.04	15.46	3.7	29.5	3.3	+0.7	55.56	115.7
36	120.1	30	91					2.67	2.65	16.08	15.91	13.41	6.5	30.9	5.5	+2.2	53.48	116.5
37	120.1	30	92					--	2.65	--	15.91	--	9.5	29.3	4.0	+1.2	--	--
38	120.1	30	93					3.10	2.65	13.42	15.91	10.32	3.2	23.1	2.8	+1.0	39.72	86.5
39	120.1	30	94					5.25	4.77	22.74	18.03	17.49	-1.8	23.1	0.6	-0.8	44.04	91.7
40	120.1	30	95					6.76	4.77	21.25	18.03	14.49	3.5	26.0	2.2	+0.5	50.75	105.7
41	120.1	30	96					12.10	4.77	29.42	18.03	17.32	4.0	19.8	2.7	+0.5	53.22	110.8
42	120.1	30	97					2.49	2.65	15.39	15.91	12.90	5.0	29.0	5.0	+1.7	48.39	105.4
43	120.1	30	98					3.76	2.65	13.24	15.91	9.46	4.8	26.2	3.7	+1.1	44.24	96.4
44	120.1	30	99					--	2.65	--	15.91	--	5.5	24.5	3.0	+1.2	--	--
45	120.1	30	100					--	4.77	15.75	18.03	--	3.3	28.4	1.5	-0.3	47.46	98.8
46	120.1	30	101					--	4.77	23.37	18.03	--	-1.6	24.9	0.7	-1.3	46.67	97.2
47	120.1	30	102					--	4.77	17.66	18.03	--	4.0	29.7	3.4	+1.5	51.36	106.5
48	120.1	30	103					--	4.77	17.20	18.03	--	7.3	28.0	1.1	+1.0	52.50	109.3
49	120.1	30	104					--	2.65	16.94	15.91	--	7.2	30.6	6.1	+2.2	54.74	119.2
50	120.1	30	105					--	2.65	--	15.91	--	10.5	31.7	5.3	+1.6	--	--
51	120.1	30	106					4.36	4.77	25.60	18.03	21.24	-1.5	24.5	0.8	-0.9	48.60	101.2
52	120.1	30	107					7.45	4.77	21.25	18.03	13.80	4.2	30.0	2.3	0.0	55.45	115.4
53	120.1	30	108					10.73	4.77	24.48	18.03	13.75	5.5	30.0	4.2	+1.7	59.98	124.9
54	120.1	30	109					4.28	4.77	15.83	18.03	11.55	8.5	26.0	2.5	0.0	50.33	104.8
55	120.1	30	110					3.44	2.65	15.31	15.91	11.87	11.0	32.5	5.5	+1.7	58.81	128.1
56	120.1	30	111					3.61	2.65	18.06	15.91	14.45	7.0	30.5	6.0	+2.2	55.56	121.0
57	120.1	30	112					2.88	2.65	13.35	15.91	10.45	11.5	40.2	7.0	+3.0	65.03	141.6
58	120.1	30	113					3.17	2.65	14.77	15.91	11.60	5.0	32.0	3.3	+0.9	51.77	112.8
59	120.1	30	114					2.54	2.65	14.47	15.91	11.93	1.3	24.0	1.3	+0.5	39.77	85.6
60	120.1	30	115					3.82	4.77	16.02	18.03	12.20	8.0	24.0	3.2	+0.9	48.02	100.0
61	120.1	30	116					5.85	4.77	19.42	18.03	14.67	10.5	26.0	3.0	0.0	56.02	116.6
62	120.1	30	117					7.05	4.77	25.63	18.03	13.98	9.3	20.8	1.5	-0.8	55.73	116.0
63	120.1	30	118					3.48	2.63	13.94	15.91	10.46	9.5	40.5	3.0	+1.3	61.94	139.1
64	120.1	30	119					4.69	2.63	17.66	15.89	12.97	6.3	36.7	4.3	+0.9	60.56	132.2
65	120.1	30	120					4.42	2.63	17.65	15.89	13.25	1.2	27.5	0.7	0.0	46.35	85.89
66	120.1	30	121					5.16	4.75	20.98	18.01	15.33	2.2	15.6	1.2	-1.1	41.78	77.0
67	120.1	30	122					6.54	4.75	22.24	18.01	14.70	8.5	25.5	3.5	+0.4	55.24	115.1
68	120.1	30	123					5.28	4.75	17.47	18.01	12.19	7.7	25.3	3.0	+0.2	50.47	105.1
69	120.1	30	124					2.90	2.62	16.42	15.88	13.52	5.5	34.7	5.3	+2.4	57.62	125.6
70	120.1	30	125					3.48	2.62	13.94	15.88	10.46	6.8	36.2	3.6	+1.1	45.88	124.1
71	120.1	30	126					4.13	2.62	17.55	15.88	13.52	2.0	27.0	2.8	+1.0	46.65	101.7

†† Cell 89 developed a partial leak in specimen C which made the confining stress indeterminate. Therefore, only the residual and induced stresses are shown for specimens 27, 28, and 29.
 ‡‡ Specimen 30 the cell had developed a total leak. Hence, subsequent cell readings were not adjusted for hydrostatic pressure.

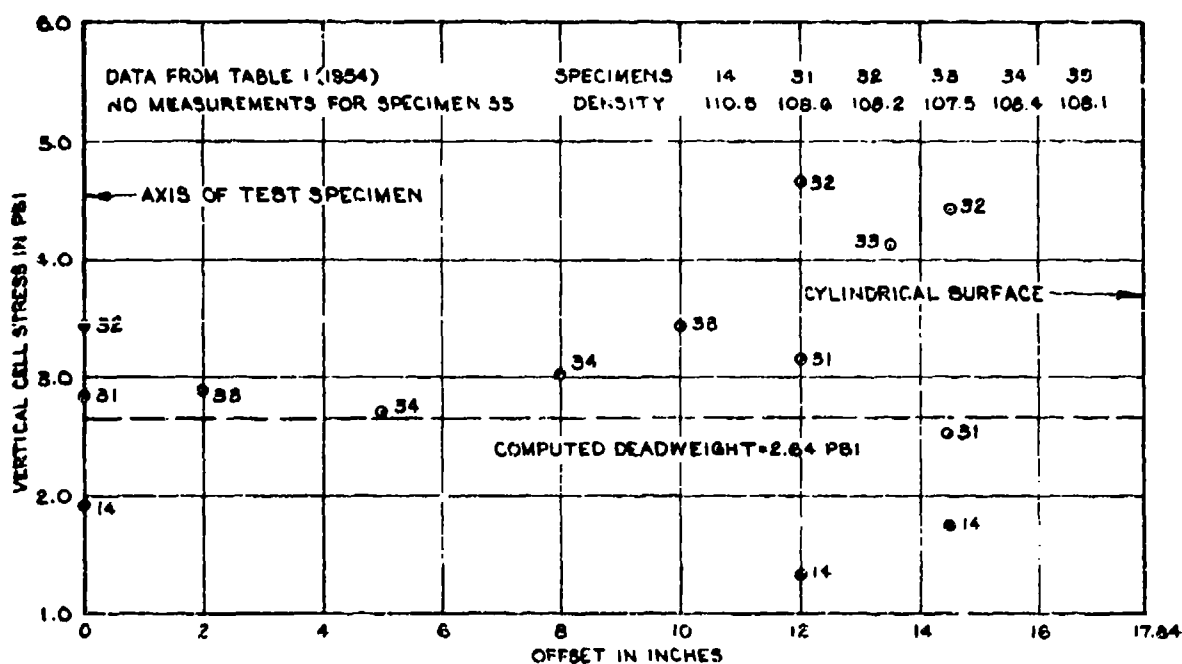
(Sheet 3 of 4)

Table 3 (Continued)

Specimen No.	Initial Density lb/cu ft	Applied Load kips	Pressure Cell			Specimen Complete			Vacuum Applied (13.20 psi)			Vertical Stresses			Total		
			No.	Capacity, psi	Elevation, in.	Location	Offset, in.	No Vacuum Measured, psi	Applied, psi	Measured for Vacuum Only, psi	Residual, psi	Induced, psi	Width of Hysteresis, psi	Hysteresis Stricity, psi	Measured, psi	Applied, psi	Measured Percent of Applied
33 (Cont'd)	107.3	30	98	50	0	0	0	6.11	4.72	21.41	17.08	15.30	3.5	19.2	44.11	47.98	91.5
			99				13-1/2 W	7.01	4.72	20.20	17.08	16.26	5.5	19.7	48.51	47.98	101.1
			87							13.19		26.4	4.6		--		--
34	106.1	30	84	100	35	0	0	2.73	2.64	14.24	15.00	11.51	6.5	34.4	55.14	45.90	120.1
			83				13-1/2 W	3.04	2.64	17.11	15.00	14.07	7.0	35.0	59.11	45.90	126.8
			82					4.93	4.76	17.33	18.32	12.40	4.0	30.7	52.03	48.02	108.4
			94	50	0	0	0	6.54	4.76	23.39	18.32	16.85	5.0	18.7	47.09	48.02	98.1
			96				13-1/2 W	7.40	4.76	20.93	18.32	13.50	4.5	19.3	44.70	48.02	93.1
			89					6.01	4.76	18.56	18.32	12.55	5.5	24.0	51.06	48.02	106.3
35	107.9	30	82	100	35	0	0	2.63	2.63	18.76	15.30	--	5.0	29.5	53.26	45.98	115.1
			84				13-1/2 W	--	2.63	13.79	15.30	--	7.7	37.6	59.09	45.98	128.8
			93					--	4.74	18.46	18.30	--	4.5	31.5	54.45	48.00	113.5
			94	50	0	0	0	4.74	4.74	23.91	18.30	--	5.5	19.8	49.21	48.00	102.5
			96				13-1/2 W	--	4.74	19.09	18.30	--	5.0	19.7	43.79	48.00	91.2
			90					--	4.74	18.93	18.30	--	7.0	23.5	49.43	48.00	103.0
36	108.0	30	84	100	17	0	0	5.00	3.65	15.51	16.91	11.51	17.5	44.7	78.34	46.91	166.9
			83				13-1/2 W	2.76	2.00	17.11	15.36	14.35	16.0	40.6	73.71	45.26	162.9
			82					1.27	1.17	14.63	14.43	13.56	14.0	41.0	69.63	44.43	156.7
			94	50	53	0	0	0.56	0.62	11.87	13.38	11.01	20.0	36.7	63.57	43.88	155.3
			89					3.19	2.82	15.56	16.48	12.35	26.4	37.6	79.56	46.08	172.7
			96				13-1/2 W	--	4.47	17.5	17.5	11.0	3.2	26.0	--	47.73	--



A. 50 PSI CELLS



• SPECIMEN 14 VIBRATED-POSSIBLE VOIDS-DATA UNRELIABLE AND NOT CONSIDERED

B. 100 PSI CELLS

FIGURE 54. MEASURED STRESSES AT MIDHEIGHT FOR DEADWEIGHT.

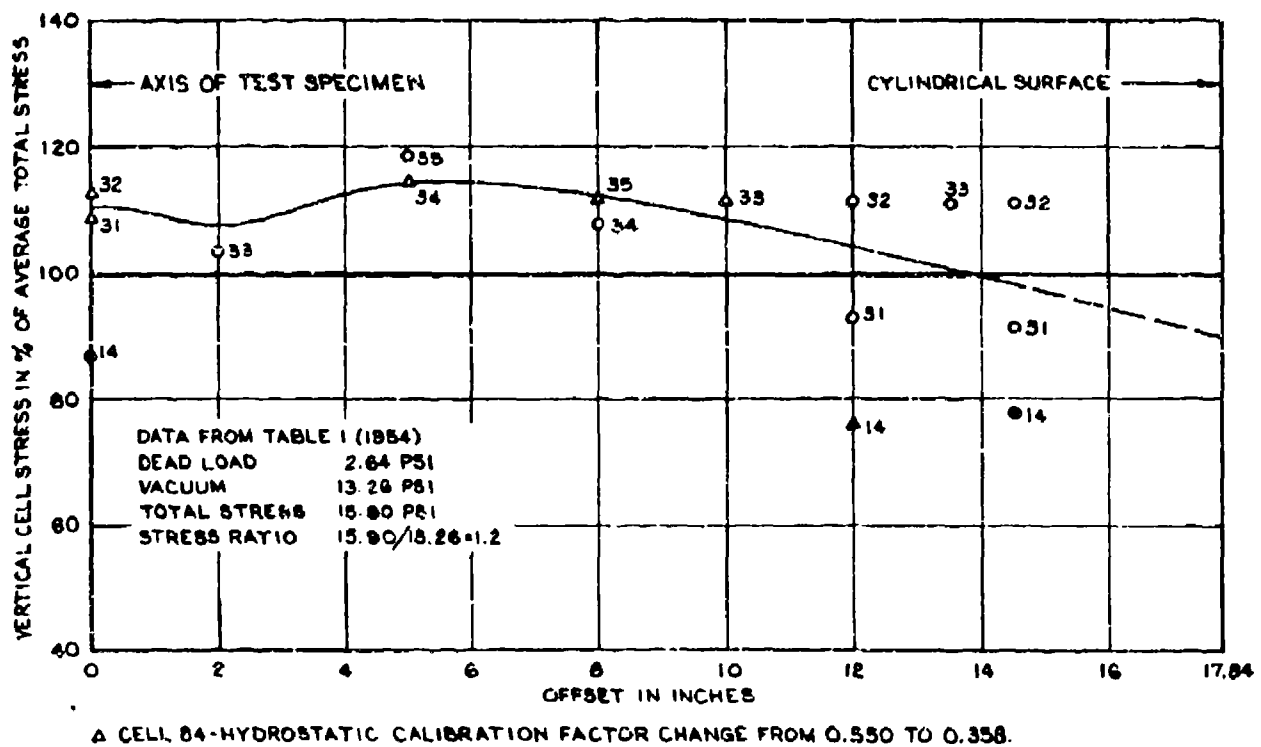
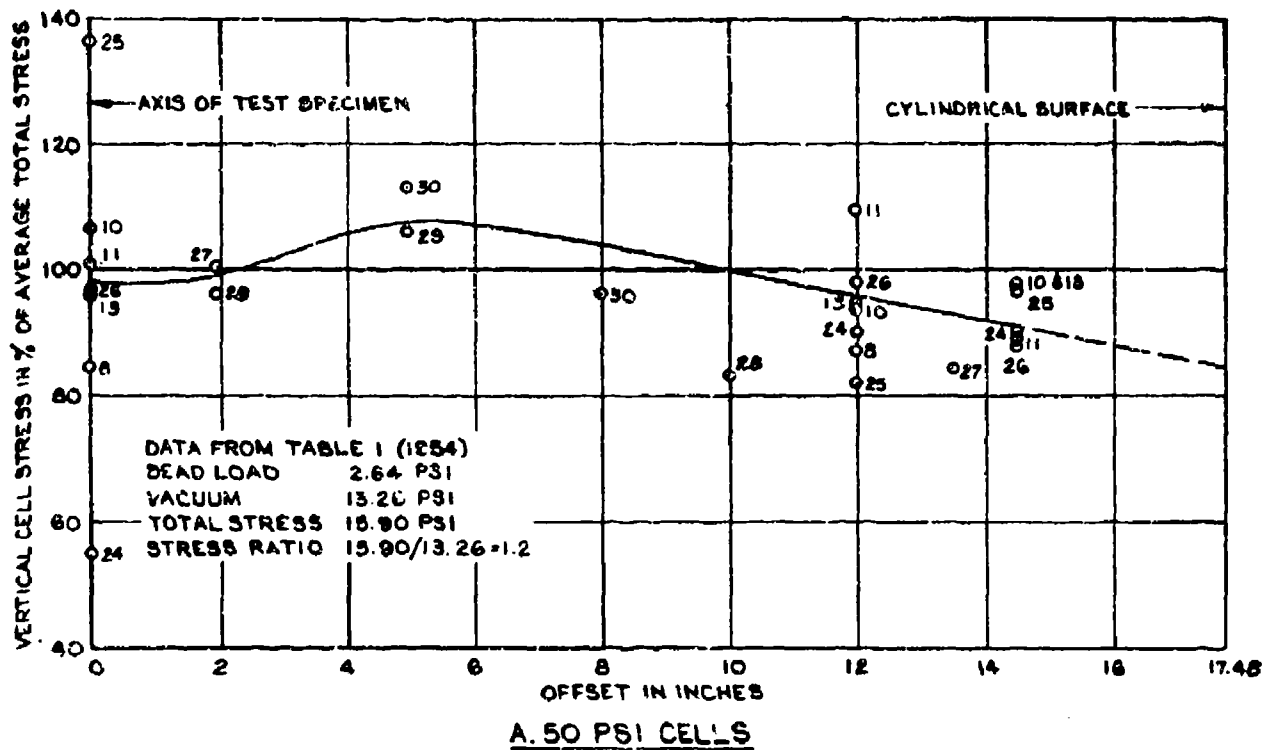
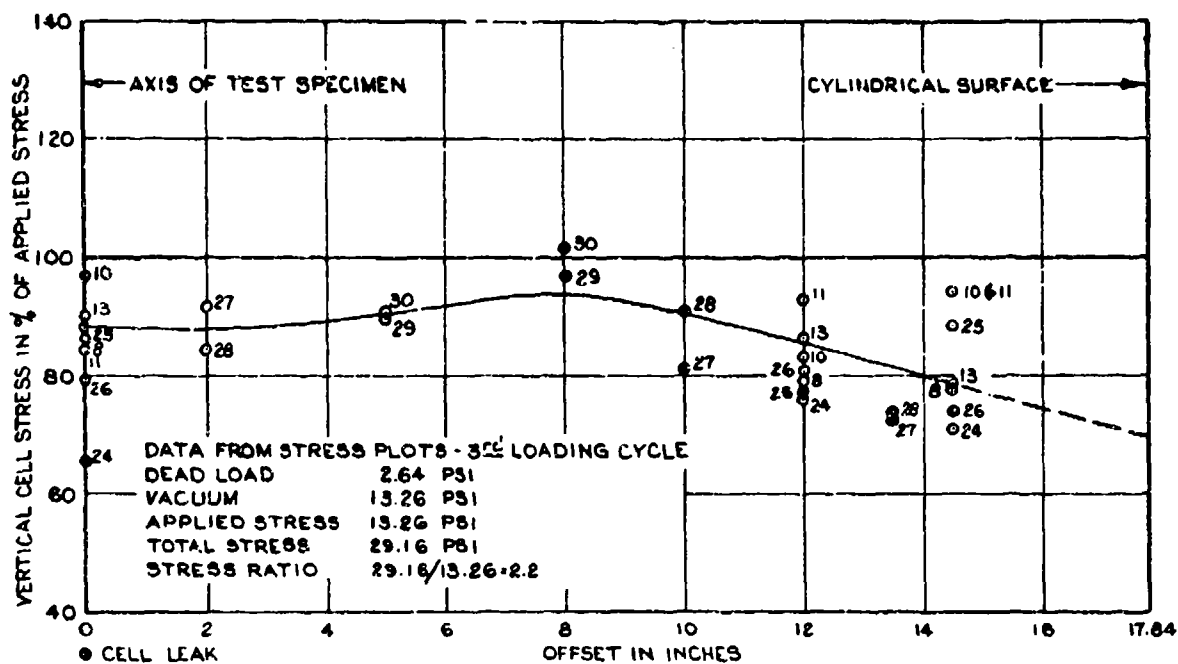
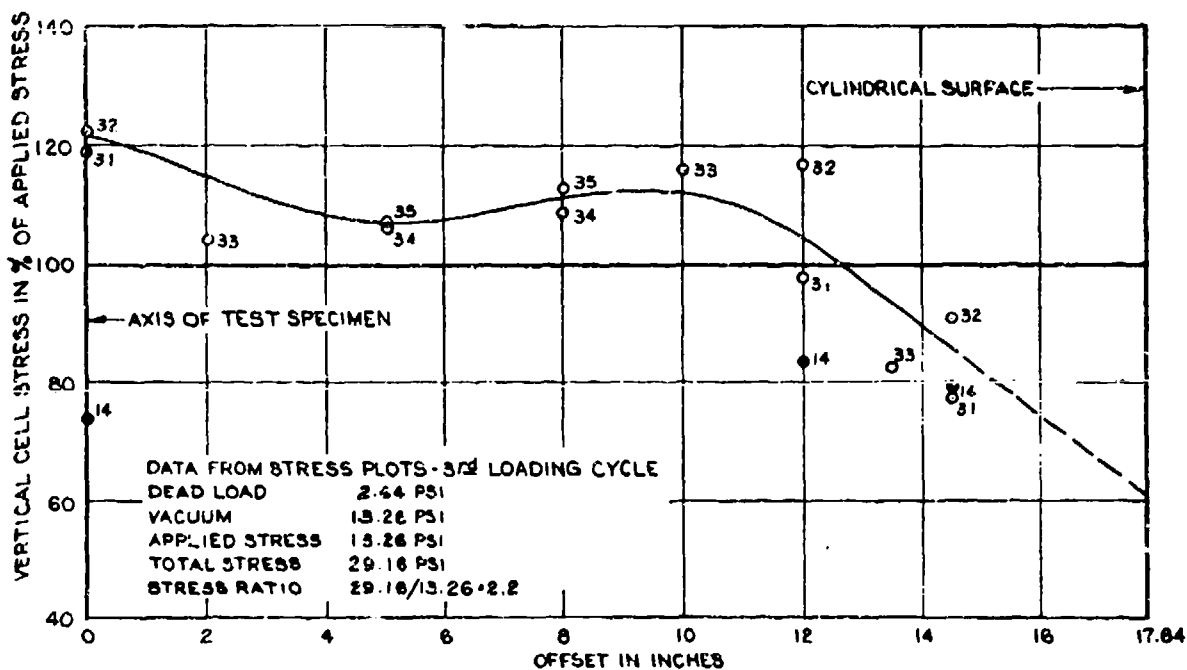


FIGURE 55. MEASURED STRESSES AT MIDHEIGHT FOR DEADWEIGHT PLUS VACUUM.



A. 50 PSI CELLS



B. 100 PSI CELLS

FIGURE 56. MEASURED STRESSES AT MIDHEIGHT FOR APPLIED AXIAL LOAD OF 13.26 PSI.

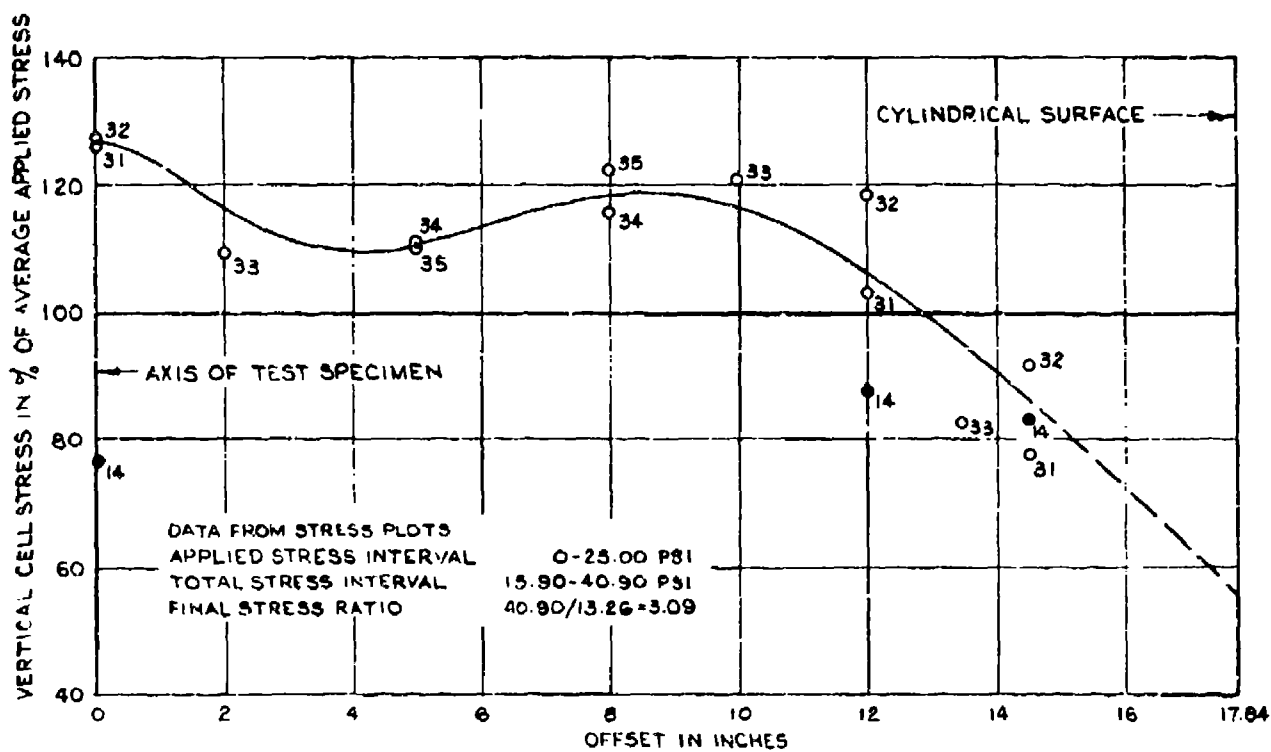
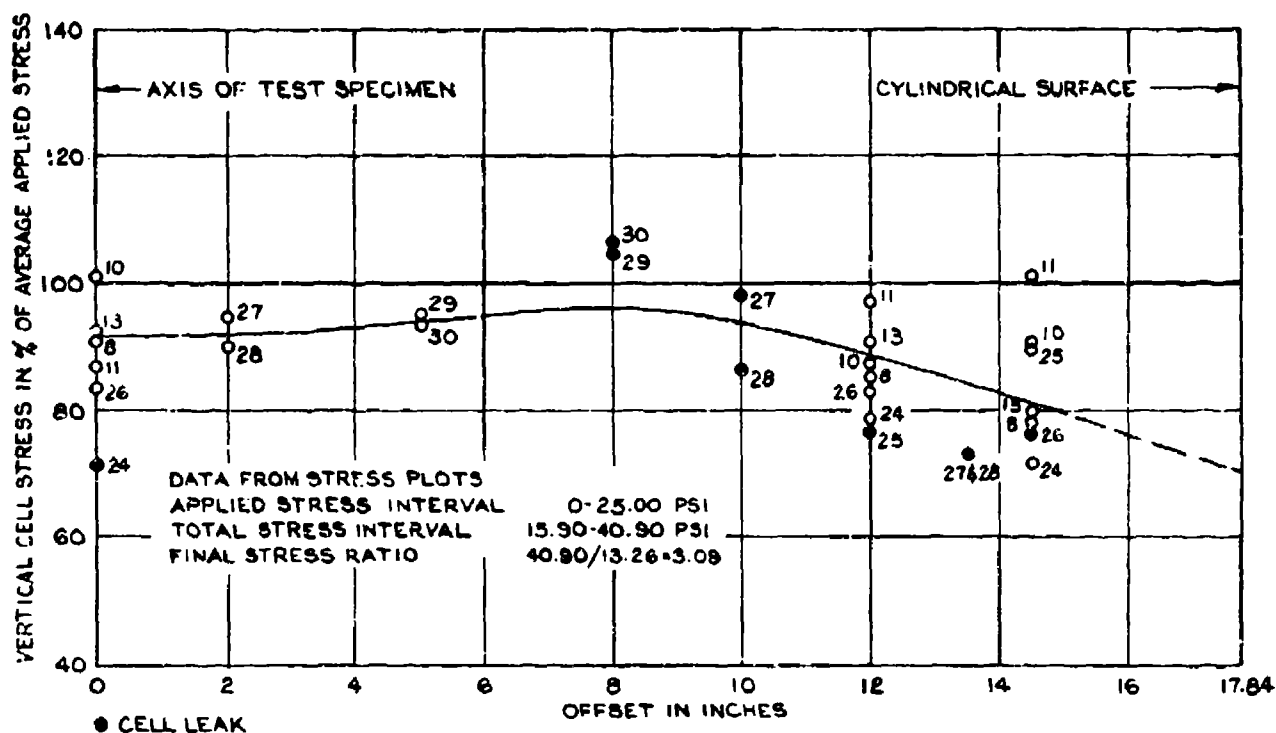


FIGURE 57. MEASURED STRESSES AT MIDHEIGHT FOR APPLIED LOAD INTERVAL, 0 - 25 PSI

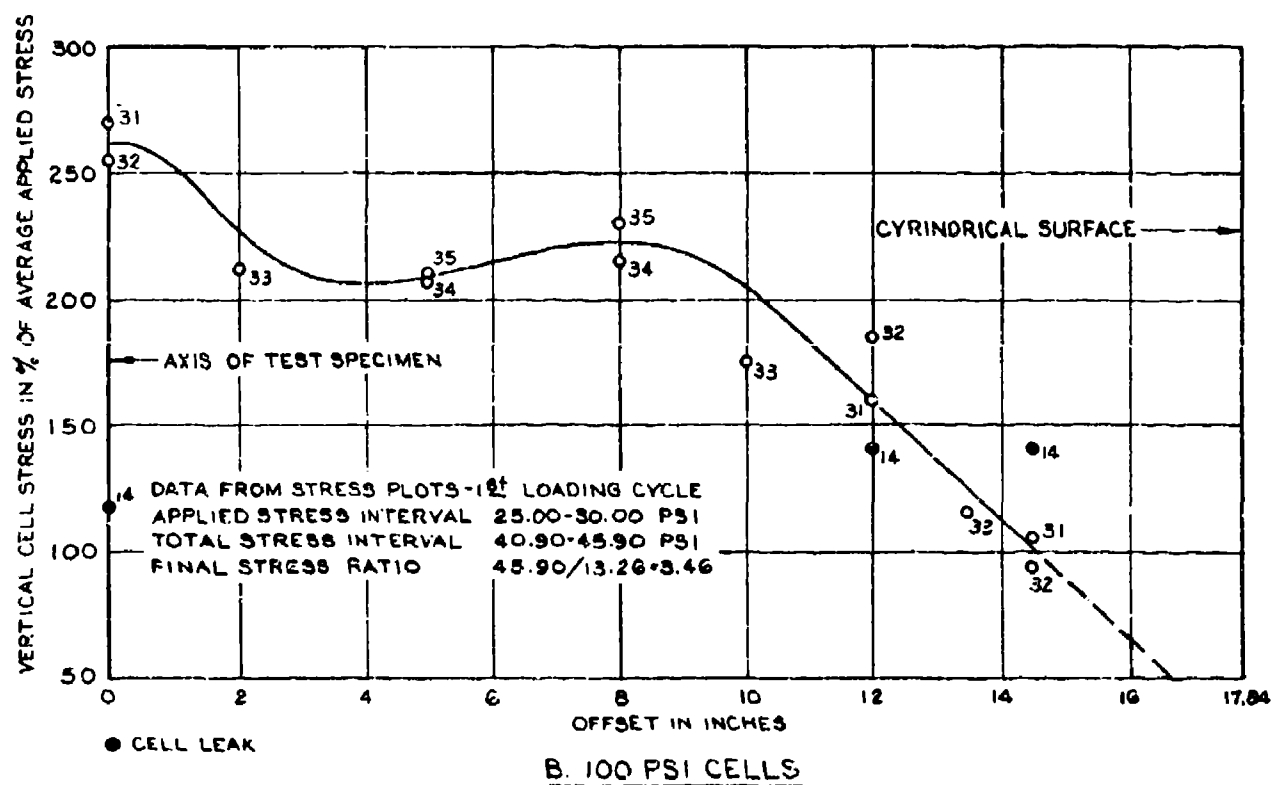
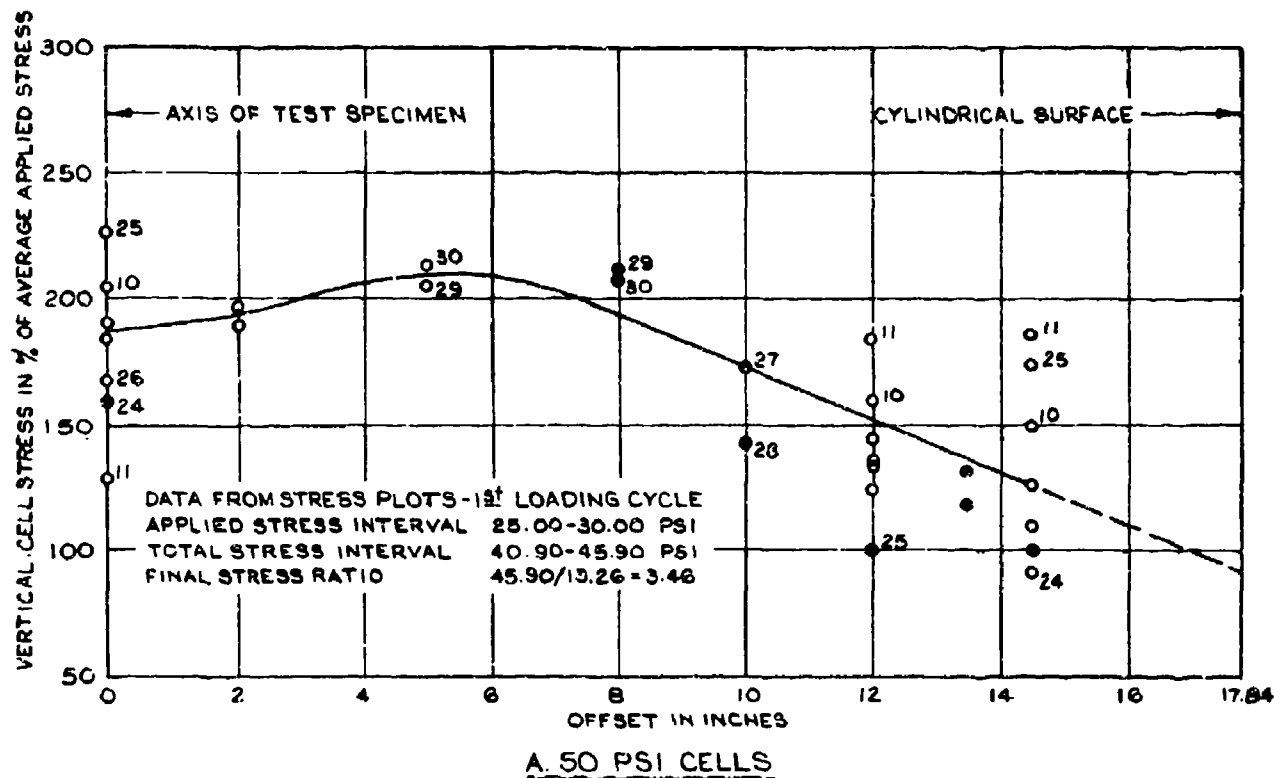


FIGURE 58. MEASURED STRESSES AT MIDHEIGHT FOR APPLIED LOAD INTERVAL 25-30 PSI.

midheight which has a slight minimum at the axis and maximum at the cylindrical surface. The observed stresses show a minimum at the axis, a maximum at a radial offset of about 5 in., and decrease to another minimum at the cylindrical surface. This stress distribution may possibly be an after-effect of friction between the test specimen and the forming jacket, now removed. The stresses caused by deadweight and vacuum are not included in the stresses shown in the following diagrams but are used to determine the stress changes caused by applied axial loads.

112. The stress increase caused by application of an axial unit load of 13.26 psi is shown in Figure 56a and b. The observed data indicate maximum stress near the axis and minimum stress at the cylindrical surface which agrees with the theory for stress distribution in a cylinder with end restraint, Figures 44 and 45, but the observed stress variations with the radial offset are much greater than the theoretical variations, Figure 45. The stresses indicated by 100-psi cells are greater than those indicated by the more compressible 50-psi cells. The central 100-psi cells show a slight overregistration and are less compressible than the test specimen, whereas the opposite applies to the 50-psi cells.

113. The same pattern and comments apply to the stresses shown in Figure 57a and b, which correspond to the average slope of the cyclic soil-cell stress lines for the applied load interval 0 to 25 psi, Figure 53, but it should be noted that the stresses are slightly higher than those obtained for the applied load interval 0 to 13.26 psi, as shown in Figure 56. In general, the soil-cell stress lines are lightly curved even for cyclic loading. Replacing these slightly curved lines with straight lines may lead to erroneous generalizations, which will be discussed in a later section on "Comparisons and Secondary Factors."

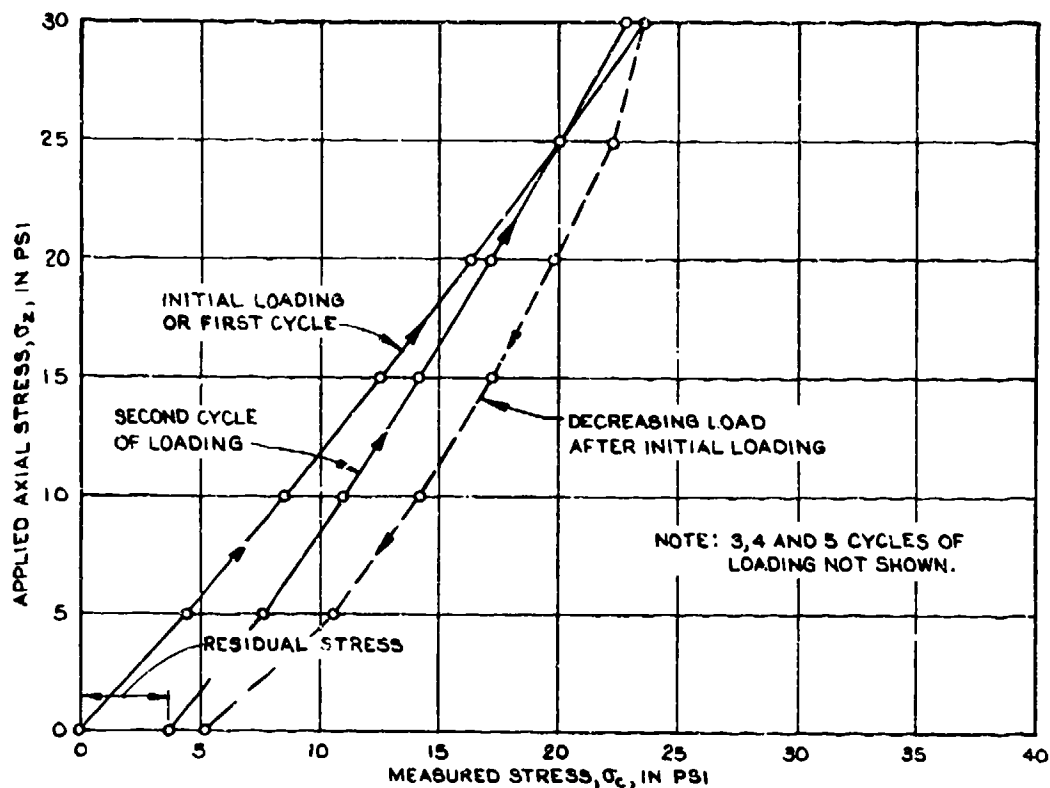
114. The soil-cell stress lines show a great increase in curvature or secant slope for the last load interval, 25 to 30 psi, Figure 53. This corresponds to a greater increase in registration ratio, σ_c/σ_z , as shown in Figures 58a and b. These observations also apply to cyclic loading when the magnitude of the load approaches that of the previous load. It may be noted that the maximum applied load, $\sigma_z = 30$ psi,

creates total stresses with a principal stress ratio of 3.42, which is close to that of failure of a test specimen of sand. The significance of this great increase of the registration ratio will be discussed in a later section and was the subject of additional investigations in the 1955 test series.

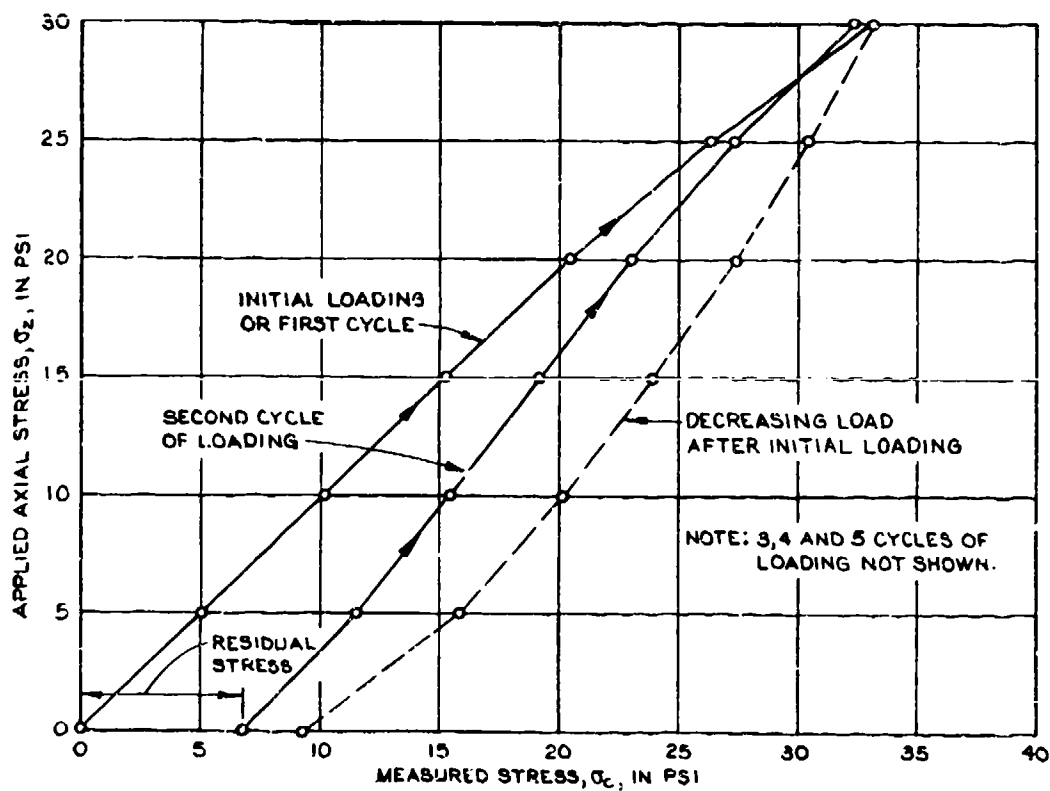
115. Stress conditions at base of test specimen. The theoretical stress distribution at the base of a cylinder with restrained ends and subjected to uniaxial loading is shown in Figure 45. However, the stresses at the base were measured by pressure cells placed directly on top of the rigid base plate. According to the simplified theory, the registration ratio of a pressure cell placed on a rigid boundary corresponds to that of a cell with twice the thickness and placed in a uniform medium, but a more rigorous investigation of this problem has not yet been made. On account of these uncertainties and because the action of pressure cells close to the midheight of a triaxial test specimen is of greater interest, this report is confined to discussion of the registration of pressure cells at the base for a change in the applied axial load.

116. Examples of soil-cell stress lines for cells at the base of the test specimen are shown in Figure 59. In contrast to the soil-cell pressure lines for a pressure cell at midheight of the test specimen, the lines in Figures 59a and b are concave upward and the registration ratio of the cells does not increase with increasing axial load or stress. It may also be mentioned that the lines for cyclic loading in some cases show a small negative residual stress, probably caused by installation difficulties and by restraint exerted by the rigid base. Negative residual stresses were not observed when the more compressible 50-psi pressure cells were used; see section on residual stresses and Figure 62.

117. An example of measured axial stresses at the base of the test specimen is shown in Figure 60. The maximum axial load was usually 30 psi, but a few tests were performed with maximum unit loads of 20, 25, and 35 psi. The diagrams are concave upwards, which is in agreement with theory, Figure 45, but the numerical values for the central part of the specimen are smaller than the corresponding theoretical value, in

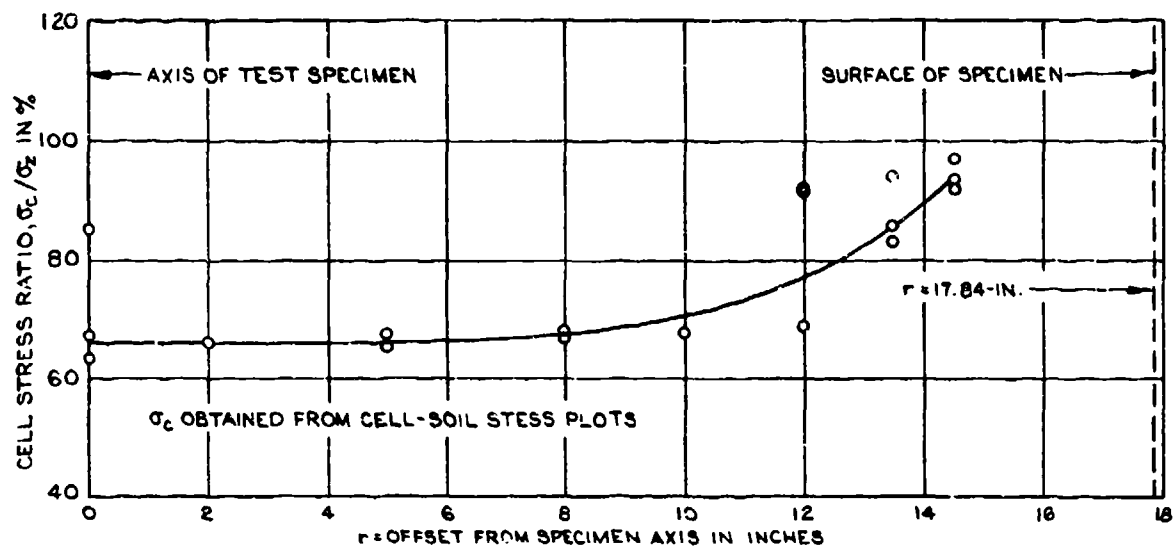


A. OFFSET 5-IN., CELL 94, CAPACITY 50 PSI

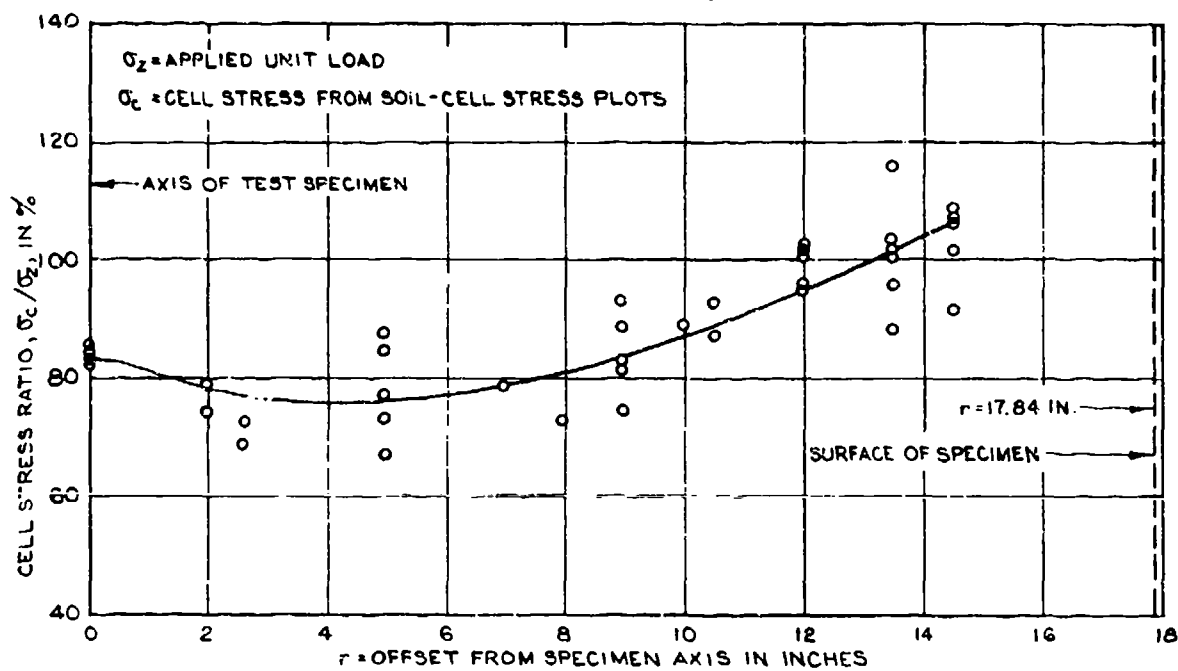


B. OFFSET 13.5-IN., CELL 89, CAPACITY 50 PSI

FIGURE 59. TYPICAL SOIL-CELL STRESS DIAGRAMS FOR BASE OF TEST SPECIMEN.



A. 50 PSI PRESSURE CELLS



B. 100 PSI PRESSURE CELLS

FIGURE 60. MEASURED STRESSES AT SPECIMEN BASE FOR APPLIED LOADS OF 20-30 PSI.

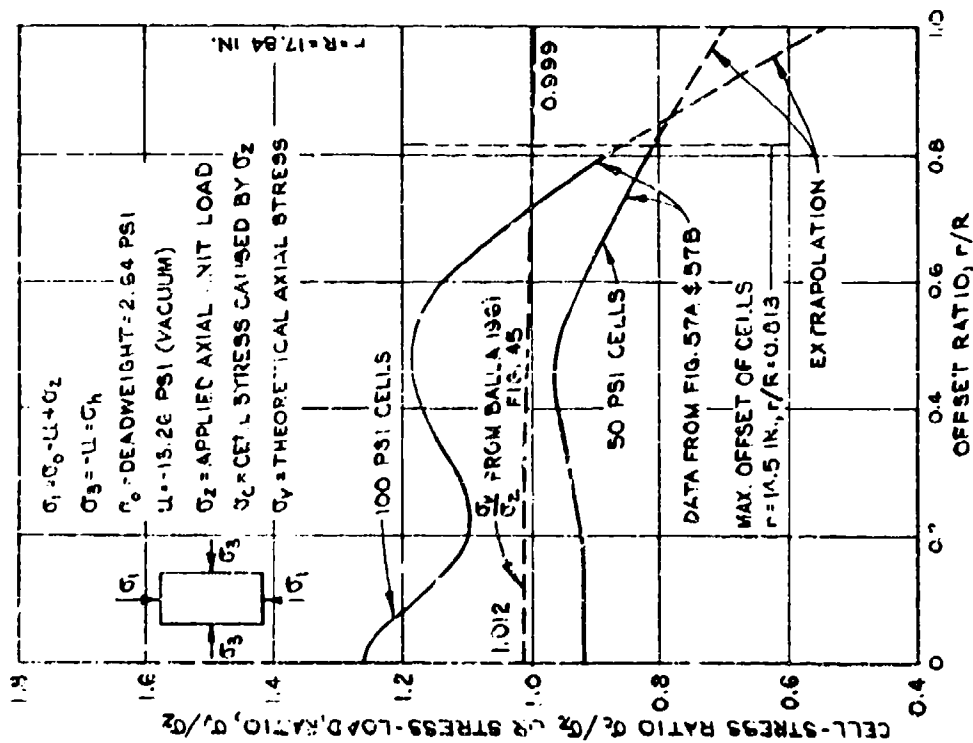
spite of the fact that the pressure cells were placed on top of the rigid base plate, which should increase the registration ratio, according to the simplified pressure cell theory.

Comparisons and analysis

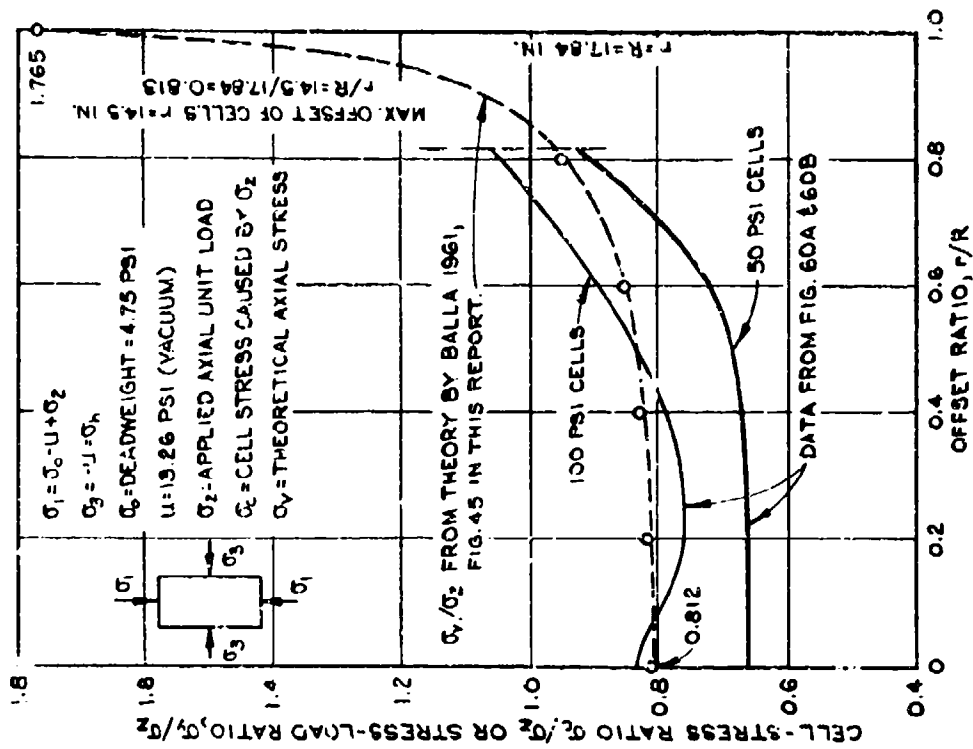
118. Experimental versus theoretical data. A simplified form of Figures 57 and 60 is shown in Figure 61, which facilitates comparison of theoretical data, Figure 45, with experimental data obtained by 50- and 100-psi pressure cells. The general form of the experimental curves agrees with that of the theoretical curves, but there are large variations in the experimental curves. In the central part of Figure 61a the theoretical diagram lies between the experimental curves obtained by 50- and 100-psi pressure cells. This may indicate that the 50-psi cells are more compressible and the 100-psi cells less compressible than the sand in the test specimen for the particular stress conditions. However, the slope of the outer part of experimental curves for the midheight section is much greater than the corresponding slope of the theoretical curve, and the stress distribution curves for 50- and 10-psi cell intersect each other. This intersection cannot be explained by available theories, and it is probable that the reliability of the extrapolation is not reliable.

119. The diagrams in Figure 61b show measured stresses at the base and that both 50- and 100-psi cells in the central area indicate stresses which are well below the theoretical stresses. The latter increase sharply close to the cylindrical surface, where stresses cannot be measured with the usual pressure cells. Simple extrapolation of experimental data up to 14.5 in. from the axis would result in much too small stresses at the cylindrical surface, in comparison with the theoretical stresses, and the reliability of the extrapolated parts of experimental curves is questionable.

120. Summation of measured stresses. The ratio of measured forces, p_m , to applied axial forces, P_z , was determined in some cases in an effort to obtain numerical estimates of the overregistration or underregistration of the pressure cells. The measured forces were determined by dividing the cross section of the test specimen into nine



A. AT MIDHEIGHT OF TEST SPECIMEN



B. AT BASE OF TEST SPECIMEN

FIGURE 61. SUMMARY OF THEORETICAL AND EXPERIMENTAL DATA ON AXIAL STRESSES.

circular segments, with a width of 2.0 in. for the inner segments and 1.84 in. for the outer segment, and then multiplying the area of each segment with the average measured stress for the segment, obtained from the stress distribution curves. The total measured force is then,

$$P_m = \sum_{n=0}^9 \Delta A_n \cdot \sigma_n \quad (92)$$

and the ratio P_m/P_z represents the weighted average overregistration or underregistration of the cells used in determining the stress distribution curve, assuming that the actual stress distribution is uniform, which is unusual. In reality, the ratio P_m/P_z is a mathematical expression for the relative position of the experimental stress distribution curve and the line $(\sigma_c/\sigma_z) = 0$. In ideal cases the ratio P_m/P_z may furnish a check on and improvement of estimated overall registration ratios, but in case of the WES tests the ratio P_m/P_z does not furnish any new information and is less reliable than the experimental stress distribution curves, because P_m depends on extrapolation of the measured stress distribution curve from an offset of 14.5 in. to the cylindrical surface at an offset of 17.84 in. The accuracy of the extrapolated part of the stress distribution curve is questionable in many cases and causes a corresponding unreliability in the computed values of P_m/P_z . Computed values of this ratio vary from 0.78 to 1.11, but stress distribution curves similar to those in Figure 58 would yield much higher values of P_m/P_z .

121. Influence of loading conditions. In discussion of the measured stresses at midheight of the test specimen, it was mentioned that the registration ratio of the pressure cells increases with increasing axial stress or the principal stress ratio, Figures 57 and 58. This agrees with the downward curvature of the soil-cell stress diagram, Figure 53. The opposite applies to pressure cells at the base of the test specimen, Figure 59. Corresponding but greater changes occur in the incremental registration ratios, $\Delta\sigma_c/\Delta\sigma_z$, which are readily determined by the secant slopes of the soil-cell stress diagrams for each

load increment, Figures 53 and 59. The results of the computations are shown graphically in Figure 62. It is seen that the incremental ratios increase to about 2.0 with increasing axial stress, constant lateral stresses, and a corresponding increase of the principal stress ratio. On the other hand, pressure cells at the base of the test specimen are subject to a relatively small decrease with increasing axial load. This decrease is probably related to the end restraint and the increase of radial stresses with increasing axial stresses. It is seen that the registration ratio is not a unique or constant property of pressure cells measuring axial stresses in a test specimen subjected to uniaxial changes in loads or stresses.

122. Changes of the cell registration ratio with the stress conditions was investigated in much greater detail during the 1955 test series, and the results are described in the next part of this report. At this time it shall only be mentioned that changes in the cell registration ratio can be decreased or eliminated by supplementing changes in axial stresses with corresponding changes in lateral stresses or by maintaining the principal stress ratio within certain critical ranges.

123. Influence of residual stresses. The foregoing paragraphs deal primarily with changes in the applied axial stress and corresponding changes in measured stresses. The total measured stresses include also measurement of stresses caused by deadweight, by vacuum and corresponding all-round soils stress, and by residual stresses after the first loading cycle, Figure 53. The residual stress reflects local stress changes in soil adjacent to the pressure cell. Measured stresses from deadweight and vacuum show only small changes with cell offset and capacity, Figure 55, and they are not affected appreciably by applied axial loads. On the other hand, the measured residual vary greatly with cell position, capacity, or compressibility, and they may cause appreciable changes in the shape and relative position of stress distribution curves for total stresses. It should also be borne in mind that the measured residual stresses represent not only true residual stresses but also stress changes caused by movement and improved seating of a cell during the first loading cycle.

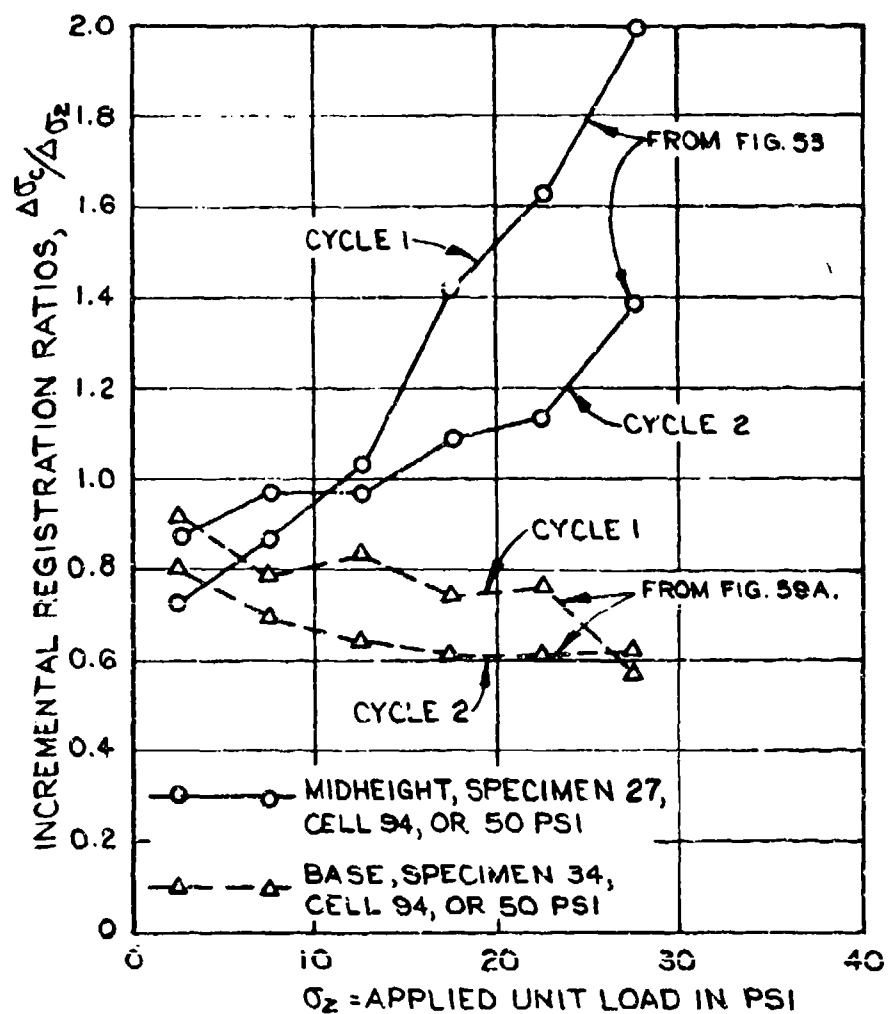


FIGURE 62. CHANGES IN INCREMENTAL REGISTRATIOH RATIO WITH INCREASING APPLIED AXIAL LOAD.

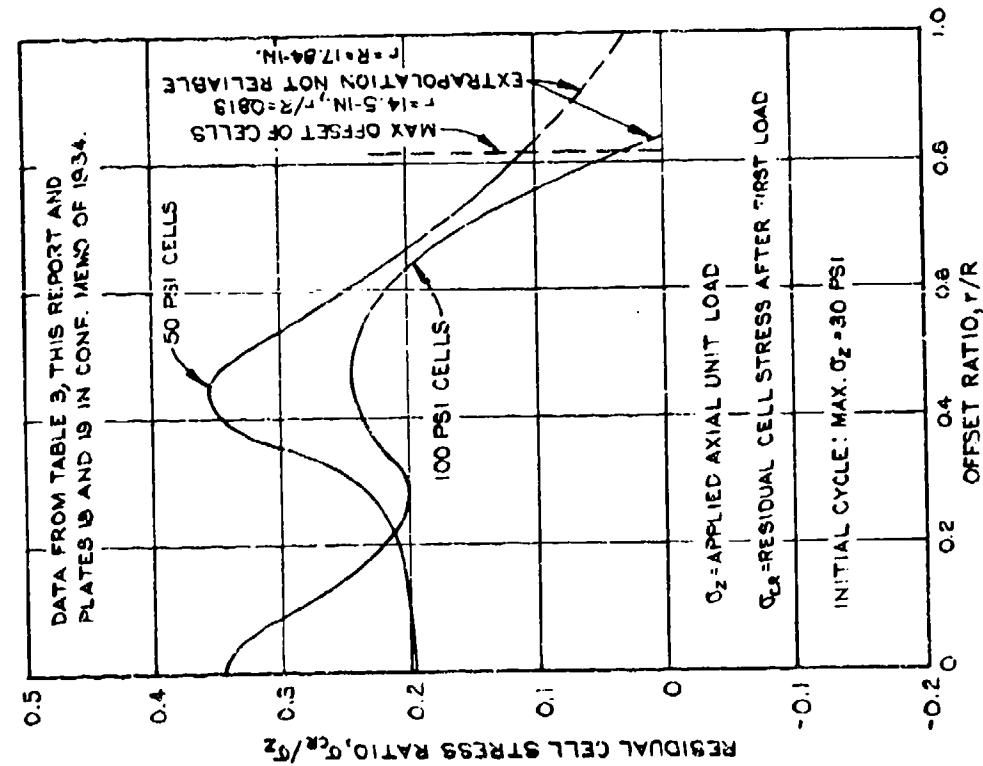
124. Examples of residual stresses measured by 50- and 100-psi pressure cells at midheight and base of test specimen are shown in Figure 63. In all cases the residual stresses at 50-psi cells are larger than those at 100-psi cells. At midheight the residual stresses decrease to very small values at the surface of the test specimen and attain an unexplained maximum at an offset ratio (r/R) of about 0.45. For cells on the rigid base plate the residual stresses increase from the center towards the edge of the test specimen, and 100-psi cells near the center indicated small negative stresses. These results are probably caused by end restraint and possibly also by small movements or adjustments in the seating of the cells.

125. Measurement of soil stresses with pressure cells without considering the influence of local residual stresses at the cells may yield quite misleading results. An effort should be made to determine, counteract, or eliminate the influence of residual stresses at the cells. The simplest and most direct method will probably be to preload the soil over a cell to the ultimate stress after the soil cover over the cell is sufficient to maintain the residual stresses. The preloading may be accomplished by construction equipment or movable weights. The difference between the cell readings before and after preloading gives an approximate value of the residual stress, which in turn may be used to establish new and compensated zero readings of the cell. Furthermore, the preloading will probably cause an improved and more reliable seating of the pressure cell. Seating loads (vacuum) were applied in the test series of 1955, and corresponding changes in pressure cell indications were observed.

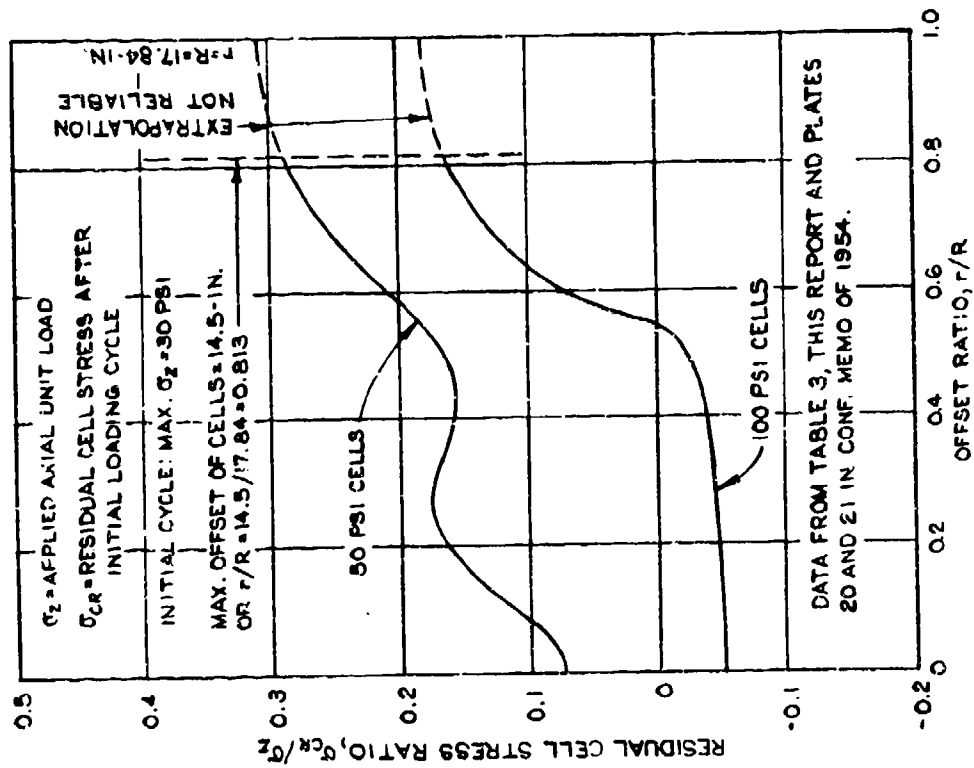
Cell Action Tests of 1955

Purposes and procedures

126. Principal objectives. The 1955 test series supplements that of 1954, and the objectives were to investigate not the stress distribution in the test specimen but the action or registration ratios of pressure cells at comparable locations but with the cells oriented in different directions to measure axial, radial, tangential, and 45° diagonal



A. AT MIDHEIGHT OF TEST SPECIMEN



B. AT BASE OF TEST SPECIMEN

FIGURE 63. MEASURED RESIDUAL STRESSES AFTER INITIAL LOADING CYCLE.

stresses for uniaxial loading and also for various triaxial loadings in which the principal stress ratios in the test specimen were maintained at constant values. Special tests were also made to investigate the effect of an inactive rim added to the standard 6-in. WES pressure cell and to determine the angle of internal friction of the sand used in the experiments.

127. Location of pressure cells. All cells were placed at an offset of 9 in. from the axis and 9 in. above or below midheight of the test specimen, Figure 51. Placement in the two planes was selected to gain more freedom in arrangement of cells or groups of cells. The angular spacing of the cells in the same plane was 90 to 120 deg, and cells in two planes were offset by half of those angles. At this location or a height ratio $h/H = 9/35 = 0.257$ and a radial offset ratio $r/R = 0.5$, the theory by Balla (1961) yields the theoretical axial stresses $\sigma_a = 1.01\sigma_z$ for uniform triaxial loading, Figure 45. These small deviations from the average unit loads are neglected in the following evaluation of the test data.

128. Equipment and test preparations. The triaxial testing equipment and the sand for the test specimen were the same as those used in the 1954 test series. The sand was compacted to a density of 108.5 pcf in all tests. Standard 100-psi WES cells were used whenever possible but were replaced with 50-psi cells in a few tests. A seating load or vacuum of 13.26 psi was applied three times after completion of the test specimen but before it was removed from the forming jacket. The forming jacket may absorb a considerable part of the lateral seating load. The axial seating stress may attain its full nominal value at the end surfaces but it is gradually reduced by sidewall friction. At midheight of the test specimen the axial seating stress may only be 40 to 50 percent of the stress on the end surfaces. The vacuum during removal of the forming jacket was 2.5 psi, which was increased to 4 to 5 psi at the start of most tests. A few pressure cells developed leaks to the space below the interior measuring diaphragm, which was taken into consideration when evaluating the cell indications. Pressure cell No. 117 was intentionally vented after possible leakage was discovered.

129. Six-inch strain gages were placed at various elevations and offsets in some tests, but the rods of the strain gages were often bent during testing, and the results obtained by the strain gages do not appear to be reliable in a quantitative sense and were not used in evaluation of the test data. Outside axial and lateral deformations were measured in all tests, and the results are used and summarized in this report.

130. Testing procedures. One series of tests were performed as uniaxial stage tests. The vacuum or confining pressure during the first stage was maintained at 4 psi, while the axial load was increased until a relatively flat slope of the stress-strain diagram was attained, Figure 64, whereupon the applied axial load was gradually decreased to zero. The vacuum was then increased to 8 psi and a new axial loading test was performed, which was followed by a third and a fourth test series both at a vacuum of 12 psi. In another series of tests the principal stress ratio was maintained at a constant value while the axial and lateral loads were increased until a limiting vacuum or $\sigma_3 = 12$ psi was attained, whereupon the loading cycle was repeated with another principal stress ratio. Several cyclic soil-cell stress diagrams were obtained for principal stress ratios of 1.0, 1.5, 2.0, 2.5, and 3.0. After the final load cycle all tests were continued as uniaxial tests without further change in maximum vacuum until large axial strains or practical failure of the test specimen occurred. The increment of the axial increase or decrease of the unit load varied between 2 and 5 psi, depending on the maximum load. The deadweight of the soil, but not residual stresses and strains at the pressure cells, was considered in computing the total stresses and the principal stress ratios. Each type of test was usually performed in triplicate. Variations of the Poisson ratios for specimen 70 were computed from observed axial and radial strain and are tabulated in Figure 64.

131. Summaries of test data. Detailed summaries of data for the principal tests of 1955 are presented in Table 4, which is an uncorrected copy of Table 1 in the Conference Memo of September 1955. The stresses shown are averages of those indicated at the end of cycles and duplicate

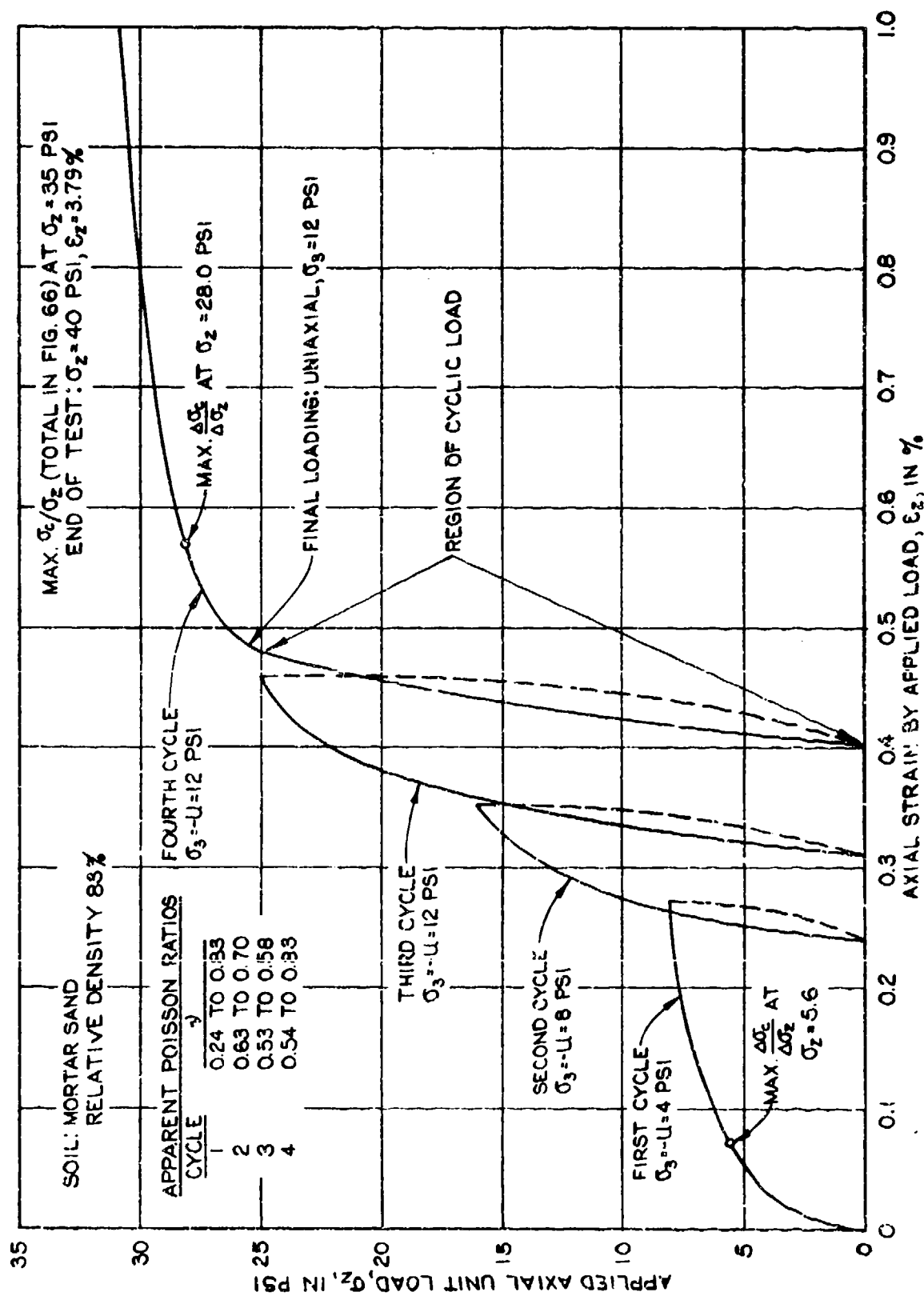


FIGURE 64. AXIAL STRESS-STRAIN DIAGRAMS FOR SPECIMEN 70-UNIAXIAL STAGE LOADING.

Summary of Appl

Specimen No.	Stress Ratio Is	Pressure Cell Elevation* in.	Pressure Cell No. for Type Stress Measured				Vertical Stress								Cyclic	
			Vertical	Diagonal	Horizontal		Applied psi	Cyclic Measured		Total Measured		Failure Slope	Applied psi	psi		
					Radial	Tangential		psi	Percent Applied	psi	Percent Applied					
48	3.0	35	91†	--	108†	--	35.6	48.4	136	40.7	59.0	145	--	--	--	
49	3.0	35	91†	--	108†	--	34.8	45.0	129	39.9	57.5	144	0.455	--	--	
50	3.0	35	86	--	82	--	34.8	47.0	135	39.9	57.0	143	0.492	--	--	
51	2.0	35	86	--	82	--	34.8	45.0	129	39.9	54.0	135	--	--	--	
67	2.5	26	82	83	119	85	26.2	33.0	126	31.8	41.5	131	0.566	18.2	19.9	
68	2.5	26	82	83	119	--	26.2	29.2	111	31.8	36.8	116	0.570	18.2	21.2	
69	2.5	26	82	83	119	100†	26.2	31.2	119	31.8	39.7	125	0.501	18.2	19.6	
67	2.5	44	86	118	117	108†	26.2	33.2	127	30.7	41.5	135	0.510	18.1	18.6	
68	2.5	44	86	118	117	108†	26.2	33.4	128	30.7	41.6	136	0.475	18.1	21.1	
69	2.5	44	86	118	117	108†	26.2	31.2	119	30.7	37.6	122	0.494	18.1	20.2	
58	2.0	26	121	85	119	120	20.0	25.0	125	25.6	33.0	129	0.513	15.1	16.8	
59	2.0	26	121	85	119	120	20.0	24.8	124	25.6	33.3	130	0.512	15.1	17.0	
60	2.0	26	121	85	119	120	20.0	22.3	112	25.6	31.3	122	0.469	15.1	17.8	
61	2.0	26	120	82	83	108†	20.0	23.8	119	25.6	32.2	126	0.506	15.1	17.2	
62	2.0	26	119	82	83	121	20.0	22.5	113	25.6	31.0	121	0.566	15.1	17.0	
63	2.0	26	119	82	83	121	20.0	22.1	111	25.6	29.5	115	0.478	15.1	17.1	
55	2.0	44	91†	85	83	108†	20.0	20.6	103	24.5	26.4	108	--	15.0	16.7	
56	2.0	44	91†	85	83	108†	20.0	26.4	132	24.5	34.4	140	0.463	15.0	16.8	
57	2.0	44	91†	85	83	108†	20.0	26.9	135	24.5	34.7	142	0.557	15.0	16.4	
61	2.0	44	85	118	86	117	20.0	23.6	118	24.5	31.0	127	0.429	15.0	16.8	
62	2.0	44	85	118	86	117	20.0	24.0	120	24.5	30.6	125	0.515	15.0	16.0	
63	2.0	44	85	118	86	117	20.0	24.0	120	24.5	31.8	130	0.466	15.0	19.2	
64	1.5††	26	83	82	108†	84	11.1	13.3	120	19.3	23.1	120	0.429	9.3	11.3	
65	1.5	26	83	82	119	84	11.1	12.3	111	19.3	21.8	113	0.501	9.3	12.1	
66	1.5	26	83	82	119	84	11.1	12.9	116	19.3	23.5	122	0.475	9.3	11.4	
64	1.5	44	120	118	85	86	11.1	14.3	129	18.2	22.7	125	0.472	9.3	10.8	
65	1.5	44	120	118	86	117	11.1	13.4	121	18.2	24.2	133	0.481	9.3	11.3	
66	1.5	44	121	118	86	108†	11.1	15.2	137	18.2	27.5	151	0.476	9.3	10.2	
64	1.0†	26	83	82	108†	84	10.1	12.6	125	15.7	20.9	133	--	10.1	12.6	
65	1.0	26	83	82	119	84	10.1	11.6	115	15.7	19.3	123	--	10.1	13.2	
66	1.0	26	83	82	119	84	10.1	11.8	117	15.7	18.3	117	--	10.1	12.5	
64	1.0	44	120	118	85	66	10.1	12.8	127	14.6	19.3	132	--	10.1	11.9	
65	1.0	44	120	118	86	117	10.1	11.8	117	14.6	19.3	132	--	10.1	11.9	
66	1.0	44	121	118	86	108	10.1	14.7	146	14.6	22.6	155	--	10.1	11.4	
70	Constant lateral††	26	82	83	119	121	33.0	41.6	126	40.2	52.6	131	0.540	20.5	21.5	
71	Constant lateral	26	82	83	119	85	33.0	44.0	133	40.2	57.0	142	0.544	20.5	21.7	
72	Constant lateral	26	82	85	119	83	33.0	41.3	125	40.2	51.3	128	0.604	20.5	19.0	
70	Constant lateral	44	86	120	117‡	108†	33.0	41.5	126	39.1	51.5	132	0.583	20.5	20.1	
71	Constant lateral	44	86	120	117‡	108†	33.0	46.5	141	39.1	56.5	145	0.441	20.5	21.3	
72	Constant lateral	44	86	120	117‡	84	33.0	45.8	139	39.1	55.8	143	0.530	20.5	20.6	

- * All cells located at 9-in. offset from center of specimen.
 ** Computed using measured diagonal and horizontal (radial) stresses.
 † 50-psi capacity cells.
 †† Tested subsequent to tests using a stress ratio of 1.0 (fourth, fifth, and sixth cycles).
 ‡ An approximate stress ratio of 1.0 was obtained by applying varying confining pressure only to specimens. Because of the weight of the head pl 1.0 cannot be obtained.
 §§ Tests using three confining pressures (4, 8, and 12 psi) applied in a ending order.
 ¶ Cell 117 vented in Tests 70, 71, and 72.

2

Table 4
Summary of Applied and Measured Stresses in Triaxial Test Specimens
1955 Test Series

Specimen No.	Failure Slope	Diagonal Stress							Horizontal Stress										Vertical Stress psi	Residual Stress psi	Horizontal Stress psi			
		Cyclic				Total			Applied Cyclic psi	Total psi	Measured				Tangential									
		Applied		Measured		Applied		Measured			Radial		Total		Cyclic		Total							
		psi	Percent Applied	psi	Percent Applied	psi	Percent Applied	psi			Percent Applied	psi	Percent Applied	psi	Percent Applied	psi	Percent Applied	psi				Percent Applied	psi	Percent Applied
145	--	--	--	--	--	--	--	--	11.1	13.6	12.0	108	14.3	105	--	--	--	--	3.6	--	0			
144	0.455	--	--	--	--	--	--	--	10.8	13.3	10.8	106	13.2	99	--	--	--	--	6.0	--	0			
143	0.492	--	--	--	--	--	--	--	10.8	13.3	11.6	107	13.1	98	--	--	--	--	3.0	--	0			
135	--	--	--	--	--	--	--	--	10.8	13.3	11.0	102	13.5	102	--	--	--	--	2.4	0.0	0			
131	0.566	18.2	109	19.9	109	22.7	23.6	106	0.435	10.1	12.5	11.5	114	13.7	110	10.3	102	12.4	99	1.5	-0.5	0		
116	0.570	16.2	116	21.2	116	22.2	26.3	118	0.539	10.1	12.5	10.6	105	13.0	104	--	--	--	--	1.5	0.4	0		
125	0.501	18.2	108	19.6	108	22.2	23.3	105	0.549	10.1	12.5	11.1	110	12.7	102	8.1	80	11.0	88	2.0	-0.5	0		
135	0.510	18.1	103	18.6	103	21.6	21.6	100	0.506	10.1	12.5	10.1	100	12.7	102	9.8	97	11.3	90	2.5	-0.5	0		
136	0.475	18.1	117	21.1	117	21.6	24.6	115	0.595	10.1	12.5	10.1	100	12.5	100	9.9	92	12.0	95	2.5	-0.3	0		
122	0.494	18.1	112	20.2	112	21.6	23.5	109	0.708	10.1	12.5	10.5	104	12.3	98	9.5	94	10.7	86	1.0	-0.5	0		
129	0.513	15.1	111	16.6	111	19.1	21.3	112	0.621	10.1	12.5	10.9	108	13.3	106	10.1	100	11.5	92	1.0	0.0	0		
130	0.512	15.1	113	17.0	113	19.1	20.7	108	0.609	10.1	12.5	10.3	102	12.0	96	10.3	102	11.7	94	2.0	-0.6	0		
122	0.469	15.1	118	17.8	118	19.1	22.4	117	0.550	10.1	12.5	10.6	105	12.8	102	10.1	100	11.9	95	2.6	0.0	0		
126	0.506	15.1	114	17.2	114	19.1	21.7	114	0.580	10.1	12.5	10.3	102	12.4	99	10.7	106	12.6	101	1.7	0.0	0		
121	0.564	15.1	113	17.0	113	19.1	20.2	106	0.540	10.1	12.5	10.7	106	12.6	101	10.1	100	11.6	93	2.5	-1.4	0		
115	0.478	15.1	113	17.1	113	19.1	20.6	108	0.403	10.1	12.5	10.5	104	12.6	101	10.2	101	12.1	97	1.0	-0.8	0		
108	--	15.0	111	16.7	111	18.5	20.3	110	--	10.1	12.5	10.1	100	11.6	93	10.1	100	12.1	97	0.9	-0.1	0		
140	0.463	15.0	112	16.8	112	18.5	20.9	113	0.479	10.1	12.5	10.2	101	11.8	94	9.9	98	11.4	91	2.0	0.0	0		
142	0.557	15.0	109	16.4	109	18.5	21.3	115	0.633	10.1	12.5	10.6	105	12.8	102	9.6	95	11.0	88	2.0	1.1	0		
127	0.463	15.0	112	16.3	112	18.5	20.5	111	0.636	10.1	12.5	11.2	111	14.7	115	10.4	103	11.5	94	1.5	0.0	0		
125	0.515	15.0	107	16.0	107	18.5	19.0	103	0.570	10.1	12.5	11.7	116	13.4	107	9.8	97	11.3	90	1.1	0.0	0		
130	0.466	15.0	128	19.2	128	18.5	23.3	126	0.465	10.1	12.5	12.3	122	13.8	110	7.4	73	8.8	70	2.2	-0.5	0		
120	0.429	9.3	113	11.3	122	15.9	17.1	107	0.455	7.5	12.5	8.3	111	13.2	106	8.2	109	12.1	97	0.4	-2.0	0		
113	0.501	9.3	130	12.1	130	15.9	18.1	114	0.620	7.5	12.5	9.9	132	14.4	115	8.5	113	12.5	100	0.5	-2.4	0		
122	0.475	9.3	123	11.4	123	15.9	18.7	118	0.470	7.5	12.5	9.4	125	13.9	111	8.7	116	12.5	100	0.0	-0.8	0		
125	0.472	9.3	116	10.8	116	15.4	16.0	104	0.595	7.5	12.5	8.2	109	11.9	95	9.3	124	13.4	107	-0.5	-1.7	0		
133	0.481	9.3	122	11.3	122	15.4	16.7	108	0.625	7.5	12.5	8.7	116	12.3	98	8.2	109	12.7	102	2.3	-1.9	0		
151	0.476	9.3	110	10.2	110	15.4	15.7	102	0.571	7.5	12.5	8.9	119	12.1	97	8.0	107	12.6	101	1.3	-1.4	0		
133	--	10.1	125	12.6	125	14.1	17.1	121	--	10.1	12.5	11.0	109	13.7	110	9.8	97	12.4	99	1.6	-0.5	0		
123	--	10.1	131	13.2	131	14.1	18.2	129	--	10.1	12.5	12.4	123	15.1	121	10.1	100	12.5	100	2.1	-0.2	0		
117	--	10.1	125	12.5	124	14.1	16.5	117	--	10.1	12.5	11.6	115	13.9	111	10.8	107	12.8	102	1.4	-0.8	0		
132	--	10.1	118	11.9	118	13.6	15.5	114	--	10.1	12.5	10.8	107	13.2	106	11.5	114	13.8	110	0.9	-0.4	0		
132	--	10.1	119	11.9	118	13.6	15.7	115	--	10.1	12.5	10.8	107	12.9	103	10.7	106	13.8	110	2.6	-0.2	0		
155	--	10.1	114	11.4	113	13.6	13.8	102	--	10.1	12.5	11.1	110	12.4	99	9.8	97	11.7	94	2.7	-1.4	0		
131	0.540	20.5	105	21.5	105	26.1	27.8	107	0.463	8.0	12.0	7.9	99	11.7	98	11.5	144	17.1	143	2.0	0.5	0		
142	0.544	20.5	107	21.7	107	26.1	28.2	108	0.456	8.0	12.0	7.4	93	11.4	95	7.4	93	11.6	97	3.5	0.6	0		
128	0.604	20.5	93	19.0	93	26.1	24.0	92	0.570	8.0	12.0	7.6	95	11.2	93	6.9	86	10.4	87	2.8	0.0	0		
132	0.583	20.5	98	20.1	98	25.6	25.4	99	0.506	8.0	12.0	8.5	106	12.5	104	6.7	84	10.2	85	2.2	0.5	0		
145	0.441	20.5	104	21.3	104	25.6	26.7	104	0.585	8.0	12.0	7.4	92	10.8	90	6.6	83	9.8	82	1.6	0.0	0		
143	0.530	20.5	101	20.6	101	25.5	25.6	100	0.551	8.0	12.0	7.7	96	10.9	91	6.8	85	9.9	83	1.3	0.0	0		

Due to the weight of the head plate and overburden, an exact ratio of

COPY AVAILABLE
PERMIT FUL

Tangential				Residual Stress				Computed Vertical Stress**			
Cyclic	Percent	Total	Percent	Vertical	Diagonal	Horizontal	Stress	Cyclic	Percent	Total	Percent
Applied	Applied	Applied	Applied	Stress	Stress	Radial	Tangential	Stress	Applied	Applied	Applied
psi	psi	psi	psi	psi	psi	psi	psi	psi	psi	psi	psi
--	--	--	--	3.5	--	0.4	--	--	--	--	--
--	--	--	--	6.0	--	0.0	--	--	--	--	--
--	--	--	--	3.0	--	-1.1	--	--	--	--	--
--	--	--	--	2.4	0.0	0.0	--	--	--	--	--
.3	102	12.4	99	1.5	-0.5	-0.5	-0.4	28.3	108	33.5	105
--	--	--	--	1.5	0.4	0.0	--	31.8	121	39.6	125
.1	80	11.0	88	2.0	-0.5	-1.0	1.0	28.1	107	33.9	107
.8	97	11.3	90	2.5	-0.5	0.2	-0.8	27.1	103	30.5	99
.9	98	12.0	96	2.5	-0.3	0.0	-0.2	32.1	123	37.1	121
.5	94	10.7	86	1.0	-0.5	-0.6	-1.1	29.9	114	34.7	113
.1	100	11.5	92	1.0	0.0	-0.2	-1.0	22.5	113	29.3	114
.3	102	11.7	94	2.0	-0.6	-0.5	-1.0	23.7	119	29.4	115
.1	100	11.9	95	2.6	0.0	-0.2	-0.6	25.0	125	32.0	125
.7	106	12.5	101	1.7	0.0	0.0	-0.6	24.1	121	31.0	121
.1	100	11.6	93	2.5	-1.4	-0.6	-0.9	23.3	117	27.8	109
.2	101	12.1	97	1.0	-0.8	-0.4	-0.6	23.7	119	28.6	112
.1	100	12.1	97	0.9	-0.1	-1.0	-0.5	25.3	117	29.0	118
.9	98	11.4	91	2.0	0.0	-0.8	-0.8	23.4	117	30.0	122
.6	95	11.0	88	2.0	1.1	-0.2	-0.9	22.2	111	29.8	122
.4	103	11.8	94	1.5	0.0	0.5	-1.0	22.4	112	26.5	108
.8	97	11.3	90	1.1	0.0	-0.9	-0.8	20.3	102	24.6	100
.4	73	8.0	70	2.2	-0.5	-1.0	-0.1	26.1	131	32.8	134
.2	102	12.1	97	0.4	-2.0	-0.8	-1.4	14.3	129	21.0	109
.5	113	12.5	100	0.5	-2.4	-2.0	-1.6	14.3	129	21.8	113
.7	116	13.5	100	0.0	-0.8	-1.8	-1.8	13.4	121	23.5	122
.3	121	13.1	107	-0.5	-1.7	-1.7	-2.0	13.4	121	20.1	110
.2	109	12.7	102	2.3	-1.9	-2.3	-0.9	15.9	125	21.1	116
.0	107	12.6	101	1.3	-1.4	-2.6	-0.7	13.5	122	19.3	106
.8	97	12.4	99	1.6	-0.5	0.0	0.3	14.2	141	20.5	131
.1	100	12.5	100	2.1	-0.2	-0.3	0.0	14.0	139	21.3	135
.8	107	12.8	102	1.4	-0.8	-0.5	-0.5	13.4	133	19.1	124
.5	114	13.8	110	0.9	-0.4	-0.1	-0.5	13.0	129	17.8	122
.7	106	13.8	110	2.6	-0.2	-0.5	0.6	13.0	129	18.5	127
.8	97	11.7	94	2.7	-1.4	-1.1	-0.4	11.7	116	15.2	104
1.5	144	17.1	143	2.0	0.5	-0.2	-0.1	35.1	106	43.9	109
7.4	93	11.6	97	3.5	0.6	0.2	0.5	36.0	109	45.0	112
5.9	86	10.4	87	2.8	0.0	-0.2	0.0	30.4	92	36.6	92
5.7	84	10.2	85	2.2	0.5	-0.2	0.2	31.7	96	38.3	98
5.6	83	9.8	82	1.6	0.0	-0.3	0.0	30.2	107	42.6	109
5.8	85	9.9	83	1.3	0.0	-0.7	-0.3	33.5	102	40.3	103

COPY AVAILABLE TO DDC DOES NOT
PERMIT FULLY LEGIBLE PRODUCTION

tests. The failure or final slope is that of a straight line replacing the last part of the soil-cell stress diagram. Likewise, cyclic test data may be represented by secants or straight lines between average stresses for the maximum cyclic loads. However, replacing slightly curved diagrams by straight lines may result in misleading generalizations, as explained in more detailed discussions of the test data. The applied diagonal stress is one-half the sum of applied axial and radial stresses, or $\sigma_d = 1/2(\sigma_z + \sigma_r)$. Conversely, the computed vertical or axial stresses in the last columns of the table are obtained from measured diagonal and radial stresses and $\sigma_z = 2\sigma_d - \sigma_r$.

132. Table 5 presents average values of measured deformations and corresponding moduli of the test specimen. Table 6 contains average values of registration ratios for the various types of tests, based on Table 4, plus average axial and radial deformations of the test specimen. The results of tests with a 6-in. cell plus a 3-in. inactive rim are shown in Figures 95-97, but the results obtained with internal strain gages and preliminary tests with a shear cell are not summarized in this report. Special tests with the large triaxial apparatus were performed to determine the angle of internal friction of the sand used in the test specimens for investigation of pressure cells. Angles of internal friction obtained with the large triaxial device varied between 38.8 and 40.8 degrees, and the average was 39.4 degrees, which is one degree larger than obtained with standard triaxial equipment.

Axial stresses for uniaxial loading

133. Tests performed. Three test specimens, Nos. 70-72, were subjected to axial stage loading for partial vacua or confining pressures of 4, 8, and 12 psi, applied in ascending order. Pressure cells were placed both above and below midheight of the test specimen or at elevations 26 and 44 in. above the base plate. The results obtained with the three test specimens are in satisfactory agreement, and only the data for test specimen 70 are presented and discussed in the following paragraphs.

134. Stress-strain relations for triaxial specimen. Stress-strain diagrams for uniaxial stage loading of specimen 70 are shown in Figure 64, which clearly indicate the previously mentioned loading

Table 5
Summary of Deformations and Moduli of Sand in Triaxial Test Specimens
1955 Test Series

Specimen No.	Stress Ratio Vertical Horizontal	Maximum Applied Load, kips			Average Vertical Specimen Deflection, in.		Initial Relative Density %				
		Cycle 1	Cycle 2	Failure	Cycle 1	Cycle 2					
								Failure			
40	3.0	24.0	24.0	47.0	0.109	0.237	2.140		0.021	0.025	0.683
50	3.0	24.0	24.0	46.0	0.200	0.228	2.893	0.022	0.026	0.604	84
51	3.0	24.0	24.0	45.0	0.196	0.227	1.752	0.026	0.030	0.656	83
57	2.5	16.0	16.0	38.4	0.097	0.114	2.177	0.005	0.006	0.610	83
60	2.5	16.0	16.0	40.3	0.094	0.108	2.487	0.004	0.006	0.685	79
60	2.5	16.0	16.0	40.3	0.090	0.097	2.740	0.001	0.004	0.701	81
55	2.0	9.9	9.9	--	0.041	0.048	--	0.002	0.003	--	84
56	2.0	9.9	9.9	40.8	0.044	0.053	2.143	-0.002	-0.002	0.707	83
58	2.0	9.9	9.9	41.2	0.047	0.054	2.806	-0.002	-0.001	0.891	84
59	2.0	9.9	9.9	41.2	0.046	0.046	3.016	-0.003	-0.001	0.903	82
60	2.0	9.9	9.9	39.9	0.041	0.046	2.595	0.002	0.001	0.817**	83
61	2.0	9.9	9.9	41.2	0.041	0.048	2.463	-0.001	-0.001	0.756	83
62	2.0	9.9	9.9	38.7	0.052	0.060	3.198	-0.003	-0.003	0.863+	83
63	2.0	9.9	9.9	39.7	0.049	0.058	2.267	-0.002	0.000	0.696	80
64	1.5**	3.7	3.7	38.5	0.029	0.037	2.284	-0.001	-0.002	0.699	84
65	1.5	3.6	3.6	39.6	0.031	0.032	2.515	-0.003	-0.009	0.772	84
66	1.5	3.6	3.6	39.6	0.022	0.025	3.003	-0.006	-0.006	0.774	78
64	1.0†	0.0	0.0	--	0.012	0.014	--	-0.005	-0.005	--	84
55	1.0	0.0	0.0	--	0.014	0.014	--	-0.006	-0.007	--	84
66	1.0	0.0	0.0	--	0.012	0.014	--	-0.005	-0.004	--	78
52	Constant lateral††	--	--	26.4	--	--	2.426	--	--	0.782	82
53	Constant lateral	--	--	11.4	--	--	1.145	--	--	0.361	83
54	Constant lateral	--	--	40.5	--	--	2.533	--	--	0.937	81
70	Constant lateral**	8.0	16.0	40.0	0.186	0.244	2.630	0.038	0.040	0.780	83
71	Constant lateral	8.0	16.0	37.5	0.200	0.250	1.675	0.013	0.012	0.521	84
72	Constant lateral	8.0	16.0	37.5	0.234	0.296	1.899	0.051	0.051	0.533	84
73	Constant lateral	8.0	16.0	37.5	0.291	0.356	2.972	0.079	0.081	0.876	77
74	Constant lateral	8.0	16.0	--	0.304	0.458	--	0.103	0.102	--	84
75	Constant lateral	8.0	16.0	--	0.272	0.381	--	0.072	0.076	--	81
76	Constant lateral	8.0	16.0	--	0.342	0.419	--	0.080	0.081	--	82
77	Constant lateral	8.0	16.0	--	0.533	0.619	--	0.163	0.163	--	79
78	Constant lateral	8.0	16.0	--	0.483	0.576	--	0.121	0.123	--	80

* The plus sign indicates one gage had exceeded the limit of its range.

** Tested subsequent to tests using a stress ratio of 1.0 (fourth, fifth, sixth cycles).

† An approximate stress ratio of 1.0 was obtained by applying varying confining pressure only to specimens. Because of the weight of the headplate and overburden, an exact ratio of 1.0 cannot be obtained.

†† Individual tests using one confining pressure: (a) specimen 52, 8-pai confining pressure; (b) specimen 53, 4-pai confining pressure; (c) specimen 54, 12-pai confining pressure.

* For first cycle constant lateral tests, the modulus of elasticity was determined from the stress at 0.02% specimen strain. For all other cycles and tests the best slope through the stress-strain curve was used to determine the modulus.

** Tests using three confining pressures (4, 8, and 12 pai) applied in ascending order.

† Specimens incorporating strain gages only.

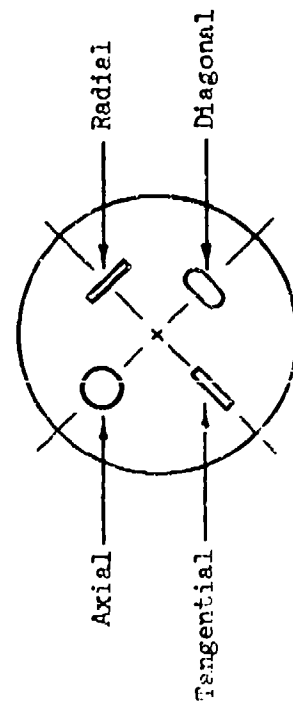
Table 6

Average Registration Ratios of Pressure Cells in Triaxial Test Specimens

1955 Test Series

Principal Stress Ratio σ_1/σ_3	Axial		Diagonal		Cyclic Load		Deformations	
	Cyclic Load σ_c/σ_z %	Final Load σ_c/σ_z %	Cyclic Load σ_c/σ_d %	Final Load σ_c/σ_d %	Radial Stress σ_c/σ_p %	Tangential σ_c/σ_ϕ %	Second Cycle Axial ΔH in.	Second Cycle Radial ΔR in.
3.0	132	212	--	--	104	--	+0.231	-0.027
2.5	122	193	111	184	105	98	+0.106	-0.005
2.0	120	205	113	178	107	101	+0.052	+0.001
1.5	116	214	120	198	119	113	+0.030	+0.006
1.0	119	--	121	--	112	104	+0.014	+0.005
σ_3 Construction uniaxial	Variable	187	100	192	(95)	(86)	+0.265	-0.041

Compression +



All four cells were usually placed in one horizontal plane 9 in. above or below midheight of the test specimen; see Figure 51. No corrections for theoretical stress distribution

procedure. The confining pressures are identical for the third and fourth cycles, and cycle four is therefore a true cyclic test. The modulus of deformation for the first stage and cycle was determined by the secant to the point of 0.02 percent strain; the moduli for the other cycles were determined by straight lines which represent the best fit for the fairly straight parts of the diagrams.

135. Measured axial stresses. Results of the pressure cell tests are summarized by the soil-cell stress plots in Figure 65, which shows the axial stresses indicated by the pressure cells versus the corresponding unit loads. Soil-cell stress diagrams for cycles 2 and 3 are not shown in Figure 65 since they are intermediate between those for cycles 1 and 4, and the loading in these two cycles was not continued until large deformations were attained. Before further evaluation of the test data is presented, it is appropriate to summarize the principal definitions and equations of the simplified theory for interaction of soil and a pressure cell.

136. Definitions and simplified theoretical relations. Taylor (1945) mentions that the simplified theory for pressure cell action actually should be applied to incremental loads and pressure cell indications, but he omitted the incremental sign, Δ , for convenience and used total stresses and deformations, which does not introduce significant additional errors in linear relationships when the moduli of deformation of soil and cell, M_s and M_c , are fairly constant. However, there is considerable difference between equations and relations for incremental and total stresses and deformations when the stress-strain diagrams are curved, as shown in Figure 66. The following summary applies primarily to incremental relations and the corresponding sign, Δ , is reintroduced when appropriate. The overregistration of a pressure cell is defined by

$$\Delta\sigma_e = \Delta\sigma_c - \Delta\sigma_z \quad \text{or} \quad \sigma_e = \sigma_c - \sigma_z \quad (93)$$

since the definition applies to both incremental and total stresses. The corresponding strains are

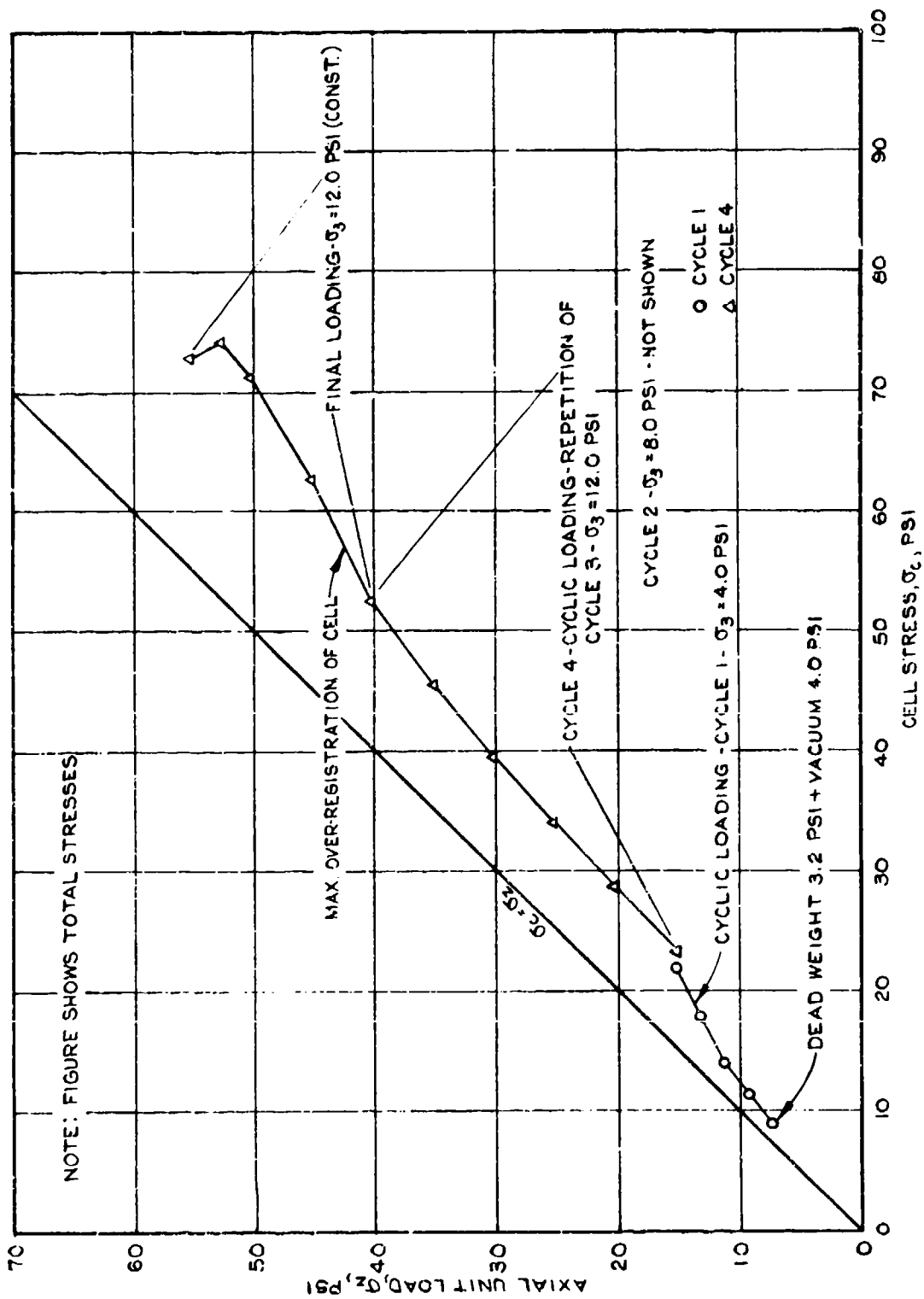


FIGURE 65. SOIL-CELL STRESS DIAGRAMS FOR UNIAXIAL STAGE LOADING.

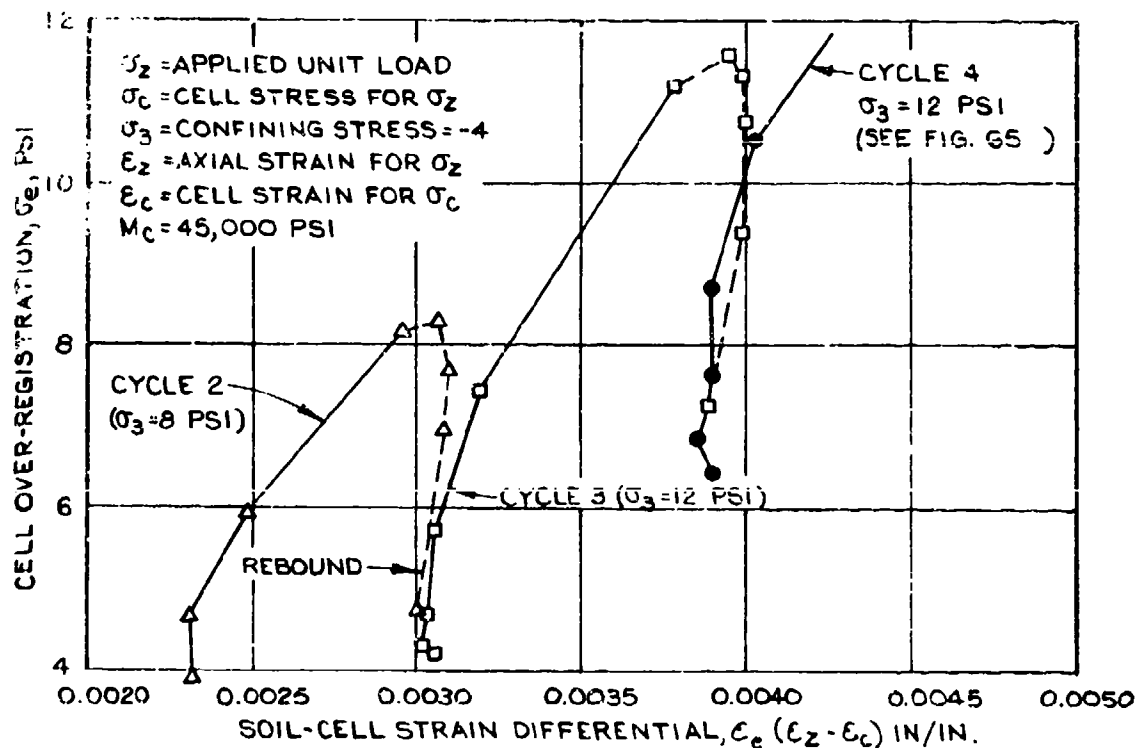
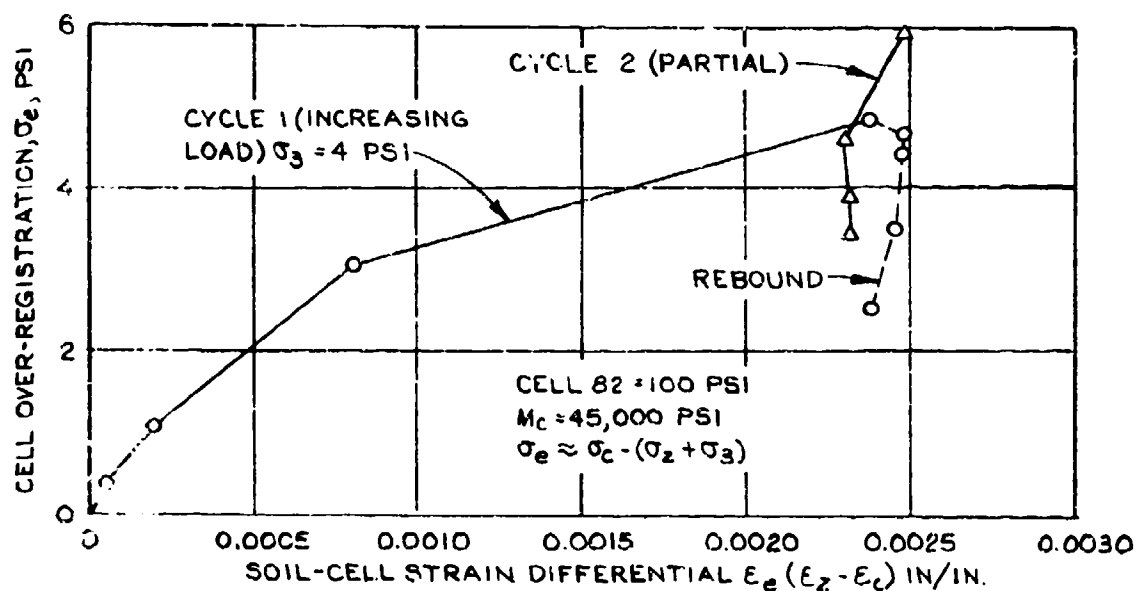


FIGURE 66A. CELL OVER-REGISTRATION VERSUS AXIAL STRAIN DIFFERENTIAL AT MIDHEIGHT; UNIAXIAL STAGE LOADING, SPECIMEN 70-CELL 82, ELEVATION 26 IN., CYCLES 1, 2, AND 3

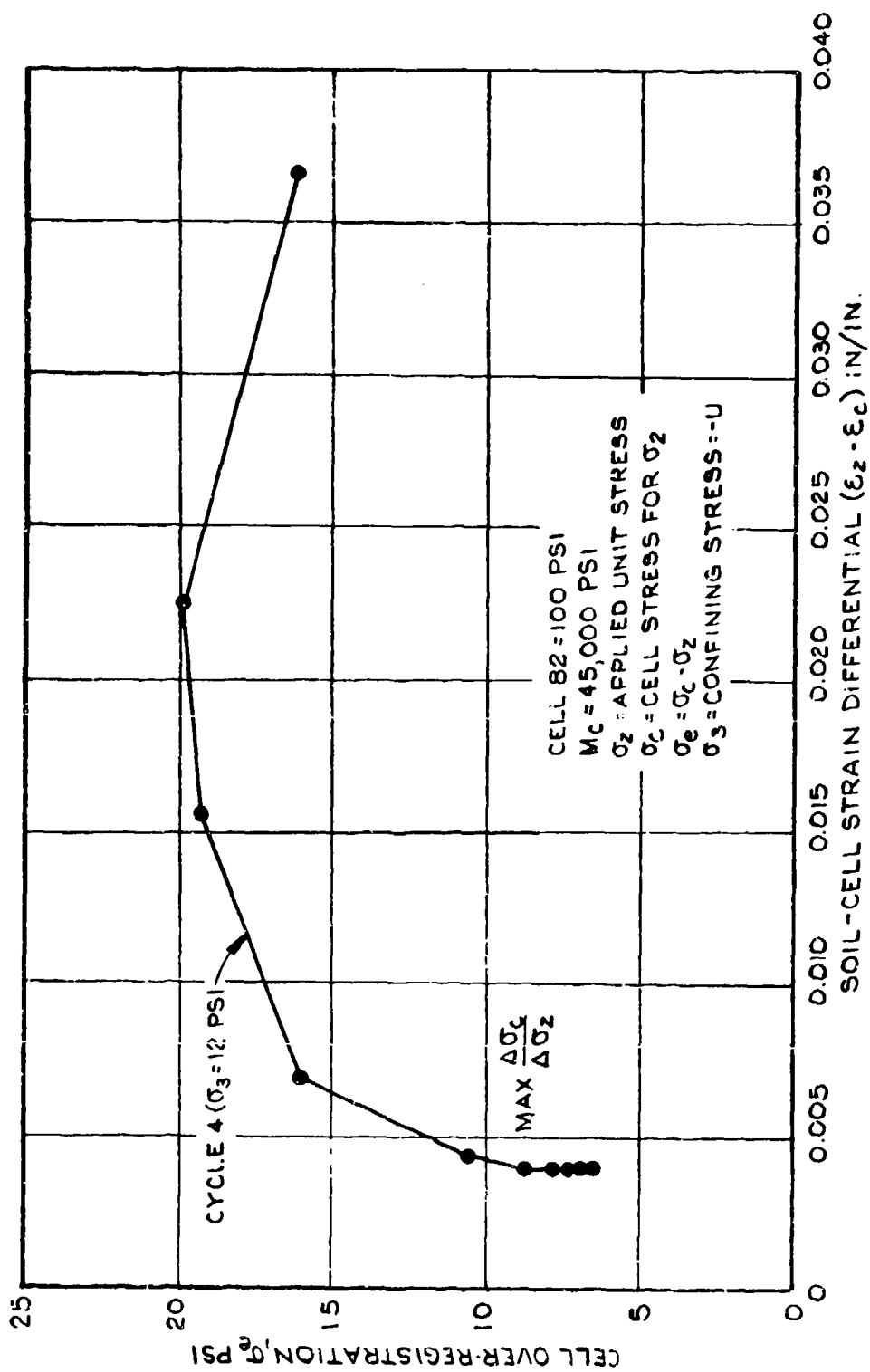


FIGURE 66B. CELL OVER-REGISTRATION VERSUS STRAIN DIFFERENTIALS; AXIAL STRESS-UNIAXIAL STAGE LOADING, SPECIMEN 70 - CELL 82-ELEVATION 26 IN. - CYCLE 4.

$$\Delta \epsilon_c = \frac{\Delta \sigma_c}{M_c} \quad \text{and} \quad \Delta \epsilon_z = \frac{\Delta \sigma_z}{M_s} \quad (94)$$

where the modulus of the cell, M_c , is reasonably constant whereas M_s is the tangent modulus of the soil as defined by the stress-strain curve and varies throughout the test. The secant modulus is commonly used for total stresses but the reliability of this procedure depends on several factors, especially the initial stress conditions of individual tests. The strain differential is

$$\Delta \epsilon_e = \Delta \epsilon_z - \Delta \epsilon_c \quad \text{or} \quad \epsilon_e = \epsilon_z - \epsilon_c \quad (95)$$

This definition is used and valid for both incremental and total strains, but the total strain cannot be computed by the simple equations for incremental strain (94), since M_s is a variable. The movement of each face of a pressure cell with respect to the soil, δ_e or $\Delta \delta_e$, is called the indentation in this report and is determined by

$$\Delta \delta_e = B \Delta \epsilon_e \quad (96)$$

when B is one-half the thickness of the pressure cell and of the soil layer under consideration. In the simplified theory for interaction of soil and cell it is assumed that the indentation also can be expressed by

$$\Delta \delta_e = D \frac{\Delta \sigma_e}{N_s} \quad (97)$$

where D is the diameter of the pressure cell and N_s is an indentation coefficient which is a function of the modulus of the soil, M_s . When the modulus of the soil varies it is expedient to introduce the indentation ratio

$$K_s = \frac{N_s}{M_s} \quad (98)$$

which is assumed to be a constant for a given soil condition, as an approximation. The relation between strain differential, indentation, and overregistration of the cell may be written

$$\Delta \delta_e = B \Delta \epsilon_e = \frac{D}{K_s} \frac{\Delta \sigma_e}{M_x} \quad (99)$$

and

$$\frac{\Delta \sigma_e}{M_s} = B \Delta \epsilon_e = \frac{B}{D} K_s \Delta \epsilon_e \quad (100)$$

With the reservations indicated above, these equations may also be applied to total stresses and strains in the evaluation of test data; that is,

$$\frac{\sigma_e}{M_s} = \frac{B}{D} K_s \epsilon_e \quad (101)$$

Referring to the discussion of the simplified theory for soil-cell interaction, Part II, paragraphs 28-67, the registration ratio of the cell may be expressed by

$$\frac{\Delta \sigma_c}{\Delta \sigma_z} = \frac{\frac{D}{B} + K_s}{\frac{D}{B} + \frac{M_s}{M_c} K_s} \quad (102)$$

and the maximum value of this ratio is attained for $M_s/M_c = 0$, which yields

$$\max \frac{\Delta \sigma_c}{\Delta \sigma_z} = 1 + \frac{B}{D} K_s \quad (103)$$

Equations 102 and 103 apply primarily to incremental loads and stresses. The equations may be used for total loads and stresses when M_s and M_c are constant, but they will in most cases yield unreliable results when either one of the moduli varies with the stress conditions. When the ratios $(\Delta\sigma_e/\Delta\epsilon_e)$ or $\max(\Delta\sigma_c/\Delta\sigma_z)$ are determined by experiments, values K_s can be obtained by Equations 100 or 103, which solved for K_s take the form

$$K_s = \frac{D}{B} \frac{\Delta\sigma_e}{\Delta\epsilon_e} \frac{1}{M_s} \quad (104)$$

and

$$K_s = \frac{D}{B} \left(\max \frac{\Delta\sigma_c}{\Delta\sigma_z} - 1 \right) \quad (105)$$

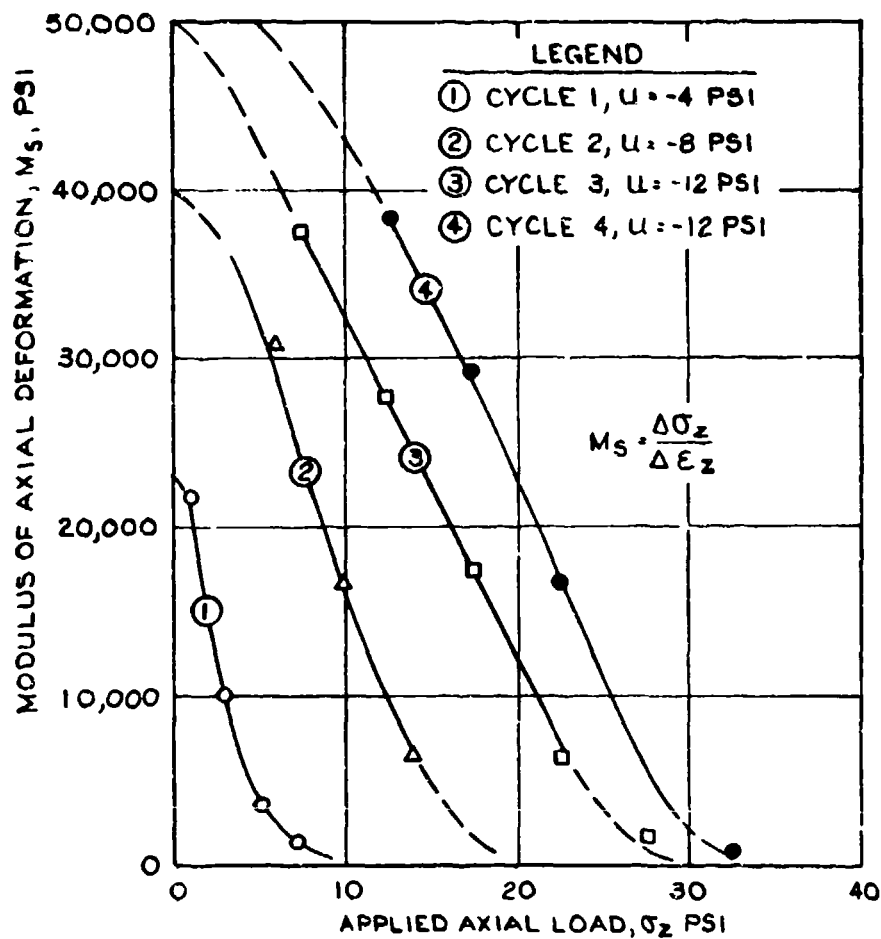
The problems caused by nonlinear stress-strain relations are discussed in several textbooks on the mechanics of continuous media or solids; for example, Erlingen (1962) and Fung (1965).

137. Overregistration versus strain differentials. It is shown in the simplified theory for interaction of soil and a pressure cell, Part II and the summary in paragraph 135, that overregistration of a pressure cell, $\sigma_e = \sigma_c - \sigma_s$, may be expressed as a function of the difference between deformation or strain of the soil and cell, $\epsilon_e = \epsilon_s - \epsilon_c$. In an effort to investigate this relationship, corresponding values of σ_e and ϵ_e for specimen 70 and cell 82 are shown in Figure 66. The values of $\sigma_s = \sigma_z$ and $\epsilon_s = \epsilon_z$ are average values for the test specimen and do not represent stress and strain concentrations close to the pressure cell; likewise, σ_c and ϵ_c are average values for the pressure cell. The deformations of the pressure cell were computed by $\epsilon_c = \sigma'_c/M_c$, and $M_c = 45,000$ psi, where $\sigma'_c = \sigma_c - u$ and u is the numerical value of the vacuum. The diagrams in Figure 66 are similar to the stress-strain diagrams in Figure 64, and a large part of the deformations or strains in the soil are potential residual strains,

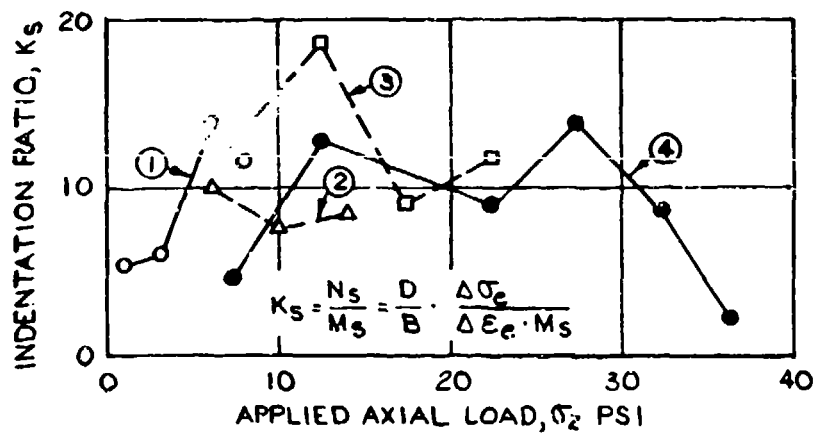
since the recovery of soil strains during the decrease of loading between the various test cycles is small. The diagram also indicates residual axial stresses, because the axial load is not decreased to zero at the end of a loading cycle but only to stresses corresponding to the vacuum or confining pressure for a particular cycle. The similarity between the diagrams in Figures 64 and 66 indicates a relationship between over-registrations and strain differentials. In the simplified theory this relationship is assumed to be represented by Equation 97 and equations derived therefrom, which have the principal parameters M_s and K_s .

138. Incremental values of the modulus M_s and the indentation ratio K_s may be determined by the diagrams in Figures 64-66, or directly from the underlying experimental data, which yield the values of M_s and K_s shown in Figure 67. The computed strains and strain differentials are often very small and at the limit of reliability of the measurements, which causes appreciable scattering in the computed values of K_s . The diagrams in Figure 67a illustrate the large variations of M_s during single tests and in different cycles, which give some indication of potential errors that may be caused by use of a single value of M_s . The scattering of individual values of K_s in Figure 67b is too great for reliable formulation of equations for changes of K_s during a test. All values of K_s computed from experimental data are much greater than those obtained by the theory of elasticity and used in examples of the simplified theory for action of soil pressure cells, but the values of K_s in Figure 67b are of the same order of magnitude as those obtained from maximum total and incremental registration ratios, which in part are caused by changes in the external load distribution, as explained in the following paragraphs. Such a change contributes to the large values of K_s in Figure 67b, but the large values of K_s may also indicate that the simplified analysis of soil-cell interaction is in need of revisions.

139. Total registration ratios. The total registration ratio is σ_c/σ_z , where σ_c and σ_z are the total changes in cell indication and in the axial stress from the start of the test to the applied axial stress σ_z in a single test cycle. Values of σ_c/σ_z for cycle 4 of



A. MODULUS OF AXIAL DEFORMATION



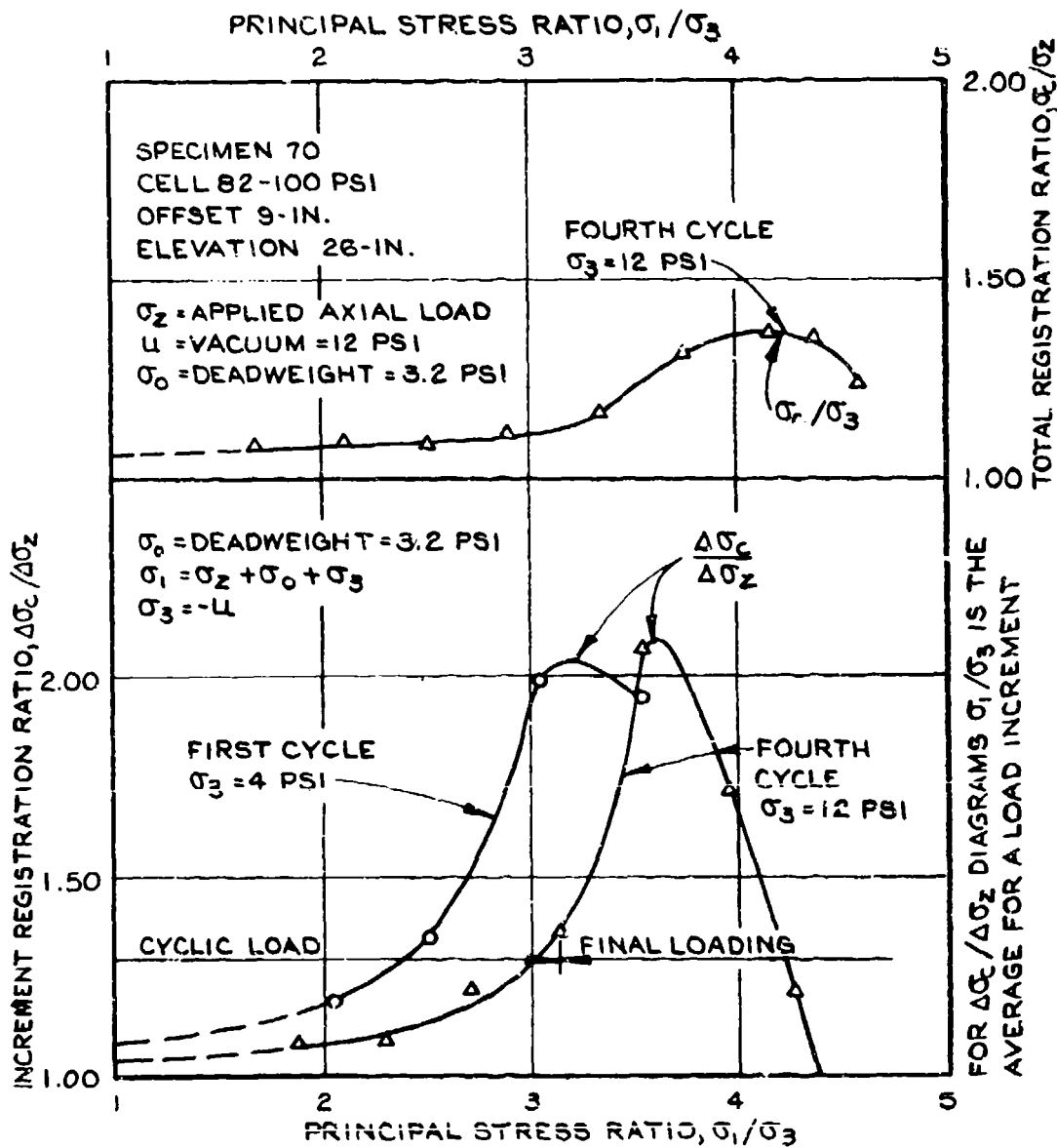
B. INDENTATION RATIO

FIGURE 67. DEFORMATION MODULI FOR UNIAXIAL STAGE LOADING.

the test with specimen 70 are shown by the diagram in the upper part of Figure 68a as a function of the principal stress ratio, σ_1/σ_3 , which permits a direct comparison of diagrams obtained in cycles with different confining pressures. The relation between the applied stress σ_z and the principal stress ratio is determined by the following equations: the confining pressure and minor principal stress is $\sigma_3 = -u$; the deadweight is $\sigma_o = 3.2$ psi; and the major principal stress is $\sigma_1 = \sigma_z + \sigma_o + \sigma_3$. At the start of a test and at low values of σ_z or σ_1/σ_3 , the total registration ratio σ_c/σ_z is less than 1.1 and in fairly good agreement with values obtained by the simplified theory for cell action. This ratio increases slowly with increasing σ_z until σ_1/σ_3 attains a value of about three whereupon a rapid increase starts and a maximum $\sigma_c/\sigma_z = 1.37$ is reached at $\sigma_1/\sigma_3 = 4.2$, corresponding to $\sigma_z = 35$ psi in Figure 64. The indentation ratio K_s at the maximum value of $\sigma_c/\sigma_z = 1.37$ may be determined by Equation 105, which yields $K_s = 12(1.37 - 1) = 4.4$. Much greater values of K_s are obtained for incremental loads as shown in Figure 67 and discussed in the next paragraph.

140. Incremental registration ratios. The simplified theory and currently available more rigorous theories for interaction of soil and pressure cells assume that the modulus of the soil is constant. As shown, Figure 67, the modulus of deformation of sand decreases with increasing axial stress and deformation for uniaxial loading, but the change of the modulus during a single load increment may be small. Therefore, the simplified theories and available more rigorous theories apply to incremental registration ratios rather than to total registration ratios when the modulus of the sand changes during a test. Incremental registration ratios, $\Delta\sigma_c/\Delta\sigma_z$, may be determined directly from test records or from soil-cell stress diagrams, Figure 65. Results obtained for cycles 1 and 4 in tests with specimen 70 are shown in the lower part of Figure 68a.* Values of $\Delta\sigma_c/\Delta\sigma_z$ for cycles 2 and 3 fall

* Alternative diagrams for incremental registration ratios are shown in Figure 68b to facilitate comparison with similar diagrams for other tests.



NOTE: SEPARATION OF THE DIAGRAMS REFLECTS THE INFLUENCE OF RESIDUAL STRESSES PLUS STAGE CHANGES OF LATERAL STRESSES AND INCLUSION EFFECT OF THE PRESSURE CELL.

FIGURE 68A. INCREMENTAL AND TOTAL REGISTRATION RATIOS FOR UNIAXIAL LOADING.

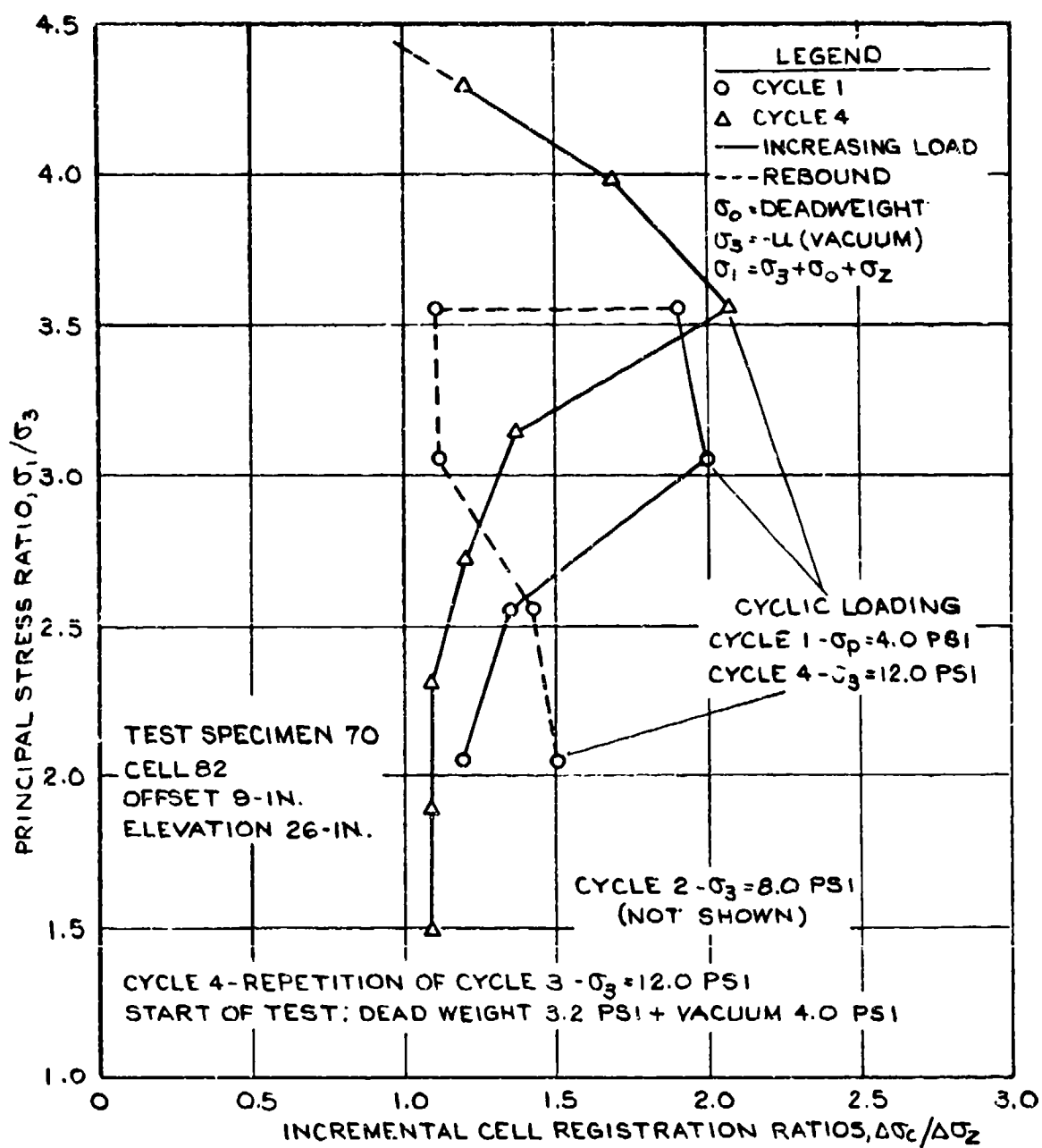


FIGURE 68B. ALTERNATIVE DIAGRAM FOR INCREMENTAL REGISTRATION RATIOS.

between the two diagrams but are not shown since the loading in these cycles was not continued until maximum values of $\Delta\sigma_c/\Delta\sigma_z$ were attained. There is but little difference between total and incremental ratios until $\sigma_1/\sigma_3 = 2$; thereafter the incremental ratios increase much faster than the total ratios and attain maximum values slightly above 2.0. The corresponding indentation ratio is obtained by Equation 105 or $K_s = 12(2 - 1) = 12$, which is many times greater than that obtained by theory for elastic materials, see Figure 14 in Part I, but it agrees well with values of K_s as a function of overregistration and strain differential, Figure 67. The maximum value of $\Delta\sigma_c/\Delta\sigma_z$ occurs at $\sigma_1/\sigma_z = 3.2$ for cycle 1, corresponding to $\sigma_z = 5.6$ psi, and at $\sigma_1/\sigma_3 = 3.6$ for cycle 4 corresponding to $\sigma_z = 26$ psi. These values of σ_z are shown in the stress-strain diagrams in Figure 64, and it is seen that the maximum values of $\Delta\sigma_c/\Delta\sigma_z$ occur at applied axial loads smaller than those causing failure or large deformations of the entire test specimen. Stress concentrations undoubtedly exist in the sand around the pressure cell, and it is possible that these stress concentrations cause local failure conditions at the above mentioned values of σ_z , which in turn may explain the rapid decrease of $\Delta\sigma_c/\Delta\sigma_z$ immediately after the maximum is attained; see following paragraphs.

141. Comparison of total and incremental registrations. The difference between total and incremental registration ratios shown in Figure 66a is explained by the fact that the $\Delta\sigma_c/\Delta\sigma_z$ curves are derivatives of the σ_c/σ_z curves. However, it should be noted that the incremental values ($\Delta\sigma_c/\sigma_z$) are plotted against the average values of (σ_1/σ_3) for each increment, whereas the total values (σ_c/σ_z) are plotted against the end values of σ_z for each load increment. There is no difference between these registration ratios when they are independent of σ_z or σ_1/σ_3 . The simplified theory for interaction of soil and cell, as well as some of the more rigorous theories are based on the assumption that the soil modulus, M_s , is constant. Therefore, these theories should not be expected to yield reliable data for the registration ratios for nonlinear stress-strain relations in a particular test, but the theories may be applied to incremental loads and

registration ratios, when variations of M_s during each load increment are negligible. Even then, errors may be caused by the fact that the linear relationship between force and indentation, indicated by Equations 99 and 100, is valid only for small stresses and indentations, as demonstrated in the next paragraph and in Figure 69.

142. Test data versus the simplified theory. Considering the data presented in the foregoing paragraph, the following comments deal primarily with incremental registration ratios and results obtained by the simplified theory for interaction of soil and pressure cells. For principal stress ratios σ_1/σ_3 less than 2.0, the difference between σ_c/σ_z , $\Delta\sigma_c/\Delta\sigma_z$, and results of the simplified theory are relatively small, but a rapid increase in $\Delta\sigma_c/\Delta\sigma_z$ followed by a rapid decrease occurs for values of σ_1/σ_3 greater than 2.0, as shown in Figure 68a. The first part of this increase is explained by the convex stress-strain diagrams for the test specimen and the corresponding decrease in M_s with increasing σ_z or σ_1/σ_3 , Figure 67. The maximum values of $\Delta\sigma_c/\Delta\sigma_z$ are usually between 2.0 and 2.1, which are much greater than the values obtained for $(M_s/M_c) = 0$ by Equation 103. The rapid increase of $\Delta\sigma_c/\Delta\sigma_z$ may be caused by a change in load concentration from the rim to the center of the cell at failure of adjacent soil. Such a change in load distribution was originally suggested by Terzaghi (1943) for plate loading tests, Figure 8, and it is supported by the behavior of a WES cell plus an inactive rim, Figures 95-97. Although the WES pressure cell is much less sensitive to nonuniform stress distribution than a pressure cell with an exposed and fixed diaphragm, a change in stress concentration from the slotted rim to the center of the cell probably causes an increase in cell registration. It should be noted that the maximum values of $\Delta\sigma_c/\Delta\sigma_z$ occur at values of σ_1/σ_3 corresponding to the rising part of the stress-strain curve, Figure 64. However, stress concentrations around the pressure cell cause failure conditions there before such conditions are attained for the entire test specimen. The rapid decrease of $\Delta\sigma_c/\Delta\sigma_z$ after the maximum strength is attained corresponds to a sudden sinkage in plate loading tests. The results of such a test in sand with a relative density of 85 percent is shown in

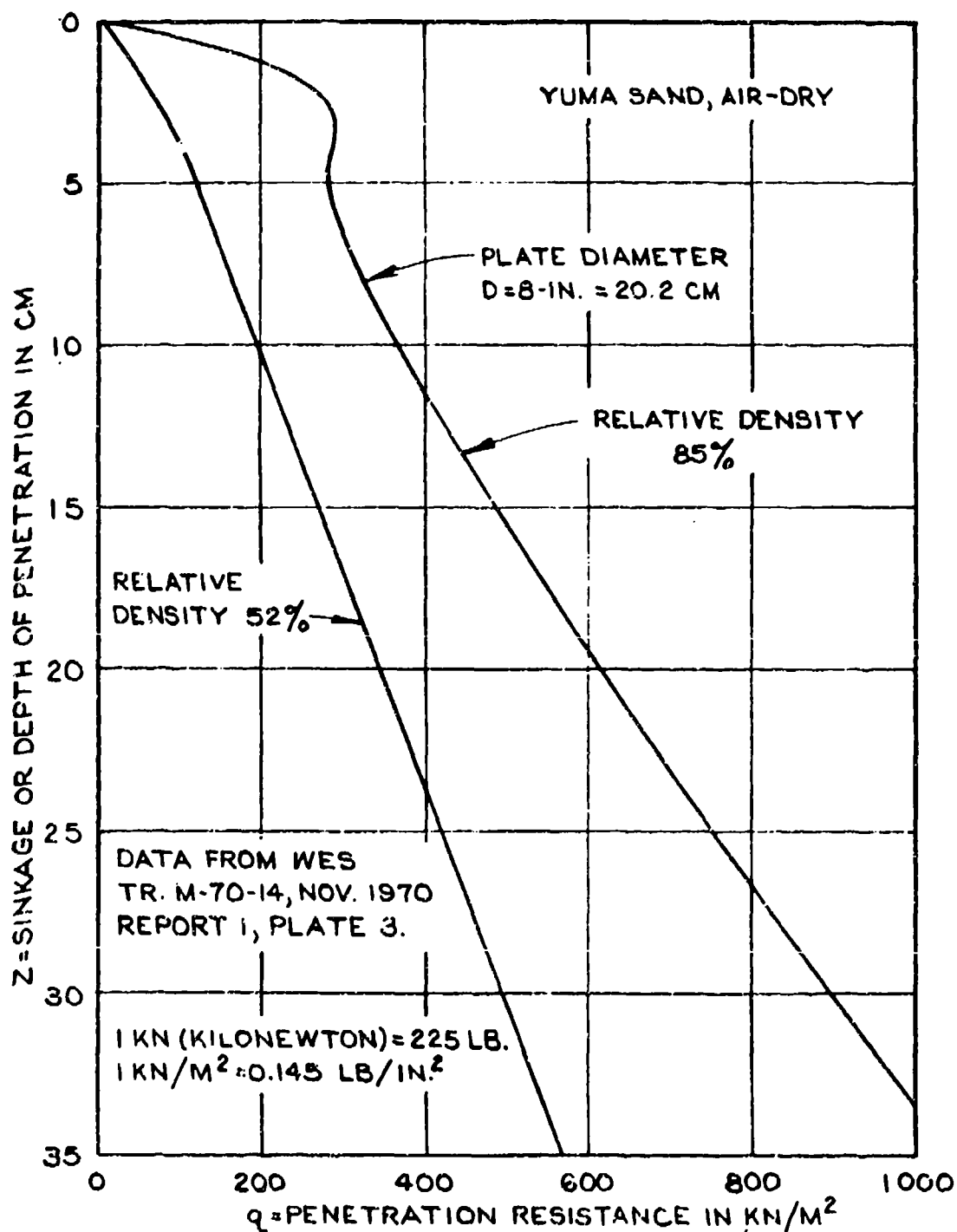


FIGURE 69A. PLATE LOADING TESTS IN YUMA SAND.

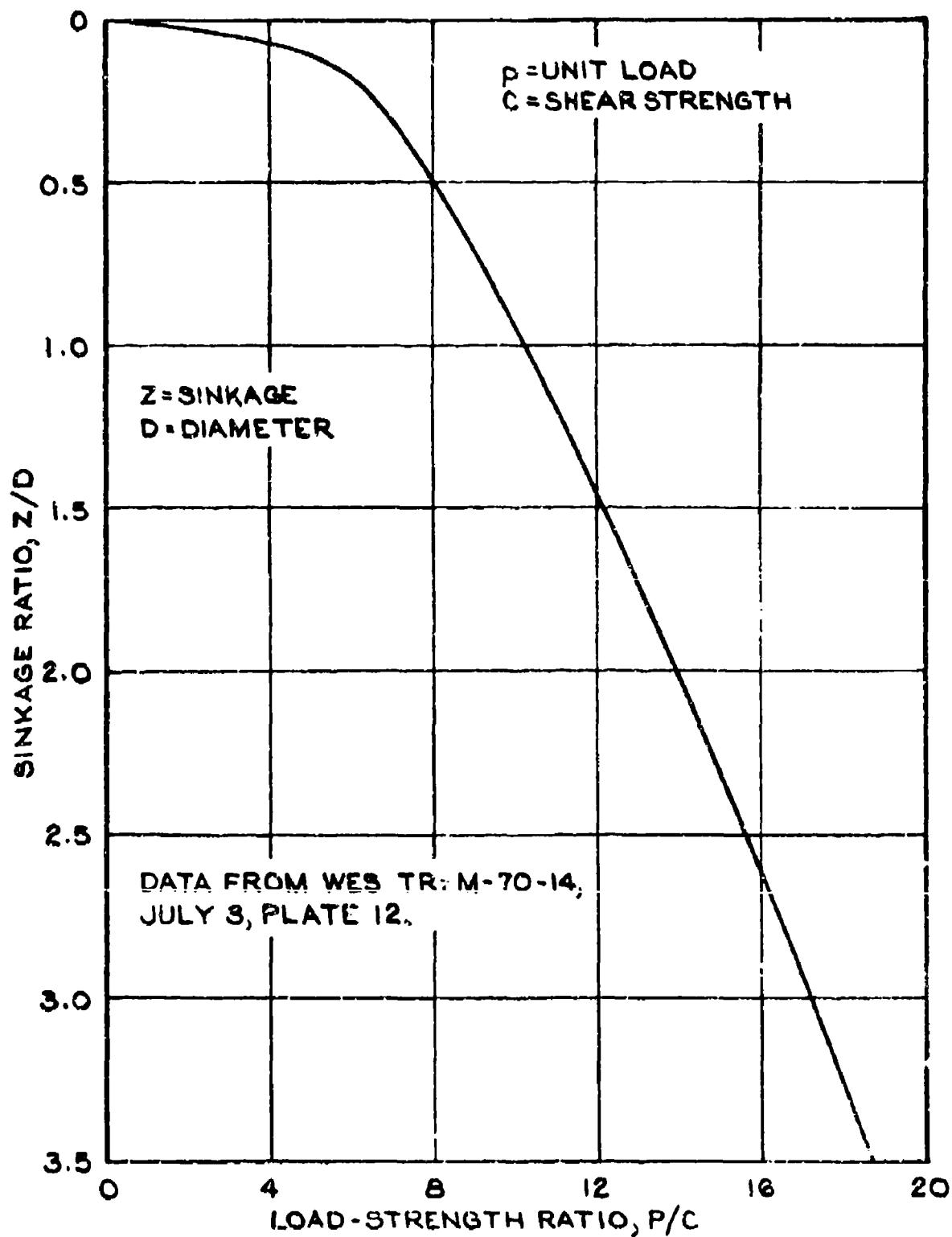


FIGURE 69B. PLATE LOADING TEST IN BUCKSHOT CLAY.

Figure 69a. The load-sinkage diagram is curved instead of being linear as assumed in the simplified pressure cell theory, Equations 99 and 100, and a sudden sinkage of the plate occurs for a load corresponding to failure conditions in the sand. The bulge of soil and sudden sinkage of the plate occur only in relatively dense cohesionless soils, but an increase in the slope of the load-sinkage diagram occurs in most soils at initial failure of the soil and is conspicuous in clay, Figure 69b. It appears that the usual relations between unit load and overregistration of a pressure cell may become unreliable at stresses corresponding to failure conditions of the soil in which the cell is embedded.

143. Pocket action problems. A possible cause of large overregistration ratios for a pressure cell is that a lens or pocket of denser soil was formed around the cell during installation procedures or previous loading cycles. Such a pocket of more rigid soil would increase overregistration of the cell; Taylor (1945, 1947). The incremental registration ratio diagrams in Figure 68 are well separated because of residual strains after each loading cycle, but the form of the diagrams and the maximum values of $\Delta\sigma_c/\Delta\sigma_z$ are nearly identical, whereas the starting registration ratio is greatest in the first cycle. Therefore, it appears that pocket action did not occur during testing in medium dense sand, and changes in the incremental registration ratio can be explained better by the convex form of the stress-strain diagrams, Figure 64, and by the shape of load-sinkage diagrams, Figure 69. However, the possibility of formation of pockets of denser sand around cells installed in loose sand cannot be excluded and should be investigated.

144. Test data versus rigorous theories by Eshelby-Askegaard. Using basic equations by Eshelby, a rigorous theory for the interaction of an elastic medium and a rigid ellipsoidal inclusion was developed by Askegaard (1963) and is reviewed in Part II of this report. A rigid inclusion corresponds to a very large value of M_c/M_s for a pressure cell or to the maximum incremental registration ratios obtained in the WES experiments. Theoretical results obtained by Askegaard for uniaxial loading of an elastic medium are shown in Figure 35a as a function of the Poisson ratio and the diameter-thickness ratio of the rigid

inclusion. Assuming a Poisson ratio $\nu = 0.3$ for the soil and with a thickness-diameter ratio of $1/6$ for the WES pressure cell, Figure 35 by Askegaard yields a registration ratio of 1.1 whereas the maximum registration ratio of the WES cell near failure was 2.0 to 2.1. These high values of σ_c/σ_s cannot be explained by the Askegaard theory, which considers only elastic but not failure conditions. As will be demonstrated in later paragraphs, the high values of σ_c/σ_s obtained by the WES cells near failure of the soil are probably caused by a change in modulus of deformation of the soil plus a shift of the load concentration from the edge to the center of the cell at failure of the soil.

145. Test data and finite element analysis by Bates. A finite element analysis of a pressure cell in a free field has been performed by Bates (1969) and is reviewed in paragraphs 68-94 of this report. The analysis is applied to a small cell with an inactive and tapered rim, and the axial rigidity is much larger than for the WES cell. The over-registration of the Bates cell is much less influenced by changes in the modulus of the material in which the cell is installed. Furthermore, the theory and experiments by Bates were not extended to failure conditions in the soil, and they should not be expected to agree with or explain the large overregistrations of the WES pressure cell.

Axial stresses for triaxial load changes

146. Previous experiments. Most investigations of the action of soil pressure cells have been performed in shallow containers with solid and rigid walls. An increase of the axial unit load also causes an increase in the radial or confining unit load, corresponding to the earth pressure at rest. However, it must also be taken into consideration that axial stresses caused by a surface load decrease with increasing depth because of the influence of sidewall friction. Various methods have been devised to determine and counteract the influence of sidewall friction. Axial loads are usually applied through a rubber cushion or as air or water pressure on a rubber membrane covering the soil in order to decrease radial restraint and nonuniformity of stresses. A rubber cushion may also be used in contact with the rigid bottom of the

contained when simulating pressure cells in a rigid wall or slab, but the action of a pressure cell in a free field cannot be properly simulated unless there is an adequate distance between the cell and the bottom of the container and unless the soil cover is sufficient to decrease surface effects to an insignificant amount. As examples of early investigations, reference is made to the first tests and report on soil pressure cells by the WES (1944) and to the investigations by Peattie and Sparrow (1954).

147. In order to decrease the influence of sidewall friction and to obtain better control of lateral stresses, Plantema (1953) performed calibration tests with pressure cells in a special triaxial device having a soil specimen with a diameter of 95 cm and a height of 72 cm, surrounded by a rubber membrane and placed in a pressure chamber, Figure 43, so that positive radial loads could be produced. Furthermore, axial loads were applied through rubber cushions at the top and bottom of the test specimen. A constant ratio between axial and radial unit loads was maintained in each test. Plantema found that the registration ratio for a particular pressure cell was subject to only small changes when the principal stress ratio remained constant. The tests indicated a slight decrease in the cell registration, Figure 43c, with increasing ratio between axial and radial soil stresses, and the cell exhibited a slight underregistration.

148. Influence of vacuum in the triaxial device. As mentioned previously, the WES triaxial device uses vacuum in the soil pores to produce radial or confining pressures. The influence of such a vacuum on the evaluation of the test data has not yet been discussed, since the vacuum was maintained at a constant magnitude during individual uniaxial tests. Both the vacuum and the applied axial load were varied simultaneously during tests, as discussed below. First of all, the stresses in the soil of the test specimen are identical whether they are produced by a vacuum in the soil pores or by a positive outside pressure on the encasing rubber membrane. The vacuum, u , is a negative pore pressure with respect to pressure of the surrounding air, and the confining radial pressure is

$$\sigma_3 = -u \quad (106)$$

With an applied unit axial load σ_z , a deadweight that produces an axial stress σ_o at the elevation of the pressure cell, and bearing in mind that the vacuum produces the soil stress σ_3 in all directions, the total axial and major principal stresses are

$$\sigma_1 = \sigma_o + \sigma_z + \sigma_3 \quad (107)$$

The deadweight does not change during individual tests, and a change in the axial soil stress can be expressed by

$$\Delta\sigma_s = \Delta\sigma_z + \Delta\sigma_{\sigma_3} \quad (108)$$

The deformations of the test specimen should correspond to these stresses and appropriate values of the soil moduli and Poisson ratios, but the total axial and radial deformations were also measured during each test.

149. An increase of the vacuum in the pores of the soil decreases the air pressure on the outside of a pressure cell, but this increase is counteracted by an equal increase in the effective soil pressure. Disregarding the effect of stress concentrations and of a possible slot in the rim of the cell and assuming that the pressure in the interior of the cell is maintained at a constant value (for example, by venting the cell to the outside air), the interior diaphragm of the cell will not react to a change of vacuum in the soil pores plus the corresponding change in soil pressure, and the cell acts as a rigid inclusion. The interior of most pressure cells in current use is hermetically sealed, and compression of the entrapped air may cause small changes in the deflection of the measuring diaphragm and corresponding indications of the cell, which in most cases are taken into consideration by calibration of the cell. On the other hand, when the interior of the cell is vented to the soil pores, the pore vacuum and changes therein also act below the measuring diaphragm, and the cell indicates only changes in

effective soil pressure on the face plate.

150. The WES pressure cell has a slot in the rim of the face plate to enable it to deflect. Air and water, but not soil, can enter this slot and counteract air and water pressures on the face plate. Consequently, the calibration factor for air and water pressures on the cell, F_u , is greater than the corresponding calibration factor for soil pressures, F_s . With the corresponding dial readings s_u and s_s of the cell analyzer, the calibration of the cell for hydrostatic pressure yields

$$\Delta u = \Delta s_u F_u \quad (109)$$

whereas calibration for direct load or soil pressure, Figure 5, yields

$$\Delta \sigma_s = \Delta s_s F_s \quad (110)$$

An increase in vacuum is considered negative, and it causes a positive increase in the effective soil pressure

$$\Delta \sigma_u = \Delta \sigma_3 = -\Delta u \quad (111)$$

Concurrent changes in vacuum, Δu , and in the axial unit load, $\Delta \sigma_z$, will then cause a total change in dial reading, $\Delta \sigma_{ct}$, which can be expressed by the foregoing equations as

$$\frac{\Delta \sigma_{ct}}{F_s} = \frac{\Delta \sigma_u}{F_s} + \frac{\Delta u}{F_u} + \frac{\Delta \sigma_z}{F_s} + \frac{\Delta \sigma_e}{F_s} \quad (112)$$

where $\Delta \sigma_e$ is the overregistration of the pressure cell. Rearranging, using Equation 111 yields

$$\frac{\Delta \sigma_{ct}}{F_s} + \frac{\Delta \sigma_3}{F_u} = \frac{1}{F_s} (\Delta \sigma_3 + \Delta \sigma_z + \Delta \sigma_e)$$

or after multiplying by F_s

$$\Delta\sigma_{ct} + \Delta\sigma_3 \frac{F_s}{F_u} = \Delta\sigma_3 + \Delta\sigma_z + \Delta\sigma_e \quad (113)$$

The equivalent measured change in soil stresses, $\Delta\sigma_c$, is then

$$\Delta\sigma_c = \Delta\sigma_{ct} + \Delta\sigma_3 \frac{F_s}{F_u} = \Delta\sigma_3 + \Delta\sigma_z + \Delta\sigma_e \quad (114)$$

and consists of the stress corresponding to the cell indication, $\Delta\sigma_{ct}$, plus the contribution of the vacuum

$$\Delta\sigma_3 \frac{F_s}{F_u} = -\Delta u \frac{F_s}{F_u} \quad (115)$$

which is measured separately by a mercury or mechanical manometer but not by the soil pressure cell. The ratio F_s/F_u represents the influence of the circumferential slot in the face plate and varies between 0.78 and 0.92 for WES pressure cells. The ratio is not equal to the ratio between the area enclosed by the bottom of the slot and that of the face plate since it also reflects the stiffness of the flexible rim, which is not the same for all the cells.

151. The incremental overregistration of the cell may be obtained from Equation 114 and is

$$\Delta\sigma_e = \Delta\sigma_c - (\Delta\sigma_z + \Delta\sigma_3) \quad (116)$$

and the corresponding registration ratio is

$$\frac{\Delta\sigma_c}{\Delta\sigma_s} = \frac{\Delta\sigma_c}{\Delta\sigma_z + \Delta\sigma_3} \quad (117)$$

where the incremental soil stress is defined by Equation 106. The

deformation of the pressure cell corresponds to the actual cell indication $\Delta\sigma_{ct}$ and not to the total change in stress, $\Delta\sigma_c$; therefore the incremental cell strain is

$$\Delta\epsilon_{ct} = \frac{\Delta\sigma_{ct}}{M_c} \quad (118)$$

The incremental soil strains may be computed from the incremental axial and lateral soil stresses, using appropriate values of the soil moduli and the Poisson ratios. However, these coefficients may vary considerably during a single test, and more reliable average values of the strains are usually obtained from outside total axial and radial deformations which were measured in each test. With an axial incremental strain $\Delta\epsilon_s$, the soil-cell strain differential is

$$\Delta\epsilon_e = \Delta\epsilon_s - \Delta\epsilon_{ct} \quad (119)$$

In tests with concurrent changes in vacuum and applied axial load, the overregistration of the soil pressure cell and the registration ratio are determined by indications of both the pressure cell and an outside manometer, and these quantities are not as simple and significant as in tests with uniaxial load changes. Therefore, the relations between overregistrations and strain differentials were not investigated in tests with triaxial load changes.

152. WES 1955 tests with triaxial load changes. The tests for triaxial load changes were essentially conducted with maintenance of a constant principal stress ratio in each test series, and this ratio was varied from 1.0 to 3.0 in the five test series performed. The principal stress ratio is

$$\frac{\sigma_1}{\sigma_3} = \frac{\sigma_3 + \sigma_z + \sigma_o}{\sigma_3} \quad (120)$$

where σ_3 is numerically equal to the pore vacuum, σ_z is the

applied axial unit load, and σ_0 is the stress corresponding to the deadweight of the soil in the test specimen above the level of the pressure cell being investigated. It was not always possible to maintain the desired principal stress ratio at small values of σ_z because of the influence of the constant value of σ_0 . The tests were usually started at a relatively low vacuum of 2.5 psi. The vacuum and the applied axial stress σ_z were increased in steps until the vacuum attained 12.5 psi, whereupon the loads were gradually decreased to the initial value and at least two cyclic tests were performed. After the last cycle the tests were continued with uniaxial loading and a constant vacuum and confining pressure of 12.5 psi. The maximum values of the vacuum were increased slightly in tests with a constant principal stress ratio of 3.0. The maximum vacuum during the cyclic part of the tests was 13.3 psi and this was increased to a constant vacuum of 14.0 psi during the final part with uniaxial loading. In the test series with a nominal principal stress ratio of 1.0, the test specimen was subjected only to vacuum and deadload but not to any applied axial load; however, the deadload σ_0 prevented actual attainment of a stress ratio of 1.0.

153. The results obtained in test series with various values of the principal stress ratio were so uniform and similar that all can be described in a single paragraph. The test data are shown in following figures,

<u>Principal Stress Ratio</u>	<u>Figures</u>
3.0	70,71,72
2.5	73,74,75
2.0	76,77,78
1.5	79,80,81
1.0	82,83,84

The stress-strain diagrams and the soil-cell stress diagrams are nearly straight during cyclic loading, and they yield nearly constant values of the soil modulus and the incremental registration ratios in the cyclic part of the tests, but the incremental registration ratios increase moderately with increasing principal stress ratios. During the uniaxial loading, following the cyclic loading, these ratios increase rapidly

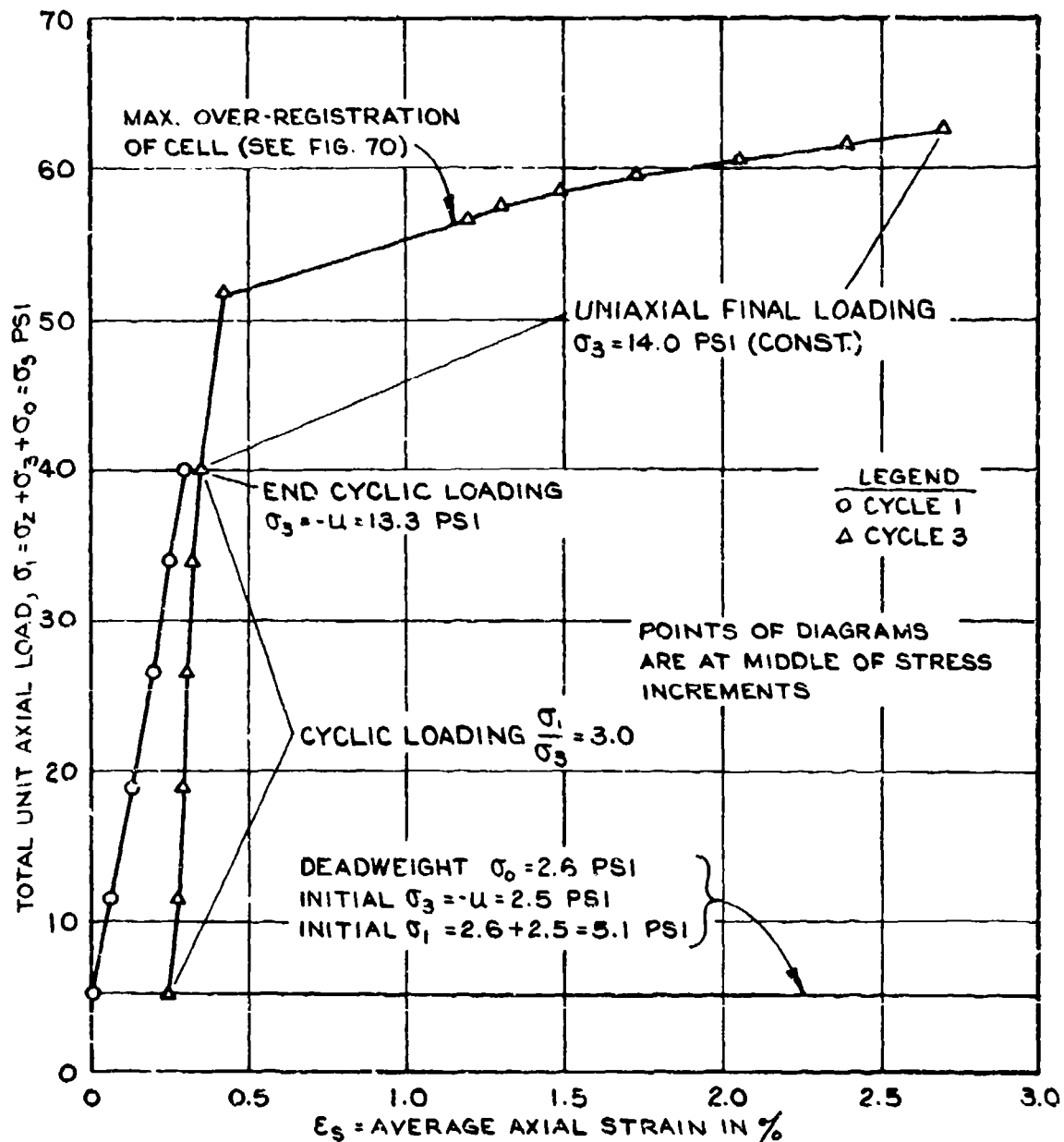


FIGURE 70. AXIAL STRESS-STRAIN DIAGRAMS FOR PRINCIPAL STRESS RATIO 3.0.

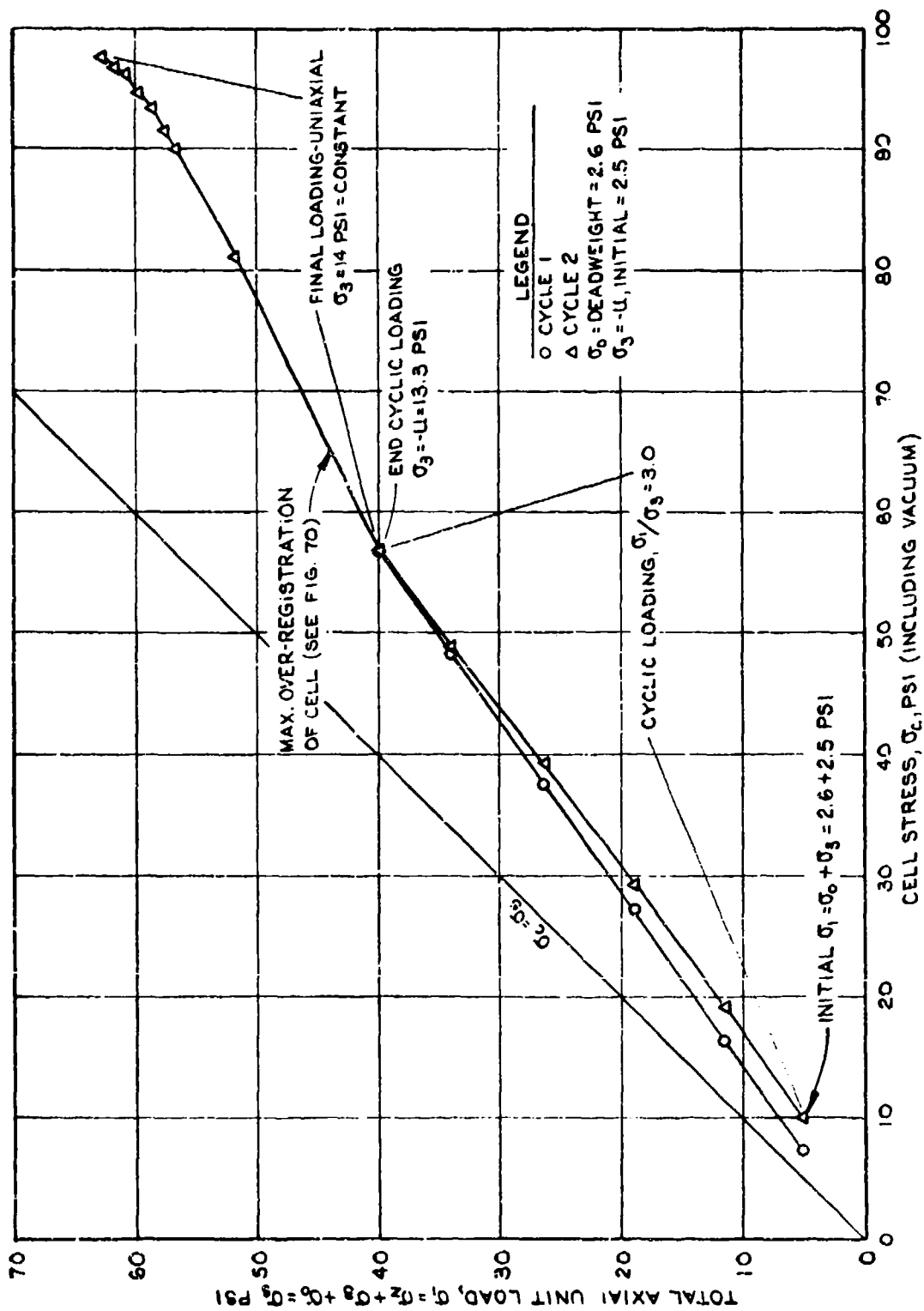


FIGURE 7. SOIL-CELL STRESS DIAGRAMS FOR PRINCIPAL STRESS RATIO 3.0.

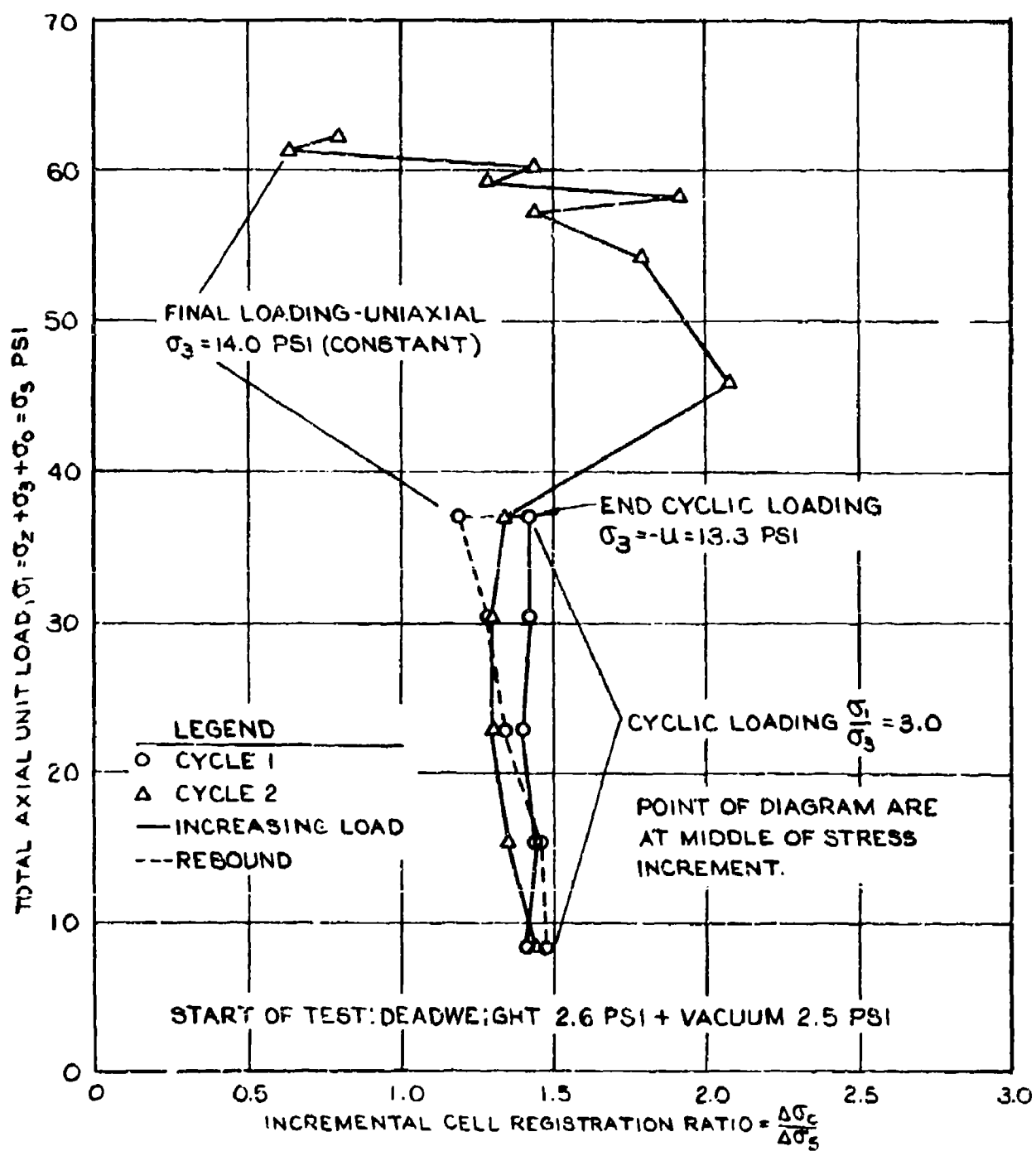


FIGURE 72. AXIAL REGISTRATION RATIOS FOR PRINCIPAL STRESS RATIO 3.0.

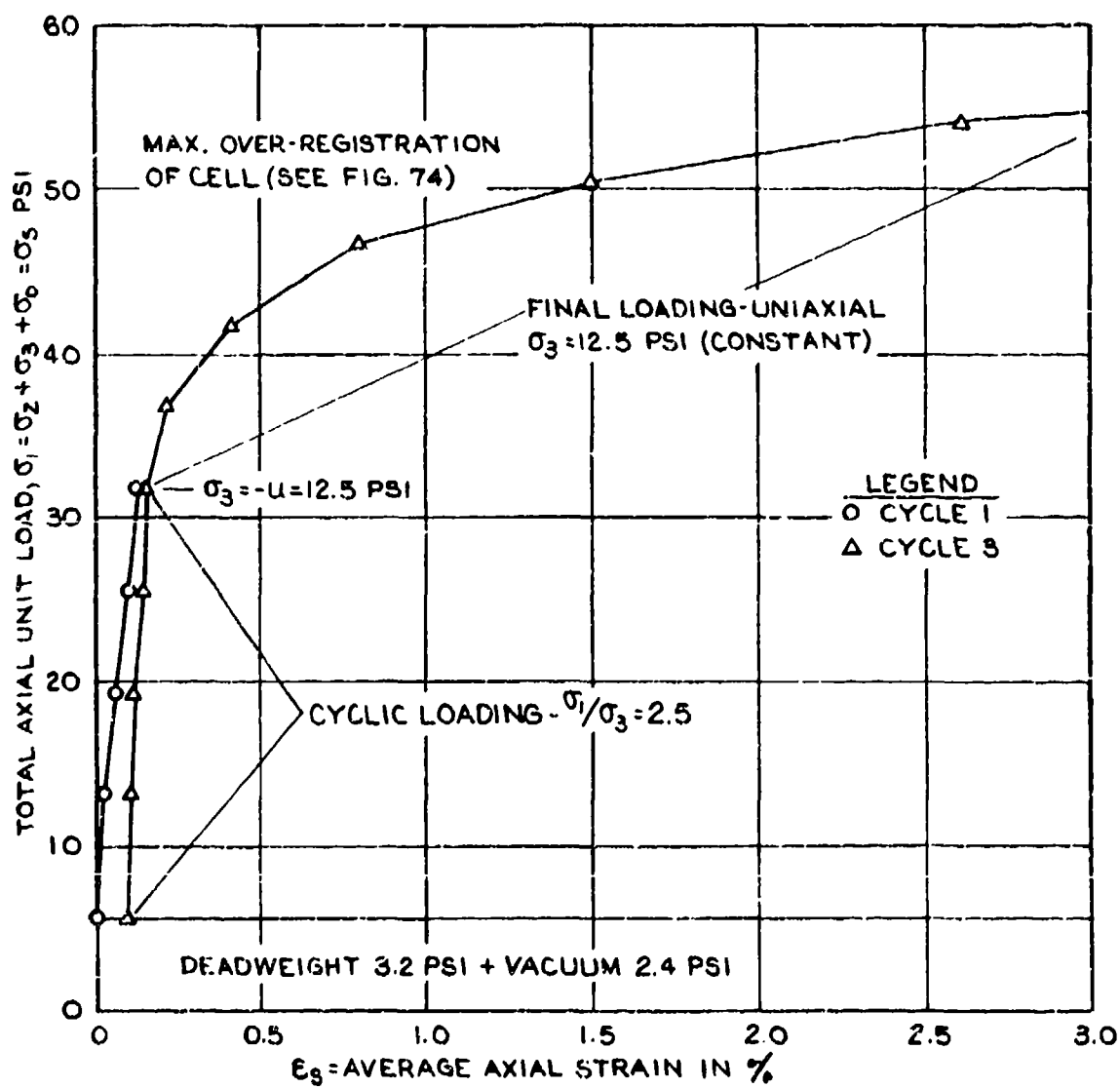


FIGURE 73. AXIAL STRESS-STRAIN DIAGRAMS FOR PRINCIPAL STRESS RATIO 2.5.

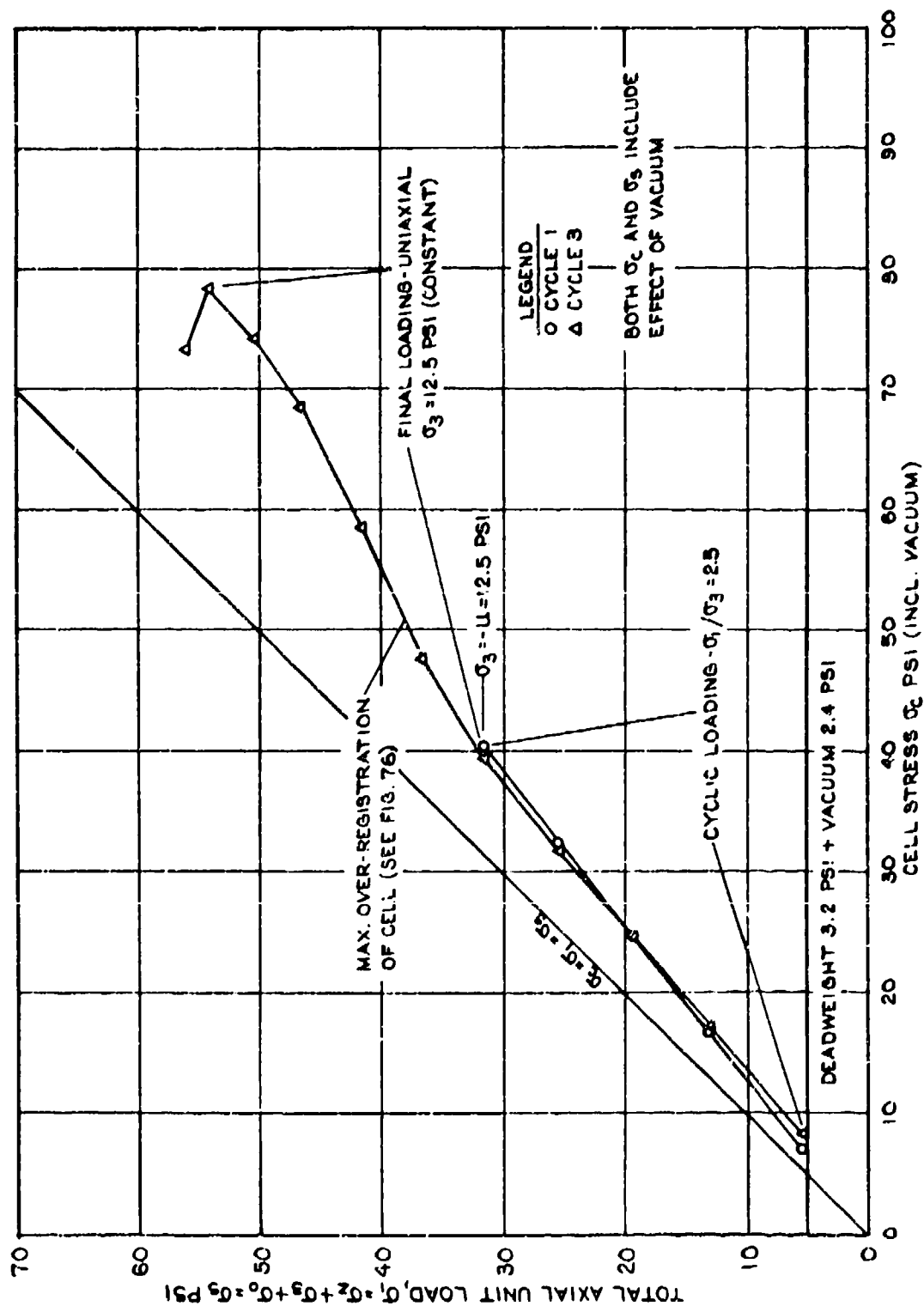


FIGURE 74. SOIL-CELL STRESS DIAGRAMS FOR PRINCIPAL STRESS RATIO 2.5

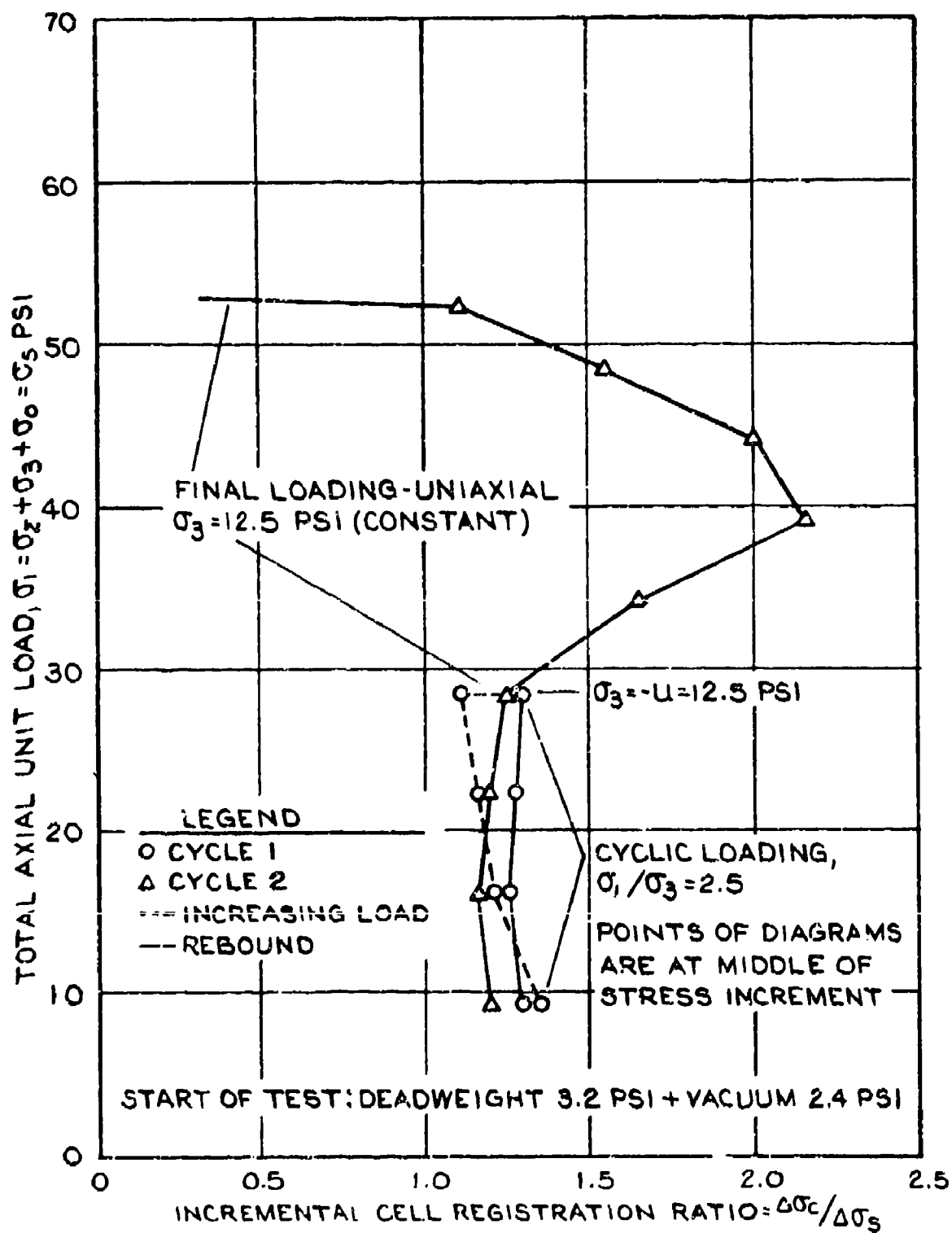


FIGURE 75. AXIAL REGISTRATION RATIOS FOR PRINCIPAL STRESS RATIO 2.5.

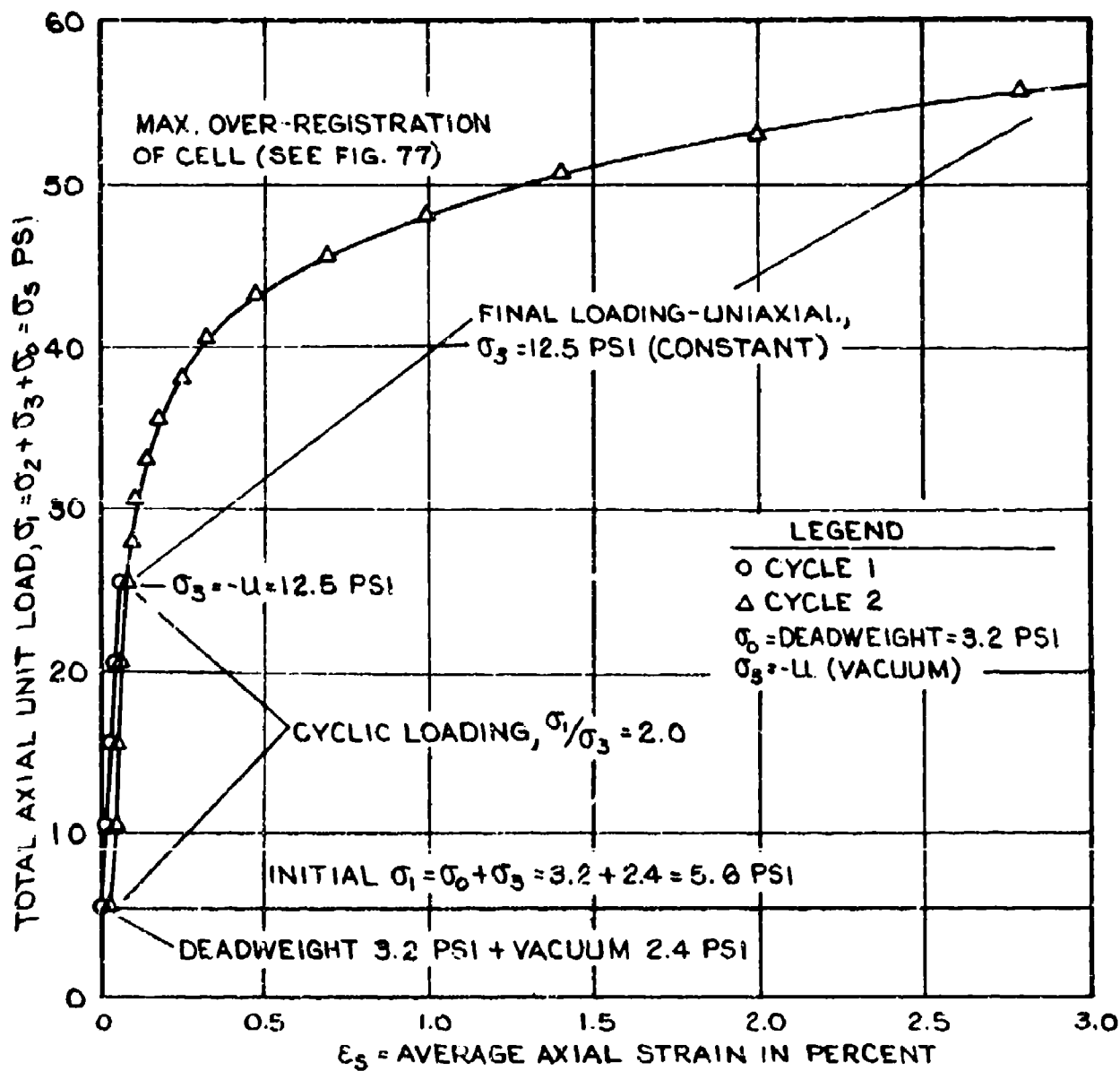


FIGURE 76. AXIAL STRESS-STRAIN DIAGRAMS FOR PRINCIPAL STRESS RATIO 2.0

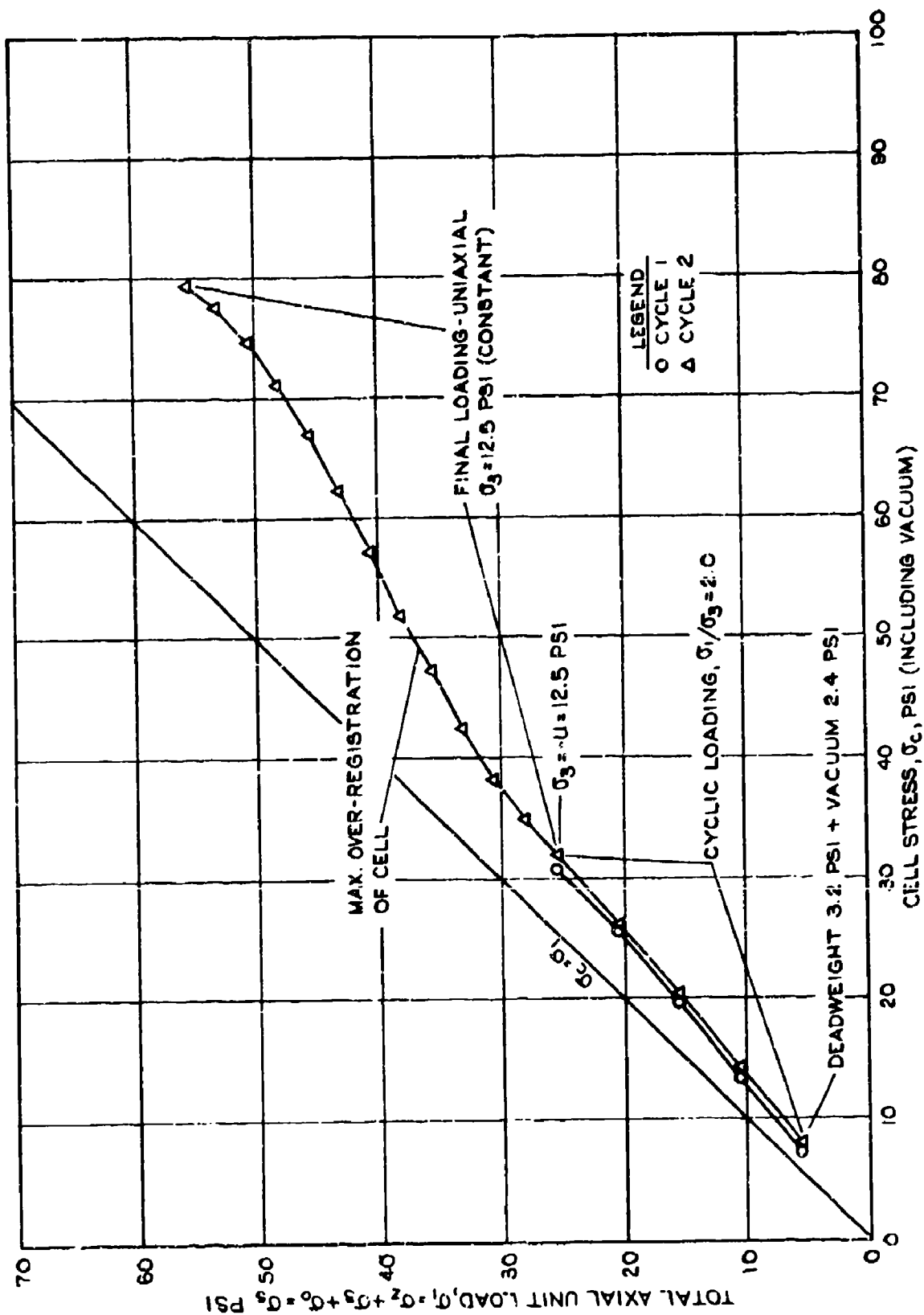


FIGURE 77. SOIL-CELL STRESS DIAGRAMS FOR PRINCIPAL STRESS RATIO 2.0

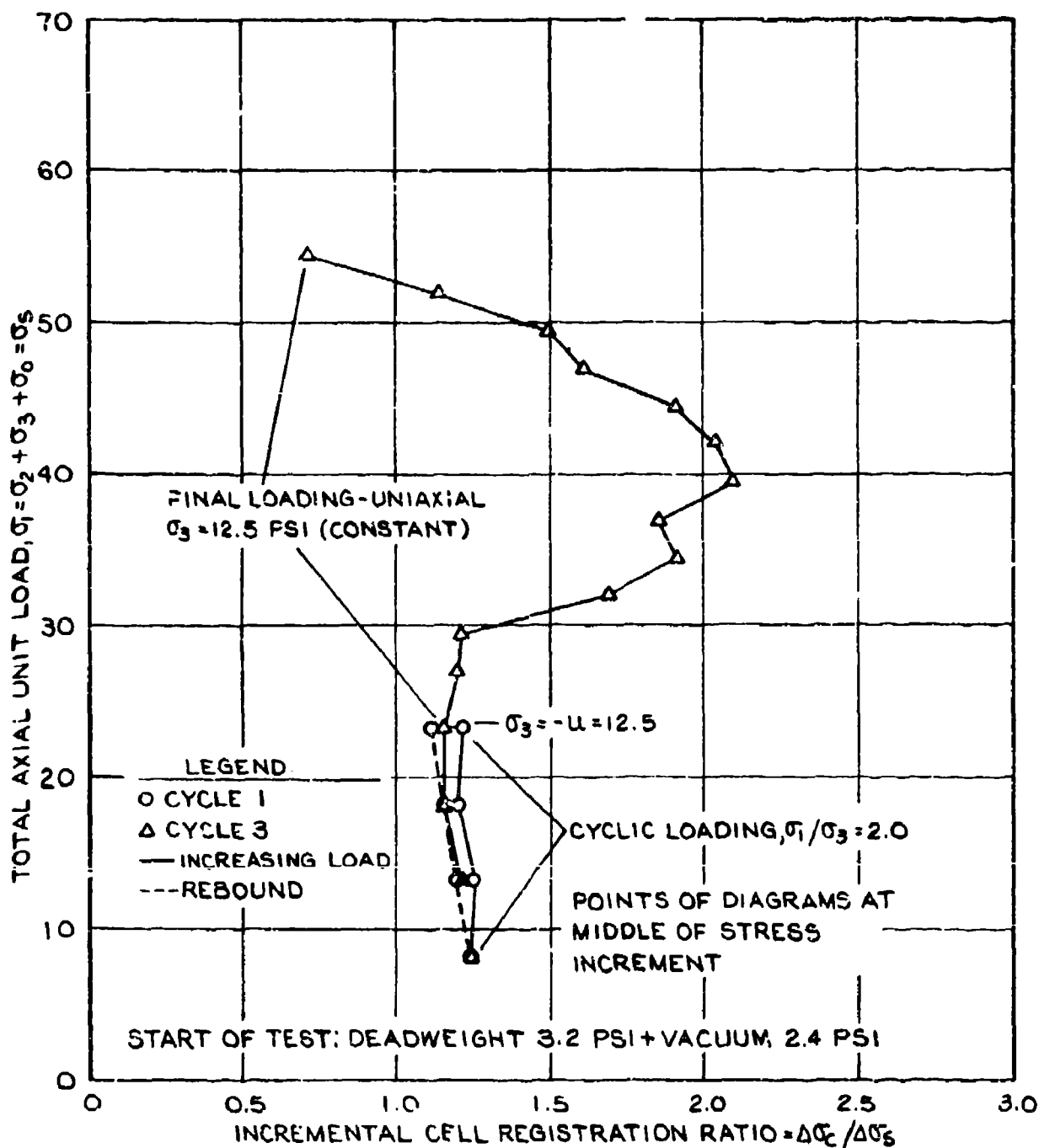


FIGURE 78. AXIAL REGISTRATION RATIOS FOR PRINCIPAL STRESS RATIO 2.0.

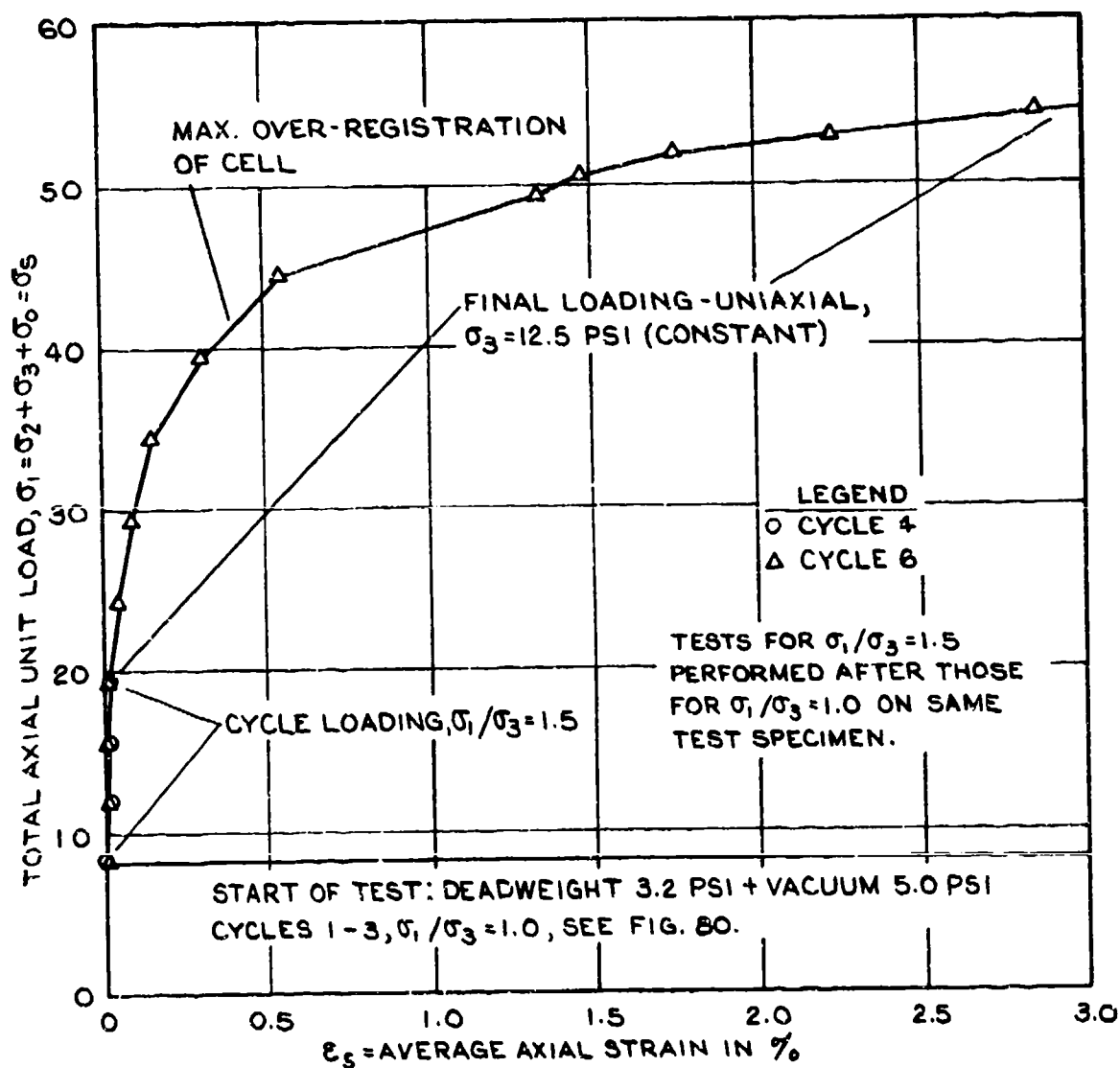


FIGURE 79. AXIAL STRESS-STRAIN DIAGRAMS FOR PRINCIPAL STRESS RATIO 1.5.

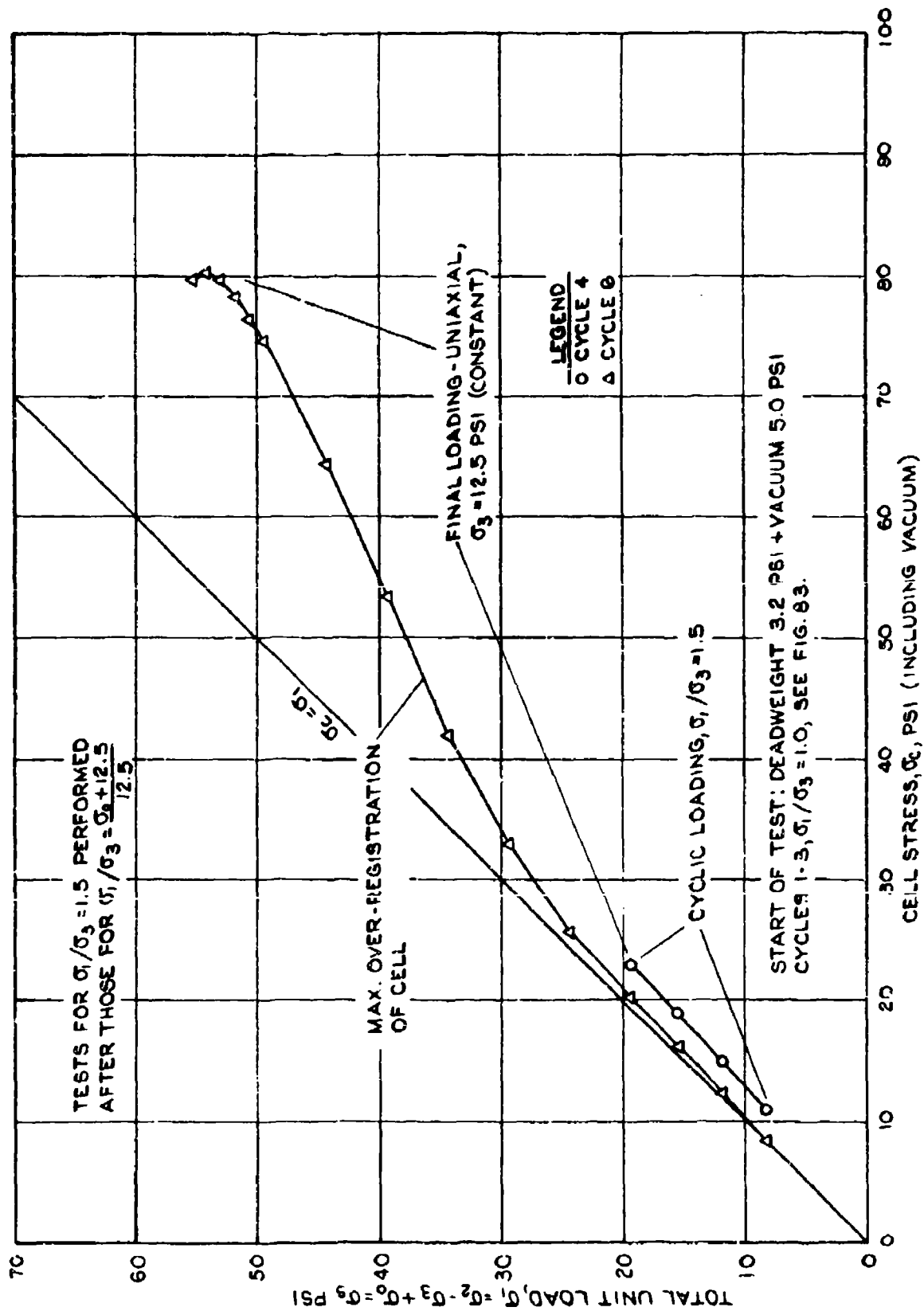


FIGURE 80. SOIL-CELL STRESS DIAGRAMS FOR PRINCIPAL STRESS RATIO 1.5

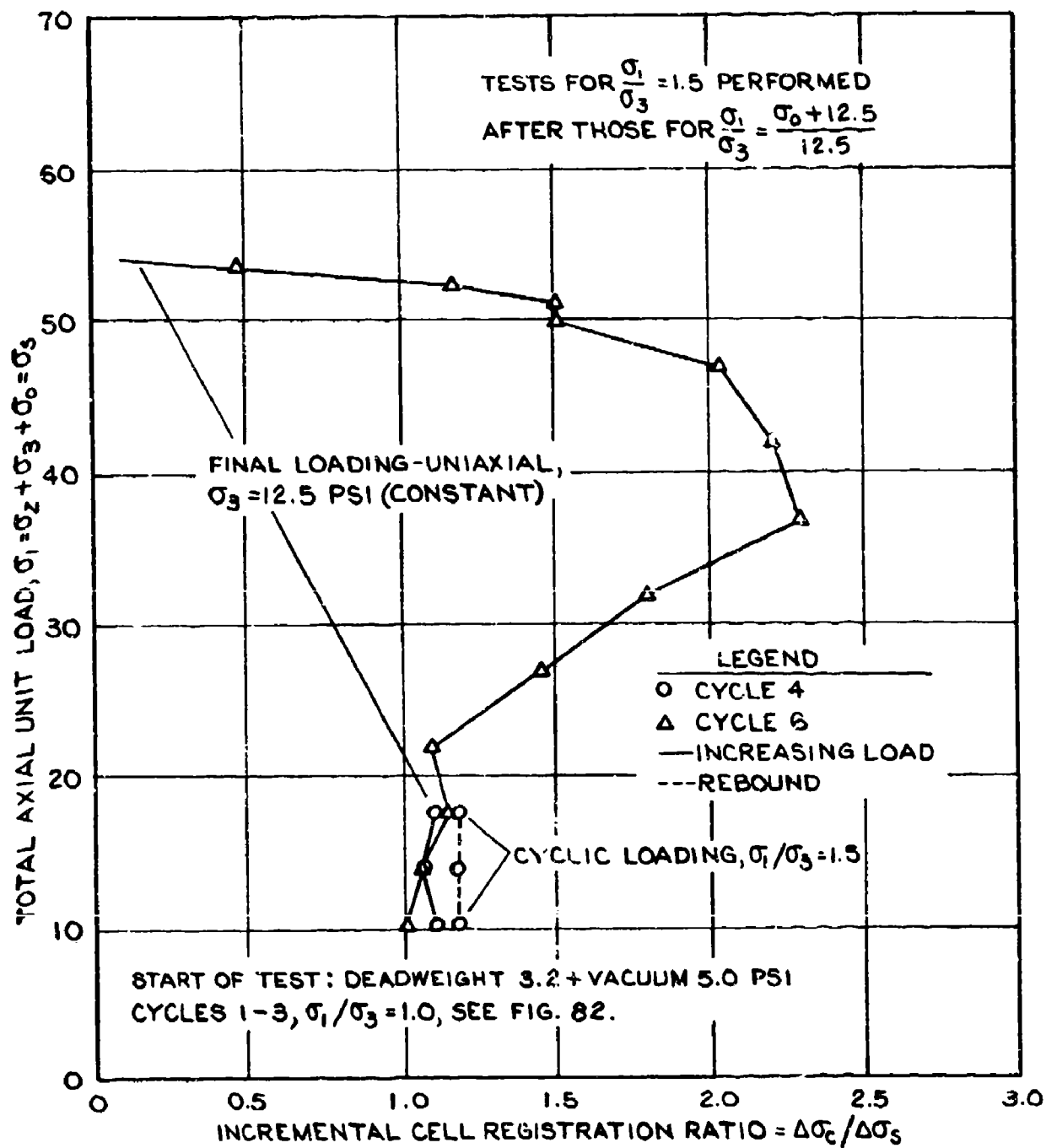


FIGURE 81. AXIAL REGISTRATION RATIOS FOR PRINCIPAL STRESS RATIO 1.5.

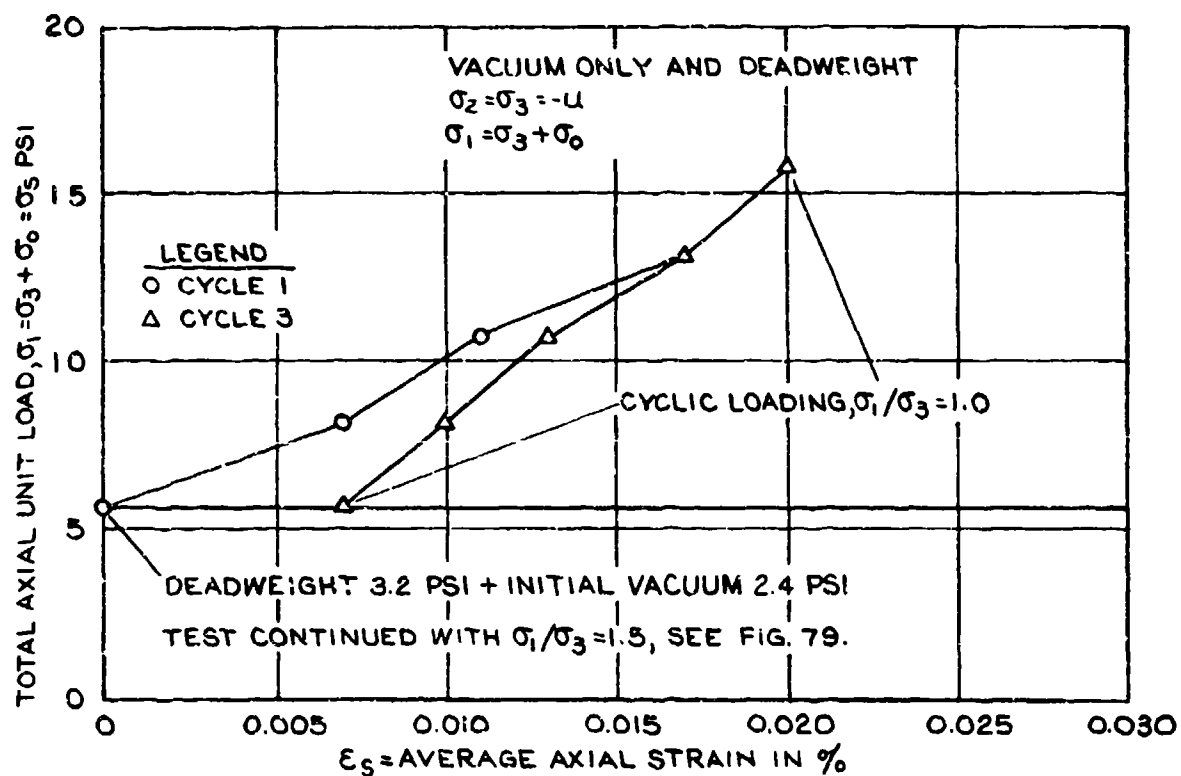


FIGURE 82. AXIAL STRESS-STRAIN DIAGRAMS FOR APPROXIMATE PRINCIPAL STRESS RATIO 1.0.

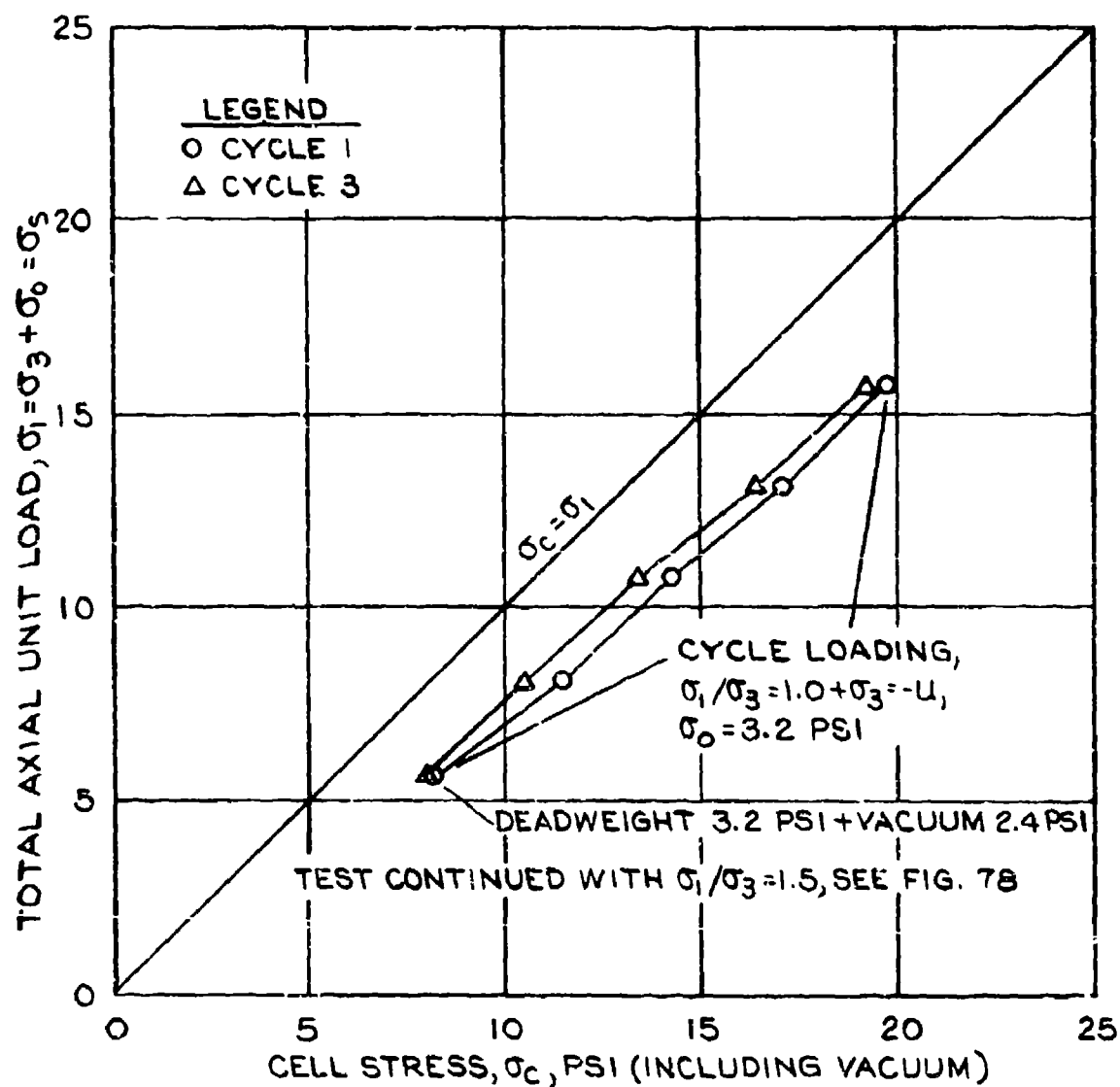


FIGURE 83. SOIL-CELL STRESS DIAGRAMS FOR APPROXIMATE PRINCIPAL STRESS RATIO 1.0.

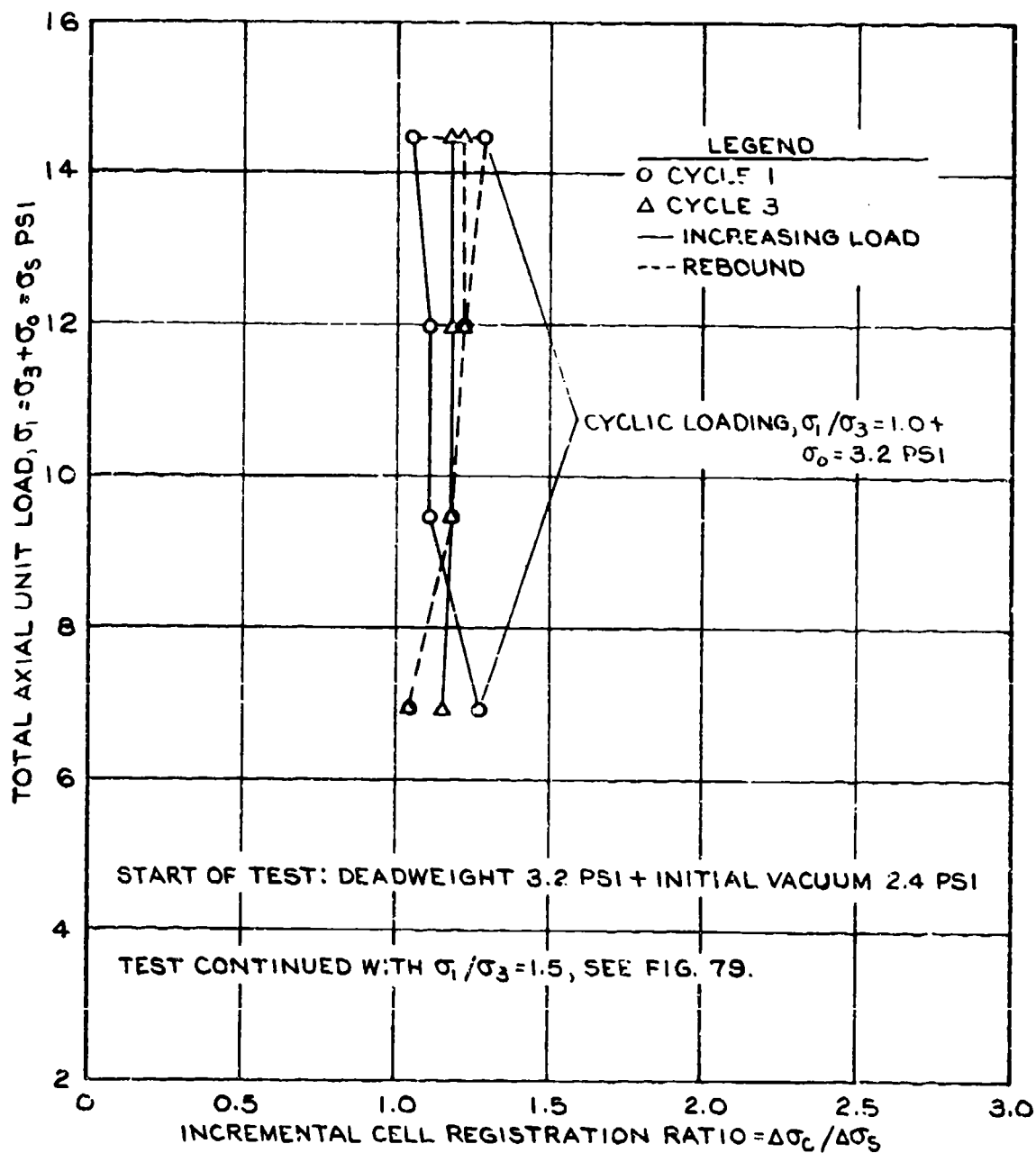
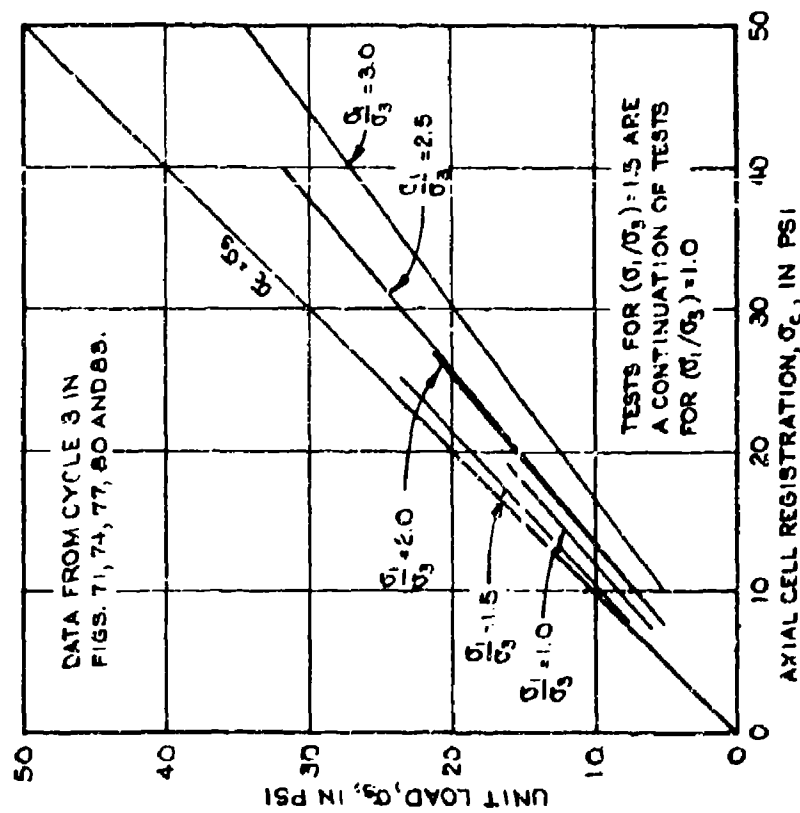


FIGURE 84. AXIAL REGISTRATION RATIOS FOR APPROXIMATE PRINCIPAL STRESS RATIO 1.0.

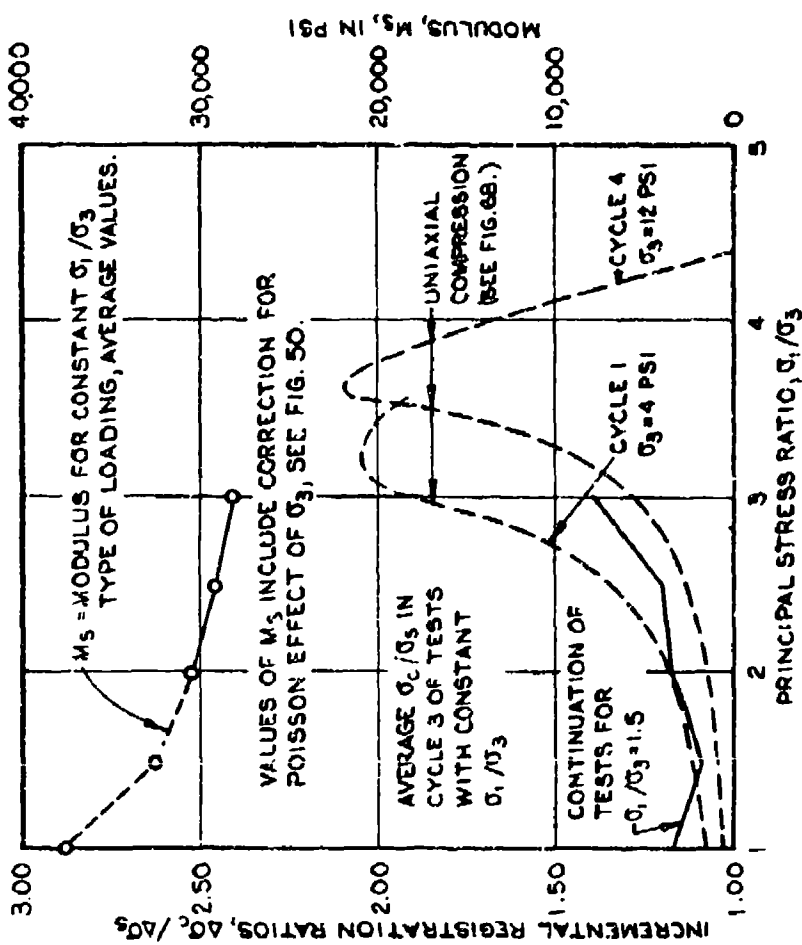
before and decrease after failure of the soil in the test specimen, as observed in the foregoing tests. The maximum value of the incremental registration ratio during the final loading varied between 2.08 and 2.30. It should be noted that a final uniaxial loading was not performed on test specimens with a principal stress ratio of about 1.0 during the cyclic loading, since these test specimens also were used in subsequent tests with a principal stress ratio of 1.5.

154. Comparison of types of loading. Typical results of tests with uniaxial loading are shown in Figure 68 and discussed in the appurtenant text. The great variations in the incremental registration ratios are caused by differences in lateral loading or confining stresses, by changes in the soil modulus, and by a shift in concentration of external pressures from the rim to the center of the pressure cell, when approaching failure of the soil, followed by a rapid decrease in bearing capacity or penetration resistance of the soil immediately after failure. The total and incremental registration ratios and governing factors are much more stable when the principal stress ratio in the test specimen is maintained at a fairly constant value during a particular loading schedule. Details of such tests are presented in Figures 70-84 and are summarized in Figure 85a and b. The total cell registrations in Figure 85a include residual stresses. Corresponding incremental registration ratios vary with the principal stress ratio but are nearly constant for a given value of the stress ratio as shown in Figures 72, 75, 78, 81, 84. These incremental registration ratios are plotted in Figure 85b and there compared with data obtained in tests with uniaxial loading. The incremental registration ratios for the two types of loading are in good agreement when considering the principal stress ratio and the loading cycle. However, a deviation occurs for $(\sigma_1/\sigma_2) = 1.5$, which undoubtedly is caused by the fact that test specimens in the loading series already had undergone a full series of loadings by vacuum or a principal stress ratio approximately equal to unity.

155. The test data summarized in Figure 85a and b show that the axial cell stresses or registration ratios increase with increasing



A. COMPARISON OF AXIAL STRESS REGISTRATION VERSUS PRINCIPAL STRESS RATIO.



B. COMPARISON OF AXIAL INCREMENTAL REGISTRATION RATIOS FOR LOADINGS WITH CONSTANT CONFINING PRESSURE AND WITH CONSTANT PRINCIPAL STRESS RATIOS.

FIGURE 85. COMPARISON OF REGISTRATIONS FOR CONSTANT PRINCIPAL STRESS RATIOS.

principal stress ratios, σ_1/σ_3 , which in part may be caused by the concurrent decrease of the soil modulus, see upper part of Figure 85b. The test data disagree with the experimental data by Plantema, Figure 43c, but the modulus of the Plantema pressure cells are only a little above or below that of the soil and the registration of the cells is very sensitive to changes in the soil modulus. The test data in Figure 85b also disagrees with theoretical data by Askegaard and Bates for low values of the Poisson ratio, Bates assumes $\nu = 0.27$, but Askegaard obtains the opposite results for high values of the Poisson ratio, Figure 35b. The WES test specimens of medium dense sand appear to have high values of the Poisson ratio, and even exhibit expansive characteristics, see Table 2. In this case the test data in Figure 85b would concur with the Askegaard theory. The WES pressure cell has a modulus which is moderately larger than that of the soil, but it reacts to changes in vacuum as a rigid inclusion. The above mentioned theories were developed for linear elastic conditions and they do not consider the influence of changes in the soil modulus and consequent changes of the registration ratio, as shown by Equation 23 of the simplified method of analysis, which yields results similar to the experimental data in Figure 85b. The inelastic swelling or consolidation of soils, and corresponding irregular values of the Poisson ratio, may also have some influence on the registration of pressure cells, but this influence has not yet been adequately investigated. Some of the many factors which govern the registration of a pressure cell are partially interdependent and may counteract each other. It is difficult to separate the influence of the individual factors, and care should be exercised in formulating general conclusions.

156. Calibration and control tests. Soil pressure cells are usually calibrated in the laboratory by direct loading of weights or by uniaxial air loading as shown in Figure 3, both correspond to $(\sigma_3/\sigma_1) = 0$. It is desirable to perform control tests for a given type of pressure cell and soil to determine the relation between registration of the pressure cell during laboratory calibration and under stress conditions in the field. If there is an appreciable difference in

registration of the cell for the two conditions, a correction diagram should be developed, similar to that proposed by Bates (1969) and Figure 42 in this report, but such a correction diagram should be based on or verified by experimental data and not on theory alone. The WES test data show that variations in incremental registration ratios are relatively small when determined for the second or third cycle of loading during which the principal stress ratio is maintained at some constant value below $(\sigma_1/\sigma_3) = 2.5$. It may be advantageous to perform such control tests with the soil placed in laterally confined soil, providing the sidewall friction is practically eliminated by use of a stacked ring device, consisting of superimposed low circular rings with rubber spacers. The principal stress ratio during such a confined test is represented by the equations

$$\sigma_3 = K_o \sigma_1 \quad \text{or} \quad \frac{\sigma_1}{\sigma_3} = \frac{1}{K_o} \quad (121)$$

K_o is the coefficient of earth pressure at rest, which for normal loading of sand may be expressed by

$$K_o = 1 - \sin \phi$$

A correction diagram should consider the influence of the many factors discussed in foregoing sections. Partial interdependence or counteraction of some of these factors should be subjected to additional investigations. Consideration should also be given to subjecting a pressure cell to a seating pressure shortly after installation, so that the stress conditions around the cell in the completed structure will correspond to second or loading cycles.

Measurement of lateral stresses

157. General relations. The principal stresses in an axisymmetrical test specimen are axial stresses, σ_z , the radial stresses, σ_p , and the tangential stresses, σ_θ . Pressure cells for measuring these stresses and diagonal stresses, σ_d , were installed in each test specimen of the 1955 test series, Figure 51. In these tests the lateral

stresses are governed by the confining pressure which in turn was caused by a vacuum in the pores of the soil. The vacuum was measured by an outside pressure gage, and the lateral pressure cells indicated only small differences between the vacuum and the soil pressures, corresponding to the deformation of the soil pressure cells, which were exceedingly small, whereas the test specimen underwent appreciable lateral deformations. The measured vacuum plus indications of the lateral pressure cells registered only small over- or under-registration, and the action of these cells was quite different from that of cells measuring axial stresses. Furthermore, the cells for measuring radial, tangential, and diagonal stresses are difficult to install, and there were more malfunctions of these cells than of cells for measuring axial stresses. Reliable test data for lateral stresses were not obtained for every test specimen. Average lateral stresses determined in the 1955 test series are summarized in Tables 4 and 6, and typical test data for properly installed lateral pressure cells are described in the following paragraphs.

158. Radial stresses. Measured radial stresses during a test with uniaxial loading of the test specimen in three stages with a vacuum or confining pressures of 4, 8, and 12 psi are presented in Figure 86. The measured stresses are shown as a function of the vacuum or nominal radial stresses, and they form a nearly straight line indicating a registration ratio close to 1.00. The influence of axial loads on the test specimen, corresponding to lateral loads on the pressure cell, are indicated by the scatter of stress readings for each vacuum or confining pressure in Figure 86 and by the hysteresis diagrams in Figure 87. In the first three test stages the applied axial load was increased until the principal stress ratio attained a value of about 3.0; however, in the fourth and final cycle of loading, also at a vacuum of 12 psi, the applied axial load was increased to 40 psi, which is close to failure of the test specimen. In this case the registered radial stresses increased to 14.1 psi in spite of the bulging of the test specimen. This increase in the measured radial stress probably reflects local soil failure at the rim of the pressure cell and a shift of stress concentration from the rim to the center of the cell.

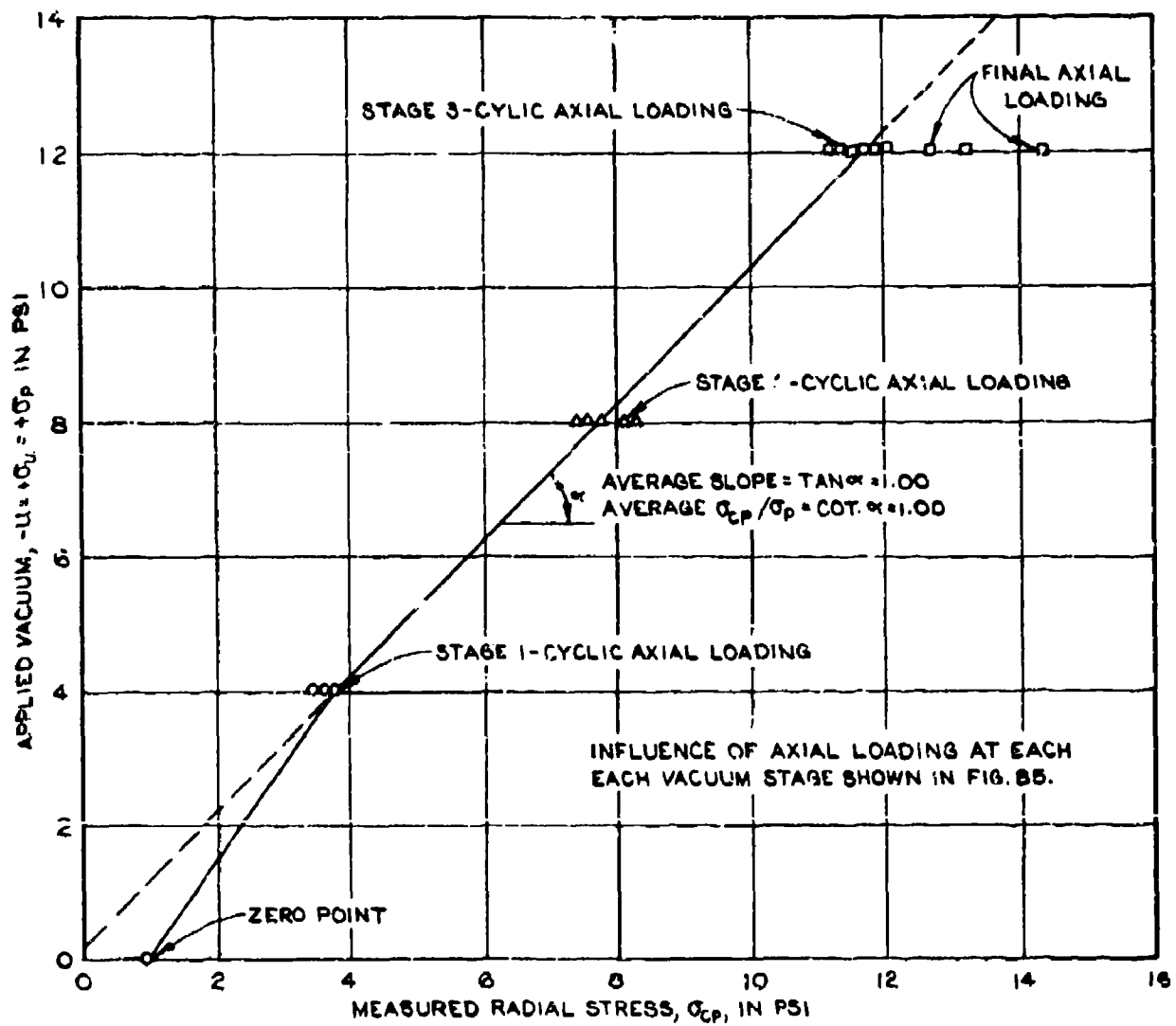


FIGURE 86. MEASURED RADIAL STRESSES FOR UNIAXIAL STAGE LOADING.

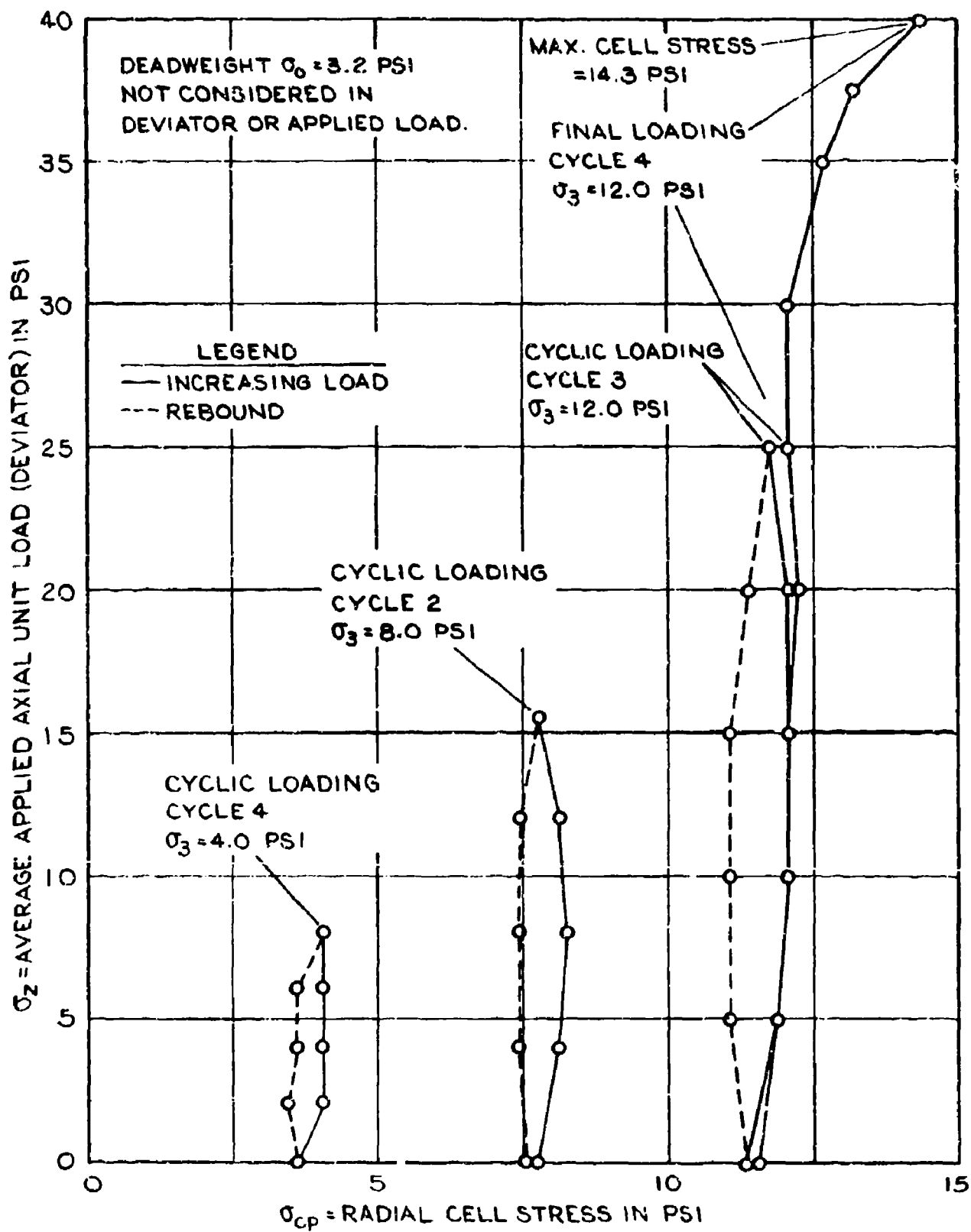


FIGURE 87. MEASURED RADIAL STRESSES IN EACH LOADING STAGE.

159. Measured radial stresses for a loading of the test specimen which maintains a principal stress ratio of 2.5 are shown in Figure 88. In this case there is only little difference between the results obtained in the first and third loading cycles because the radial stresses primarily are caused by the confining pressure or the vacuum in the pores of the test specimen, which is measured by an outside air pressure gage and not by the soil pressure cell. The diagram for the third cycle is not straight but has a slight double or S curvature. The registration ratios for the individual load increments are shown in the figure and vary between 0.90 and 1.12, and the average registration ratio is 1.03. A fourth loading cycle was extended as uniaxial compression for a vacuum of 12.0 psi, and the registered radial stress rose to 15.3 psi corresponding to a total registration ratio of 1.53. These numerical results agree reasonably well with those obtained for uniaxial stage loading and are shown in Figure 87, and the final increase in cell registration is probably also in this case caused by a shift in load concentration from the rim to the center of the cell.

160. Tangential stresses. The results of measurements of tangential stresses for uniaxial stage loading of the test specimen are shown in Figure 89, which is very similar to the diagram in Figure 89 for measured radial stresses. However, the inclination of the diagram corresponds to an average registration ratio of 0.85 in contrast to 1.00 for a radial stress. The average registration ratio of tangential stresses for all tests is also smaller than the corresponding ratio for radial stresses, Table 6. Measured tangential stresses during applied axial load at each vacuum stage are indicated by the horizontal lines through observed stresses at the three vacuum stages of 4, 8, and 12 psi. Further details for plotting diagrams similar to those in Figure 87 are not available at the time of writing the final draft of the report. The diagram in Figure 90 is substituted for one corresponding to Figure 89. This diagram shows measurements obtained with a WES pressure cell of 50-psi rated capacity and considerably more compressible than cells with 100-psi rated capacity. This more compressible pressure cell shows an average additional underregistration ratio 0.90 for tangential stresses,

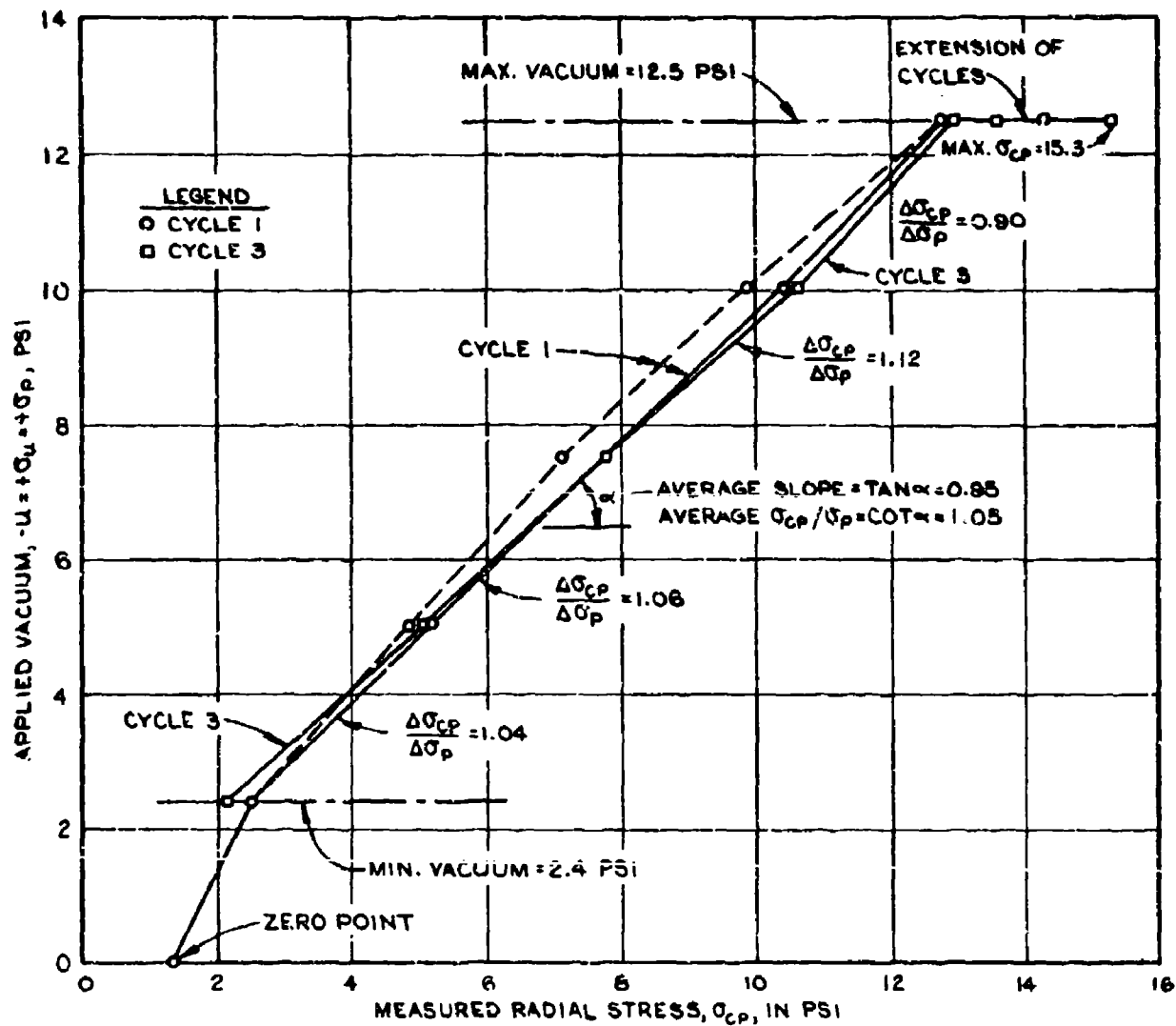


FIGURE 88. MEASURED RADIAL STRESSES FOR PRINCIPAL STRESS RATIO 2.5.

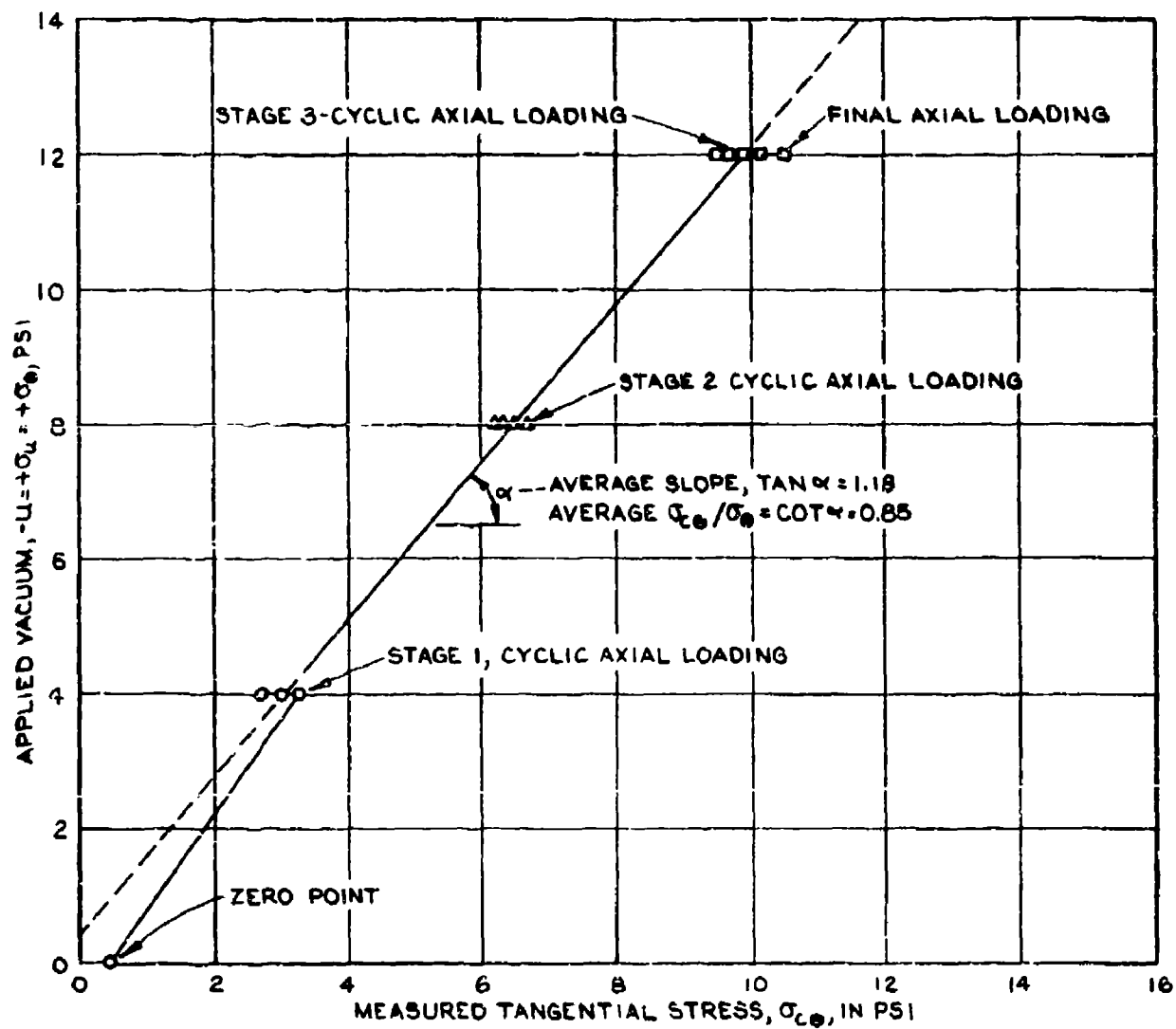


FIGURE 60. MEASURED TANGENTIAL STRESSES FOR UNIAXIAL STAGE LOADING.

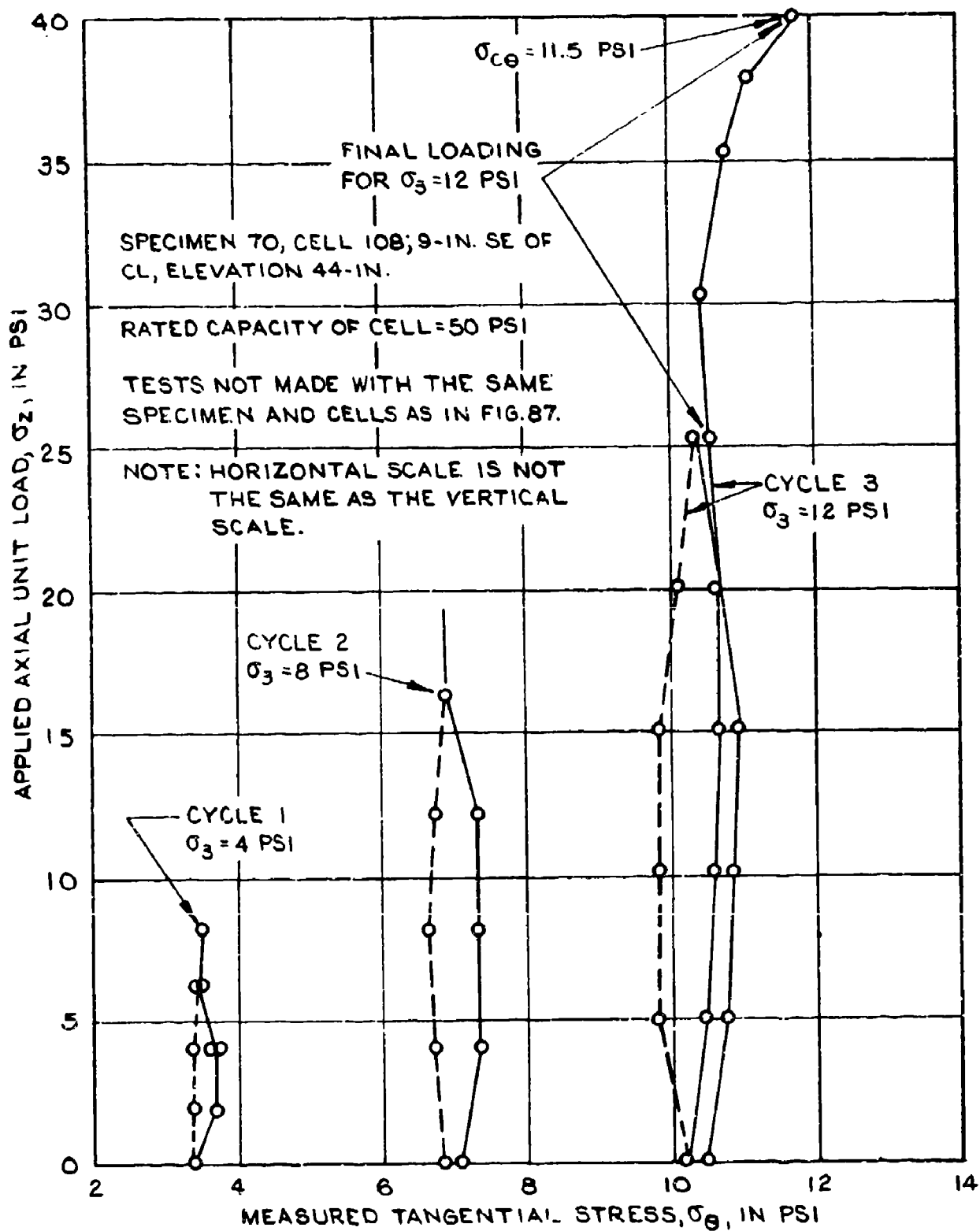


FIGURE 90. MEASURED TANGENTIAL STRESSES IN EACH LOADING STAGE.

the shape or hysteresis of the diagrams obtained for axial loadings at the three vacuum stages are nearly identical to those in Figure 87. After completion of the third loading cycle a fourth loading was performed also at the vacuum or confining pressure of 12 psi and it was continued to an applied vertical load of 40 psi which is close to failure of the test specimen. At this axial pressure the measured tangential stress is 11.5 psi which corresponds to a registration ratio of 0.96. This ratio is greater than those obtained at the end of the regular loading cycles, but it is smaller than the corresponding ratio for radial stresses, Figure 87.

161. An example of measured tangential stresses during a loading procedure which maintains a principal stress ratio of 2.5 in the test specimen is shown in Figure 91. Stress measurements during the third loading cycle indicate incremental registration ratios which vary from 0.85 to 1.08. The average registration ratio for a complete cycle is 1.02, whereas the corresponding ratio in measurement of radial stresses is 1.05, Figure 88.

162. Summary and comments. The test data presented in the foregoing paragraphs are supported by many other tests, as shown in Tables 4 and 6. Both the details in Figures 86-91 and the summaries in the tables show that the measured radial stresses are slightly but also systematically larger than the measured tangential stresses, although according to theoretical investigations by Balla (1961) and Brady (1971) the difference between these stresses should be practically negligible for a linearly elastic material. It is possible that there is a systematic difference in the placement and effective preloading of the pressure cells, but a definite explanation of the difference between measured radial and tangential stresses cannot be formulated on basis of available data. The measured radial and tangential stresses are appreciably smaller than the measured axial stresses. The most logical explanation of this difference is that the magnitude of the lateral stresses is governed by the confining lateral stress or the vacuum which is measured by an outside pressure gage, and that the radial and tangential pressure cells are only subjected to very small changes in loads and deformations.

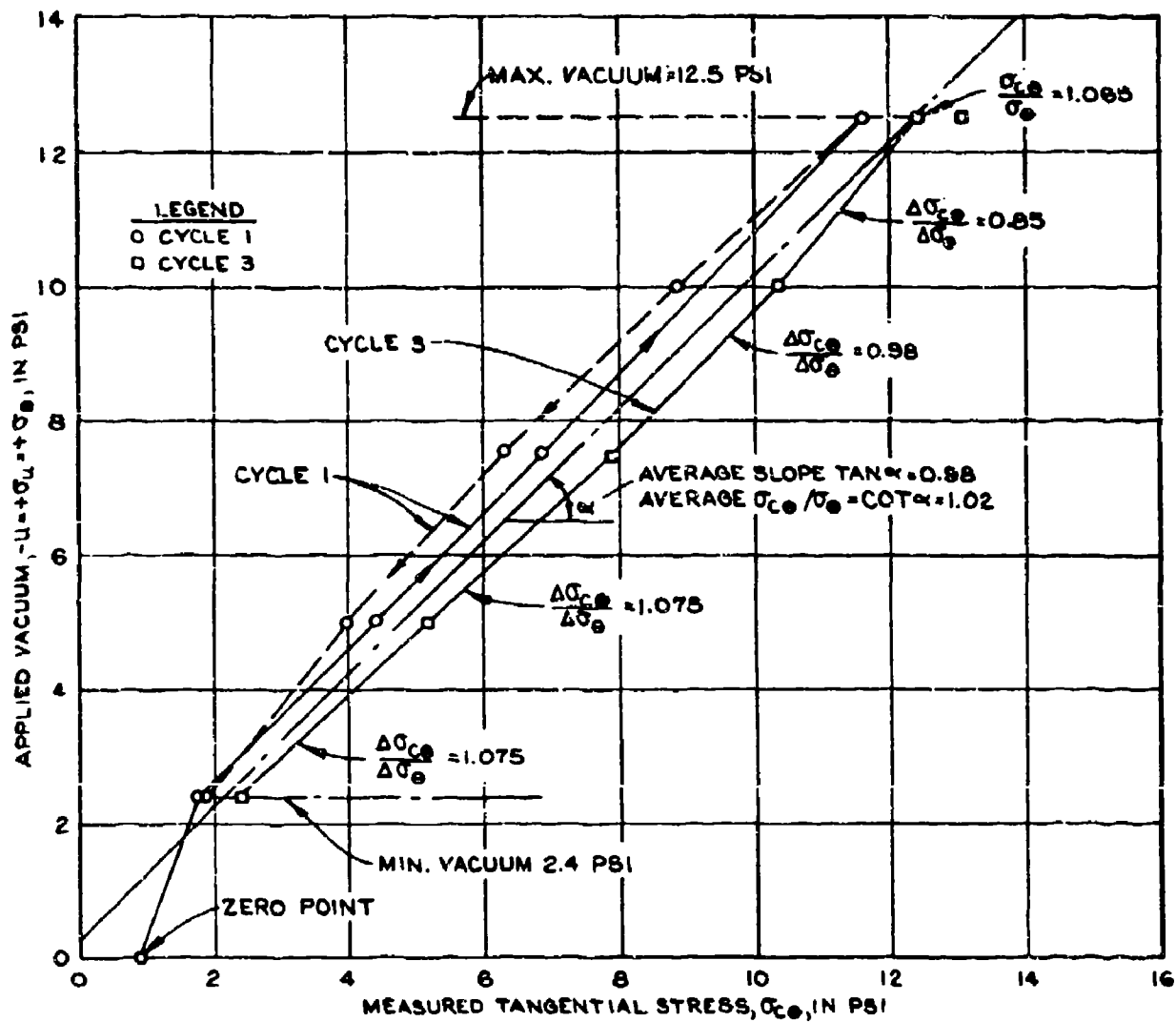


FIGURE 91. MEASURED TANGENTIAL STRESSES FOR PRINCIPAL STRESS RATIO 2.5.

Furthermore, outside unit loads in the plane of cells measuring axial stresses are equal to the lateral stresses, whereas one of the stresses in the plane of cells for measuring lateral stresses is the much larger axial stress, and this should decrease the measured lateral stresses as indicated in the theory by Askegaard, bearing in mind that the apparent Poisson ratio for the medium dense sand in the test specimens is larger than 0.5, Figure 35b. However, Figures 87 and 90 indicate that the measured radial and tangential stresses vary relatively little with changes in the applied axial load. It should be noted that the registered radial and tangential stresses increase materially when the stress conditions in the surrounding sand approach those of failure, as do the registered axial stresses, but they do not attain a maximum value for the applied axial loads. The calibration factors for axial stresses should not be applied in measurement of radial and tangential stresses without modification. A correction factor was found theoretically by Bates (1969) for a given set of parameters, but such a factor cannot be determined from experimental data presented in this report, because of the disturbing influence of vacuum changes in the pores of the soil. A change in this vacuum is counteracted by a nearly equal change in effective soil pressure. As a result, that actual change in pressures on and deformations of a vertical soil pressure cell are very small compared to the changes in effective lateral soil pressures. Additional tests are needed with equipment which can produce a change in outside lateral or confining pressure without a significant change in pore pressures of the test specimen.

Measurement of inclined or diagonal stresses

163. Basic relations. Diagonal planes are inclined planes which form an angle of 45 deg with the axis of the test specimen; normal stresses on these planes are the diagonal stresses, which are designated by σ_d . Pressure cells for measuring diagonal stresses were placed in most of the specimens of the 1955 test series; Figure 51. There are two conjugate directions of diagonal planes, forming an angle of 90 deg with each other, but all pressure cells were placed in the direction

shown in Figure 51. Templates were used in placing diagonal cells. The following simple relations exist for axial, radial, and diagonal stresses on unit loads:

$$\begin{aligned}\sigma_1 &= \sigma_a = \sigma_o + \sigma_u + \sigma_z \\ \sigma_3 &= -u = \sigma_u = \sigma_p \\ \sigma_d &= \frac{1}{2} (\sigma_1 + \sigma_3) = \frac{1}{2} (\sigma_a + \sigma_u)\end{aligned}\tag{122}$$

The principal stresses are σ_1 and σ_3 which in this case are equal to the axial and radial stresses, σ_a and σ_p . The pore pressure (vacuum) is $-u$ and the corresponding compressive stress is $\sigma_u = -u$. The unit load from deadweight at the elevation of the cell is σ_o , and the unit load applied to the top cap of the specimen is σ_z . Equation 122 is first used to compute the unit load on diagonal planes, but all the equations should also apply to the measured stresses as discussed in a subsequent paragraph.

164. Example of test data. Corresponding measured stresses and strains for diagonal planes are shown in Figure 92. The normal diagonal stresses were computed by Equation 122 and the corresponding diagonal strains by

$$\epsilon_d = \frac{1}{2} (\epsilon_1 + \epsilon_3)\tag{123}$$

or from the measured total axial and lateral deformations. The diagram in Figure 92 for the last normal load cycle shows that the rate of strain decreases when the stress conditions in the specimen approach those of failure and that the axial strain finally becomes negative corresponding to dilation of the test specimen at failure. This corresponds to the large values of the Poisson ratio obtained from the total axial and lateral deformations, summarized in Tables 2 and 5, and in Figure 64.

165. A soil-cell stress plot for diagonal stresses and uniaxial stage loading of the test specimen is shown in Figure 93. These diagrams

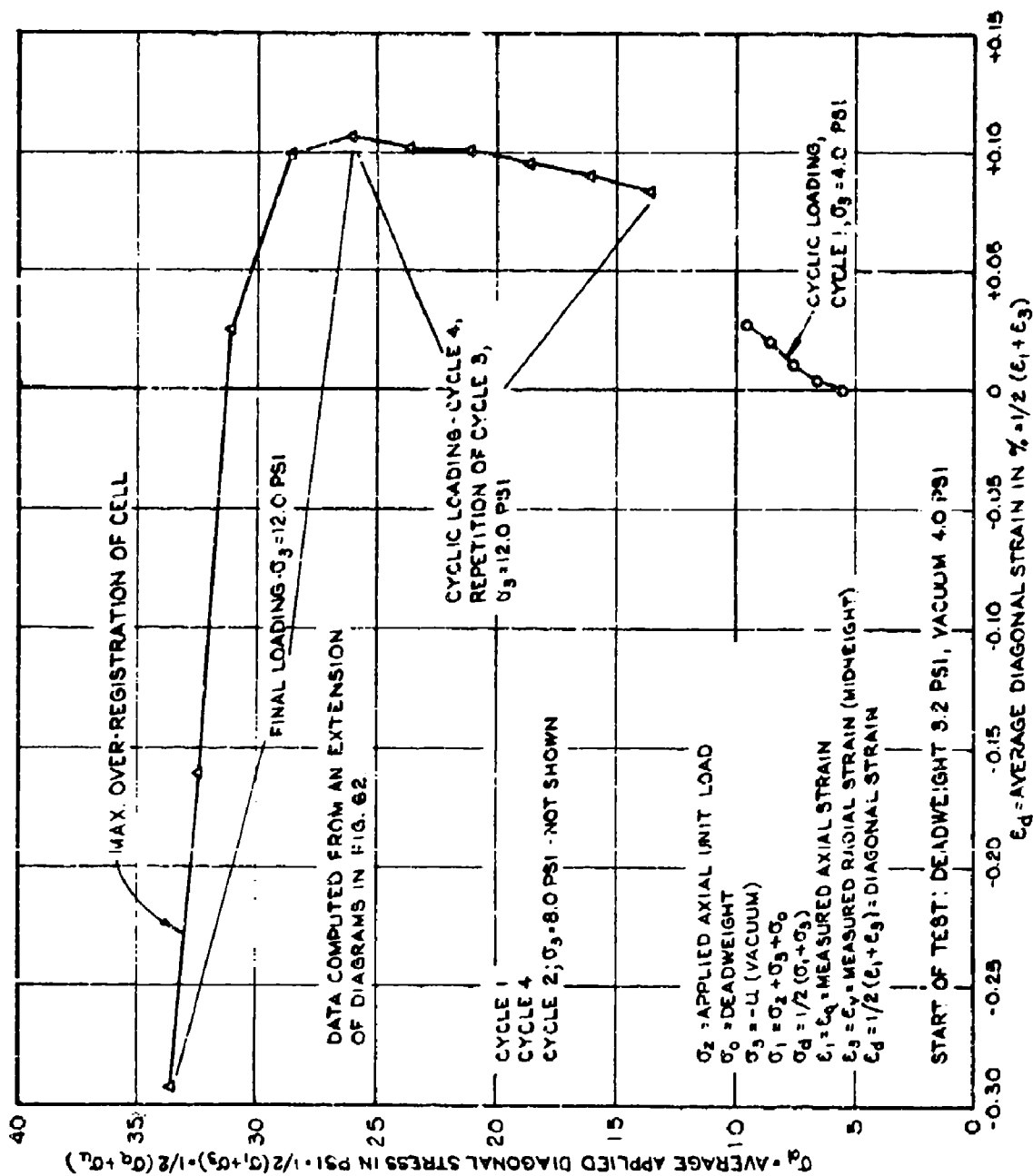


FIGURE 92. DIAGONAL STRESS-STRAIN DIAGRAMS FOR UNIAXIAL STAGE LOADINGS.

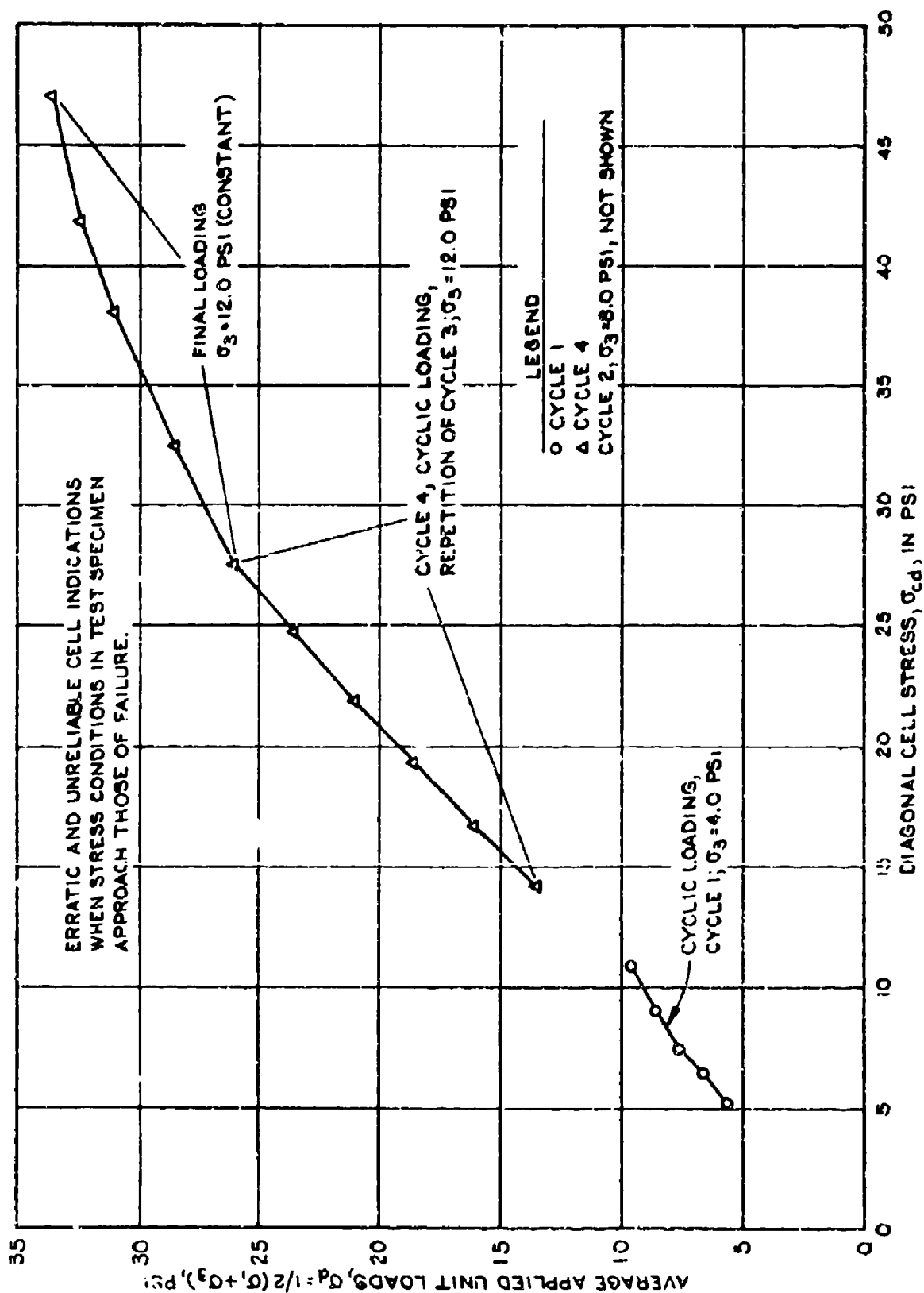


FIGURE 93. DIAGONAL SOIL-CELL STRESS DIAGRAM FOR UNIAXIAL STAGE LOADING.

are fairly straight in comparison with similar diagrams for axial stresses and uniaxial loading, Figure 93. There is a distinct break in the curve at the end of cyclic testing and continuation of the axial loading for a vacuum of 12 psi, but stress and strain relations during the final loading are relatively irregular. Incremental registration ratios corresponding to these stress-strain diagrams are shown in Figure 94. The incremental registration ratios increase quite regularly during the cyclic loading, but this increase is more rapid and irregular during the final loading, and the ratio does not seem to attain a finite maximum value before completion of the test, as observed in measurement of axial stresses, Figure 68. This result agrees with data obtained for radial and tangential stresses.

166. Compatibility of measured stresses. Equation 122 for determination of applied diagonal unit loads should also be valid for measured diagonal stresses. Using the notation for measured stresses, Equation 122 becomes,

$$\sigma_{cd} = \frac{1}{2} (\sigma_{ca} + \sigma_{cp}) \quad (124a)$$

or solved for σ_{ca}

$$\sigma_{ca} = 2\sigma_{cd} - \sigma_{cp} \quad (124b)$$

In Table 4 values of σ_{ca} or the right side of Equation 124b, are compared to applied axial unit loads for average cyclic loads and the final unit loads, and the ratios σ_{ca}/σ_a are also shown in the table. It is seen that values of σ_{ca} , determined from measured values of σ_{cd} and σ_{cp} , are larger than the applied axial unit load, which is reasonable since the overregistration or error in σ_{cd} is greater than in σ_{cp} . The table reflects average values obtained by replacing slightly curved diagrams with straight lines.

Tests with WES soil pressure cell within an inactive rim

167. Tests performed. Several soil pressure cells with an

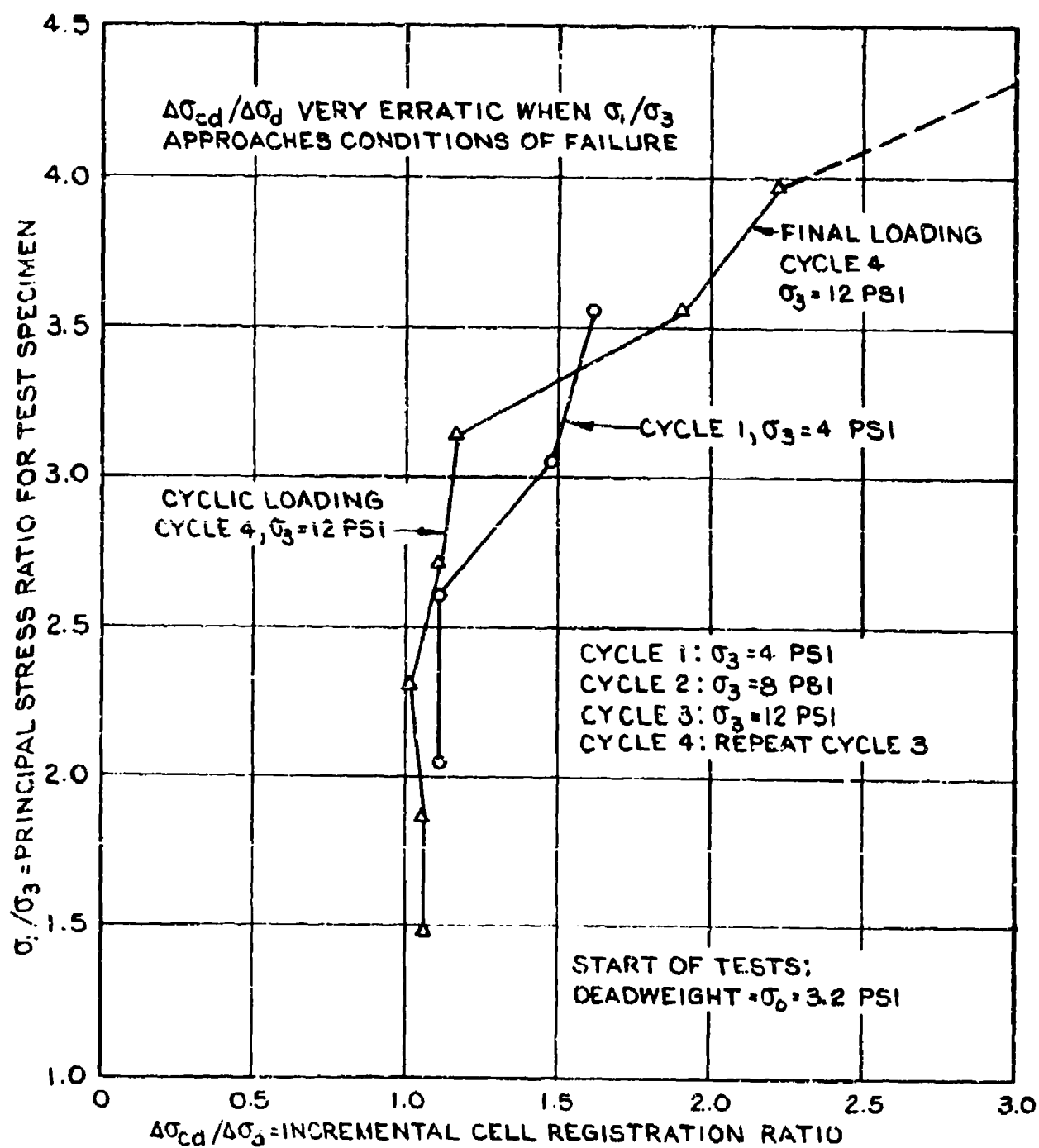


FIGURE 94. DIAGONAL CELL REGISTRATION RATIOS FOR UNIAXIAL STAGE LOADING.

inactive rim and an exposed measuring diaphragm are described in the first part of this report, but test data for these pressure cells cannot be compared directly with data for a WES soil pressure cell having a full active face and an interior measuring diaphragm. In order to obtain comparable data for determination of the influence of an inactive rim, a standard WES 100-psi cell was placed inside a rim with a radial width of 3.0 in., as shown in Figure 97. The rim consisted of upper and lower halves and a central washer. Use of the steel washer in some tests and the rubber washer in other tests was expected to yield data for estimating the influence of compressibility of the inactive rim. The cell-rim assembly was placed at midheight in a test specimen and subjected to uniaxial loading with a vacuum and corresponding confining pressure of 13.26 psi. Initially, three cyclic tests were made to a maximum axial applied load of 30 psi, corresponding to a maximum principal stress ratio $\sigma_1/\sigma_3 = 3.5$. This initial cyclic loading was followed by two to three tests to a maximum applied axial load of 40 psi, corresponding to $\sigma_1/\sigma_3 = 4.2$. The tests were made using test specimens Nos. 39-46 of dense sand with a unit weight of 110 pcf. These tests were performed between the main test series of 1954 and 1955.

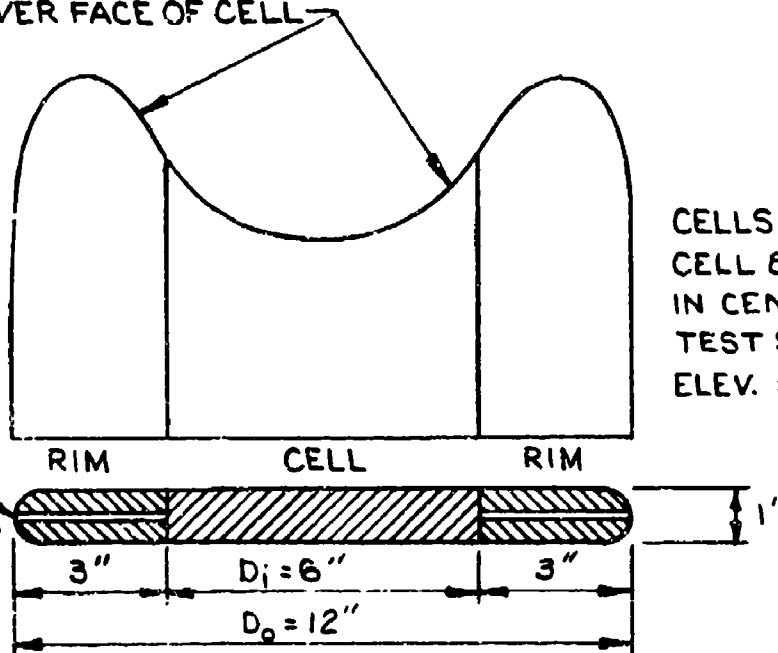
168. Test results. Examples of soil-cell stress diagrams are shown in Figure 95a for tests with a steel washer in the inactive rim and in Figure 95b for tests with a rubber washer in the rim. Only one load cycle is shown for each of the maximum applied axial loads of 30 and 40 psi. The soil-cell stress diagrams are fairly straight up to an applied axial load of 30 psi, but a sharp break in the diagrams occurs when the applied load exceeds 30 psi. It is noted that the slopes of the diagrams for the fourth cycle are steeper than those for the first cycle, which corresponds to a decrease in the registration ratio, as also shown by the diagrams for incremental registration ratios in Figure 96. However, there is a great increase in the incremental registration ratio when the applied axial load exceeds 30 psi or when the principal stress ratio in the surrounding soil approaches that corresponding to failure. This increase in registration ratio is probably caused by a transfer of load and stress concentration from the rim to the center

PROBABLE INITIAL STRESS
DISTRIBUTION OVER FACE OF CELL

CONSTANT
LATERAL
PRESSURE
 $\sigma_3 = 13.26$ PSI

CELLS 82 AND 85
CELL 85 - 100 PSI
IN CENTER OF
TEST SPECIMEN
ELEV. = 35-IN.

1/8" STEEL OR
RUBBER WASHER



WASHER	NO. OF TESTS	REGISTRATION RATIO, σ_c / σ_z , IN %	
		σ_1 / σ_3 1.3 TO 3.5	σ_1 / σ_3 3.5 TO 4.2
STEEL	6	86 TO 112	125 TO 215
RUBBER	2	97 TO 118	140 TO 150
ALL TESTS	8	AVERAGE 101	AVERAGE 160

DATA FROM FOURTH LOAD CYCLE

NOTE: ALL CELLS HORIZONTAL AND MEASURE AXIAL
STRESSES.

FIGURE 95. SUMMARY OF TEST DATA FOR WES PRESSURE CELL PLUS
INACTIVE RIM.

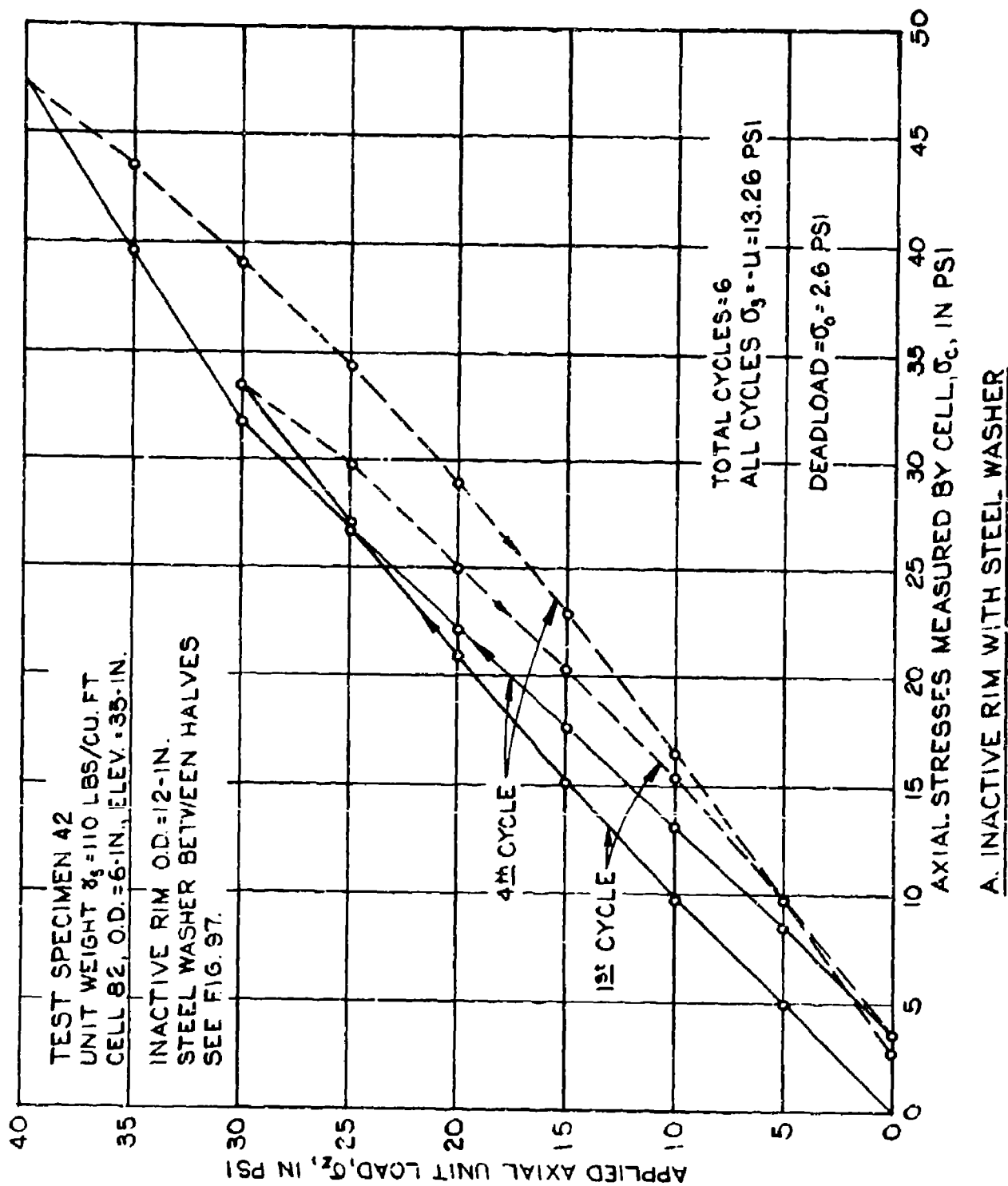


FIGURE 96. SOIL-CELL STRESS DIAGRAMS FOR WES CELL PLUS INACTIVE RIM.

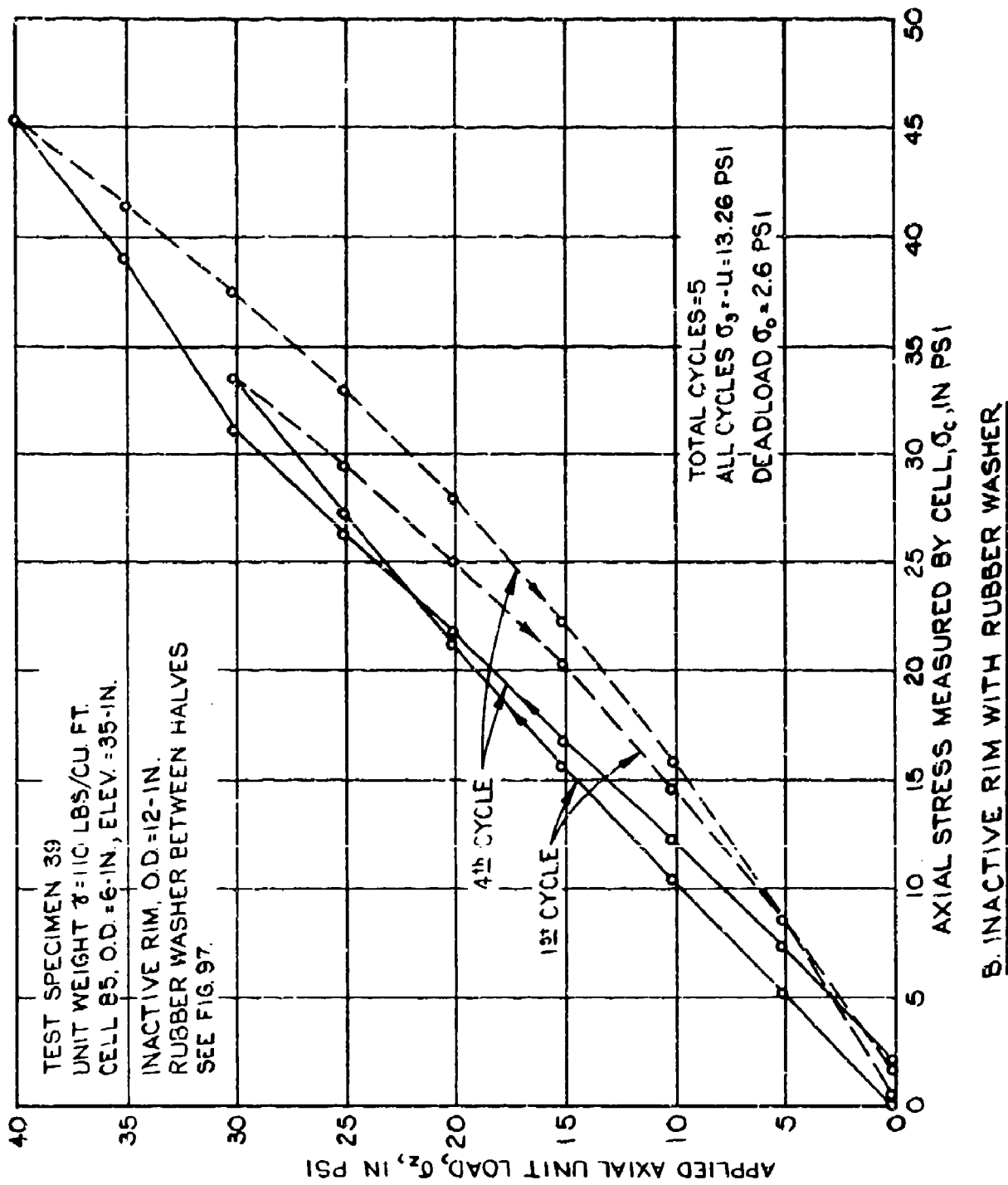


Figure 96 (Continued)

of the cell-rim assembly. These test results are in agreement with an additional proof of the thesis by Terzaghi (1943) concerning changes in stress distribution below a rigid plate when the load creates stress conditions approaching those of soil failure, see Figure 8.

169. Results corresponding to the fourth cycle of all tests are summarized in Figure 97. There is considerable scatter of the test data, but the average registration ratios for σ_1/σ_3 less than 3.5 are much smaller than those obtained with WES pressure cells without an inactive rim. Registration ratios for a rubber washer in the rim are slightly larger than those obtained with a steel washer in the rim, but this relationship is reversed for the larger registration ratios obtained for σ_1/σ_3 greater than 3.5. These maximum registration ratios are also smaller than corresponding ratios for cells without inactive rims. However, it is possible that the maximum registration ratios for a cell-rim assembly, although quite irregular, may continue to increase for applied axial loads greater than 40 psi, and corresponding greater principal stress ratios, because the unit weight and strength of the test specimens used in these tests were somewhat larger than the average unit weight and strength of the test specimens in the main test series of 1955.

170. Comments on the influence of an inactive rim. Peattie and Sparrow (1954) and others have shown that an inactive rim may decrease the overregistration of a rigid soil pressure cell. This conclusion is verified by the above mentioned test data for a standard WES soil pressure cell placed inside an inactive rim. However, the test data also indicate that the initial advantage of an inactive rim is decreased and may disappear when stress conditions in the surrounding soil approach those of failure, because failure conditions cause a shift of stress concentrations from the edge to the central part of the cell-rim assembly. The relative compressibility of the inactive rim should have some influence on the magnitude and location of the stress concentration, and thereby the errors in the cell registration, but differences between results obtained with steel washers and rubber washers are too small and varied to enable formulation of reliable numerical conclusions. It is also possible that a bevelled or tapered shape of the rim will reduce

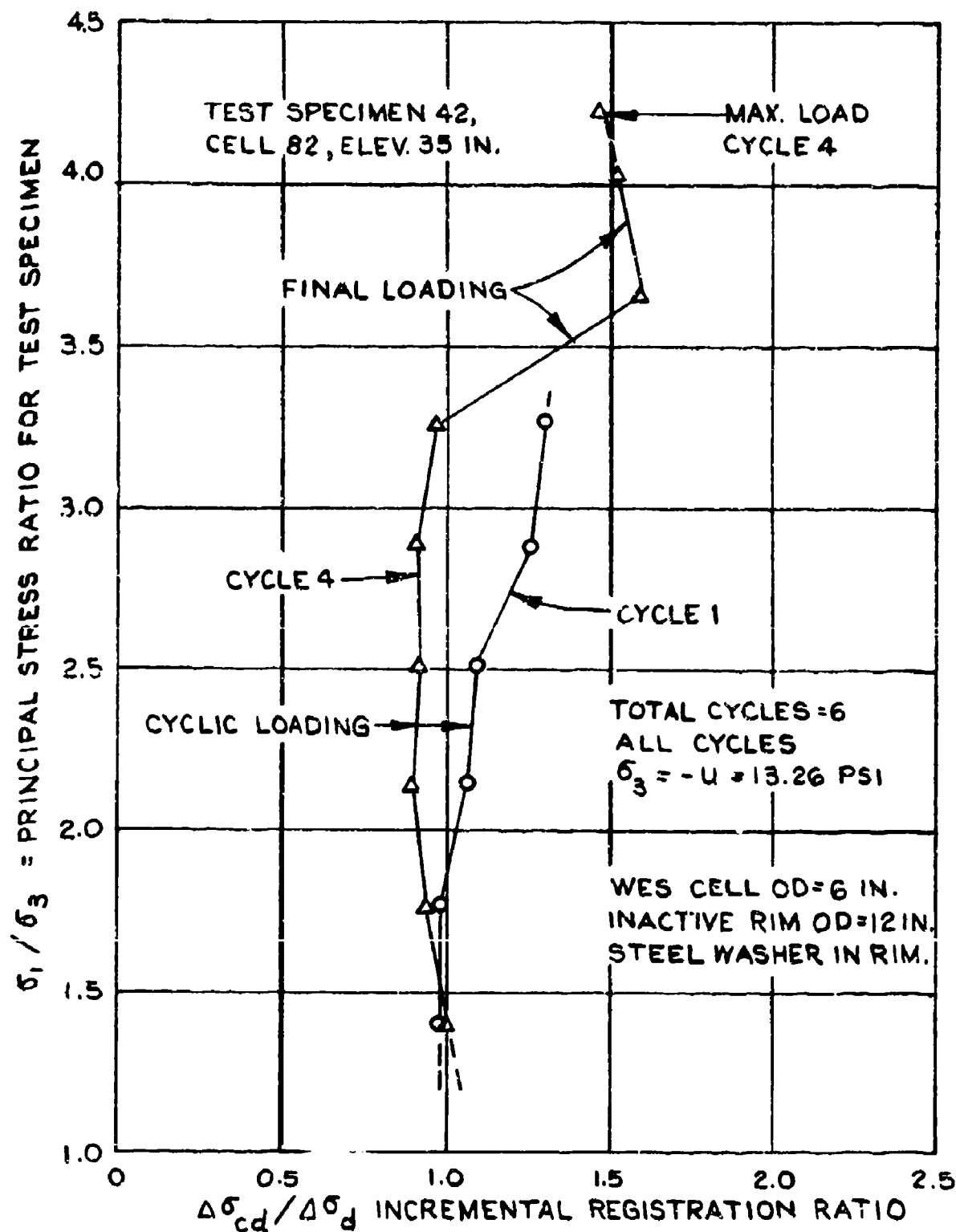


FIGURE 97. REGISTRATION RATIOS FOR WES PRESSURE CELL PLUS INACTIVE RIM.

stress concentration and possible errors in stress registration by a pressure cell. A tapered edge has been used by Bates, Figure 11, and Carlson has proposed a semicircular shape of the outer edge in a recently revised design of his stress meter.

1.71. A WES-type pressure cell plus an inactive rim requires movement between the face plate of the cell and the inactive rim. Such movement may in time be impeded by entrance of foreign material and development of friction and adhesion. Most of the currently used pressure cells with inactive rims avoid this potential difficulty and achieve a much simpler design by use of one or two exposed measuring diaphragms, Figures 2, 9, 11, 12. The registration of such a fixed diaphragm is very sensitive to nonuniformity of the load and it may be damaged by stones in the soil or proximity of rock. Heavy face plates or diaphragms decrease this danger as well as sensitivity of the cell to changes in the ratio of moduli of cell and soil or rock. A heavy diaphragm may not yield adequate resolution of stresses unless resistivity strain gages are replaced by far more sensitive solid-state strain gages. The latter are satisfactory for cells used in laboratory experiments but are not yet considered to be sufficiently stable for field investigations under adverse conditions and of long duration.

PART IV: SUMMARY AND CONCLUSIONS

General Data

172. The report contains a review of the principal types of soil pressure cells, a summary of various hypotheses proposed for soil-cell interaction, and a long delayed account of experiments with soil pressure cells performed by the WES in 1954-55.

173. The soil is usually assumed to be a uniform, elastic material, whereas it is imperfectly elastic and subject to irregular changes in its properties. It has nonlinear stress-strain relations, including hysteresis and residual stresses and strains. It may exhibit volume changes and apparent values of the Poisson ratio which are incompatible with the formal theory of elasticity, and it is a two- or three-phase system of solids, liquids, and gases.

174. The principal types of soil pressure cells are (a) relatively large and very thin pressure pads with a special control valve, Figure 10, (b) cells with fully active face plates, a transfer liquid, and an interior measuring diaphragm, Figures 3 and 4, and (c) cells with an inactive rim and exposed measuring diaphragms on one or both faces, Figures 9, 11, 12.

175. The action of a cell may be expressed by the registration ratio or ratio between the registered stress change and the actual change in field stresses. The total registration ratio, σ_c/σ_s , refers to the total stress changes in a loading cycle, and the incremental registration ratio, $\Delta\sigma_c/\Delta\sigma_s$, refers to changes caused by a single load increment. The error in cell registration is the difference

$\sigma_e = \sigma_c - \sigma_s$, and the error ratio is σ_e/σ_s .

176. Pressure cells are inclusions in the soil and change the stress conditions in the soil in the vicinity of the cell. The cell actually measures the inclusion stresses normal to the face of the cell. These stresses are influenced by lateral soil stresses and the Poisson ratio, whereas lateral or radial stresses on the cell itself has no significant influence on the cell registration.

177. It has long since been established experimentally that the registration error or error ratio of a soil pressure cell decreases with decreasing thickness-diameter ratio of the cell, h/D ; Benkelman and Lancaster (1940), Waterways Experiment Station (1944). However, solutions for pressure cells embedded flush with a rigid boundary have been obtained by means of the basic relations of the theory of elasticity, and the results can be expressed approximately by the equations in Figures 34c and d. Theories show that a pressure cell placed just in contact with a rigid boundary acts as a cell of twice the thickness in a free field, whereas a cell embedded flush with a rigid boundary always underregisters. For a cell stiffer than the soil there should be a partial embedment at which the registration error is zero, Figures 21-24.

Hypotheses for Soil-Cell Interaction

178. One of the earliest and simplest hypotheses for soil-cell interaction may be called the indentation analogy. It consists of estimating the difference in deformations of the cell and a soil layer of equal thickness, and comparing this difference with the force on and indentation of a rigid plate of the same diameter, at the soil surface. Estimating this indentation involves use of the Prandtl or equivalent equations by Boussinesq. The indentation analogy method yields reasonable explanations of the actions of a pressure cell, but the numerical results may be in error to a considerable extent, primarily because the Boussinesq equations apply only to forces at the soil surface, whereas the Mindlin equations should be used for forces inside a soil mass, Figure 26. Examples of applications of the indentation analogy to a pressure cell in a free field are shown in Figures 15 and 16.

179. Application of the indentation analogy method to a pressure cell at or in a rigid boundary may cause numerical errors which are greater than for a cell in a free field.

180. Solutions for the soil-cell interaction by use of incremental annular elements were developed by Carlson (1935, 1939) and Monfore (1950), who solved the resulting simultaneous equations by iteration

methods. Numerical solutions may be obtained more efficiently by computers and finite element methods, Bates (1969) and Figures 38-40. These methods yield numerical solutions for specific soil types and cells, but the results should not be generalized without additional investigations.

181. The registration of a soil pressure cell depends on the magnitude of inclusion stresses normal to the face of the cell, but these stresses are in part a function of the lateral soil stresses and the value of the Poisson ratio. Using basic equations by Eshelby (1957), Askegaard (1963) obtained semiclosed solutions for inclusion stresses at a rigid ellipsoidal body, which are represented graphically in Figure 35. The diagrams show the influence of lateral stresses and the Poisson ratio on the inclusion stresses and cell registration which will be discussed again in the paragraphs on calibration.

182. Pressure cells with an inactive rim combine problems of a cell in a free field and a cell in a rigid boundary for which a computer solution has been obtained by Tory and Sparrow (1967). Numerical solutions for specific cells and soils are shown graphically in Figure 37. This form of pressure cell is advantageous for many stress conditions.

183. The influence of shallow embedment of a pressure cell may be estimated by comparison with the test data for circular trapdoors by McNulty (1965), Figures 28-32. Approximate data may also be obtained by use of the approximate trapdoor theories by Terzaghi (1936, 1943) and by Mason (1965).

WES Experimental Data of 1954-55

184. The tests were performed in 1954-55 using a large vacuum-type triaxial device, Figures 46 and 47, and with WES pressure cells in test specimens of medium dense sand. The soil of the test specimens had expansive characteristics and apparent Poisson ratios greater than 0.50, which combined with variations of the vacuum in the soil pores limits the applicability or generalization of the test data.

185. The principal objective of the WES 1954 test series was to determine the axial stress distribution in a test specimen with

restrained ends. The pressure cells were placed as shown in Figure 5a, and they were not subjected to a seating load. The scattering in the test data was large, but the data show definitely that the minimum stress at the ends occurs in the center of the test specimen, whereas the maximum stress at midheight of the specimen occurs in the center. This agrees with theories proposed by Filon, Balla, Brady, and others.

186. The main objective of the 1955 test series was to investigate the cell action under various types of loading. The cells were placed at half radius a little above and below midheight of the test specimen, Figure 5b. The cells were subjected to a seating pressure of 13.26 psi, before the forming jacket was removed and the actual tests were started.

187. The first cell action tests were conducted with uniaxial stage loading; that is, the vacuum or confining pressure was constant during a particular test, but it was increased in successive stages from 4 to 8 and 12 psi. An example of the test data is shown in Figure 68, where changes of total and incremental registration ratios are given as a function of the principal stress ratio. The rate of changes in the registration ratio increases with increasing principal stress ratio but this change is small at the start of the test and may then be attributed to changes in the modulus of deformation of the soil. The rapid changes close to failure of soil cannot be explained in this manner, and it is likely that they represent changes in stress distribution or a shift in stress concentration from the periphery to the center of the pressure cell, similar to that for rigid circular loading plates, as observed by Terzaghi and others, Figure 8. This shift is reversed immediately after failure of the soil occurs. This explanation assumes that the sensitivity of the WES cell decreases to some extent from the center to the periphery.

188. In a second series of tests the principal stress ratio was maintained at constant value during loading in a particular tests, but it was varied for the different test series. After reaching the limit corresponding to the maximum possible vacuum, the test was continued as a uniaxial test with the equivalent confining pressure. Typical test

data are shown in Figures 71-85, which show that the registration ratio is more sharply defined in these tests than in uniaxial tests; and they are also in better agreement with stress conditions encountered in the field. Results yielded by the two types of loading are compared in Figure 85a and b. For values of σ_1/σ_3 close to those of failure of the soil, uniaxial loading yields a large and rapid increase of the incremental registration ratio because of a probable shift in stress concentration, as previously mentioned. For smaller and usual values of the principal stress ratio, loading with maintenance of this ratio yields larger values of the registration ratio than those obtained by uniaxial loading, which probably reflects the influence of larger lateral stresses on the inclusion effect of the cell, but the influence of changes in the vacuum should also be considered because they cause changes in deformations of the soil without corresponding deformations of the pressure cell.

189. Examples of the measurement of lateral, or radial and tangential, stresses in the soil are shown in Figures 80-91 and in Tables 4 and 6. The corresponding registration ratios vary from slightly below to slightly above 1.00 and are always smaller than those for corresponding axial stresses. The lateral stresses are produced by changes in vacuum or pore pressure, which is measured by an outside manometer and causes very little deformation of the pressure cell. Reliable data on the inclusion effect of a pressure cell placed on edge, or the shape factor of a cell so placed, are not yet available. It is difficult to estimate the reliability of measurements of lateral stresses until additional tests are made in which a partial vacuum in the soil pores is replaced with a positive outside confining pressure on the test specimen.

190. An example of the results of measurement of diagonal or inclined stresses is shown in Figures 92-94. The measurements are compatible with those of axial and lateral stresses, but since the diagonal stresses are a simple function of the axial and lateral stresses, these measurements do not provide a real check on the measured diagonal stresses. The remarks on measurement of lateral stresses in the

foregoing paragraph apply also the measurement of diagonal stresses.

191. In a few cases, stresses were measured by uniaxial loading of a WES pressure cell surrounded by a 3-in. wide inactive rim as shown in Figure 95. The compressibility of the inactive rim could be changed by annular steel or rubber inserts. The registration ratios obtained for normal values of σ_1/σ_3 varied considerably, but the average was close to 1.00; however, when the tests were continued and approached failure of the test specimen, the registration ratios increased similarly to those shown in Figures 68 and 85. These tests furnish an illustration of the advantages of the principle of an inactive rim, and they support the assumption that the rapid rise of registration ratios in Figures 68 and 85 are caused by a shift in stress concentrations on the cell.

Principal Pressure Cell Parameters and Design Data

192. It has long been known that the inclusion effect or error in pressure cell registration is nearly proportional to the thickness-diameter ratio of the cell, h/D , Benkelman and Lancaster (1940), Waterways Experiment Station (1944). It is often stated that the value of h/D should not exceed 1/6 to 1/5, but it appears that the ratio h/D should preferably be much smaller.

193. It has also been known that the error in cell registration of axial stresses in the test specimen increases but approaches a limiting value with increasing modular cell-soil ratio, M_c/M_s , Figure 15. The correction factor becomes nearly constant when the modular ratio is greater than about four or five; that is, the factor does not increase appreciably with further increases of M_c/M_s .

194. The error in cell registration also increases with increasing principal stress ratio for cohesionless soils, Figure 85, but the cell registration increases rapidly followed by an equally rapid decrease, so that the cell registrations become unreliable, when the stress conditions in the soil at the cell approaches those of failure.

195. The Poisson ratio of the soil greatly influences the inclusion effect of the lateral stresses which in turn governs the cell

registration of axial stresses, Figure 35. Furthermore, soils may undergo volume changes and exhibit apparent Poisson ratios which are incompatible with the formal theory of elasticity. Better estimates of soil-cell interaction can undoubtedly be made by developing and using improved constituent equations for stresses and strains in soils.

196. The shape of the usual soil pressure cell is a right cylindrical disc with sharp edges, which increases stress irregularities and stress concentration at the periphery of the cell. Attempts have recently been made to decrease such stress concentrations by bevelling or rounding the outer edge of the cell. Adequate analytical and experimental data on the influence of the shape of a soil pressure cell and the direction of the principal soil stresses are not yet available.

197. The WES (1944) has suggested that a maximum permissible deflection of a soil pressure cell with fully active face plates should be less than $1/2000$ of the diameter. The suggestion cannot be applied directly to a pressure cell with an inactive rim and an exposed, fixed measuring diaphragm. Preliminary data for the permissible deflection of such diaphragms may be made by use of the theories by Gravesen (1959) and Askegaard (1961), or by substituting the average diameter of the measuring diaphragm and its average deflection in the above mentioned rule, but the problem deserves further theoretical and experimental investigations. However, the deflection of a diaphragm becomes less important when the diaphragms are provided with very sensitive strain gages for a required resolution of the stresses, which permits use of relatively thick diaphragms with corresponding small deflections.

Types of Cells, Sensors, and Soils

198. The principal types of soil pressure cells are reviewed in the first part of the report, but only three types are mentioned in this summary. The original German pressure pad is used again after introduction of the check valve by Glötzl, Figure 10, which permits measurement of the pressure in the liquid between the face plates with a very small movement of the liquid. Special sensors are not needed. The

cell is fairly large, appears to be stable, and is suited for measurement of earth pressures in large earth structures. Detailed data on the influence of stones in the soil and irregular stress distribution are not yet available.

199. Of the many designs proposed for common use, a pressure cell with an inactive rim is currently the most promising one. The cell may have two exposed measuring diaphragms for cells in a free field, Figure 9, but one diaphragm is sufficient for cells embedded in a rigid boundary material. The stresses are actually obtained by correlation with strains in the diaphragm, determined by strain gages or sensors. The diaphragms should be as thick as possible to provide resistance to stones and other irregularities but also consistent with the sensors used and the required resolution of stresses.

200. A recent and novel design of a soil pressure cell is shown in Figure 11. The cell has an inactive rim, and the space between the cover plates is filled with a liquid. The pressure in the liquid is measured by a special, miniature, solid-state liquid pressure gage. It is possible that the cell requires cover plates which are too thin to prevent damage by stones in the soil.

201. The strain gages used in early pressure cells were vibrating wires or mechanically attached resistivity wires; the former were primarily used in Europe and the latter in the United States. In later years mechanically attached wires are often replaced with resistivity foils, bonded to the diaphragms with epoxy cements, which appear to function satisfactorily. In recent years conventional resistivity foils have for some purposes been replaced with solid-state resistivity foils, primarily in the United States, which have more than fifty times greater sensitivity than the ordinary resistivity foils and can be used for both static and dynamic measurements, replacing the large piezoelectric crystal placed between thin cover plates of a cell but were not suitable for static stress measurements. However, the long-term stability of solid-state foils has not yet been demonstrated satisfactorily, and this type of gage is primarily used for short-term experiments, but rapid improvements are being made in the manufacture of solid-state gages.

202. The soil-cell interaction depends on the properties of both soil and cell. Preliminary experiments by Peattie and Sparrow (1954) indicate that the principal deviation is exhibited by dense cohesionless materials, Figure 27a, and the materials used in the WES experiments of 1954-55 fall in this category. Tests have not yet been made in strongly overconsolidated and undisturbed cohesive soils. Additional experiments are needed.

Calibration of Soil Pressure Cells

203. The over- or under-registration of a soil pressure cell is equivalent to or a function of the inclusion effect. As shown by Askegaard, Figure 35, the inclusion effect depends not only on the axial or vertical stresses in a free field but also on the lateral stresses in the soil and its Poisson ratio and on the configuration of the cell. Furthermore, the total registered stress may be changed by the pressure of air and/or water in the pores of the soil. Therefore, the calibration factor is not a constant for a given pressure cell. However, as shown in Figure 35, the inclusion effect is small for some combined values of the Poisson ratio and the thickness-diameter ratio.

204. The commonly used methods for calibration of soil pressure cells are direct loading, axial hydraulic, or pneumatic loading by equipment similar to that shown in Figure 5a. The calibration factors thus obtained need modification by a coefficient which reflects the influence and the direction of the stresses, the Poisson ratio, and the pore pressures. Therefore, the usual calibration tests should be supplemented by the following tests in order to determine the correction coefficients, but it is possible that these tests need only be performed for each type of cell and soil, general stress condition, and Poisson ratio.

205. First, the calibration factor should be determined for hydrostatic water or air pressure and be compared with the factors for equipment commonly used for measurement of pore pressures. Secondly, the cell should also be calibrated when embedded in soil and subjected to all the inclusion stresses and for both horizontal and vertical positions of the

cell. It would be desirable to perform such tests in a large triaxial device with positive confining pressure. However, it may be adequate to make the tests under confined consolidation in a stacked ring device, Figure 5b, since similar stress conditions are commonly encountered in the field.

206. Currently, the results of static calibrations are also being used in evaluation of measurements of dynamic stresses. Fully satisfactory methods for dynamic calibration have not yet been developed or published. It may be difficult to differentiate between dynamic stresses in solids and pore fluids, since the measurements may be subject to a time lag, depending on permeability of the soil.

207. Influence of variations in numerical values of the Poisson ratio should be taken into consideration when generalizing the results of experiments or theoretical investigations.

Installation of Soil Pressure Cells

208. The first requirement for installation of a soil pressure cell is preparation of a plane contact or seating surface. Stones should be removed and a thin layer of fine sand may be used to obtain a smooth surface, but the thickness of such a sand layer should not be large enough to cause appreciable pocket action in the soil around the cell. According to Hadala (1967), cells should be placed at an interface of compacted, cohesionless soils, but cells in cohesive soils should preferably be placed in a shallow excavation of the same diameter as the cell. Backfill soil should be carefully placed, tamped, or compacted around and over the cell.

209. It is suggested that a seating pressure be applied when the cover attains a thickness sufficient to protect the cell against damage. A seating pressure of 13.26 psi was applied in the WES tests of 1955 before removal of the forming jacket and starting the actual tests. The scatter in the test data was much smaller than in the tests of 1954. The minimum or optimum seating pressure has not yet been determined.

210. The curvature of the stress-strain diagram for a first

loading cycle and corresponding changes in the soil modulus also cause considerable variations in the cell registration. More uniform and consistent results would be obtained if the cell and surrounding soil were preloaded so that conditions during the actual measurements correspond to cyclic loading. Such preloading may be difficult to achieve in the field, but it deserves consideration and investigation.

211. Vertically placed pressure cells for measurement of lateral stresses should also be installed to obtain essential data on the stress conditions and, when required, to determine correction coefficients to the general calibration factors. Seating pressures and preloading are difficult to apply to vertical cells, and systems of diametrically placed loads may be used to avoid lateral displacements of the pressure cells during seating and preloading.

212. The foregoing paragraphs apply also, with minor modifications, to pressure cells installed at or in a rigid boundary. Special difficulties are encountered when installing pressure cells in undisturbed soil; it is very difficult to avoid some disturbance of the soil and some pocket action in the backfill.

Operating Procedures

213. Evaluation of the registration of a soil pressure cell is made by use of the effective calibration factors, after correction for the influence of pore pressures, which must be known, reliably estimated, or determined separately. The registration of a soil pressure cell reflects its reaction to the total inclusion stresses, including the pore pressures. The modification coefficients are functions of the soil properties, the stress conditions, the design of the cell, and its orientation. All these parameters should be carefully considered in the evaluation of the total registrations of the cells.

214. Soil stresses and pore pressure in the field may be subject to cyclic variations, which may cause zero shifts of the pressure cells and some changes in the effective calibration factors. Attempts should

be made to determine all these changes, by use of the cyclic stress-strain diagrams for the soil.

215. Attention is again called to the possibility that differences between stresses based on laboratory and field experiments in many cases are not caused by errors in the actions of the pressure cells but on difficulties reproducing actual field conditions in the laboratory, where artificial boundary conditions or restrictions often must be introduced. These remarks also apply to many other laboratory soil investigations.

PART V: SUGGESTIONS FOR ADDITIONAL INVESTIGATIONS

216. Further development of soil pressure cells is possible and needed and some specific investigations are enumerated in the following paragraphs. Advantage should be taken of all published data, but repetitions of experiments should be avoided except for the purpose of clarification or checking. The suggestions do not cover all needed investigations.

First Priority

Review papers on soil pressure cells published after January 1971.

Make desirable additions to this report.

Investigate variations in sensitivity with distance from center of the WES soil pressure cell. Use multiple point loads or annular loads.

Theoretical Investigations

Finite element analysis of uniform inclusion. Disc shape, uniaxial loading, horizontal, and vertical orientation of disc.

Finite element analysis of WES soil pressure cell, different axial and lateral moduli, uniaxial and triaxial loading, horizontal and vertical orientation of cell, Poisson ratio 0.1, 0.3, 0.49.

Optimum shape of cell. Constant diaphragm diameter, plus variable inactive rim. Various thickness-diameter ratios.

Relation between cell error and thickness-diameter ratio for vertical cell, uniaxial loading, various Poisson ratios of the soil.

Analysis of cell with optimum form, close to, resting on, straddling, or embedded in rigid boundary material.

Influence of distance to free boundary.

Influence of changes in pressure of air or liquid in soil pores.

Influence of creep and extraneous volume changes

Influence or limits of approximations for nonlinear stress-strain relations of the soil.

Assemble results of foregoing paragraphs into simplified rules.

Testing Equipment

- Develop auxiliary equipment for the stacked-ring device.
- Develop and build large triaxial testing device with positive or external confining pressure.
- Develop special equipment for testing pressure cells at a rigid boundary.
- Develop special equipment for field investigations.

Installation of Pressure Cells

- Compare irregularities in first and second loading cycles in the 1954-55 test series.
- Optimum seating pressure for horizontal pressure cells.
- Optimum seating pressure for vertical soil pressure cells.
- Maximum thickness of uniform sand layer for direct seating.
- Field procedures and limitations.

Experimental Investigations for Free Field Conditions

- High pressure tests in the stacked ring device.
- High pressure tests in large triaxial device.
- Comparison with test data in vacuum-type triaxial device.
- Tests for optimum shape of cell; constant central part plus variable inactive rim of bevelled and rounded or ellipsoidal shape.
- Relation of error to thickness-diameter ratio for vertical cell.
- Influence of depth below free boundary.

Experiments with Pressure Cells at Rigid Boundary

- Influence of distance from rigid boundary, vertically and laterally, vertical and horizontal cells.
- Cells resting on rigid boundary.
- Cells straddling rigid boundary.
- Cells embedded flush in rigid boundary material.

Influence of Soil Types on Cell Action

- Medium loose sand.
- Medium dense sand.
- Sand with gravel and stones.
- Normally consolidated soft clay.

Influence of Soil Types on Cell Action (Continued)

Overconsolidated firm or stiff clay.

Swelling soils.

Soft shales.

REFERENCES

About 70 technical articles and books are mentioned in the text of this report. These references are listed in alphabetical order on the following pages, and they are referred to in the text by author and year of publication. This method is the most convenient listing of references so far developed. The authors name and the year of publication of the article often gives the reader sufficient information without having to look up the complete reference. Furthermore, references may be added or deleted without having to change reference numbers throughout the text. However, if desired the references may be given numbers and listed in the order of their being mentioned in the text, as is still being done by some individuals and institutions. This list of references contains primarily technical papers published before January 1971, although a few articles published after this date are also included, but it is emphasized that the list of references does not constitute a complete bibliography on the subject of soil pressure cells.

- Ahlvin, R. G. (1956), "Waterways Experiment Station Large Triaxial Apparatus," Highway Research Board Bulletin 141, pp 19-25.
- Askegaard, V. (1959), "The Measurement of Pressure Between an Infinitely Rigid Wall and a Compressible Medium," Festskrift til (Publication in honor of Professor Anker Engelund, Copenhagen, 1930), pp 9-25.
- Askegaard, V. (1961), "Measurement of Pressure Between a Rigid Wall and a Compressible Medium by Means of Pressure Cells," Structural Research Laboratory, Technical University of Denmark, Bulletin No. 14, Copenhagen.
- Askegaard, V. (1963), "Measurement of Pressure in Solids by Means of Pressure Cells," Structural Research Laboratory, Technical University of Denmark, Bulletin No. 17, Copenhagen.
- Askegaard, V., Berholdt, M., and Nielsen, J. (1972), "Probleme by der Messung des Silodruckes mit Hilfe von Druckzellen (Problems in Measuring Silo Pressures by Means of Pressure Cells)," Die Bautechnik, Vol 49, pp 83-36.
- Balla, A. (1961), "Stress Conditions in Triaxial Compression," Transactions, American Society of Civil Engineers, Vol 128, Part 1, pp 1074-1101.
- Bates, R. C. (1969), "SMRL Soil Stress Cell," Proceedings, Engineering Geology and Soils Engineering Symposium, University of Idaho, Moscow, Idaho, pp 9-32.
- Bedesam, W. B. (1964), "A Continuum Theory for Soil-Structure Interaction in Granular Media," Thesis, University of Illinois, Urbana, Illinois.
- Benkelman, A. C. and Lancaster, R. J. (1940), "Important Considerations in the Design and Use of Soil Pressure Cells," Proceedings, Highway Research Board, Vol 20, pp 299-313, and in Public Roads, Vol 21, pp 235-243, 1941.
- Brady, B. T. (1971), "An Exact Solution to the Radially End-Constrained Circular Cylinder Under Triaxial Loading," International Journal of Rock Mechanics Mining Sciences, Vol 8, pp 165-178.
- Carlson, R. W. (1935), "Five Years Improvement of the Elastic-Wire Strain Meters," Engineering News Record, Vol 114, pp 696-697.
- Carlson, R. W. (1939), "Development and Analysis of a Device for Measuring Compressive Stress in Concrete," Thesis, Department of Civil and Sanitary Engineering, Massachusetts Institute of Technology.
- Carlson, R. W. and Pirtz, D. (1952), "Development of a Device for Direct Measurement of Compressive Stress," Journal of American Concrete Institute, Vol 24, pp 201-215, and Discussions.

Chelapati, C. V. (1964), "Arching in Soils Due to the Deflection of a Rigid Horizontal Strip," Test Note N-591, U. S. Naval Civil Engineering Laboratory, Port Hueneme, California.

Coutinho, A. (1949), "Theory of an Experimental Method for Determining Stresses Not Requiring Accurate Knowledge of the Modulus of Elasticity," Publications, International Association for Bridge and Structural Engineering, Vol 9, p 83.

D'Appolonia, E. and Newmark, N. M. (1951), "A Method for Solution of the Restrained Cylinder Under Compression," Proceedings, U. S. National Conference on Applied Mathematics, pp 217-226, published by American Society of Mechanical Engineers.

Eason, G. and Shield, R. T. (1960), "The Plastic Indentation of a Semi-Infinite Solid by a Perfectly Rough Circular Punch," Journal, Applied Mathematical Physics, Vol 11, pp 33-43.

Erlingen, A. C. (1962), Nonlinear Theory of Continuous Media, McGraw-Hill, New York.

Eshelby, J. D. (1957), "The Determination of the Elastic Field of an Ellipsoidal Inclusion, and Related Problems," Proceedings, Royal Society, London, Series A, Vol 241, pp 376-396.

Filon, L. N. G. (1902), "The Elastic Equilibrium of Circular Cylinders Under Certain Practical Systems of Load," Philosophical Transactions, Royal Society, London, Series A, Vol 198, pp 147-233.

Finn, W. D. (1960), "Stresses in Soil Masses Under Various Boundary Conditions," Thesis, University of Washington.

Franz, G. (1958), "Unmittelbare Spannungsmessung in Beton und Baugrund (Direct Measurement of Stresses in Concrete and Foundation Soil)," Der Bauingenieur, Vol 133, pp 190-195.

Fung, F. C. (1965), Foundation of Solid Mechanics, Prentice-Hall, Englewood Cliffs, New Jersey.

Geddes, J. D. (1966), "Stresses in Foundation Soils Due to Vertical Subsurface Loading," Geotechnique, pp 231-255.

Girijavallabhan, C. V. and Mehta, K. C. (1969), "Stress-Strain Relationships from Compression Tests on Non-Linear Materials," American Society of Civil Engineers Symposium on Application of Finite Element Methods in Civil Engineering, pp 457-480, Nashville, Tennessee.

Glötzl, Franz (1958), "Ein Neues Hydraulisches Fernmessverfahren für Mechanische Spannungen und Drücke. Archiv für Technisches Messen (A New Hydraulic Method for Remote Measurement of Stresses and Pressures),"

Archiv für Technisches Messen, Lieferung 265, pp 21-23, Oldenbourg, Munich.

Goldbeck, A. T. and Smith, E. B. (1916), "An Apparatus for Determining Soil Pressures," Proceedings, American Society for Testing and Materials, Vol 16, No. 2, pp 310-319.

Gravesen, S. (1959-A), "Elastisk Halvrum Begrænset af en Stiv Plade med Cirkulært Stempel (Elastic Halfspace Bounded by a Rigid Plate with a Circular Piston)," (Publication in honor of Professor Anker Engelund, Technical University of Denmark, pp 22-89, Copenhagen).

Gravesen, S. (1959-B), "Elastic Semi-Infinite Medium Bounded by a Rigid Wall with a Circular Hole," Bygningsstatistiske Meddelelser, Vol 30, pp 93-111, Copenhagen.

Hadala, P. F. (1967), "The Effect of Placement Method on the Response of Soil Stress Gages," Technical Report No. 3-803, U. S. Army Engineer Waterways Experiment Station, CE, Vicksburg, Miss.

Hamilton, J. J. (1960), "Earth Pressure Cells, Design, Calibration, and Performance, Technical Paper No. 109, Building Research Station, Canadian National Research Council, Ottawa.

Hast, Nils (1945), "Measuring Stresses and Deformations in Solid Materials," Ingenör-Vetenskaps-Akademien, Bulletin No. 178, Stockholm.

Hvorslev, M. J. (1957), Discussion of "Stress Distribution in Compression Tests," Proceedings, Fourth International Conference on Soil Mechanics and Foundation Engineering, Vol 3, pp 105-106, London.

Ingram, J. K. (1968), "Development of a Free-Field Stress Gage for Static and Dynamic Measurements," Technical Report No. 1-914, U. S. Army Engineer Waterways Experiment Station, CE, Vicksburg, Miss.

Kallstenius, T. and Bergau, W. (1956), "Investigation of Soil Pressure Measuring by Means of Cells," Proceedings, Royal Swedish Geotechnical Institute, No. 12, Stockholm.

Kulhawy, F. H., Duncan, J. M., Seed, H. B. (1969), "Finite Element Analysis of Stresses and Movements in Embankments During Construction," Contract Report S-69-8, prepared for U. S. Army Engineer Waterways Experiment Station by University of California, Berkeley, California.

Mindlin, R. D. (1936), "Force at a Point in the Interior of a Semi-Infinite Solid," Physics, Vol. 7, pp 195-200.

McNulty, J. W. (1965), "An Experimental Study of Arching in Sand," Technical Report No. 1-674, U. S. Army Engineer Waterways Experiment Station, CE, Vicksburg, Miss.

Mason, H. G. (1965), "Effects of Structural Compressibility on Active and Passive Arching in Soil-Structure Interaction," Defense Atomic Support Agency, DASA 1718, URS 645-8.

Mason, H. G. et. al. (1963), "A Study of Dynamic Soil-Structure Interaction Characteristics of Real Soil Media," paper for ASCE Meeting in San Francisco, data also presented in report to Air Force Special Weapons Center, AFSWC-TDR-63-3075.

Monfore, G. E. (1950), "An Analysis of the Stress Distribution in and near Stress Gauges Embedded in Elastic Soils," Structural Laboratory Report No. SP 26, U. S. Bureau of Reclamation, Denver, Colorado.

Peattie, K. R. and Sparrow, R. R. (1954), "The Fundamental Action of Earth Pressure Cells," Journal of the Mechanics and Physics of Solids, London, Vol 2, pp 141-155.

Pettibone, H. C. and Bates, R. C., "Cable Troubles with the SMRL Soil-Stress Cell," Proceedings, 8th Annual Engineering Geology and Soils Engineering Symposium, Pocatello, Idaho, p 145.

Pickett, G. (1944), "Application of the Fourier Method to the Solution of Certain Boundary Problems in the Theory of Elasticity," Journal of Applied Mechanics, American Society of Mechanical Engineers, Vol 11, pp A-176 to A-182.

Plantema, G. (1953), "A Soil Pressure Cell and Calibration Equipment," Proceedings, Third International Conference on Soil Mechanics and Foundation Engineering, Zurich, Vol 1, pp 283-288.

Seaman, L. (1966), "One-Dimensional Stress Propagation in Soils," Report DASA 1757, Stanford Research Institute.

Shield, R. T. (1955), "On Plastic Flow of Metals Under Conditions of Axial Symmetry," Proceedings, Royal Society, London, Vol 233-A, pp 267-286.

Shield, R. T. and Drucker, D. C. (1953), "The Application of Limit Analysis to Punch Indentation Problems," Journal of Applied Mechanics, American Society of Mechanical Engineers, Vol 75, pp 453-460.

Shockley, W. G. and Ahlvin, R. G. (1960), "Nonuniform Conditions in Triaxial Test Specimens," Proceedings, American Society of Civil Engineers Research Conference on Shear Strength of Cohesive Soils, Boulder, Colorado, pp 341-357.

Sirieys, P. M. (1964), "Champs des Contraintes Autour des Tunnels en Elastoplasticité," Rock Mechanics and Engineering Geology, II-1, pp 65-75.

Smith, T. et al. (1961), "Evaluation of Commercial Pressure Cells," Material and Research Department, Division of Highways, State of California, Research Report 636342.

Spangler, M. G. (1948), "Underground Conduits--An Appraisal of Modern Research," Transactions, American Society of Civil Engineers, Vol 113, pp 316-343.

Taylor, D. W. (1945), "Review of Pressure Distribution Theories and Earth Pressure Cell Investigations," Chapter 2 in report to the U. S. Army Engineer Waterways Experiment Station of November 1945.

Taylor, D. W. (1947), "Pressure Cell Considerations," Triaxial Shear Research and Pressure Distribution Studies on Soils, Chapter 2, pp 211-236, U. S. Army Engineer Waterways Experiment Station, CE, Vicksburg, Miss.

Taylor, D. W. (1948), Fundamentals of Soil Mechanics, Wiley, New York.

Terzaghi, K. (1936), "Stress Distribution in Dry Sand and in Saturated Sand Above a Yielding Trap Door," Proceedings, First International Conference on Soil Mechanics and Foundation Engineering, Cambridge, Vol 1, pp 307-311.

Terzaghi, K. (1943), Theoretical Soil Mechanics (Trapdoor, pp 66-76, contact pressure pp 390-393), Wiley, New York.

Terzaghi, K. and Peck, R. B. (1967), Soil Mechanics in Engineering Practice, 2d Ed. (contact pressure pp 281-283), Wiley, New York.

Timoshenko, S. and Goodier, J. N. (1951), Theory of Elasticity, 2d Ed., McGraw-Hill, New York.

Van Horn, A. D. (1963), "An Analytical Method for Determining Loads," A Study of Loads on Underground Structures, Part III, Iowa Engineering Experiment Station, Iowa State University, Ames, Iowa.

Tory, A. C. and Sparrow, R. W. (1967), "The Influence of Diaphragm Flexibility on the Performance of an Earth Pressure Cell," Journal of Scientific Instruments, Vol 44, pp 781-785.

Trollope, D. H. and Lee, B. C. E. (1961), "The Measurement of Soil Pressures," Fifth International Conference on Soil Mechanics Foundation Engineering, Paris, Vol 2, pp 403-409.

Walén, C. (1942), "Ett Fall av Deformation i Halvöändligt Elastiskt Medium (A Case of Deformation in a Semi-Infinite Elastic Medium)," Teknisk Tidskrift, Vol 72, No. 34, pp 383-385, Stockholm, Sweden.

Walter, Kriebel, Kaplan (1971), "URS Free Field Soil Stress Gage; Design, Construction, and Evaluation," URS Report 758.

Waterways Experiment Station (1944), "Soil Pressure Cell Investigation," Technical Memorandum No. 210-1, Vicksburg, Miss.

Waterways Experiment Station (1949), "Earth Pressure in Soil Masses, Pressure Cell Performance in Limited Test Section," Interim Report, Vicksburg, Miss.

Waterways Experiment Station (1951), "Pilot Tests on New Four-Gage Cell," Report No. 2, Vicksburg, Miss. (Part of report on investigation of pressures and deflections of pavements.)

Waterways Experiment Station (1952), "Stress Measurements in Flexible Edge of WES Earth Pressure Cell," Not published, Vicksburg, Miss. (Memorandum on earth pressure cell development.)

Waterways Experiment Station (1954-A), Memorandum on "Test Data for Discussion at the Stress Distribution Conference in July 1954," Not published, Vicksburg, Miss.

Waterways Experiment Station (1954-B), "Summary of Earth Pressure Cell Development to 1954," Miscellaneous Paper No. 5-21, Vicksburg, Miss.

Waterways Experiment Station (1955), Memorandum on "Test Data for Discussion at the Stress Distribution Conference in September 1955," Not published, Vicksburg, Miss.

Waterways Experiment Station (1957), "Investigation of the Improved Carlson Stress Meter," Technical Paper No. 6-454, Vicksburg, Miss.

Wiehle, C. H. (1965), "Soil-Structure Interaction Under Dynamic Loads," Final Report, Defense Atomic Support Agency, DASA 1711, URS 645-7.

Woodman, E. H. (1955), "Pressure Cells for Field Use," Bulletin 40, Waterways Experiment Station, Vicksburg, Miss., (WES earth pressure cell pp 11-20).

APPENDIX A: NOTATION

1. The notation used in this report is a compromise between that recommended by the International Society for Soil Mechanics and Foundation Engineering and the notations used in the initial investigations by the Waterways Experiment Station and in the various publications reviewed and quoted in this report.

A	Area
2B	Total thickness of pressure cell
2B _p	Total thickness of soil pocket around cell
2B _w	Total thickness of weak soil cover for cell
c	Cohesion or adhesion of soil
C	Coefficient for plate sinkage, general, Equation 12
C _a	Cell action factor or correction coefficient
d	D _a = diameter of active diaphragm
D	Diameter of pressure cell or rigid inclusion
D _a	Active diameter of pressure cell
D _i	Inside diameter of inactive rim
D _o	Outside diameter of inactive rim
E _c	Elastic modulus of cell material
F	Friction force
F _s	Calibration factor for soil or direct loading of cell
F _u	Calibration factor for hydrostatic loading of cell
G _c	Rigidity modulus of cell material, $G_c = E_c/2(1 + \nu)$
h	Thickness of ellipsoidal inclusion, Figure 32a
H	Depth of burial or soil cover for cell
H _r	Embedment of cell in wall or slab
H _s	Protrusion of cell from wall or slab, $H_r + H_s = 2B$
K	Ratio of lateral to vertical earth pressures
K _b	Coefficient-Boussinesq equations
K _m	Coefficient-Mindlin equations
K _o	Coefficient of earth pressure at rest
K _s	Soil indentation ratio, $K_s = N_s/M_s$

M_c	Deformation modulus of cell for soil loading
M_d	Deviator deformation modulus of soil, $M_d = \epsilon_1 / (\sigma_1 - \sigma_3)$
M_e	Equivalent deformation modulus
M_p	Deformation modulus of soil pocket
M_r	Deformation modulus of the more rigid soil at interface
M_s	Deformation modulus of soil, general, Poisson ratio considered
M'_s	Equivalent modulus nonlinear relations
M_u	Deformation modulus of cell for hydrostatic loading
M_w	Deformation modulus of soil in more compressible or weak cover
N	Z/D = depth ratio
N_r	Indentation relations for the more rigid soil at interface
N_s	Soil indentation coefficient in general
p	Unit pressure, soil or liquid
p_a	Liquid pressure in cavity for uniaxial loading of soil
p_r	Unit soil load measured
p_s	Applied uniaxial soil load, unit load
p_t	Liquid pressure in cavity for triaxial loading of soil
P	Total effective load or force
P_e	Total effective soil load on cell or cavity of cell
P_m	Maximum total force
q	Unit load on soil surface
q_a	Unit axial load
q_r	Unit radial load
Q	Point load or total load
R	Radius of cell or cavity, $2R = D$, also ratio or coefficient
R_c	Modular ratio cell to soil, $R_c = M_c / M_s$
R_s	Modular ratio soil to soil, $R_s = M_s / M_r$, Equation 55
s	Linear coefficient for shrinkage or swelling
S	Total shear force
t	Thickness of diaphragm
T°	Temperature change

u	Unit pressure of water or air in soil pores
V	Volume or volume change
W	Weight or force
z_1	Critical depth or cover; limit of influence
x,y,z	Coordinates
α_c	Coefficient of thermal expansion of pressure cell
α_s	Coefficient of thermal expansion of soil
γ	Unit weight
δ	Deformation or deflection; in coordinate direction $\delta_x, \delta_y, \delta_z$
δ_a	Average deformation, deflection, or depth
δ_c	Deformation of pressure cell
δ_{ce}	Cell deformation for extraneous soil strain ϵ_{se}
δ_e	Differential deformation or indentation by cell, $\delta_e = \delta_s - \delta_c$
δ_m	Maximum deformation or depth
δ_p	Deformation of soil pocket
δ_r	Deformation of more rigid soil layer at interface
δ_s	Deformation of soil, general or weak layer at interface
δ_{se}	Extraneous deformation of soil, Equation 64
Δ	Indicates incremental change in loads, stresses, deformations
ϵ	Strain general; coordinate directions $\epsilon_x, \epsilon_y, \epsilon_z$
ϵ_c	Strain in pressure cell, generally average axial strain
ϵ_s	Strain in soil, generally average axial strain
ϵ_{se}	Extraneous soil strain, Equation 64
ϵ_{sr}	Residual soil strain
μ	Coefficient of friction in soil, $\mu = \tan \phi$
ν	Poisson ratio, generally for soil
σ	Normal stress; in coordinate directions $\sigma_x, \sigma_y, \sigma_z$
σ_c	Normal stress measured by pressure cell, general
σ_{ca}	Axial stress indicated by cell
σ_{cd}	Diagonal stress indicated by cell
σ_{ce}	Cell indication for extraneous soil strain ϵ_{se}

σ_{ct}	Total stress indicated by cell, $\sigma_{ct} = \sigma_{cu} + \sigma_{cu}$
σ_{cu}	Pore pressure indicated by cell, $\sigma_{cu} = u$
σ_{cp}	Radial stress indicated by cell
$\sigma_{c\phi}$	Tangential stress indicated by cell
σ_e	Error in pressure cell registration $\sigma_e = \sigma_c - \sigma_s$
σ_e/σ_s	Error ratio or relative error $(\sigma_e/\sigma_s) = (\sigma_c/\sigma_s) - 1$
σ_F	Pressure on face of cell
σ_i	Normal stress in rigid inclusion
σ_o	Normal cell stress from dead load
σ_r	Normal residual cell stress
σ_s	Normal stress in soil, general
σ_{sc}	Soil stress equivalent to extraneous soil strain
σ_{se}	Soil stress equivalent to extraneous soil strain ϵ_{se}
σ_u	$-u$ = soil stress corresponding to x_1
σ_w	Normal average stress in weak soil cover for cell
$\sigma_{xi}, \sigma_{yi}, \sigma_{zi}$	Normal stresses in rigid inclusion
$\sigma_{xs}, \sigma_{ys}, \sigma_{zs}$	Normal stresses in basic soil matrix
σ_{zh}	Stress by Boussinesq equations
σ_{zi-A}	Axial normal stress in rigid inclusion, uniaxial loading
σ_{zi-T}	Axial normal stress in rigid inclusion, triaxial loading
σ_{zm}	Stress by Mindlin equations
$\sigma_1, \sigma_2, \sigma_3$	Principal stresses
τ	Shear stress, general
τ_c	Cohesion component of soil strength
τ_f	Failure shear strength of soil
τ_r	Shear stress in horizontal and vertical planes
τ_ϕ	Friction component of shear strength
ϕ	Angle of internal friction of soil at peak strength

Reproduced From
Best Available Copy

In accordance with ER 70-2-3, paragraph 6c(1)(b),
dated 15 February 1973, a facsimile catalog card
in Library of Congress format is reproduced below.

Hvorslev, Mikael Juul

The changeable interaction between soils and pressure
cells; tests and reviews at the Waterways Experiment
Station, by M. Juul Hvorslev. Vicksburg, U. S. Army
Engineer Waterways Experiment Station, 1976.

1 v. (various pagings) illus. 27 cm. (U. S. Water-
ways Experiment Station. Technical report S-76-7)

Includes bibliography.

1. Pressure cells (Soils). 2. Soil-pressure cell
interaction. (Series: U. S. Waterways Experiment
Station, Vicksburg, Miss. Technical report S-76-7)
TA7.W34 no.S-76-7

Reproduced From
Best Available Copy